Physiopathology and therapies in myopathies linked to the mechanoenzyme dynamin

Xènia Massana Muñoz

UNIVERSITÉ DE STRASBOURG

ÉCOLE DOCTORALE DES SCIENCES DE LA VIE ET DE LA SANTÉ

Institut de Génétique et de Biologie Moléculaire et Cellulaire
CNRS UMR 7104 – INSERM U 964

THÈSE

présentée par :

Xènia MASSANA MUÑOZ

soutenue le : **14 septembre 2020**

Pour obtenir le grade de :
Docteur de l'université de Strasbourg

Discipline/ Spécialité : Aspects moléculaires et cellulaires de la biologie

Physiopathology and therapies in myopathies linked to the mechanoenzyme dynamin

THÈSE dirigée par :

Mr. Le Docteur Jocelyn LAPORTE	Directeur de recherche INSERM, Université de Strasbourg
Mme. Le Docteur Belinda COWLING	Chargée de recherche INSERM, Université de Strasbourg

RAPPORTEURS :

Mr. Le Docteur Marc BITOUN	Directeur de recherche INSERM, Université Sorbonne
Mme. Le Docteur Fanny PILOT-STORCK	Professeur, Université Paris-Est
Mr. Le Docteur Fabien ALPY	Chargée de recherche INSERM, Université de Strasbourg

AUTRES MEMBRES DU JURY :

Mme. Le Docteur Hélène TRONCHERE	Chargée de recherche INSERM, Université Paul Sabatier

Acknowledgements

I will start by thanking the jury that took the time to read this thesis and come here to be part of my defense. I would like to thank Marc and Fabien for their involvement also in my thesis follow-up committees during these years.

I thank Jocelyn and Belinda because they made me feel at home since the beginning. I learnt so much with you, thank you for hosting and taking care of me during this four years of thesis. Your patience and motivation have been the energy taking me through this journey. Now: Belinda, you now have a collection of GIF so you remember me and we'll always have 'Australia vs Spain' games to bet; Jocelyn, now you know how cool Catalan people can be and as a side PhD project I learnt how to make you laugh.

I spent 4 years at IGBMC surrounded of an amazing team, and eventually they became my friends. Thanks to all of you for the time we shared and for your greatest unconditional help, you made this PhD smoother.

Cricri I had so much fun sharing my days with you. Thank you for taking care of me when I couldn't handle blacksix mice or when I needed help. I really hope our paths cross in the future. Lots of Phil Collins songs for you!

Vale, if each of us is already crazy by herself when we mixed the two of us it became fantastic! Thank you for teaching me so much and all the moments we shared: from dinners, microscope gossiping sessions, waiting for guys to pick up your fridge while painting the walls of your apartment, etc. I cannot wait to be your touristic guide in Barcelona!

Aymen, my football teammate that almost kills us when had torticollis and was not able to turn the neck to see if there were other players. I enjoyed a lot sharing coffees, lab days and football matches with you.

Suzie, thank you for the many phone calls you made when I arrived here and was not able to say a single word in French… thanks to you I had internet at home, a bunch of AAVs to inject and someone always willing to help me.

Sarah1, apart from our crazy days in Paris, it was great having you around during this time, your cooking skills made my PhD journey better, thank you for being there.

Vasu, wherever you are, good luck!

Sarah2, I had a soul sister in France and I spent more than 20 years without knowing it… You were an enormous support during this confinement and thesis writing, thanks for taking care of me and being always there. But you know, let's be honest, you never waited for me to take the morning coffee… I love you anyways.

David, time was too short at your side but enough to discover a soulmate! I hope you remember me every time Bob is in the radio, now that your daughter will start learning Spanish you will need to be learning the normal sentences... you know what I mean. And I won't forget Marie, who made me realize that I'm not done to supervise, I get too sentimental.

To Pascal, because we were the only ones understanding the real magic of photons, fluorophores and microscopes. And Spanish latino songs.

My bench pseudobro (Q1), may the viruses be with you. There is not stupid question that does not deserve your 'Googleing' abilities. Good luck and whenever you need a bit of motivation, we'll always have inspirobot.

Juliana, cactus cactus cactus, you know what I mean. Thank you for your help in this last (stressing) period of the PhD.

Coralie, thank you for helping me in this confinement time I wish karma pays you back and… may the force be with you in your PhD journey!

To all my football and padel mates, thank you for creating a safe environment where I could shout, run and liberate all the stress. But most importantly thank you because I still keep my ankles, knees and wrists.

To my 'lunch groups', thank you for the time we shared either at 11.30h or 12.30h. RU food tasted better by your side.

A special thanks to Ayesha that took her confinement time to improve my manuscript, thank you for your commas, Oxford.

Raquel y Roberto, resulta que tenía dos almas gemelas viviendo en Madrid y tuve que encontrarme con ellas en Estrasburgo. No me caben aquí todas las palabras de agradecimiento que tengo para vosotros, siempre habéis salido en mi rescate y este doctorado no habría sido posible sin vuestro apoyo, que siempre ha sido un salvavidas incluso cuando he perdido la motivación. Espero que vuestros caminos queden cerquita del mío porque me costara mucho

imaginar perderos de vista. Y si no… siempre habrá fideuas que nos reúnan! Os quiero mucho (sorbiendo mocos). (Raquel, Barcelona tiene mar…).

Arantxa, Bea, Laia, Pau, Rafa, habéis sido mi familia desde que llegue aquí y sin vosotros esto habría sido mucho (muchísimo) más complicado. Entre cervezas, cenas, caminatas y mudanzas a pie, hemos arreglado el mundo mil veces, solucionado problemas de 'quiero ir a España' y descubierto que el doctorado resulto ser un poquito más complejo de lo que habíamos previsto (menos Rafa que ya estaba curado de espanto y nos hizo natillas para darnos fuerzas). Pensar que cuando me vaya de Estrasburgo significara separar nuestros caminos me duele, pero sonrío al pensar que gracias a vosotros me llevo la maleta llena de sonrisas y recuerdos, gracias por estar ahí! Os quiero!

Tot això no hauria estat possible sense el suport inesgotable de la meva família. Mama, Adrià, Iaia, Rafa... sempre heu estat la meva estrella polar, el far que em recorda on està casa meva. Ja sabeu que no les vaig tenir totes en què la meva defensa acabes passant, però en aquests anys he après que no importa la distància perquè el vostre amor travessa fronteres i fa que les coses més difícils siguin fàcils. Us estimo moltíssim i de nou us agraeixo tota la forca que m'heu transmès perquè aquesta tesi avui estigui escrita. De vosaltres he après, i aprenc cada dia, que encara que de vegades les coses semblin difícils sempre hi ha motius per lluitar-les i tirar-ho tot endavant. Sou un pilar en la meva vida i ens queden tantes partides de parxis per fer!

Jordi no hi ha prou pàgines en aquesta tesi (perque les vas fer servir totes per la teva ☺) per totes les gràcies que t'haig de donar. Des que estem al costat de l'altre ens hem vist créixer com a persona i hem passat per situacions de tota mena, qui ens havia de dir que arribaríem fins aquí aquella nit que per atzar vam aplicar al doctorat a un tal IGBMC? I qui ens hauria de dir que escriuríem la nostra tesi en 40m2 confinats l'un al costat de l'altre? Gràcies per donar-me la força que m'ha faltat en alguns moments i per ser el meu company de viatge. Ha sigut un confinament molt complicat però tu ho has fet molt més fàcil i senzill pintant-ho amb somriures. T'estimo! EDIT: Deu meu... quin final d'escriptura més mogut... de veritat calia trencar-se un dit?

And of course this would have not been possible without IGBMC PhD Programme that funded me in this adventure and the help from many IGBMC platforms staff: Virus production, Histology service, Electron Microscopy and Photonic Microscopy. Special thanks to Nadia and Pascale for their patience and help.

And thanks to you for taking your time in reading these acknowledgements, in case your name is not here, don't be mad, come to see me and I'll try to fix it.

To the memory of my father Jordi, I would like to tell him: I MADE IT

En memoria de mi padre Jordi, solo querría decirte: LO CONSEGUI

Pel meu pare Jordi, només voldria dir-te: HO HE ACONSEGUIT

[…]
tu ja no hi ets i el temps ara em transcorre
entre el record de tu, que m'acompanyes,
i aquell esforç, que prou que coneixes,
de persistir quan res no ens és propici.
Des d'aquests mots molt tendrament et penso
mentre la tarda suaument declina.
Tots els colors proclamen vida nova
i jo la visc, i en tu se'm representa
sorprenentment vibrant i harmoniosa.
No tornaràs mai més, però perdures
en les coses i en mi de tal manera
que em costa imaginar-te absent per sempre.

***Lletra a Dolors**, Miquel Marti i Pol*

Contents

List of figures

Note: the figures included in the two publications they are not listed here as they are incorporated into manuscripts.

List of abbreviations

AAV	Adeno-associated virus
AChR	Acetylcholine receptors
AD-CNM	Autosomal dominant centronuclear myopathy
ALR	Autophagic lysosome reformation
AMPH	Amphyphisin 1
AP2	Adaptor protein 2
AR-CNM	Autosomal recessive centronuclear myopathy
ASO	Antisense oligonucleotide
BIN1	Amphyphisin 2
BSE	3-helix bundle signaling element
CME	Clathrin-mediated endocytosis
CMT	Charcot Marie Tooth neuropathy
CNM	Centronuclear myopathy
DHPR	Dihydropyridine Receptor
DI-CMT	Dominant intermediate form of Charcot Marie Tooth neuropathy
DNM	All dynamins
DNM1, DNM2, DNM3	Dynamin 1, 2 or 3
DRP1	Dynamin-related protein 1
E18.5	Embryonic day 18.5
ECC	Excitation-contraction coupling
ECM	Extracellular matrix
ER	Endoplasmic reticulum
GED	GTPase effector domain
GTP	Guanosine triphosphate
HE	Hematoxylin eosin
KO	Knock-out
MTM1	Myotubularin 1
MTOC	Microtubule-organizing center
NADH	Nicotinamide adenine dinucleotide tetrazolium reductase

NMJ	Neuromuscular junction
P2 or P10	Post-natal day 2 or 10
PH	Pleckstrin homology domain
PH-GRAM	Pleckstrin Homology-Glucosyltransferase, Rab-like GTPase Activator and Myotubularin domain
PIK3C2b	Phosphatidylinositol-4-Phosphate 3-Kinase Catalytic Subunit Type 2 Beta
PIK3C3	Phosphatidylinositol 3-Kinase Catalytic Subunit Type 3
PRD	Proline-rich domain
PtdIns	Phosphatidylinositol
PtdIns(3)P	Phosphatidylinositol 3-phosphate
PtdIns(5)P	Phosphatidylinositol 5-phosphate
PtdIns(3,5)P2	Phosphatidylinositol 3,5-bisphosphate
PtdIns(4,5)P2	Phosphatidylinositol 4,5-bisphosphate
RID	Rac1-Induced recruitment Domain
RSS	Radial sarcoplasmic strands
RYR1	Ryanodine receptor 1
SCs	Satellite cells
SDH	Succinate dehydrogenase
SH3	Src-homology domain 3
SID	SET-protein interaction domain
SR	Sarcoplasmic reticulum
TA	Tibialis anterior muscle
TGN	Trans-golgi network
VPS34	Phosphatidylinositol 3-kinase VPS34
XLCNM	X-linked myotubular myopathy or X-linked centronuclear myopathy

Part 1
Introduction

1. Introduction to skeletal muscle

Striated muscle is divided into two types: skeletal muscle and cardiac muscle. Cardiac muscle works as a set of muscle cells with self-stimulating abilities with intermediate energy requirements. On the other hand, skeletal muscle is a set of innervated, voluntary muscle cells that have a high energy demand and fatigue upon use (Mukund & Subramaniam, 2020). In humans, skeletal muscles are the most abundant tissue of the body. They function to maintain body posture and temperature as well as to allow movement and generate force (Frontera & Ochala, 2015).

Skeletal muscle is derived from mesodermal tissue, one of the three germ layers determined in early gestation. At the beginning, muscle progenitor cells, also known as myoblasts, proliferate. A change in gene expression results in the differentiation from myoblasts to mononucleated myocytes that eventually fuse to form multinucleated mature muscle fibers that have the ability to contract (Chal & Pourquie, 2017). During this process, myonuclei are initially internalized and once the fiber is mature they migrate to the periphery. One of the hypothesis of this localization is to ensure that all the contractile machinery has enough space in the cytosol (Cadot, Gache, & Gomes, 2015).

A small population of precursor muscle cells remain quiescent associated with myofibers, called adult satellite cell (SCs) (Mukund & Subramaniam, 2020; Relaix, 2006).

Mature skeletal muscle is a highly organized organ, its structure is a group of integrated tissues. Each skeletal muscle has three layers of connective tissue (Figure 1) (Mukund & Subramaniam, 2020):

- Epimysium: ensures structural integrity and separation from other tissues.
- Perimysium: is a layer that covers groups of fibers, also called fascicles.

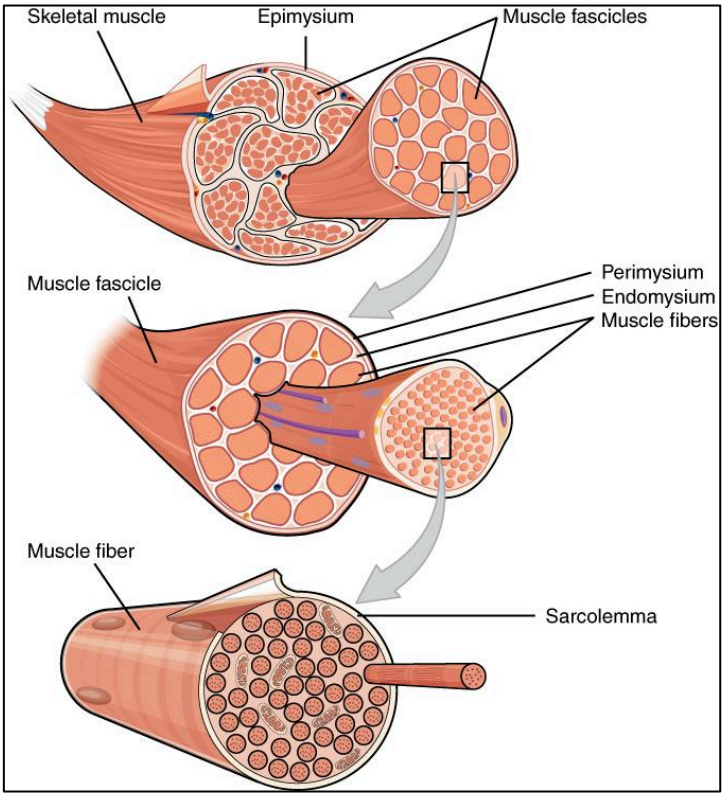

Figure 1. Muscle structure.

From https://opentextbc.ca/anatomyandphysiology/chapter/10-2-skeletal-muscle/

- Endomysium: inside each fascicle every individual skeletal muscle fiber is covered by this last thin layer of connective tissue that is in contact with the cell membrane.

A muscle fiber is surrounded by the sarcolemma, or muscle cell membrane. Inside the sarcolemma we find bundles of myofibrils that are covered by reticulum and Transverse-tubules (T-tubules), which are invaginations of the plasma membrane (Al-Qusairi & Laporte, 2011). Each myofibril is composed by groups of sarcomeres that are the contractile units of skeletal muscle. Skeletal muscles contain a high number of mitochondria. They can undergo mitochondrial biogenesis in case of high energy demand in response to exercise (Peterson, Johannsen, & Ravussin, 2012). (Figure 2)

The sarcomere is an organized structure comprised of actin (or thin filaments) and myosin filaments (or thick filaments) organized in parallel. Myosin heads will interact with actin, allowing muscle contraction. When viewed by electron microscopy, sarcomeres display a set of light and dark lines which have been named according to their light or dark coloration. The relative intensities of the bands are related to their protein content (Sweeney & Hammers, 2018).

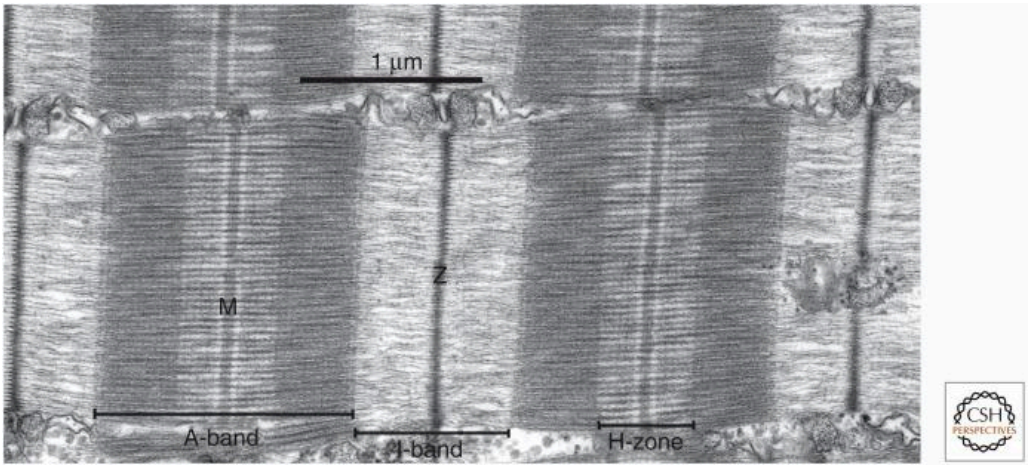

Figure 2. Electron micrograph showing the different bands and lines of the sarcomere.

From (Sweeney & Hammers, 2018)

Myofibers have a specific intracellular structure named sarcoplasmic reticulum (SR) in contrast to the role of endoplasmic reticulum (ER) which is mainly related to protein modification, SR is specialized in calcium storage and release during muscle contraction. When calcium is released from the SR, this causes a conformational change in actin-associated myosin, inducing sarcomere shortening and muscle contraction. Calcium exposes myosin head binding sites to actin, facilitating this process (Kuo & Ehrlich, 2015).

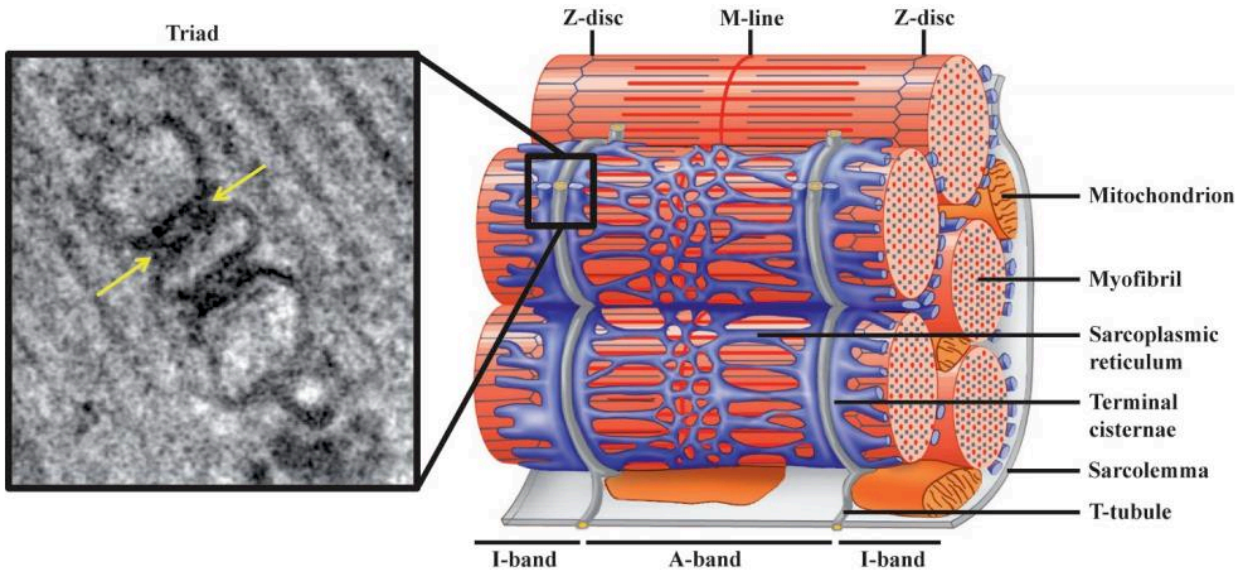

Figure 3. Image of myofiber organization with zoom on triad structure.

From (Al-Qusairi & Laporte, 2011)

Triads are specific muscle structures responsible for excitation-contraction coupling (ECC) (Figure 3). They are composed by a T-tubule tightly associated with two SR on both sides. (Al-Qusairi & Laporte, 2011). There are several proteins involved in ECC:

- Dihydropyridine Receptor (DHPR): a voltage gated calcium channel located at T-tubule membrane.
- Ryanodine receptor (RyR1): a calcium release channel located at SR.
- Calsequestrin: calcium buffering protein in the lumen of SR.
- Calmodulin: one of the different calcium channel regulators.

Muscle contraction is triggered by an excitation signal from a motor neuron to a muscle fiber, this signal is transmitted in a specific area named neuromuscular junction (NMJ). At this junction, the acetylcholine released by the motor neurons will be sensed by acetylcholine receptors (AChR) from the muscle cell (Mukund & Subramaniam, 2020; Nishimune & Shigemoto, 2018). This will lead to a depolarization of the plasma membrane transmitted through the T-tubule and finally causing a conformational change in DHPR. This change will also lead to an opening of RyR1, enabling the release of calcium from SR resulting in muscle contraction (Frontera & Ochala, 2015).

2. Dynamin 2

Dynamin was first discovered as a GTPase enzyme that was co-purified with microtubules (Shpetner & Vallee, 1989). Later studies on flies showed that *shibire* mutants from *Drosophila melanogaster,* which displayed a temperature-sensitive paralytic phenotype (at temperatures higher than 29ºC), were carrying a mutation in the dynamin gene (van der Bliek & Meyerowitz, 1991). In this mutants, there is a strong paralysis due to a depletion of synaptic vesicles and accumulation of endocytic pits at the plasma membrane (Koenig & Ikeda, 1989).

The dynamin superfamily is a group of large GTPases (more than 70kDa) with low affinity for guanine nucleotides (GTP) that can form polymers along membrane structures (Ramachandran & Schmid, 2018).

There are 3 genes encoding 'classical' dynamins in mammals: Dynamin 1 (*DNM1*), Dynamin 2 (*DNM2*) and Dynamin 3 (*DNM3*). They have an 80% homology, with most sequence variation located at the Proline-Rich domain, responsible for protein interaction. Expression of Dynamin 1 is restricted to neurons. Dynamin 3 is mainly expressed in brain, testis and lungs. Dynamin 2 is ubiquitously expressed (Gonzalez-Jamett et al., 2014).

2.1. Dynamin 2 gene

Human *DNM2* gene is located on the short arm of chromosome 19 (19p13.2). The gene is a 114kb region and is comprised of 22 exons (Figure 4A) (Durieux, Prudhon, Guicheney, & Bitoun, 2010). Several splice isoforms have been described: exons 10a and 10b have the same length and are alternatively spliced; and 13b (also named 13ter) that can be spliced (Cao, Garcia, & McNiven, 1998). Recently, a new exon named 12b has been discovered. Both 12b and 13b exons can be included or excluded in the different transcripts found in skeletal muscle. However, the expression of 12b exon is restricted to skeletal muscle, suggesting the presence of a muscle-specific isoform of Dynamin 2 (Cowling et al., 2017). Of note, exon 12b and 13b have not been found in the same transcript so far (unpublished data).

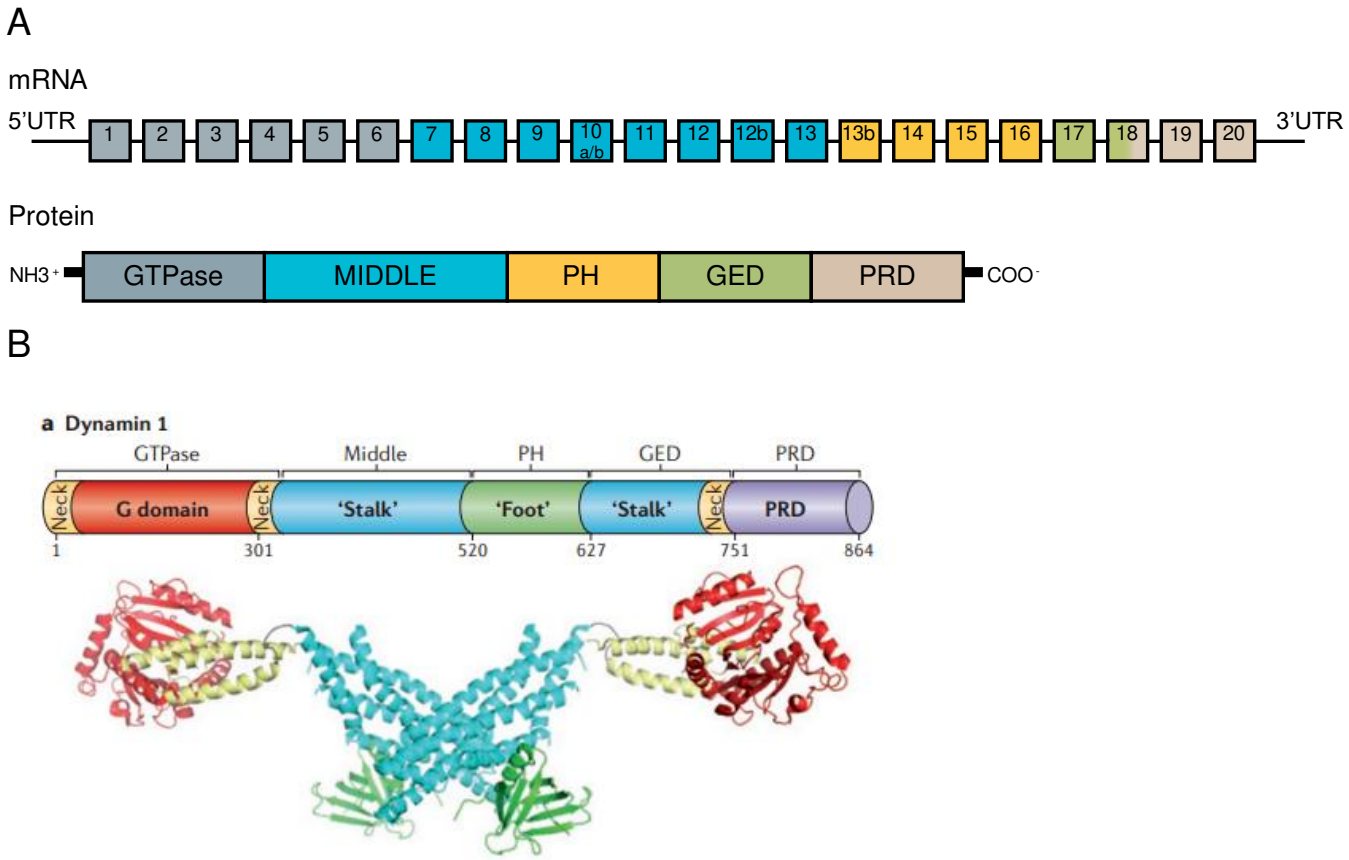

Figure 4. Dynamin 2 domain organization.

(A) Exonic and protein domain structure of Dynamin 2. (B) Dynamin 1 structural domain organization from (Ferguson & De Camilli, 2012).

2.2. Dynamin 2 protein

Dynamin 2 protein is 866 to 876 amino acids, with a molecular weight of around 100kDa. The knowledge of the dynamins mainly comes from studies of neuronal DNM1.

Classical dynamins are multidomain proteins. There are two different nomenclatures: one based on each domain function (Figure 4A) and another one based on the three-dimensional structure of DNM1 (Figure 4B) (Antonny et al., 2016; Ferguson & De Camilli, 2012):

- GTPase or G domain: involved in the hydrolysis of GTP to GDP. It is important also for high order oligomerization.

- MIDDLE or Stalk: allows the dimerization in a cross-like fashion, with the two G domains oriented in opposite directions.
- Pleckstrin homology (PH) or Foot: binds to PtdIns(4,5)P2 when the protein is in an open-conformation state.
- GTPase effector domain (GED): acts a regulatory part of the GTPase activity
- Proline-rich domain (PRD): allows the interaction with proteins containing Src-homology domain 3 (SH3) domain.
- Neck: also known as 3-helix bundle signaling element (BSE).

Dynamins need to oligomerize to be able to fission membranes, and spontaneously polymerize into rings and helices when incubated in low ionic strength solutions (Hinshaw & Schmid, 1995). The dimer is considered the basic dynamin unit (Faelber et al., 2011). Structural studies defined 3 different interfaces at Stalk domain that were important for oligomerization: first, the dimerization occurs via interface 2 (Figure 5, labelled as I2) then the dimers oligomerize to form a tetrameric structure. Studies on DNM3 showed that the tetramerization can occur via two additional interfaces: 1 and 3 (I1 and I3 respectively in Figure 5) (Reubold et al., 2015). Although the exact interactions between subunits are not conserved through all dynamin family, the basic assembly to form helicoidal polymers are shared by dynamin members from bacteria to mammals (Ramachandran & Schmid, 2018). The following scheme shows the different interactions between domains of the DNM3 tetramer (Figure 5).

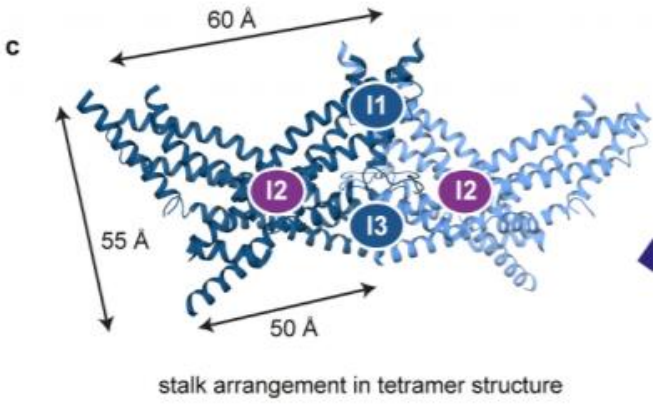

Figure 5. Image of two dynamin dimers.

Each dimer is shown in blue and light blue. They are interacting to form a tetramer. The different interfaces are labelled as: I1, I2 and I3. From (Reubold et al., 2015)

The interaction of interface 3 is the most important for the creation of helicoidal structures, whereas interface 1 allows the interaction with a neighbour dimer. The tetramer seems to have the ability to bend the membrane facilitating the high order oligomerization (Reubold et al., 2015). Membrane constriction to inner diameters of less than 16 nm needs active GTP turnover as well as interaction of G domains across helical turns. The diameter of the polymer is around 50 nm (Antonny et al., 2016).

G domain has also a role in oligomerization since dynamin oligomerization is favoured in presence of GTP or non-hydrolyzable analogs while GTP hydrolysis leads to a disassembly of the oligomer (Danino, Moon, & Hinshaw, 2004; Warnock, Baba, & Schmid, 1997). Of note, mutations located in PH domain have been shown to interfere with GTPase activity, suggesting a cross-talk between this two domains (Kenniston & Lemmon, 2010).

PH domain has been typically related to PtdIns(4,5)P2 binding, although previous studies showed that it may have the ability to bind other phosphoinositides (Klein, Lee, Frank, Marks, & Lemmon, 1998). When found alone, it has low affinity to PtdIns(4,5)P2 and its affinity increases with polymerization. The presence of an additional loop has been proposed to have membrane curvature or sensing properties that may enhance PtdIns(4,5)P2 affinity (Ramachandran et al., 2009; Zheng et al., 1996). However, this domain is not only important for lipid binding: the tetramer coexists in two different conformations, active or autoinhibited in a closed conformation by an interaction of PH and Stalk domains (Reubold et al., 2015). Another function that has been proposed for PH domain is to facilitate PtdIns(4,5)P2 cluster around DNM binding sites (Bethoney, King, Hinshaw, Ostap, & Lemmon, 2009).

PRD domain is related to protein-protein interaction. It has a PXXP motif that enables the interaction with SH3 containing proteins, like the interaction occurring between dynamin and amphyphisin (Grabs et al., 1997).

There are two models proposed to explain dynamin fission activity (Antonny et al., 2016):

- The disassembly model (Figure 6): in which there is a first step where dynamin will bind and constrict lipid membrane enabling the formation of hemifission intermediates which are not stable. The second step occurs after GTP is hydrolyzed, thus loosening the scaffold, allowing the hemifission intermediates to proceed to complete fission. This model is not fully accepted since: the first step requires a high coordination of nucleotide state of all dimers (i.e. all of which should be loaded with GTP at the same time) and the second step may be unlikely as the time that dynamin requires to disassemble is longer than the

viscoelastic time of the membrane, meaning the membrane will not be sufficiently destabilized to drive hemifission (Bashkirov et al., 2008).

- Constriction model (Figure 7): dynamin is acting as a motor where the energy created by GTP hydrolysis is spent in a mechanical work to slide adjacent turns in the helix. They propose that there are several cycles of binding/power stroke/dissociation powered by GTP hydrolysis leading to membrane constriction (Chappie, Acharya, Leonard, Schmid, & Dyda, 2010; Praefcke & McMahon, 2004). This model may be more likely based on current knowledge.

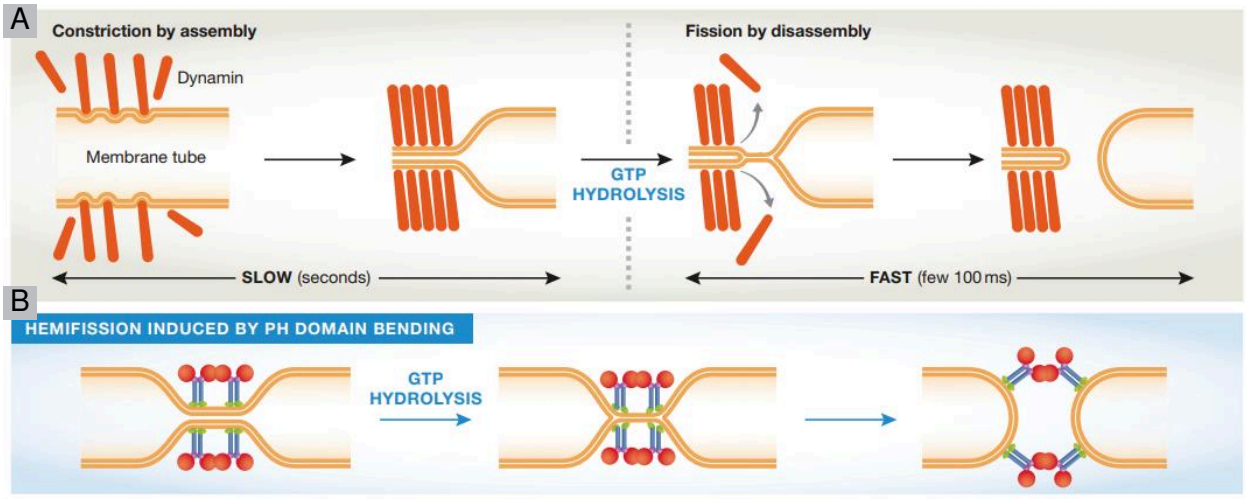

Figure 6. Disassembly model

(A) Schematic view of the process. (B) Scheme showing the different DNM domains and their role in the process (see text). From (Antonny et al., 2016).

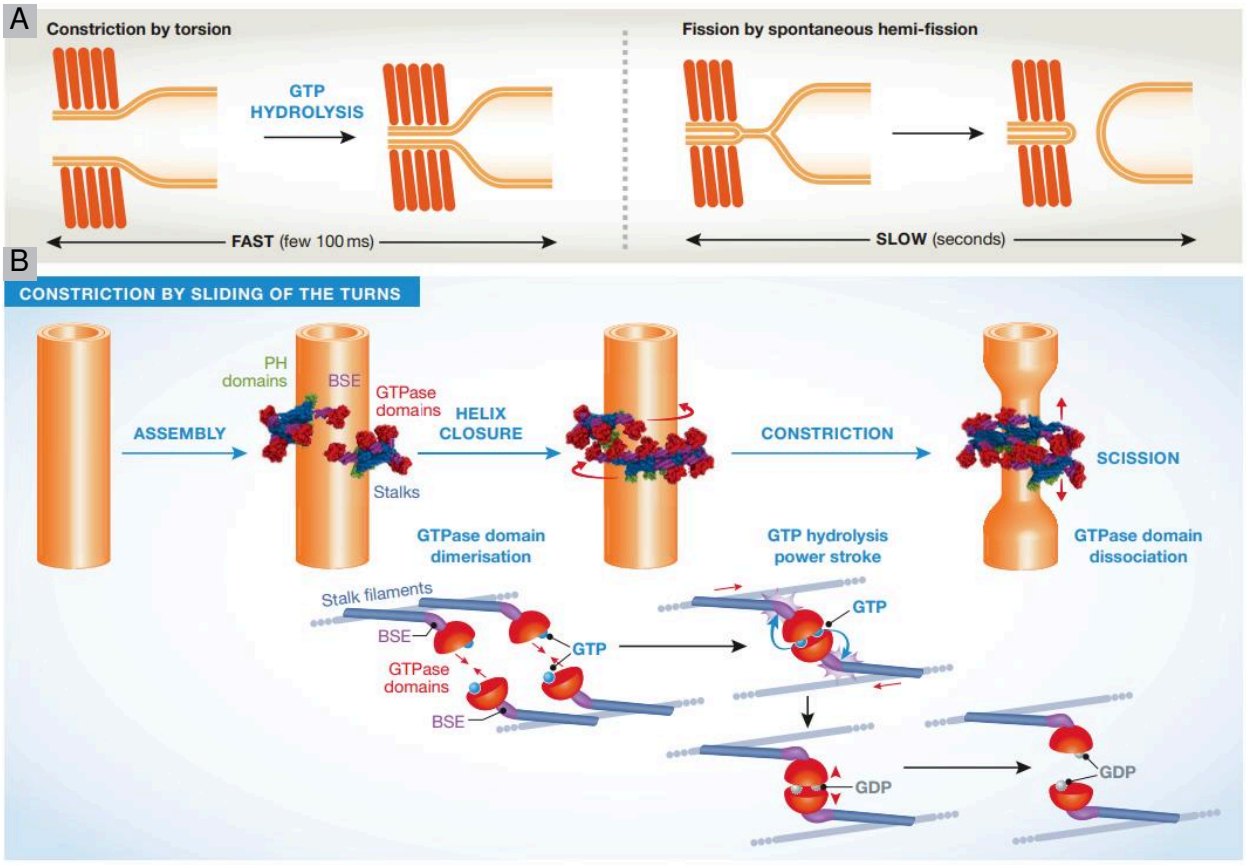

Figure 7. Constriction model

(A) Schematic view of the process. (B) Scheme showing the different DNM domains and their role in membrane fission (see text). From (Antonny et al., 2016).

To conclude, DNMs displays 3 main properties: (1) the ability to self-oligomerize, (2) GTP-induced conformational change leading to constricting of the polymer and the membrane, and (3) induction of membrane fission dependent on GTP hydrolysis.

2.3. Function

Transport and vesicle formation

DNM was related to endocytosis since its early discovery. Studies on *shibire* mutants from *Drosophila melanogaster* (explained in Section 2) had a decreased number of vesicles and accumulation of 'collared pits', suggesting a blockage in the endocytic process (Kosaka & Ikeda, 1983).

Nowadays, we know that DNM2 has an important role in endocytosis, as it was demonstrated in mammalian cells with DNM mutants with reduced GTPase activity (van der Bliek et al., 1993).

Initially, DNM is recruited to the membrane by interaction with PtdIns(4,5)P2 (Zoncu et al., 2007) and BAR domain proteins (such as amphiphysin 1 (AMPH), amphiphysin 2 (BIN1) and sorting nexin 9 (SNX9) (Grabs et al., 1997; Lundmark & Carlsson, 2004)). As discussed before, once recruited to the membrane, DNM2 can then polymerize into an helical structure around the neck of nascent vesicles. When GTP is hydrolyzed there is a power stroke that releases the new vesicle.

There are two types of vesicular trafficking: clathrin-dependent and clathrin-independent. In clathrin-mediated endocytosis (CME), clathrin is the scaffold protein to maintain vesicle structure. It has been shown that clathrin colocalizes with DNM2 during this process (Mettlen, Pucadyil, Ramachandran, & Schmid, 2009). Additionally, in skeletal muscle clathrin heavy chain and DNM2 are part of the costamere, a specific structure that allows mechanical interaction between the fiber and extracellular matrix (Vassilopoulos et al., 2014).

In clathrin-independent vesicle transport, DNM2 is required for its role in membrane fission such as in caveolae formation (Oh, McIntosh, & Schnitzer, 1998). Caveolin, a specific protein related to this structure, was found to partially colocalize with DNM2 in hepatocytes (Henley, Krueger, Oswald, & McNiven, 1998).

Intracellular membrane trafficking

DNM2 has also been found in the Trans-Golgi network (TGN), where it participates in vesicle budding and membrane fission (S. M. Jones, Howell, Henley, Cao, & McNiven, 1998).

DNM2 is also localized to endosomes where it has a dual role: to transport vesicles from late endosomes to the Golgi compartment and the recycling from early endosomes (Gonzalez-Jamett et al., 2013). However the role of DNM2 in this process remains controversial as different studies found no relation between DNM2 and Golgi transport and others claim that when inhibiting DNM2, protein transport from Golgi to plasma membrane is inhibited (S. M. Jones et al., 1998; Kasai, Shin, Shinotsuka, Murakami, & Nakayama, 1999). The different cell types analysed in these experiments may be a confounding factor contributing to the different conclusions made by the authors.

The role of DNM2 in exocytosis is still not clear. Studies on different cell types suggest that DNM2 GTPase activity is important for vesicle release, regulating vesicle fusion with plasma membrane (Reid et al., 2012; Trouillon & Ewing, 2013).

DNM2 and Cytoskeleton

DNM2 was first identified as a microtubule-associated protein (Shpetner & Vallee, 1989). Studies showed that PRD domain is able to directly bind microtubules (Herskovits, Shpetner, Burgess, & Vallee, 1993).

DNM2 polymerizes spontaneously in presence of actin bundles and microtubules (Ferguson & De Camilli, 2012). It binds microtubules by interacting with its PRD domain (Dong, Misselwitz, Welfle, & Westermann, 2000). Reducing DNM2 by siRNA impacts on the amount of acetylated tubulin which is a more stable form and reduces its growing capacity (Thompson, Cao, Chen, Euteneuer, & McNiven, 2004). This suggests DNM2 impacts on microtubule polymerization.

DNM2 is a component of the centrosome, the main microtubule organizing centre (MTOC), where it binds to gamma-tubulin. The function is unknown, but it seems to impact on mitotic spindle alignment (Thompson, Skop, Euteneuer, Meyer, & McNiven, 2002).

Actin cytoskeleton remodelling is a process that contributes to the correct functioning of cell migration, vesicle formation and mitochondrial fission among other processes. DNM2 has been shown to directly interact with actin via its MIDDLE domain: DNM2 binds to short actin filaments and aligns them into bundles (Gu et al., 2010). Two additional proteins involved in actin cytoskeleton interact with DNM2: Actin-binding protein 1 (Abp1, a Src-kinase) and cortactin (involved in CME) (Kessels, Engqvist-Goldstein, Drubin, & Qualmann, 2001; Mooren, Kotova, Moore, & Schafer, 2009). Both proteins are involved at different steps of clathrin-mediated endocytosis. Cortactin-DNM2 interactions together with Arp2/3 (actin related proteins complex) have been found to be important in the global organization of the actomyosin cytoskeleton and to ensure the correct reorganization that will allow lamelipodia formation (Krueger, Orth, Cao, & McNiven, 2003).

Focal adhesions are large assemblies that allow the interaction between the extracellular matrix and the cell. Integrins are glycoproteins part of this complex. To allow cell migration, focal adhesions should be disassembled. DNM2 participates in disassembly of focal adhesions as well as in beta1-integrin recycling (Brinas, Vassilopoulos, Bonne, Guicheney, & Bitoun, 2013).

Apoptosis

DNM2 overexpression has been shown to cause cell toxicity in HeLa cells by p53 apoptotic pathway (Fish, Schmid, & Damke, 2000). A 5-fold increase was shown to be sufficient to cause it. The capacity to induce apoptosis seems to be restricted to DNM2 since DNM1 overexpression, which was increased up to 200-fold, did not cause cell death. Interestingly, overexpression of DNM2 K44A mutant, defective for GTPase activity, was not able to reproduce the same phenotype, whereas overexpression of DNM2 without PRD domain was causing even a stronger apoptotic effect (Fish et al., 2000).

Mitochondria fission

Mitochondrial fission is a complex process that requires multiple steps. First, endoplasmic reticulum and actin cytoskeleton should cooperate to constrict mitochondrial membrane so DRP1 can assemble on the mitochondrial outer membrane. DRP1 then further constricts until membrane fission occurs (Yu, Lendahl, Nister, & Zhao, 2020). In 2016 Lee et al proposed that this process required DNM2 and not DRP1 as the main actor making membrane fission. They suggest that indeed actin and endoplasmic reticulum constrict mitochondria so DRP1 can bind to mitochondrial outer membrane, but the role of DRP1 is to sufficiently constrict mitochondrial membrane so DNM2 can polymerize around it and induce membrane fission (Lee, Westrate, Wu, Page, & Voeltz, 2016).

Three years later, Fonseca et al showed contrary results, claiming DRP1 does not require DNM2 cooperation to ensure mitochondrial fission (Fonseca, Sanchez-Guerrero, Milosevic, & Raimundo, 2019).

This topic remains controversial and further studies should bring more information on the role of DNM2 in mitochondrial fission.

Autophagic lysosome reformation (ALR) and lipid droplet breakdown

In liver or hepatocytes DNM2 has a specific function in helping lipid droplet breakdown. During lipophagy, lipid droplets are enclosed by membranes creating an autophagosome. Lysosomes will fuse with autophagosomes and help in cargo degradation. Once the process is finished, and to replenish the number of lysosomes in the cell, there is a formation of a tube from the

autolysosome that will be fissioned to form a protolysosome. This process is known as autophagic lysosome reformation (ALR) (Y. Chen & Yu, 2017). In the tubulation step, there is interaction of clathrin, adaptor-protein 2 (AP2) and PtdIns(4,5)P2 enrichment in the tubule. Interestingly, they are all components needed for CME. DNM2 has been proposed to participate in fissioning this tubule and creating protolysosomes (Y. Chen & Yu, 2017).

It has been found that lipophagy also requires DNM2 activity in hepatocytes. Inhibition of DNM2 prevented lipid droplet breakdown in hepatocytes due to a defect in ALR (Schulze et al., 2013). Additionally, *Dnm2*$^{R465W/+}$ present a defect in autophagosome maturation, suggesting this process may be impaired as well (Durieux et al., 2012).

Viral entry

Viral entry into host cells requires a cascade of events including: receptor binding, membrane fusion and endocytosis. Viruses following an endocytic pathway to enter into their host cells require DNM2 to fission vesicles where they will be transported along the cell. However, it has been shown that DNM2 can stabilize fusion pores (Sun & Tien, 2013). Viruses like HIV have been proposed to enter their host cells by a fusion process in which DNM2 allows the creation of the fusion pore at low oligomeric state (D. M. Jones et al., 2017).

Functions of DNM2 specific to skeletal muscle

In most cells DNM2 localizes at the plasma membrane, perinuclear region, Golgi network and endosomal compartment (Zhao, Maani, & Dowling, 2018). In skeletal muscle it localizes also in tissue-specific structures such as NMJ (see 1. Introduction to skeletal muscle) and proximal to the Z-line (Zhao et al., 2018).

In skeletal muscle there are specific structures that ensure muscle contraction. As introduced in Section *1. Introduction to skeletal muscle*, triads are muscle-specific structures responsible for excitation-contraction coupling (ECC). The biogenesis of this structure requires extensive membrane remodelling during muscle development. Several membrane binding proteins have been related to this structure such as caveolin and BIN1 (Al-Qusairi & Laporte, 2011). Immunofluorescence experiments showed colocalization of DNM2 with alpha-actinin at the Z-line but not with DHPR receptor on T-tubules in mature muscles (Cowling et al., 2011). During development, T-tubules initially have a longitudinal orientation and are then reoriented in the final

transverse orientation. In fact, later studies showed that in embryonic day 18.5 (E18.5) DNM2 and BIN1 colocalize in longitudinal tubules, consistent with a role of this two proteins in T-tubule biogenesis (Cowling et al., 2017). Moreover, BIN1 is a binding partner of DNM2 by interacting with its PRD domain (Nicot et al., 2007).

Recently Fongy et al showed that DNM2 mutations reduce the number of nuclei per myofiber, suggesting a role in muscle growth and myocyte fusion (Fongy et al., 2019).

Costameres are muscle-specific protein structures aligned with Z-line of peripheral myofibrils. They are localized between plasma membrane and myofibrils and have both a mechanical and signalling role during muscle contraction by stabilizing muscle fibers by binding with the ECM. Costameres are enriched in actin and DNM2 and require clathrin heavy chain to ensure their formation and maintenance (Vassilopoulos et al., 2014). This shows an additional muscle-specific role of DNM2 maintaining myofiber integrity.

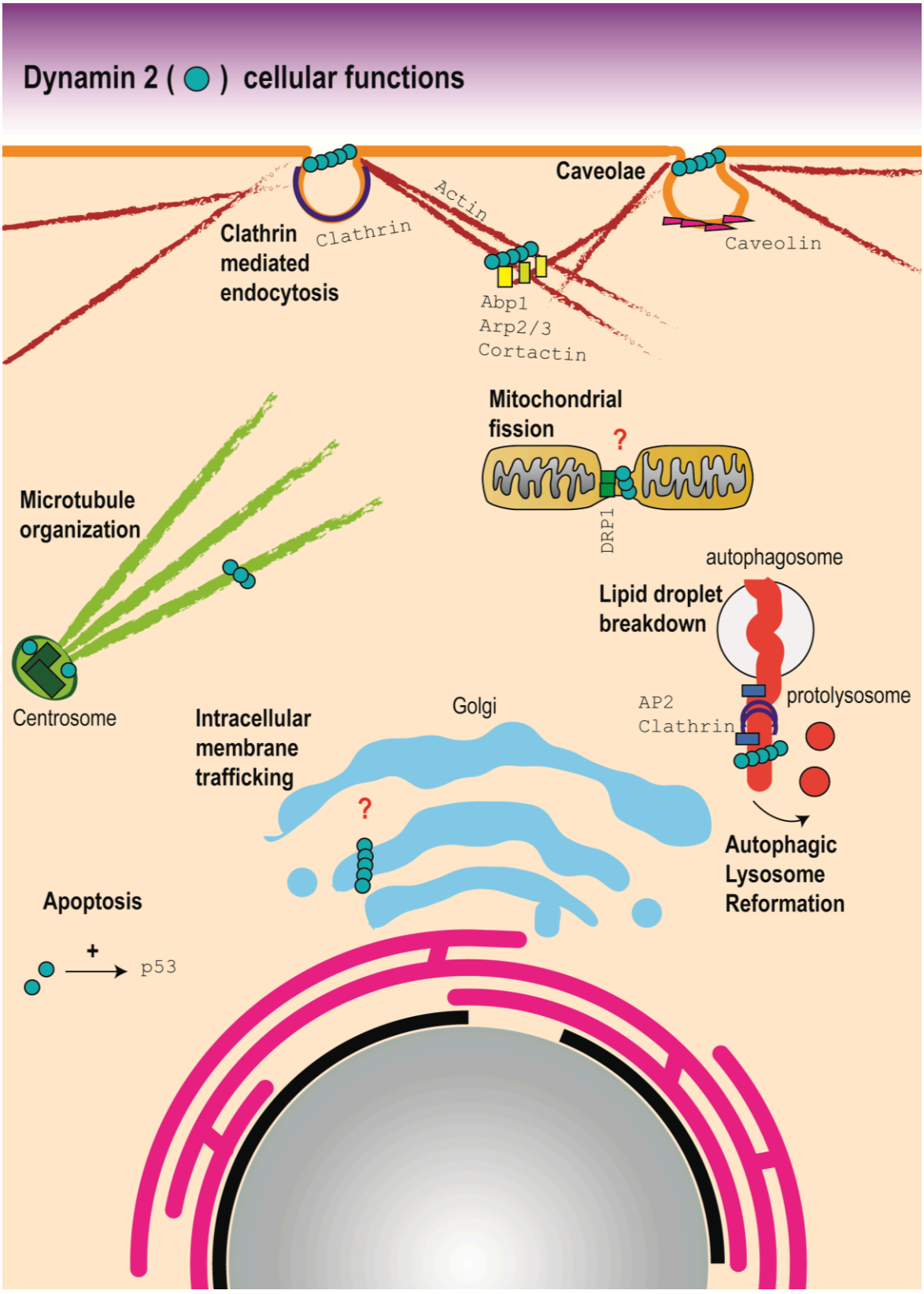

Figure 8. Summary of DNM2 cellular functions.

2.4. Artificial mutations studied in vitro

Several mutations, artificial or pathogenic, have been studied in vitro to better understand dynamin function. In this section only artificial mutations will be discussed, patient-related mutations will be reported in sections 2.5 and 2.6. A summary of all mutations presented in this thesis is in Figure 14.

K44A

K44A is the most common dominant negative mutation, and is localized in the GTPase domain. In vitro studies showed K44A mutant has very low affinity for GTP partially inhibiting GTPase and fission activity (Damke, Baba, Warnock, & Schmid, 1994).

At the structural level K44A forms more constricted helicoidal structures compared to WT protein (Sundborger et al., 2014).

When expressed in cells the K44A mutant blocks clathrin-related vesicle formation, lipid droplet breakdown, lamellipodia formation and actin cytoskeleton remodelling (Damke, Binns, Ueda, Schmid, & Baba, 2001; Gu et al., 2010; Schlunck et al., 2004; Schulze et al., 2013). Similarly to ΔPRD, discussed below, K44A is not able to rescue mitochondrial fission in DNM2-depleted cells (Lee et al., 2016).

K142A

K142A is a DNM2 mutant with an almost normal GTPase activity but no conformational change is observed after GTP hydrolysis. Expression of this mutant in cells results in a blockage in CME (Marks et al., 2001).

R399A

This mutation localizes in the MIDDLE domain. R399A mutant is unable to form high order oligomers, and remains blocked in a dimeric state. It has 50% less efficient lipid binding and 90% reduced GTPase activity when compared to WT protein (Ramachandran et al., 2007). The higher reduction observed in GTP hydrolysis may be due to the fact that this mutant cannot form high oligomeric structures that could propagate the conformational change needed to catalyse its enzymatic activity (Ramachandran et al., 2007).

Interestingly, the combination of this mutation with pathogenic DNM2 mutations where GTPase activity was increased, can return the catalytic activity to normal levels (Chin et al., 2015)

ΔPRD

This mutant has a deletion of the entire PRD domain, disrupting the interaction with SH3-domain containing proteins.

Structural studies showed that ΔPRD behaves similarly to WT DNM and is able to form helicoidal structures around membrane tubules (Zhang & Hinshaw, 2001).

However, ΔPRD is not able to bind SH3-domain containing proteins like BIN1 or cortactin, affecting DNM2 localization and function (McNiven et al., 2000). Interestingly, this mutant is not able to rescue mitochondrial fission in DNM2-depleted cells (Lee et al., 2016). Recent reports showed that expression of ΔPRD DNM2 in DNM triple-KO cells is not able to rescue CME (Rosendale et al., 2019).

2.5. Associated diseases

Dominant mutations in *DNM2* have been associated to two different diseases: Autosomal dominant centronuclear myopathy (ADCNM, MIM#160150), Charcot Marie Tooth Neuropathy (CMT, MIM#606482).

Only one mutation has been reported at homozygous state causing lethal congenital contracture syndrome (Koutsopoulos et al., 2013)(MIM#615368).

2.5.1. Charcot Marie Tooth

Charcot Marie Tooth disease (CMT) is a peripheral neuropathy characterized by loss of sensation, neuropathic pain, distal muscle weakness and atrophy and skeletal deformations such as *pes cavus* (Gonzalez-Jamett et al., 2014; Nave & Werner, 2014). Patients affected with CMT usually experience disease onset in the two first decades of life with various degrees of severity. A subset of patients also develop cataract and neutropenia (abnormally low concentration of neutrophils in blood) (Claeys et al., 2009).

CMT is genetically heterogeneous and is divided in two different categories (Berciano, 2011):

- CMT 1: Including demyelinating forms of the disease with reduced nerve conduction velocities.

- CMT 2: Including axonal forms of the disease where nerve conduction velocities are normal but conduction amplitudes are decreased, mostly due to a loss of myelination from large-calibre axons.

There are also 4 dominant intermediate forms of the disease (DI-CMT): DI-CMTA, DI-CMTB, DI-CMTC and DI-CMTD. These forms exhibit characteristics from both demyelinating and axonal forms (Tanabe & Takei, 2012). Mutations in *DNM2* are associated to DI-CMTB (Zuchner et al., 2005) and CMT 2 (Fabrizi et al., 2007). When peripheral nerves are observed at histological level they display abnormal myelination (Figure 9).

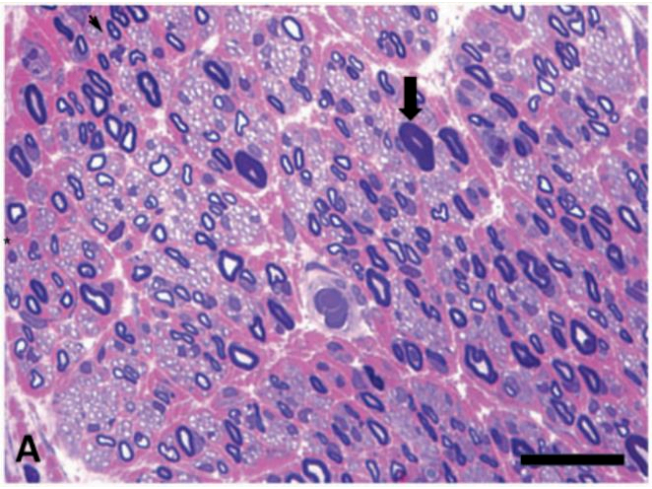

Figure 9. Sural nerve biopsy from a CMT-DNM2 patient carrying the K562E mutation.

Arrow points to an axon with abnormally think myelin layers. From (Claeys et al., 2009).

Since mutations in *DNM2* are also causing centronuclear myopathy, a muscle biopsy was performed in CMT-DNM2 affected patient to evaluate a possible overlap between the two diseases. No clinical muscle phenotype was observed in this patient (Bitoun et al., 2008) (Figure 10).

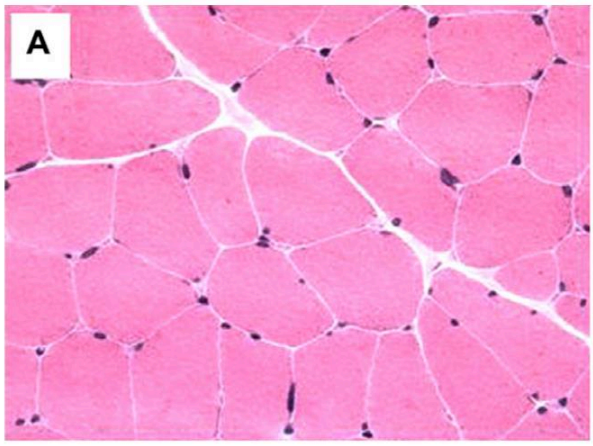

Figure 10. Muscle biopsy from a CMT patient carrying K559del mutation.

Section was stained with Hematein-eosin. Note the absence of nuclei internalization. From (Bitoun et al., 2008).

Mouse models for *DNM2*-related CMT

Very recently Pereira et al. reported the creation of the first *Dnm2* mouse model carrying a CMT mutation. Surprisingly their study concludes that this mouse model does not display signs of a peripheral neuropathy but of a mild myopathy (Pereira et al., 2020).

Dnm2$^{+/K562E}$ mice were analyzed by different electrophysiological and behavioural tests that led the authors to conclude that the mutation caused a decrease in muscle force without affecting nerve physiology. Myofibers from this animals have reduced fiber size but no significant change was detected in nuclei position (Figure 11) (Pereira et al., 2020).

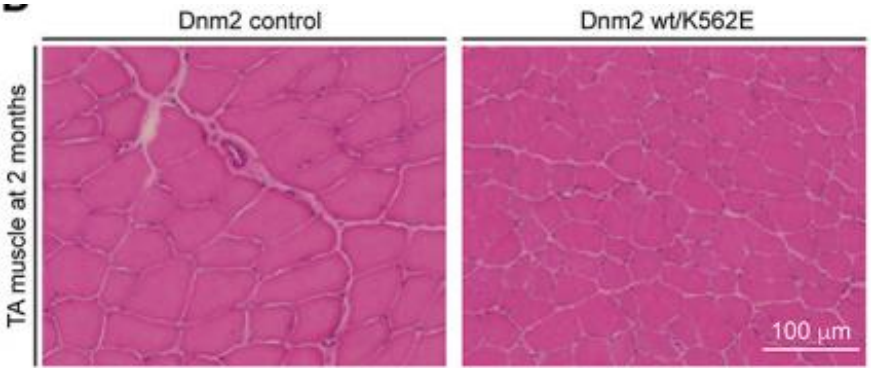

Figure 11. Tibialis anterior muscle section from 2-month old control and *Dnm2*$^{+/K562E}$

Muscles were stained with Hematoxylin Eosin (HE). Note the difference in myofiber size from *Dnm2*$^{+/K562E}$ animals compared to control. From (Pereira et al., 2020).

Transcriptomic analysis of soleus muscles from heterozygous K562E mice showed a downregulation of transcripts related to oxidative metabolism (i.e. mitochondrial oxidative phosphorylation and energy metabolism). On the other hand, there was an enrichment of transcripts related to ECM organization and inflammatory response that was confirmed at histological level by an increase of macrophage number (Pereira et al., 2020).

Overall these results point to a possible overlap between DNM2-related CMT and myopathy.

2.5.2. Centronuclear myopathy

Congenital myopathies are a group of muscle disorders characterized by various degrees of muscle weakness. Centronuclear myopathy (CNM) is a type of congenital myopathy. As suggested by the name, it is characterized by the central position of the nuclei in patient myofibers. There are two types of centronuclear myopathies:

- X-linked myotubular myopathy (XLCNM) caused by mutations in myotubularin 1, *MTM1*. It has an estimated incidence of 17 per million of all births (Vandersmissen et al., 2018). It will be briefly discussed in the next section.
- Autosomal recessive or dominant CNM caused by mutations in amphiphysin 2 (*BIN1*), dynamin 2 (*DNM2*), ryanodine receptor (*RYR1*), myotubularin-related protein 14 (*MTMR14*), titin (*TTN*) or striated muscle preferentially expressed protein kinase (*SPEG*). Non-XLCNM has an incidence of 7 per million births (Vandersmissen et al., 2018). Only *BIN1* and *DNM2*-related CNM will be discussed in this thesis. BIN1-related CNM will be briefly mentioned in the next section.

Currently, there are no available therapies for CNM patients.

2.5.2.3 Autosomal dominant DNM2 related CNM

Dominant mutations in *DNM2* cause Autosomal Dominant CNM (AD-CNM, MIM#160150) (Bitoun et al., 2005). It is estimated that 21 newborns per year are carriers of mutations in *DNM2* causing ADCNM. Clinically, patients are very heterogeneous: from mild forms in adult patients to severe forms appearing at birth. Patients with moderate phenotype have delayed milestones, moderate muscle weakness, ptosis and ophthalmoplegia (Figure 12A). On the other hand, patients with neonatal onset have generalized weakness, hypotonia, facial weakness with open mouth, ptosis and ophthalmoplegia (Bitoun et al., 2007). Other phenotypes that can be associated to AD-CNM are: scoliosis, reduced jaw opening and mild pes cavus (Bitoun et al., 2007; Bohm et al., 2012).

Biopsies from AD-CNM patients show radial arrangement of sarcoplasmic strands that are positive for oxidative staining (named radial sarcoplasmic strands, RSS), nuclear centralization and internalization together with type I fiber predominance and hypotrophy (Figure 12B). Sometimes there is an increase of adipose endomysial tissue replacing muscle tissue (Toussaint et al., 2011). Those features are only found in *DNM2*-related cases (Romero & Bitoun, 2011).

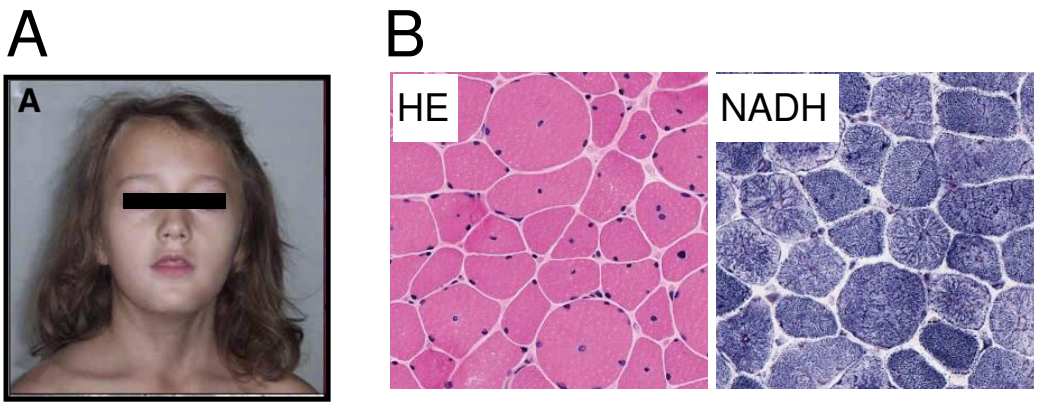

Figure 12. Main features of DNM2-related AD-CNM

(A) Picture of DNM2 showing facial muscle weakness. (B) Histological analysis of patient muscles showing fiber size variability in HE and radial strands by oxidative staining (NADH). Images from a patient carrying R465W mutation. (Aghbolaghi & Lechpammer, 2017; Romero & Bitoun, 2011)

Ultrastructural analysis by electron microscopy confirmed the presence of RSS impacting on the myofibril size inside the fiber. Surrounding the nuclei accumulation of mitochondria, sarcoplasmic reticulum, Golgi and glycogen can be observed (Toussaint et al., 2011).

The most common mutation in AD-CNM is the missense mutation R465W localized in the MIDDLE domain (Zhao et al., 2018).

Animal models for *DNM2*-related CNM

The first knock-in mouse model was generated in 2010 expressing R465W mutation. Heterozygous mice (*Dnm2*$^{+/R465W}$) developed a mild progressive myopathy whereas homozygous mice (*Dnm2*$^{R465W/R465W}$) were dying at birth, some of them surviving until 1 week of age. *Dnm2*$^{+/R465W}$ mice lived as long as WT without any defect in growth curve. Histological muscle analysis displayed defects at mitochondrial and sarcoplasmic reticulum organization. No obvious nuclei internalization was observed for this animal model (Figure 13) (Durieux, Vignaud, et al., 2010). However, a recent study showed that isolated fibers from the same animal display defects of number and spatial distribution of myonuclei (Fongy et al., 2019). Other ultrastructural analysis revealed defects in the T-tubule network and calcium homeostasis (Durieux, Vignaud, et al., 2010).

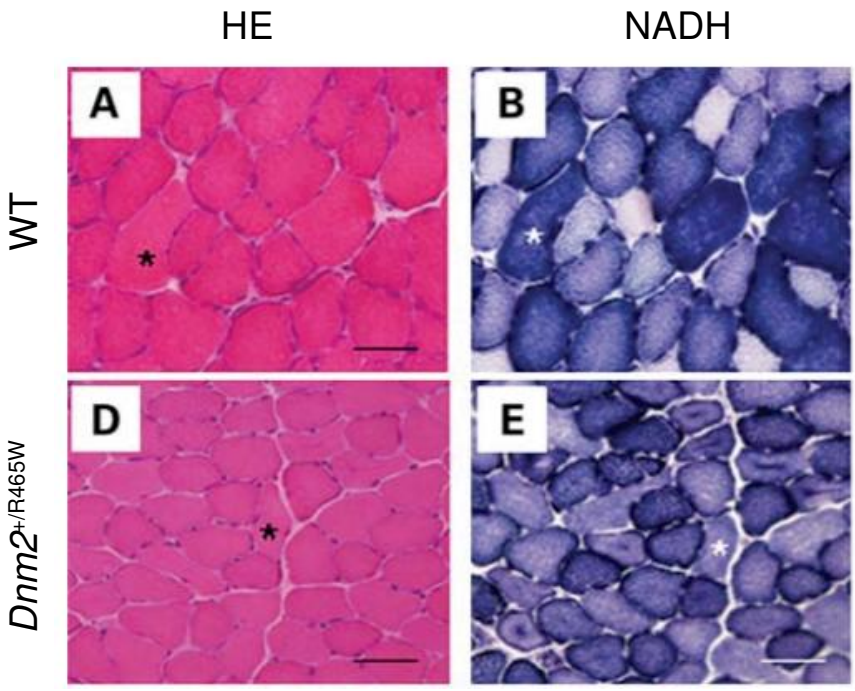

Figure 13. Histological analysis of TA muscles from *Dnm2*$^{+/R465W}$ mouse model.

HE and NADH images from TA muscles of Dnm2+/R465W animals. NADH staining shows an abnormal accumulation at the center of the fiber. From (Durieux, Vignaud, et al., 2010)

The following year Cowling et al. published a model with AAV-mediated expression of WT and R465W DNM2 in skeletal muscle. Interestingly, increased expression of WT-DNM2 induced some

muscle defects but to a lesser extent than R465W mutant. The overexpression of WT-DNM2 or R465W mutant impacted on muscle force, fiber size and nuclei position. These results combined suggest that CNM-DNM2 mutations are gain of function (Cowling et al., 2011). This is supported by in vitro data in which CNM-DNM2 mutants appeared to have higher GTPase activity compared to WT protein (Kenniston & Lemmon, 2010).

2.6. Insights into DNM2 pathogenic mutations

Most of the *DNM2* pathogenic mutations are clustered in the PH domain and interface between the PH and MIDDLE domains (Bohm et al., 2012).

CMT mutations

Note: K562E is also called K558E; 555delta3 is also called 551delta3, since other reports took other DNM2 isoform as a reference. Here I only used K562E and 555delta3 nomenclature.

Most of the CMT-DNM2 mutations are located at PH domain, in a lipid binding pocket, although some others are found in MIDDLE and PRD domains (Bohm et al., 2012; Claeys et al., 2009).

There are two main DNM2 cellular processes that have been related to CMT: membrane binding and microtubule association. Initial experiments hypothesized that CMT-DNM2 mutants have reduced membrane binding in favour of binding to microtubules (Zuchner et al., 2005).

As explained before, there is a specific loop in PH domain which has been related to membrane-curvature sensing and lipid binding affinity (Bethoney et al., 2009). Most of the mutations of CMT-DNM2 mutations are located in this loop, potentially affecting lipid binding (Bohm et al., 2012). In vitro, CMT-DNM2 mutants, like K562E, are not able to bind lipids and display low GTPase activity (Kenniston & Lemmon, 2010). They have low fission activity in vitro (Chin et al., 2015). The same mutant when overexpressed in cells was not able to localize at plasma membrane, blocking CME and displaying a similar effect to K44A (GTPase defective mutation). On the other hand, mutants like 555delta3 or G358R did not block endocytosis in COS7 cells, suggesting that DNM2 was still able to localize in the membrane (Koutsopoulos et al., 2011; Tanabe & Takei, 2009). Some CMT mutations caused DNM2 aggregates in perinuclear region (Zuchner et al., 2005).

It remains controversial if microtubule association is a key process affected in presence of CMT-DNM2 mutants since different reports found contrary results. When DNM2 was initially related to CMT, cells transfected with CMT-DNM2 mutants displayed microtubule disorganization with

DNM2 colocalization (Zuchner et al., 2005). Later, another study in cells transfected with 555delta3 showed that this mutant has a high affinity to bind microtubules. The authors hypothesized that microtubule-dependent transport would be then inhibited since most of the surface would unavailable because of DNM2 binding. However, the overexpression of K562E did not affect microtubule stability suggesting microtubule binding is not impaired in all CMT-DNM2 mutations (Tanabe & Takei, 2009).

Furthermore, organization of actin cytoskeleton was disturbed in various cell types overexpressing K562E mutant (Yamada, Kobayashi, Zhang, Takeda, & Takei, 2016).

Schwann cells and oligodendrocytes are the cells responsible to ensure myelination in peripheral nerves and central nervous system, respectively (Nave & Werner, 2014). Schwann cells wrap around axons of large diameter with myelin, forming a multi-layered membranous system that secures fast conduction of action-potentials. At physiological level, CMT mutations impact CME in Schwann cells and motor neurons and reduce myelination in a dorsal root ganglia culture model (Sidiropoulos et al., 2012). Interestingly, DNM2 appears to be necessary for Schwann cells survival and function, suggesting only peripheral nervous system requires DNM2 for an effective axon myelination. Oligodendrocytes without DNM2 expression were able to survive and ensure central nervous system myelination (Gerber et al., 2019).

Taken together, different cellular processes are implicated in the pathomechanisms causing CMT-DNM2 mutations, and the specific cellular process affected may depend on the location of the mutation in patients.

CNM mutations

The most common CNM-*DNM2* mutations are (Zhao et al., 2018):

- R465W, found in 25% of affected families
- E368K and R369W, in 20% of families
- Mutations in residue S619 in 15% of patients
- Mutations in residue S618 in 10% of patients

CNM-DNM2 mutant proteins are able to form more stable oligomers and they display a higher GTPase activity in vitro (Chin et al., 2015). Lipid binding remains unaffected in CNM mutants. Their high GTPase activity rates seems to be independent to lipid binding, so called lipid unsensitised (Kenniston & Lemmon, 2010). More specifically, S619L mutation, causing a severe

form of CNM, behaves as a lipid unsensitised form of DNM2 with high GTPase activity independent of lipid binding together with a high fission activity. S619L has higher propensity to self-assemble into oligomers (Kenniston & Lemmon, 2010).

In transfected cells, CNM mutants affect DNM2 localization and cause the aggregation of the protein in the cytosol (Gonzalez-Jamett et al., 2017). This has been also observed in *Dnm2*$^{R465W/+}$ mice, where DNM2 aggregates in the cytosol with Dysferlin (Durieux, Vignaud, et al., 2010). DNM2 accumulation has been also observed in a patient with E368K mutation (Kierdaszuk et al., 2013). Of note, two CMT-DNM2 mutants were shown to cause DNM2 aggregation when expressed in cells (Koutsopoulos et al., 2011).

It remains controversial whether DNM2-CNM mutations have an effect on CME as the data generated appears to depend on the cell line used. For example, COS7 cells transfected with R465W displayed impaired CME whereas no effect was observed in HeLa, C2C12, patient fibroblasts or motor neuronal cells transfected with the same mutation (Bitoun et al., 2009; Koutsopoulos et al., 2011; Sidiropoulos et al., 2012).

As discussed previously, DNM2 may have a role in T-tubule biogenesis or maintenance. In vitro and in vivo experiments suggested that DNM2-CNM mutants are defective in this process, giving a possible explanation of the tissue-specificity of the disease (Chin et al., 2015; Gibbs, Davidson, Telfer, Feldman, & Dowling, 2014).

In this thesis only the following mutations will be further studied:

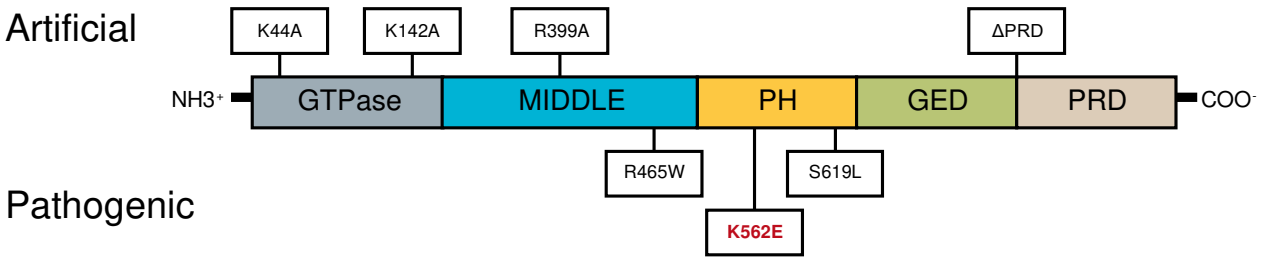

Figure 14. Summary of DNM2 mutations included in this thesis

The mutations listed in this figure are the ones that will be considered in this thesis. Upper part shows artificial mutations, below pathogenic mutations for CNM and CMT (in red) diseases.

3. The ‘MAD’ Pathway

Myotubularin 1 (MTM1), Amphyphisin 2 (BIN1) and Dynamin 2 they have been hypothesized to be in the same pathway. In this section the different proteins will be briefly introduced as well as the interactions between them.

3.1. Membrane remodeling

As discussed in previous sections, DNM2 is a large GTPase involved mostly in membrane fission events. There are several studies that place the three different proteins in the same pathway. The main feature they have in common is that their function is mostly related to membranes:

- MTM1 is a lipid phosphatase regulating membrane phosphoinositides
- BIN1 is a BAR-domain protein with membrane-curvature sensing properties
- DNM2 is a large GTPase as well as a mechanoenzyme able to fission membranes.

3.2. Myotubularin 1

The locus for *MTM1* was first identified by linkage analysis in the X chromosome (Thomas et al., 1990). Several studies on patients affected with X-linked myotubular myopathy, a disease caused by deletions in *MTM1*, allowed to finally clone and identify the *MTM1* gene (Laporte et al., 1996).

MTM1 is ubiquitously expressed and has a muscle-specific alternative transcript thanks to the use of an alternative polyadenylation signal. *MTM1* gene is 100kb long including 15 exons (Laporte et al., 2000). This gene encodes for Myotubularin 1 protein and it was the first member identified of the Myotubularin protein family.

MTM1 protein has the following different domains (Figure 15A) (Raess, Friant, Cowling, & Laporte, 2017):

- PH-GRAM domain (Pleckstrin Homology-Glucosyltransferase, Rab-like GTPase Activator and Myotubularin): allows binding to lipids, especially to phosphatidylinositol-3,5-biphosphate (PtdIns(3,5)P2) but it can also interact with effector proteins.
- RID domain (Rac1-Induced recruitment Domain): can interact with Desmin and plasma membrane.
- Phosphatase domain: it is a catalytic domain. It contains a motif conserved among other phosphatases that is required to dephosphorylate phosphoinositides

- SID (SET-protein interaction domain)
- Coiled coil
- PDZ binding site: mediates protein-protein interactions

Most of the members from the myotubularin family can interact with themselves or other myotubularins.

MTM1 catalyzes the dephosphorylation of PtdIns(3,5)P2 to PtdIns(5)P and PtdIns(3)P to PtdIns (Figure 15B) (Lorenzo, Urbe, & Clague, 2006; Tronchere et al., 2004).

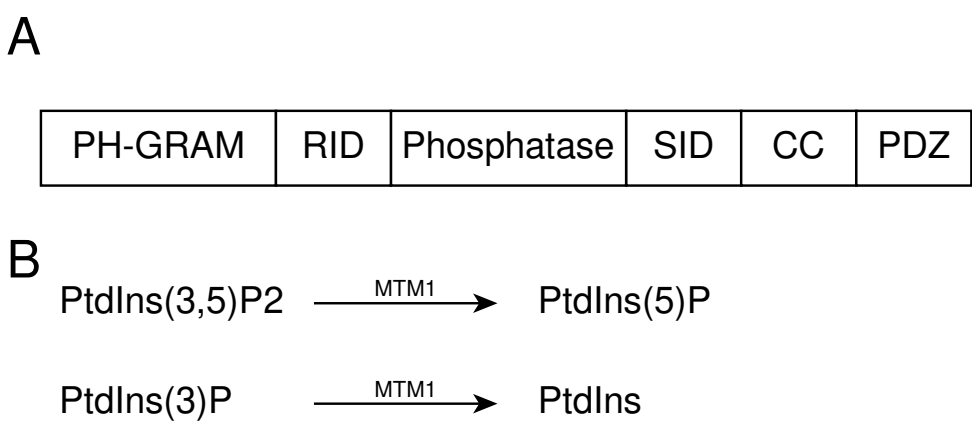

Figure 15. Scheme of MTM1

(A) Protein domains and (B) catalytic reactions.

Phosphoinositide signalling has many implications in the cell. One of the most important relates to cellular transport and membrane recycling. In this regard, substrates of MTM1 have specific localizations: PtdIns(3)P are components of early endosomes, PtdIns(3,5)P2 are mainly found in endosomes. The product from its catalytic activity, PtdIns(5)P, are components of late endosomes (De Craene, Bertazzi, Bar, & Friant, 2017). MTM1 has also been found to have a role in autophagy (Al-Qusairi et al., 2013; Gavriilidis et al., 2018). In skeletal muscle, immunogold labelling showed that MTM1 localizes in the SR (Amoasii et al., 2013).

Mutations in *MTM1* cause a severe form of centronuclear myopathy. Interestingly, mutations in other members of the myotubularins protein family, for example *MTMR2*, cause Charcot Marie Tooth neuropathy (Raess, Cowling, et al., 2017).

3.2.1. X-linked myotubular myopathy (XLCNM)

Mutations in *MTM1* cause XLCNM (MIM#310400) (Laporte et al., 1996), which is one of the most severe congenital muscle disorders with an incidence of 1/50.000 newborn males. More than 300

mutations have been identified on this gene, most of them are loss-of-function mutations that cause a strong decrease of MTM1 protein (Buj-Bello, Biancalana, Moutou, Laporte, & Mandel, 1999; Laporte et al., 1997).

XLCNM is clinically characterized by severe hypotonia, muscle atrophy and generalized weakness at birth. Very often patients present respiratory insufficiency and swallowing difficulties, requiring ventilation support and a feeding tube to prevent early death (Figure 16A). Some patients develop external ophthalmoplegia, a condition characterized by weakness of the eye muscles (Romero & Bitoun, 2011). The large majority of patients die within the first months of life, only a small proportion survive into childhood and even adulthood (Jungbluth, Wallgren-Pettersson, & Laporte, 2008).

Female carriers can present a wide spectrum of clinical and pathological involvement: from severe muscle weakness with loss of ambulation to no muscle weakness but signs of an asymmetric phenotype (Cocanougher et al., 2019).

Histological analysis of patient muscle biopsies shows a high number of small fibers with centralized nuclei and type I fiber predominance (Figure 16B). Ultrastructural visualization shows that myofibrils are misoriented and preferentially localize at the periphery of the fiber. In contrast, central areas of the myofiber are mostly occupied by glycogen and mitochondrial aggregates. Oxidative staining, such as Nicotinamide adenine dinucleotide tetrazolium reductase (NADH) or succinate dehydrogenase (SDH), shows that some fibers have accumulation around the cytosol. Due to their appearance they are called necklace fibers (Figure 16C).

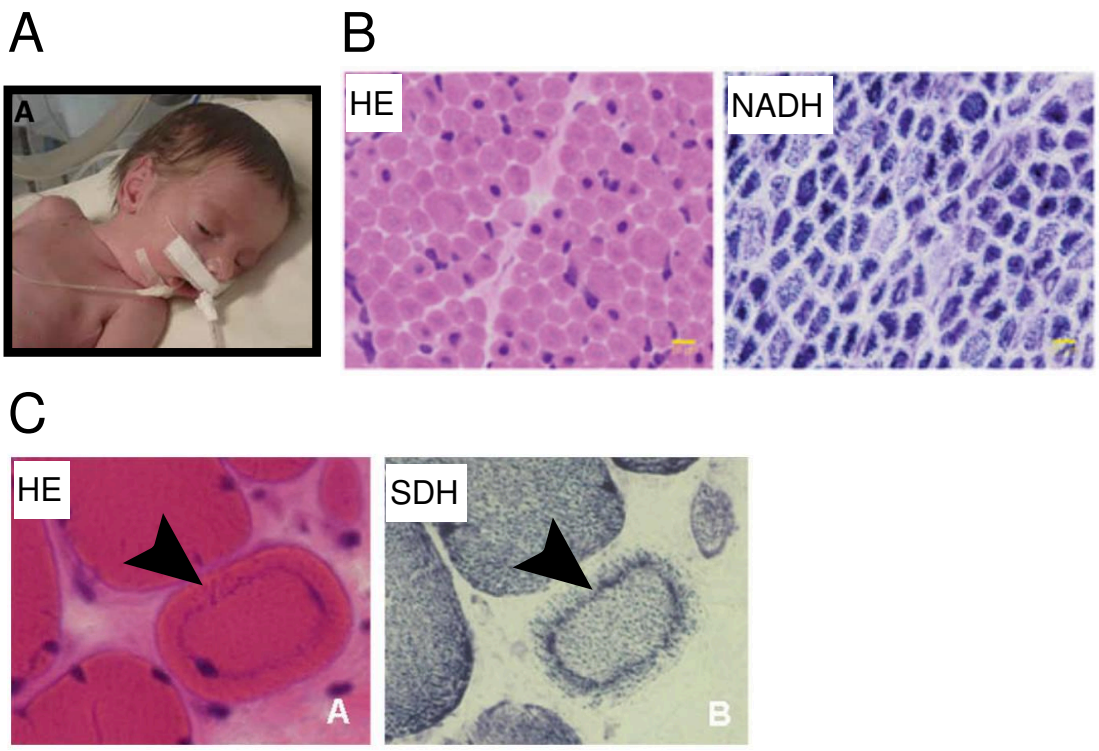

Figure 16. Overview of XLCNM features.

(A) Affected boy. (B) Histology analysis showing centralized nuclei in HE and abnormal accumulation in oxidative NADH staining. (C) Zoomed images, arrowhead points at necklace fibers in HE and oxidative staining (SDH). Adapted from (Romero, 2010; Romero & Bitoun, 2011; Toussaint et al., 2011).

Animal models for XLCNM

Several animal models have been created in order to study XLCNM.

The first animal model generated was a mouse model with a deletion of *Mtm1* exon 4 (*Mtm1*$^{-/y}$) (Buj-Bello et al., 2002). These mice have a reduced lifespan, not surviving more than 7 weeks due to a progressive myopathy that impacts their ability to breath and feed. *Mtm1*$^{-/y}$ mice have reduced body weight and muscle weakness starting at 3 weeks of age. At 6 weeks of age they develop kyphosis and ptosis. Morphological analysis showed myofiber hypotrophy with around 30% of fibers with internalized nuclei. Oxidative staining revealed the presence of necklace fibers, with accumulation of staining at the sarcolemma. Ultrastructural analysis indicated that mitochondria were affected showing an abnormal shape and localization. Abnormal triads were also reported together with a reduction in triad number.

In 2009, using morpholino antisense technology, they generated a zebrafish model with reduced amount of myotubularin protein (Dowling et al., 2009). This reduction lead to impaired motor activity and changes in muscle morphology. At histological level, they observed abnormally

shaped and positioned nuclei and fiber hypotrophy. Electron microscopy analysis pointed to defects in T-tubules and abnormal membranous accumulations in some fibers.

In 2010 it was reported the first case of dogs affected with sporadic cases of XLCNM (Beggs et al., 2010). The myopathy appeared at around 10 weeks of age. Affected dogs exhibited pelvic limb weakness that progressed to an inability to rise or walk. Morphological analyses showed myofiber size variability with necklace fibers when stained with oxidative staining.

A second mouse model was generated carrying the R69C mutation in the *Mtm1* gene (Pierson et al., 2012). This animal has a less severe phenotype than the previously mentioned KO. The presence of the mutation induces exon 4 skipping, leading to a premature termination of myotubularin translation. However, some full-length *Mtm1* mRNA was still detected. In *Mtm1*$^{R39C/y}$ animals, muscle weakness is appearing at 2 months and they survive up to 16,5 months.

3.3. Amphyphisin 2

Since this thesis is not focused on Amphyphisin 2, it will only be briefly introduced.

Amphyphisin 2, also known as Bridging interactor 1 (BIN1) was initially identified as an interactor of the oncogene Myc. The same year the human gene was cloned. There are two different Amphyphisin genes: Amphyphisin 1 which is mainly expressed in neurons and Amphyphisin 2 which is ubiquitously expressed. Similarly to DNM2, BIN has a muscle-specific isoform which contains a specific exon not found in other tissues. There are also cardiac and neuronal specific isoforms.

3.3.1. Autosomal recessive BIN1 related CNM

Recessive or compound heterozygous mutations in *BIN1* cause Autosomal Recessive or Dominant CNM (AR-CNM, MIM#255200 and (Bohm et al., 2014)). The phenotype observed in patients is variable: from moderate to severe. Main features of AR-CNM include: delayed motor milestones, muscle atrophy, weakness, facial diplegia and ophthalmoplegia (Toussaint et al., 2011).

Morphological analysis from muscles of AR-CNM patient reveals several small rounded type I fibers with central nuclei. A special feature from AR-CNM is the clustering of several nuclei in the center of the fiber (Figure 17). Ultrastructure analysis shows accumulation of mitochondria and tubular structures around the nuclei (Cowling, Toussaint, Muller, & Laporte, 2012; Romero, 2010).

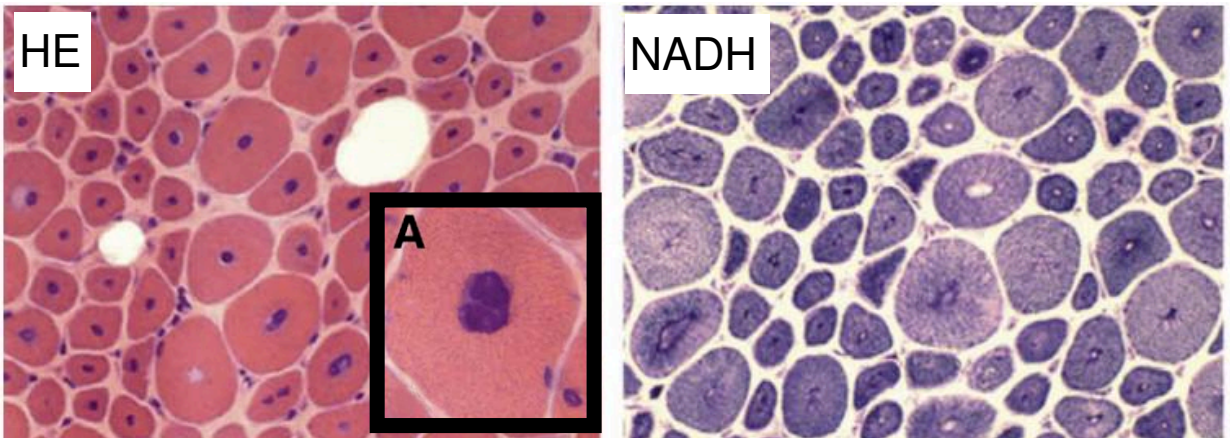

Figure 17. Histological features of BIN1 AR-CNM.

HE staining shows fiber size variability. Zoomed image depicts several nuclei accumulated in the center of the fiber. NADH Oxidative staining presents radial staining. Adapted from (Romero, 2010; Romero & Bitoun, 2011).

3.4. Interactions between MTM1, BIN1 and DNM2

Since MTM1, BIN1 and DNM2 have been related to membrane remodelling and mutations in their genes cause CNM disease, it has been proposed that they are part of the same pathway. Moreover, studies modulating DNM2 and BIN1 levels have showed positive effects in *Mtm1*$^{-/y}$ and *Bin1*$^{-/-}$ mouse models (Cowling et al., 2014; Cowling et al., 2017; Lionello et al., 2019).

In vitro experiments showed that BIN1 can interact with DNM2 by an SH3 – PRD domain interaction from each protein. This was confirmed by transfection experiments where it was showed that BIN1 without SH3 domain was not able to collocalize with DNM2. Interestingly, cotransfection of both proteins promotes membrane tubulation in cells (Nicot et al., 2007).

Bin1$^{-/-}$ mice have a poor life expectancy, all of them dying perinatally. It has been shown that reducing DNM2 by genetic cross rescues lifespan of *Bin1*$^{-/-}$ (Cowling et al., 2017).

So far, there is no data showing a direct interaction between MTM1 and DNM2.

In conclusion, different experiments showing direct interaction between MTM1, BIN1 and DNM2 and the therapeutic effect of modulating this proteins in CNM models with mutations in their partner genes, suggest they are in a common pathway. Membrane tubulation seems to be a common role with all three proteins and it remains to be discovered if additional partners participate in this process.

4. Therapies in centronuclear myopathies

Nowadays, no specific therapy exists to treat CNM although some proof-of-concept have been established and some approaches are being tested in patients.

4.1. Dynamin 2 as a therapeutic target

In 2014 Cowling et al. found that XLCNM patients and mouse model have an increased DNM2 level. They identified a 1.5-fold increase in DNM2 level in *MTM1*-XLCNM affected patients. In *Mtm1*$^{-/y}$ mice, reducing this level by genetic cross rescues the disease phenotypes and lifespan. Interestingly *Dnm2*$^{+/-}$ mice are clinically and physiologically similar to WT littermates (Cowling et al., 2014). This was another evidence suggesting DNM2 in CNM acts in a gain-of-function way, and that bringing its activity/quantity to normal levels has a therapeutic effect.

Recently, Chen et al. proposed that miR199a1, a microRNA involved in muscle development and targets nonmuscle myosin IIA (NM IIA), was the one responsible for XLCNM pathology (X. Chen et al., 2020). miR199a1 is one of the intragenic microRNA found in *DNM2* gene (Aranda, Canfran-Duque, Goedeke, Suarez, & Fernandez-Hernando, 2015). Their study suggests that *miR199a1* is upregulated along with *Dnm2* in *Mtm1*$^{-/y}$ animals. They also showed that a genetic cross of *Mtm1*$^{-/y}$ with *miR199a*$^{-/-}$ mice improved *Mtm1*$^{-/y}$ lifespan by 30%. The main hypothesis was that miR199a-1 targets NM IIA, which is an important protein in *de novo* assembly of contractile myofibrils (Wang, Fan, Sanger, & Sanger, 2018), inhibiting muscle postnatal development. They also pointed at signal transducer and activator of transcription 3 (STAT3) as the main transcription factor causing the upregulation of *Dnm2* and *miR199a1*, since there was an upregulation of STAT3 levels and phosphorylation in *Mtm1*$^{-/y}$ animals (X. Chen et al., 2020).

To establish a translatable therapeutic approach based on DNM2 reduction, antisense oligonucleotides (ASO) targeting *Dnm2* transcript were injected in *Mtm1*$^{-/y}$ mice. ASO are molecules that promote RNA degradation by the RNase H pathway (Seth et al., 2008). ASO treatment efficiently prevented and reverted disease phenotypes associated to MTM1 loss in mice (Tasfaout et al., 2017). The same approach was tested using shRNA-dependent DNM2 reduction showing an improvement of muscle phenotype (Tasfaout et al., 2018). In *Dnm2*$^{R465W/+}$ the same strategy with ASO and shRNA-dependent DNM2 reduction was also tested giving an improvement in muscle function (Buono et al., 2018). Of note, no increase in DNM2 protein has

been described in *Dnm2*$^{R465W/+}$ (Durieux, Vignaud, et al., 2010). In this mice, 50% of total DNM2 level was enough to rescue the muscle phenotypes observed (Buono et al., 2018). Altogether shows DNM2 reduction is a promising therapeutic approach that may be commonly used in different CNM forms.

Other therapeutic proof-of-concept have been established to treat DNM2-related ADCNM. Two different approaches aimed to specifically correct or inactivate the mutated alleles. First, Trochet et al successfully replaced the mutated sequence in *Dnm2*$^{R465W/+}$ mice through spliceosome-mediated RNA trans-splicing (Trochet, Prudhon, Jollet, Lorain, & Bitoun, 2016). Another study, used siRNA technology against sequences of human or murine with R465W. After screening, the best candidate was tested in *Dnm2*$^{R465W/+}$ by AAV-mediated shRNA expression. 3 months post-injection, AAV-injected mice showed an improvement in muscle function (Trochet et al., 2018). Lastly, CRISPR/Cas9 system allowed to correct the mutation in *Dnm2*$^{R465W/+}$ immortalized myoblasts. This approach rescued a defect in endocytosis and autophagy that were previously linked to R465W DNM2 mutation (Rabai et al., 2019).

4.2. Other therapeutic approaches

Other therapeutic approaches have been tested in different animal models, most of them in *Mtm1*$^{-/y}$.

PtdIns are molecules implicated in many processes in the cell and they have a signalling role. MTM1 acts as a PtdIns phosphatase catalysing the conversion from PtdIns(3,5)P2 to PtdIns(5)P and PtdIns(3)P to PtdIns (Section 3.2. Myotubularin 1). Loss of MTM1 has been shown to cause PtdIns(3)P accumulation (Amoasii et al., 2013). Several kinases are implicated in PtdIns(3)P generation such as: class-II kinases (for example PIK3C2) and class-III kinases (such as VPS34 and PIK3C3) (De Craene et al., 2017). Several strategies were explored to see if PtdIns(3)P level normalization had a positive effect in XLCNM animal models. Removal of PIK3C2β had positive effects both in Drosophila melanogaster (Velichkova et al., 2010). Following this study, *Mtm1*$^{-/y}$ mouse with a PIK3C2β muscle-specific deletion was created. Loss of PIK3C2β protein in mice prevented the myopathy and improved survival, body weight and muscle clinical phenotypes. Surprisingly, this was not achieved when removing PIK3C3, which worsened the CNM phenotype(Sabha et al., 2016). Following these studies, several inhibitors were tested in zebrafish *mtm1* model. panPIK3 inhibitors had a positive effect in treated mtm1 larvae at survival, morphological and motor levels (Sabha et al., 2016). This was also observed in *Mtm1*$^{-/y}$ mouse.

However, nowadays there are no specific PIK3C2β inhibitors and PIK3C1 and PIK3C3 inhibition did not improve the observed XLCNM phenotype.

Defects in neuromuscular junction have been reported in XLCNM and ADCNM animal models, suggesting DNM2 and MTM1 may have a role in NMJ regulation (Gibbs et al., 2013; Mercier et al., 2016). Electron microscopy imaging from patient muscle biopsies showed shallow primary synaptic clefs with few vesicles, indicating poor NMJ transmission (Robb et al., 2011). Acetylcholinesterase are enzymes responsible to degrade acetylcholine neurotransmitter. XLCNM and DNM2-related ADNCM patients treated with an acetylcholinesterase inhibitor (pyridostigmine) showed a significant clinical improvement by increasing acetylcholine half-life (Gibbs et al., 2013; Robb et al., 2011).

Other therapeutic approaches have been tested in animal model, such as:

- Myostatin inhibition: myostatin is a skeletal muscle-specific protein that regulates fiber size by binding to different receptors. Myostatin inhibition promotes muscle growth and appears as a potential therapy in CNM where there is a strong muscle atrophy (Koch et al., 2020).
- Autophagy regulation: Autophagy is a process that has been found dysregulated in *Mtm1*$^{-/y}$ and *Dnm2*$^{R465W/+}$ models (Durieux et al., 2012; Gavriilidis et al., 2018). Inhibition of mTOR, which is a negative regulator of autophagy, had positive effects on Mtm1-/y muscle, reducing desmin accumulation and increasing muscle mass (Fetalvero et al., 2013). Since autophagy defects have been reported in models from both MTM1 and DNM2 related CNM, its regulation can be a common therapeutic approach for both forms.

5. Objectives of this thesis

Bottlenecks

First, there is a lack of understanding how DNM2 leads to CNM or CMT diseases and the reason for this tissue specificity. It is not clear if an overlap between this two diseases exists.

There is not a clear idea of how different mutations in DNM2 cause different forms of CNM (with adult or neonatal onsets) and CMT disease. It is not fully understood which mechanisms in skeletal muscle are impaired by those mutations.

In vitro data has shown how artificial mutations in DNM2 protein can modulate its different activities: from GTP hydrolysis to membrane binding and oligomerization. It is not known if there are specific activities of DNM2 which are linked to specific muscle functions.

Reducing DNM2 has shown promising effects in different CNM models but it was not tested in severe DNM2-related CNM.

Aims

- To gain insight in DNM2 mutations and their pathomechanisms in skeletal muscle.
- To better understand how artificial mutations can impact on DNM2 function in healthy and XLCNM-affected muscle.
- To establish a faithful mouse model for severe form of DNM2-related CNM.
- To validate a therapeutic approach in a mouse model for severe form of DNM2-related CNM

Strategies

Different strategies and tools were used including: AAV intramuscular injection, genetically modified mouse models, skeletal muscle characterization techniques as well as basic molecular biology tools.

Part 2
Results

Publication 1: Different in vivo impacts of Dynamin 2 mutations implicated in Charcot-Marie-Tooth neuropathy or centronuclear myopathy

Introduction

Mutations in the ubiquitously expressed DNM2 GTPase cause CMT or CNM. However it remains unclear why there is this tissue specificity and how this mutations impact differentially in skeletal muscle physiology.

In vitro studies suggested CNM mutations are gain-of-function, displaying a higher GTPase activity that is not modulated by lipid binding. On the other hand, CMT mutations have very low GTPase activity and they are defective in lipid binding (see section 2.6. Insights into DNM2 pathogenic mutations).

In this study we overexpressed different DNM2 mutations associated to CNM or CMT using AAV in skeletal muscle of WT mice and compared the phenotypes obtained.

Aims of the study

To understand the different pathomechanisms associated to DNM2 mutations related to CNM or CMT diseases, and their effect in skeletal muscle.

Results

- We observed that overexpressing WT-DNM2 and CNM-DNM2 mutations decreases muscle force and increases the percentage of fibers with internalized and centralized nuclei. Overexpression of both WT and CNM-DNM2 recreate a CNM-like phenotype.
- Overexpression of CMT-DNM2 caused a decrease in muscle force without recapitulating most of CNM features such as internalized nuclei or myofiber atrophy, suggesting another pathomechanism is involved and affects skeletal muscle.
- Ultrastructural analysis of muscles injected with CNM-DNM2 mutants revealed enlarged mitochondria. This phenotype was not present in CMT-DNM2.
- We observed defects in all mutants in T-tubule circularity and NMJ integrity. CMT-DNM2 mutant had the strongest decrease in NMJ count giving a possible explanation of the decreased force observed.

Conclusion

WT and CNM mutants recreate a CNM-like phenotype, suggesting CNM mutations are gain-of-function. The different analysis performed in this study point to different pathomechanisms associated to CNM and CMT-DNM2 mutations affecting skeletal muscle: CNM mutants seem to primarily affect mitochondria in muscle, while CMT mutant seems to impact neuromuscular junction.

Contribution

In this study, I performed all AAV intramuscular injections, histological and ultrastructural analysis and immunofluorescence experiments. I analyzed all the data obtained from force measurements and histology images. I also participated in muscle force measurements.

Suzie Buono cloned and produced all pAAV plasmids with different DNM2 mutations and performed muscle force measurements.

Pascale Koebel produced all the AAV used for intramuscular injections.

This work was supervised by Jocelyn Laporte and Belinda Cowling.

OXFORD

Human Molecular Genetics, 2019, Vol. 28, No. 24 4067–4077

doi: 10.1093/hmg/ddz249
Advance Access Publication Date: 19 October 2019
General Article

GENERAL ARTICLE

Different in vivo impacts of dynamin 2 mutations implicated in Charcot–Marie–Tooth neuropathy or centronuclear myopathy

Xènia Massana Muñoz[1,2,3,4], Suzie Buono[1,2,3,4], Pascale Koebel[1,2,3,4], Jocelyn Laporte[1,2,3,4,*,†] and Belinda S. Cowling[1,2,3,4,5,*,†]

[1]Institut de Génétique et de Biologie Moléculaire et Cellulaire, Illkirch, France [2]Centre National de la Recherche Scientifique, UMR7104, Illkirch, France [3]Institut National de la Santé et de la Recherche Médicale, U1258, Illkirch, France [4]Université de Strasbourg, Illkirch, France [5]Dynacure, 67400 Illkirch, France

*To whom correspondence should be addressed. Email: jocelyn@igbmc.fr or belinda@igbmc.fr

Abstract

Dynamin 2 (DNM2) is a ubiquitously expressed GTPase implicated in many cellular functions such as membrane trafficking and cytoskeleton regulation. Dominant mutations in *DNM2* result in tissue-specific diseases affecting peripheral nerves (Charcot–Marie–Tooth neuropathy, CMT) or skeletal muscles (centronuclear myopathy, CNM). However, the reason for this tissue specificity is unknown, and it remains unclear if these diseases share a common pathomechanism. To compare the disease pathophysiological mechanisms in skeletal muscle, we exogenously expressed wild-type DNM2 (WT-DNM2), the *DNM2*-CMT mutation K562E or *DNM2*-CNM mutations R465W and S619L causing adult and neonatal forms, respectively, by intramuscular adeno-associated virus (AAV) injections. All muscles expressing exogenous WT-DNM2 and CNM or CMT mutations exhibited reduced muscle force. However, only expression of CNM mutations and WT-DNM2 correlated with CNM-like histopathological hallmarks of nuclei centralization and reduced fiber size. The extent of alterations correlated with clinical severity in patients. Ultrastructural and immunofluorescence analyses highlighted defects of the triads, mitochondria and costameres as major causes of the CNM phenotype. Despite the reduction in force upon expression of the *DNM2*-CMT mutation, muscle histology and ultrastructure were almost normal. However, the neuromuscular junction was affected in all *DNM2*-injected muscles, with the *DNM2*-CMT mutation inducing the most severe alterations, potentially explaining the reduction in force observed with this mutant. In conclusion, expression of WT and CNM mutants recreate a CNM-like phenotype, suggesting CNM mutations are gain-of-function. Histological, ultrastructural and molecular analyses pointed to key pathways uncovering the different pathomechanisms involved in centronuclear myopathy or Charcot–Marie–Tooth neuropathy linked to *DNM2* mutations.

Introduction

Dynamins are mechanoenzymes able to fission membrane and interact with cytoskeletons. These large GTPase enzymes are thus involved in many cellular processes ranging from cytoskeleton regulation to membrane remodeling and endocytosis (1–3). Classical dynamins are composed of several functional domains: a GTPase domain at the N-terminal which is able to

†The authors wish it to be known that, in their opinion, the last two authors should be regarded as equal contributors.

Received: September 9, 2019. **Revised:** September 29, 2019. **Accepted:** September 30, 2019

hydrolyze GTP, a middle domain and a GTPase effector domain (GED) forming the stalk and involved in protein oligomerization, a pleckstrin homology (PH) domain binding phosphoinositides and a C-terminal proline-rich domain (PRD) which binds SH3-containing proteins (2,4). Dynamin 2 (DNM2), encoded by the *DNM2* gene is the ubiquitously expressed classical dynamin. Despite its ubiquitous expression, dominant mutations in *DNM2* have been associated to two different diseases affecting different tissues: centronuclear myopathy (CNM), and Charcot–Marie–Tooth peripheral neuropathy (CMT). It is unclear how different mutations in the ubiquitous exons of *DNM2* lead to very different diseases and if the pathomechanisms of these two diseases partially overlap.

CMT neuropathies, or hereditary motor and sensory neuropathies (HMSNs), are a group of inherited peripheral neuropathies. The main symptoms are loss of the sensation of touch, pain, muscle weakness and atrophy (5,6). The classification of CMT into two forms relies on the histological and electrophysiological characteristics: demyelinating forms (CMT1) causing a defect in nerve conduction velocity, and axonal forms (CMT2) in which nerve conduction velocity is near normal (7). Additionally, forms of CMT with intermediate electrophysiology have been described (dominant intermediate, DI-CMT). In 2005, heterozygous mutations in *DNM2* were reported to cause a DI-CMTB intermediate form (OMIM 606482) (8,9). Patients with DI-CMTB caused by the K562E mutation in DNM2 protein display mild reductions in nerve conduction velocity, loss of myelinated axons, rare segmental demyelination and remyelination with onion bulb formation and focal hypermyelination (9).

Heterozygous mutations in *DNM2* have also been associated with autosomal dominant CNM (CNM1; OMIM 160150) (10,11). CNM is a congenital muscle disease characterized by muscle weakness and myofiber atrophy (12,13). Individuals affected by CNM present with facial weakness and delayed motor milestones. At the histological level, muscle fibers present abnormally localized nuclei at the center of the fiber, fiber type I predominance and atypical sarcoplasmic reticulum organization as radial strands (14). The severity of the disease is variable, and cases of *DNM2* related-CNM have been reported with neonatal or adulthood onset (10,15). The most common mutation present in patients with the severe neonatal onset form is the S169L mutation. Severe hypotonia is often present, and patients may require mechanical ventilation (16). In comparison, the R465W mutation is the most common mutation found in patients with adolescent or adult-onset of the disease and is associated with milder disease symptoms (11). To date, a genotype–phenotype correlation has not been identified *in vivo*.

The cellular functions of DNM2 rely on its ability to hydrolyze GTP, oligomerize and bind lipids (1). Lipid binding promotes GTP activity that correlates with oligomerization. Several years ago, the tetrameric structure of the dynamin superfamily was solved which helped in predicting the effect of mutations related to CNM and CMT diseases (17). It was suggested that mutations may not strongly affect protein misfolding, but may rather impair its regulation. *In vitro* studies have shown that the K562E-CMT mutant was not able to bind lipids, in contrast to CNM mutants that were able to bind lipids in an equivalent manner to the WT protein (18). Furthermore, the GTPase basal activity was also differentially altered in R465W- and S619L-CNM versus K562E-CMT mutants: the CNM-related mutants had high GTPase activity irrespective of lipid binding while the CMT mutant displayed low GTPase activity even in the presence of lipids (18,19). In addition, CNM mutants formed abnormally stable oligomers (19). These combined studies suggest that various disease-causing *DNM2* mutations affect different molecular properties of DNM2 function in vitro.

The reason for this tissue specificity and the heterogeneous severity of the different *DNM2* mutations is currently unknown, and it remains unclear if these diseases share a common pathomechanism. To investigate these questions, we selected the most common DNM2-CNM mutations, R465W and S619L causing adult and neonatal forms respectively, and the *DNM2*-CMT mutation K562E, and compare the cellular and physiological effects of their exogenous expression in skeletal muscle *in vivo* in mice.

Results

Exogenous expression of CNM and CMT patient mutations in WT mouse muscle results in reduced muscle force

To investigate the effect of specific DNM2 mutations in skeletal muscle, we selected the *DNM2*-CNM mutations R465W and S619L causing adult and neonatal forms of CNM, respectively (10,15), and the *DNM2*-CMT mutation K562E causing CMT neuropathy (9) (Fig. 1A). The R465W-CNM mutation is located in the middle/stalk domain at the interface between dynamin dimers, whereas the S619L-CNM mutation is located in the PH domain, at the interface between the PH and stalk domains (Fig. 1B). While the K562E-CMT mutation is also in the PH-domain, 3D modeling suggests that this mutation is in a loop potentially contacting lipid membranes. Expression of patient mutations from human cDNA was achieved by performing intramuscular injections using AAV1 into the tibialis anterior (TA) muscles of 3-week-old wild-type mice. At this age, muscles have completed the early stages of postnatal muscle restructuring and growth and from 3–5 weeks undergo muscle hypertrophy to reach near-adult muscle mass, which will reach its maximum at 8 weeks of age (20). Mice were analyzed 2 weeks post injection at 5 weeks of age, and patient mutations were analyzed in comparison to wild-type DNM2 (WT-DNM2) or empty vector (empty) injection. No difference in TA muscle mass relative to body weight was detected between groups (Fig. 1C). Expression of WT-DNM2 resulted in a trend ($P = 0.10$) for reduced muscle force (Fig. 1D), as described previously (21). Expression of the K562E-CMT mutation through AAV1 injection into the muscle resulted in a significant drop in absolute muscle force in contrast to empty control muscles ($P = 0.002$). Expression of the R465W-CNM and S619L-CNM mutations also resulted in a strong reduction in force ($P = 0.0003$ and $P < 0.0001$, respectively). These results were confirmed on specific muscle force, relative to muscle mass (Fig. 1E). Exogenous expression of DNM2 proteins was confirmed for all DNM2-injected muscles by immunoblot analysis and densitometry, relative to empty-injected control (Fig. 1F and G). While WT-DNM2 and CNM-DNM2 mutations result in a 3–10-fold increase in DNM2 expression relative to endogenous levels, expression of the K562E-CMT mutation resulted in a stronger increase (approximately 25-fold) despite administration of equivalent AAV1 titers. The *DNM2* RNA level was then investigated by RT-qPCR, and similarly to the protein level, *DNM2* RNA in muscle was higher for the K562E-CMT mutation (Fig. 1H). Of note, there was an inverse correlation between the levels of DNM2 proteins and the decrease in force, with the K562E-CMT mutant being the most expressed with a mild reduction in muscle force in contrast to the S619L-

CNM mutant being the least expressed with the strongest reduction in force. The R465W-CNM mutant was intermediate in expression and impact on the force. These data are consistent with the fact that the S619L-CNM mutation is observed in patients with the strong myopathic phenotype while the K562E-CMT mutant is observed in patients with a primary neuropathy (11).

In vivo expression of CNM and CMT patient mutations induce distinct histopathological phenotypes

We next determined whether the reduction in muscle force correlated with specific histopathological phenotypes. Transverse TA sections were stained with hematoxylin and eosin (HE) to determine the fiber size and nuclei position within muscle fibers. Indeed, decreased fiber size and centralization of nuclei are main hallmarks of CNM. In contrast to empty injected control muscles, R465W-CNM and S619L-CNM mutations induced strong nuclei mislocalization within the muscle fibers, with the latter mutant exhibiting the most severe alteration (Fig. 2A and B), consistent with this mutation inducing the most severe phenotype in patients (15). Similarly, WT-DNM2 also induced mislocalization of nuclei to a lesser degree, as shown previously (21). Furthermore, exogenous expression of CNM mutations and WT-DNM2 induced reduced fiber size (Fig. 2C), consistent with a CNM histopathological phenotype. These results support a gain-of-function mechanism in CNM. In contrast, nuclei positioning was not significantly altered in K562E-CMT-injected muscles (Fig. 2A and B), despite the strong increase in DNM2 expression (Fig. 1F and G). This correlates with normal muscle histology reported for a DNM2-CMT patient (23). In addition, fiber size was not affected (Fig. 2C). Overall, this suggests a potential loss-of-function mechanism in DNM2-CMT.

To further investigate the histological phenotype, muscles were stained with succinate dehydrogenase (SDH) and nicotinamide adenine dinucleotide (NADH), indicating oxidative activity from the mitochondria and the mitochondrial/reticulum, respectively. WT-DNM2 and DNM2-CNM mutations induced an abnormal staining pattern with accumulation towards the center and periphery of fibers, in both SDH and NADH staining (Fig. 2A). In addition, SDH staining was visibly reduced in the severe S619L-CNM mutation, suggesting a strong defect in mitochondrial function. Interestingly, in K562E-CMT muscles NADH staining was severely affected in contrast to SDH staining which was largely unaffected. Of note, slight sub-sarcolemmal accumulation of NADH was previously seen in the muscle of a DNM2-CMT patient (23). Overall, these results suggest that different pathomechanisms occur in CNM and CMT resulting in distinct histopathological features.

Ultrastructural defects in muscles overexpressing CNM but not CMT *DNM2* mutations

As histological analysis suggested defects in myofiber organization as a potential cause of decreased force for the DNM2-CNM mutants, we next analyzed AAV1-transduced muscles at the ultrastructural level by transmission electron microscopy. Muscles transduced with R465W-CNM exhibited misaligned Z-lines, enlarged abnormally shaped mitochondria with associated membrane accumulations and altered triad structures (Fig. 3A). Triads are comprised of one t-tubule surrounded by two junctional sarcoplasmic reticuli. We investigated if this structure was abnormal in the different muscles (Fig. 3B). Quantitative analysis revealed that the number of identifiable triads per sarcomere was significantly reduced in R465W-DNM2-transduced muscles (Fig. 3C). This correlated with an increased circularity of t-tubules (Fig. 3D). The more severe S619L-CNM mutation exhibited the strongest increase in t-tubule circularity; however, one striking difference was the enlarged mitochondrial structures with the internal cristae network clearly perturbed (Fig. 3A), correlating with the reduced SDH staining observed (Fig. 2A). Overexpression of WT-DNM2 also induced some minor mitochondrial abnormalities, with misaligned Z-lines, altered triad number per sarcomere and increased circularity of t-tubules (Fig. 3A–D). These combined results suggest DNM2-CNM mutations induce CNM-like clinical, histological and ultrastructural phenotypes when overexpressed *in vivo* in WT muscles, and these phenotypes correlate with the CNM severity observed in patients.

In contrast, K562E-CMT expression did not induce any obvious ultrastructural defects apart from an increase in t-tubule circularity (Fig. 3A, B and D), consistent with the normal histological phenotype (Fig. 2A), and patient muscle biopsies (23).

DNM2-CNM mutants are linked to defects in t-tubule and costamere markers

As ultrastructural analysis suggested t-tubule and triad defects in muscles expressing *DNM2*-CNM mutants, we next performed immunofluorescence analysis of dihydropyridine receptor alpha (DHPRalpha), a marker of t-tubules, on longitudinal sections. Expression of WT-DNM2 and K562E-CMT led to a DHPRalpha staining comparable to empty control (Fig. 4A). In contrast, both R465W-CNM and S619L-CNM displayed disorganized DHPRalpha staining patterns. This defect confirmed the observation of altered triad structures by electron microscopy and aligned with the severity of the CNM mutations, with muscle expressing the S619L-CNM mutant most severely affected.

To further investigate the molecular mechanism that could explain the defects in muscle force observed with *DNM2*-CNM mutants, we focused on DNM2 and known functional partners. DNM2 localization in the sarcomere was previously reported to be associated to Z-lines (21). We investigated the localization of DNM2 on longitudinal muscle sections using an antibody recognizing both exogenous and endogenous DNM2 proteins. AAV1-empty-injected muscles displayed striated transverse staining on longitudinal sections (Fig. 4A) consistent with Z-line localization as seen previously (21). DNM2 appeared to be mislocalized in muscles expressing both CNM mutants. In particular, the more severe S619L mutation induced areas of longitudinal staining (Fig. 4A, arrow). In contrast, K562E-CMT exhibited a similar DNM2 localization to empty control muscles (Fig. 4A).

DNM2 plays an important role in clathrin-mediated endocytosis (2,24) and together with clathrin participates in the correct attachment of the muscle fibers to the extracellular matrix (25). Immunolabeling of clathrin heavy chain (CHC) was performed on longitudinal muscle sections from TA muscles. In AAV1-empty injected muscles, CHC exhibited the expected transverse staining pattern reminiscent of costameres (Fig. 4B). Muscles transduced with K562E-CMT exhibited a transverse staining pattern indistinguishable from control sections. However, muscles transduced with R465W-CNM and S619L-CNM showed a more disorganized staining pattern for CHC. Additional peri-nuclear staining in WT-DNM2 and S619L-CNM transduced muscles was also observed. Caveolin-3 is an important regulator of clathrin-independent endocytosis and participates in t-tubule biogenesis. In adult muscle, caveolin-3 is localized at the sarcolemma. We

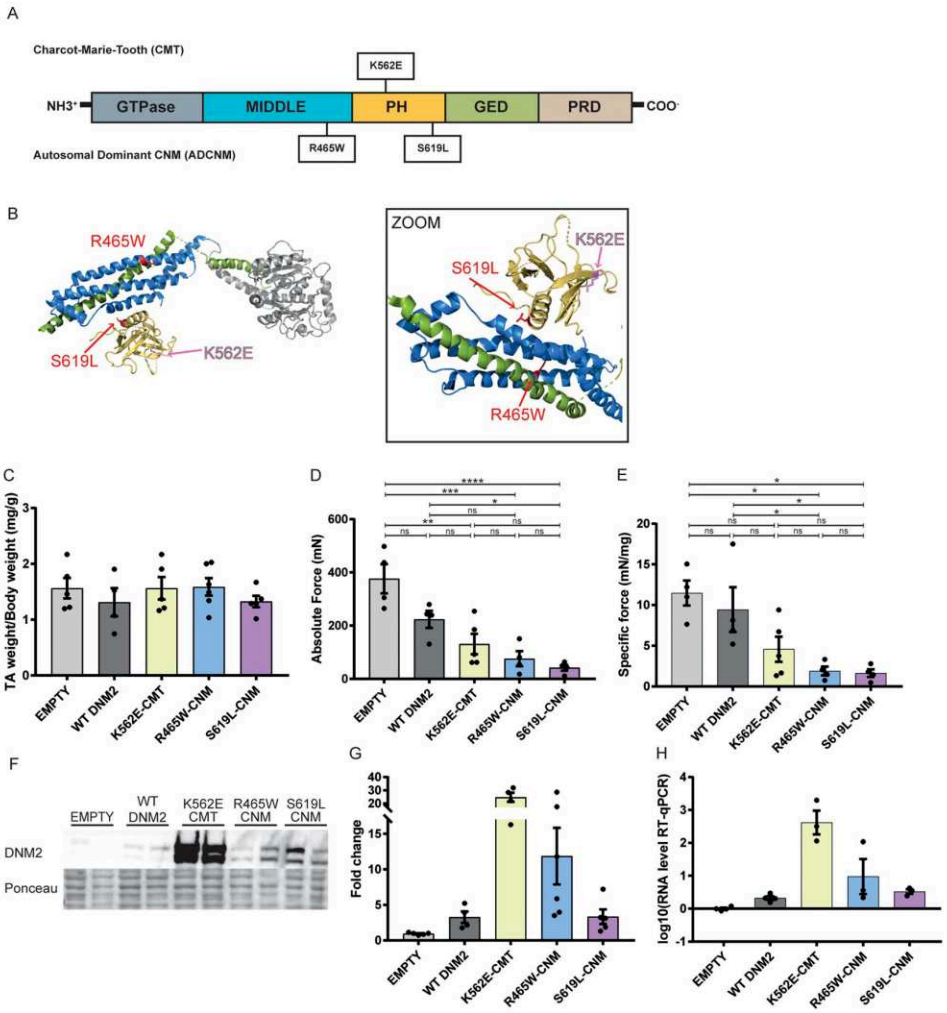

Figure 1. AAV-mediated expression of CNM and CMT patient mutations in muscle results in reduced muscle force. (A) Domain organization of DNM2 and localization of the mutations studied in this work. The middle and GED domains form the structural stalk domain. (B) Mutations were visualized on equivalent amino acid of DNM3 published structure (4), showing CNM mutations (in red) and CMT mutation (pink) used in this study. (C) Ratio of TA muscle weight and total body weight ($n = 4$–6 muscles). (D) Absolute maximal muscle force measured 2 weeks after injection ($n = 4$–6 muscles). (E) Specific force corresponding to the absolute maximal muscle force divided by muscle weight ($n = 4$–6 muscles). (F) Skeletal muscle lysates immunoblotted for DNM2 and stained with Ponceau solution to determine total protein. (G) Relative expression of total DNM2 signals revealed by an anti-DNM2 antibody and standardized to Ponceau staining. Expression is represented as fold change in contrast to empty-AAV injected muscles ($n = 4$–6 muscles). (H) Transcript expression of the different DNM2 constructs quantified by RT-qPCR after DNAse treatment. Total DNM2 level was detected using primers recognizing *DNM2* and *Dnm2* and normalized to *Rpl27* expression. Statistical analysis: Shapiro–Wilk normality test and Brown–Forsythe test for equal variances, followed by one-way ANOVA or Kruskal–Wallis ANOVA, followed by multiple comparisons test with Tukey–Kramer or Dunn's correction; $^{***}P < 0.0001$; $^{*}P < 0.05$; ns not significant. P values > 0.40 are not displayed in the graph.

did not detect obvious changes in caveolin-3 distribution in any groups (Fig. 4B).

Dysferlin is another muscle protein implicated in t-tubule biogenesis, membrane trafficking and membrane repair. While dysferlin localization appeared normal upon expression of the K562E-CMT mutant, expression of WT-DNM2 or DNM2-CNM mutants induced an abnormal accumulation of dysferlin around the centralized nuclei (Supplementary Material, Fig. S1A).

Overall, the structural defects induced by *DNM2*-CNM mutants parallel disorganization of t-tubule and costamere markers and are probably the cause of decreased muscle force. Conversely, expression of the K562E-CMT mutant did not have a strong impact on muscle fiber organization, raising the question of the molecular mechanism for the decrease in muscle force observed.

DNM2 overexpression leads to neuromuscular junction defects

Muscle force generation depends on muscle innervation through the neuromuscular junction (NMJ) formed by contact between a motor neuron and a muscle fiber. Neuromuscular junctions were

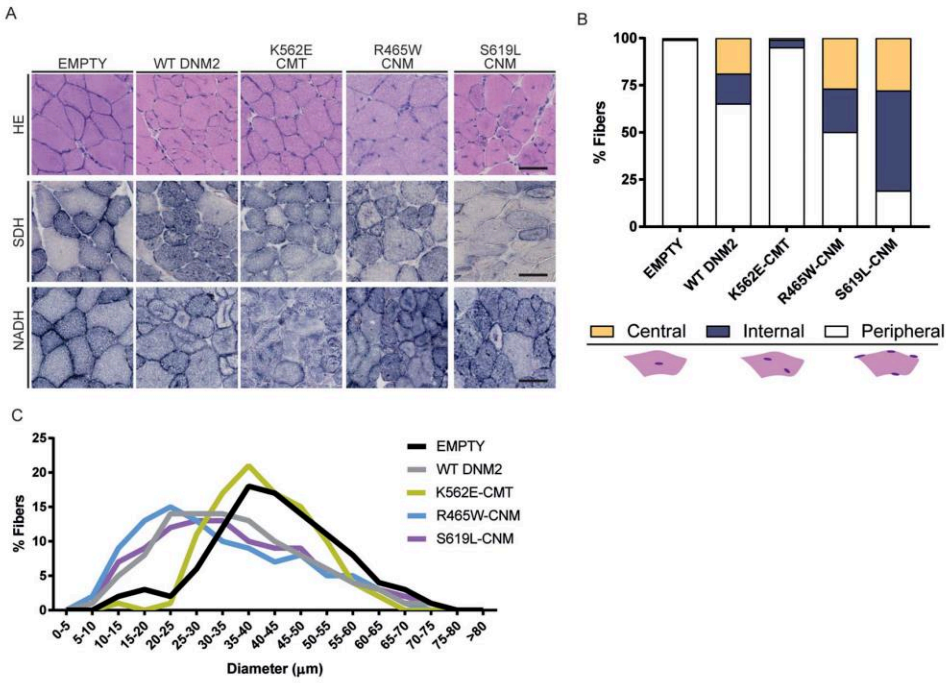

Figure 2. Overexpression of CNM and CMT patient mutations induce distinct histopathological phenotypes. (A) Transverse 8 µm TA sections from AAV-transduced muscles stained with hematoxylin and eosin (HE), SDH or reduced NADH. Scale bar = 50 µm. (B) Percentage of myofibers with central, internal or peripheral nuclei (n = 400–500 fibers × 4–6 muscles). (C) Transverse 8 µm TA sections were analyzed for fiber diameter. Fiber diameter (minimum Feret's diameter) is grouped into 5 µm intervals and represented as the percentage of the total fibers in each group (n = 400–500 fibers × 4–6 mice).

visualized with fluorescently labeled alpha-bungarotoxin which stains nicotinic acetylcholine receptors located in NMJs. In contrast to AAV1-empty control muscles, all muscles injected with the different DNM2 constructs exhibited a strong alteration in NMJ shape that appeared more elongated (Fig. 5A). We calculated the circularity for different NMJs present in transduced muscles. In particular, there was a tendency for reduced circularity, in contrast to control muscles, in all NMJ from the different constructs, except for CNM-R465W (Fig. 5B). In addition, NMJ fragmentation was highly increased in all the analyzed constructs in contrast to NMJ from empty-injected muscles (Fig. 5C). However, the surface of NMJs was similar between DNM2 constructs and AAV1-empty control (Fig. 5D). Moreover, the number of NMJs in the analyzed muscles was strongly reduced in K562E-CMT-expressing muscles (Fig. 5E). The largest reduction was observed in K562E-CMT-injected muscles. Overall, NMJ defects correlated with decreased muscle force with all DNM2 constructs including WT-DNM2. The strongest defects observed with the CMT mutant could explain in part the reduction in force observed in injected muscles, despite the lack of significant muscle histopathological features.

Discussion

While DNM2 is ubiquitously expressed, different dominant point mutations in *DNM2* result in two tissue-specific disorders. It was unclear however if these diseases arise from a common pathomechanism. In this study, we investigated the molecular, cellular and physiological alterations induced by *DNM2* mutations in two distinct human diseases: CNM (neonatal and adult onset forms) and Charcot–Marie–Tooth neuropathy, with a focus on skeletal muscle. Moreover, the basis of the difference in severity between the mutations leading to CNM was not previously defined.

Differential functional impact of CNM and CMT mutations

CNM patients present with a myopathic phenotype varying from neonatal to adult onset, with a wide range of severity. Most often symptoms are limited to skeletal muscles. Conversely, CMT neuropathy patients exhibit predominantly neuronal symptoms. Bitoun *et al.* reported no obvious muscle defects in a biopsy of a CMT patient with the K559del mutation in the PH domain (23). However, another patient with a *DNM2* mutation exhibiting both CNM and CMT-like features has been reported (26). This patient was carrying a mutation in the middle/stalk domain (G359D), where typically CNM mutations are located and close to another mutation already reported in CNM. Histological analysis of the patient's muscle revealed variation in fiber size and fiber atrophy, and a sural nerve biopsy showed a severe loss of large myelinating fibers (26). Nevertheless, the effect of CMT-related mutations on skeletal muscles has not been extensively explored.

Muscle weakness is common to both CNM and CMT patient presentation (11). Here, we showed that the exogenous expression of CNM and CMT *DNM2* mutations led to muscle force decrease in mice. However, expression of both CNM mutations led to muscle structural alterations mimicking the histopathological hallmarks seen in CNM patients with hypotrophic myofibers with mislocalized nuclei, central accumulation of

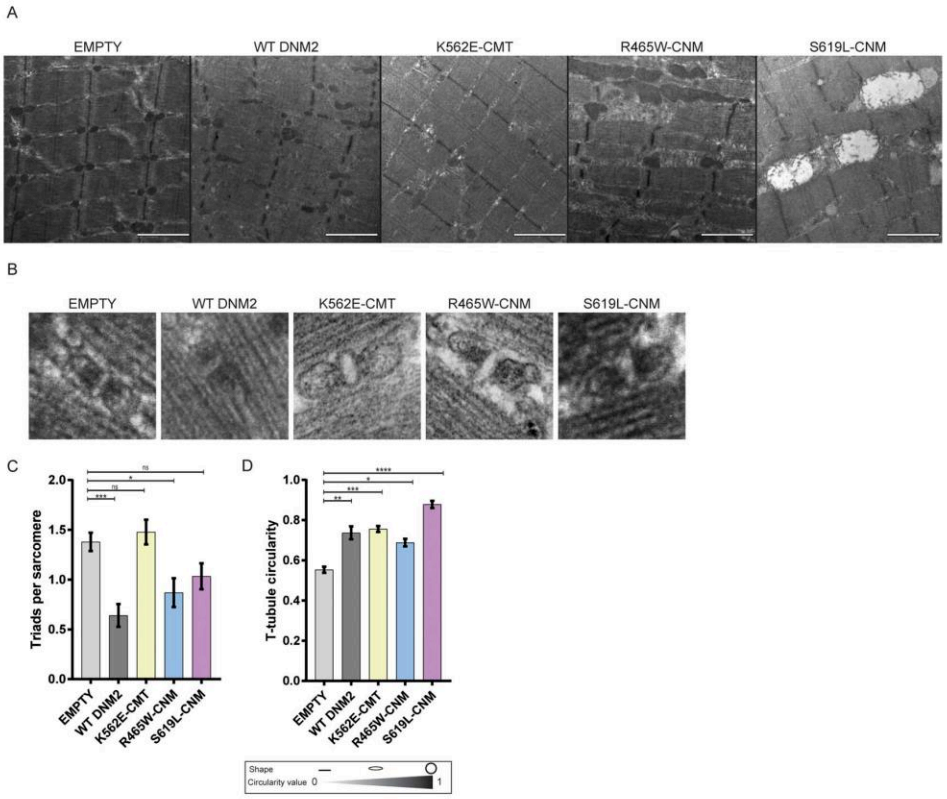

Figure 3. *In vivo* expression of CNM mutations results in ultrastructural defects. (A) AAV-transduced TA muscles imaged by transmission electron microscopy. Images show an overview of muscle sarcomeric ultrastructure, mitochondrial shape and triad structure. Scale bar = 2 µm. (B) Zoomed image in triad structure. (C) Graph representing the number of triads per sarcomere (mean ± SEM) (n = 10–30 sarcomeres × 2 mice per groups). (D) Circularity of t-tubule using 1 = perfect circle and 0 = straight line (mean ± SEM) (n = 10–30 t-tubules per group). Statistical analysis: Shapiro–Wilk normality test and Brown–Forsythe test for equal variances, followed by Kruskal–Wallis ANOVA, and multiple comparisons test with Dunn's correction; $^{***}P < 0.0001$; $^{*}P < 0.05$; ns not significant. P values > 0.40 are not displayed in the graph.

oxidative activity, decreased triads number and abnormal t-tubule shape, while expressing a CMT mutant left the muscle structure almost intact.

Importantly, overexpression of WT-DNM2 also caused the CNM phenotype with the same histological and structural findings, as shown previously (21), suggesting increasing DNM2 may be pathogenic for skeletal muscles. This is supported by data suggesting overexpression of DNM2 may be in part responsible for the CNM phenotype observed in the X-linked form of the disease due to mutations in the lipid phosphatase MTM1. Indeed, DNM2 protein level was found increased in muscle from mice and patients lacking MTM1, and normalization or decrease of DNM2 through transgenesis, shRNA or antisense oligonucleotides prevented and reverted the X-linked CNM in mice (27–30). DNM2 reduction with similar approaches also ameliorated the phenotypes of the transgenic mouse mice *Dnm2*$^{R465W/+}$ (31), supporting that reduction of DNM2 overall activity counteracts DNM2-CNM mutation effects. Of note, the heterozygous KO *Dnm2*$^{+/-}$ mice do not develop CNM suggesting that CNM mutations are not loss-of-function (27).

Most mutations causing CNM are localized at the interface between the middle/stalk domain and the PH domain (4,32). This interface was proposed to have an autoinhibitory effect on the PH domain insertion into the membrane and consequently dynamin oligomerization and GTPase activity. As CNM mutations located there disrupt potential hydrogen bounds between the middle/stalk and PH domains, it is expected that CNM mutations alleviate the autoinhibition, leading to DNM2 'hyperactivation'. In agreement, in vitro studies showed that CNM mutations induce a higher GTPase hydrolysis activity of DNM2 regardless of their binding to lipids, combined with increased oligomer stability (18,19). Several studies in cells also suggested CNM mutations increase the oligomeric state and stability of DNM2 (33,34), and endocytosis of transferrin was found increased in murine muscle cells with the R465W mutation and in CNM patient myoblasts with R465W or R369Q mutations (35).

Altogether, our present in vivo data combined to the literature support that the DNM2-CNM mutations are gain-of-function.

Conversely, expressing the K562E-CMT mutant in WT muscles did not cause any of the CNM histopathological hallmarks with the exception of an increase in t-tubule circularity. In particular, myofiber size and nuclei position were normal (Fig. 2A–C), despite the high level of protein expression (Fig. 1F and G). Our data suggest that DNM2-CMT mutations are not gain-of-function. Most mutations causing CMT are localized in the loops

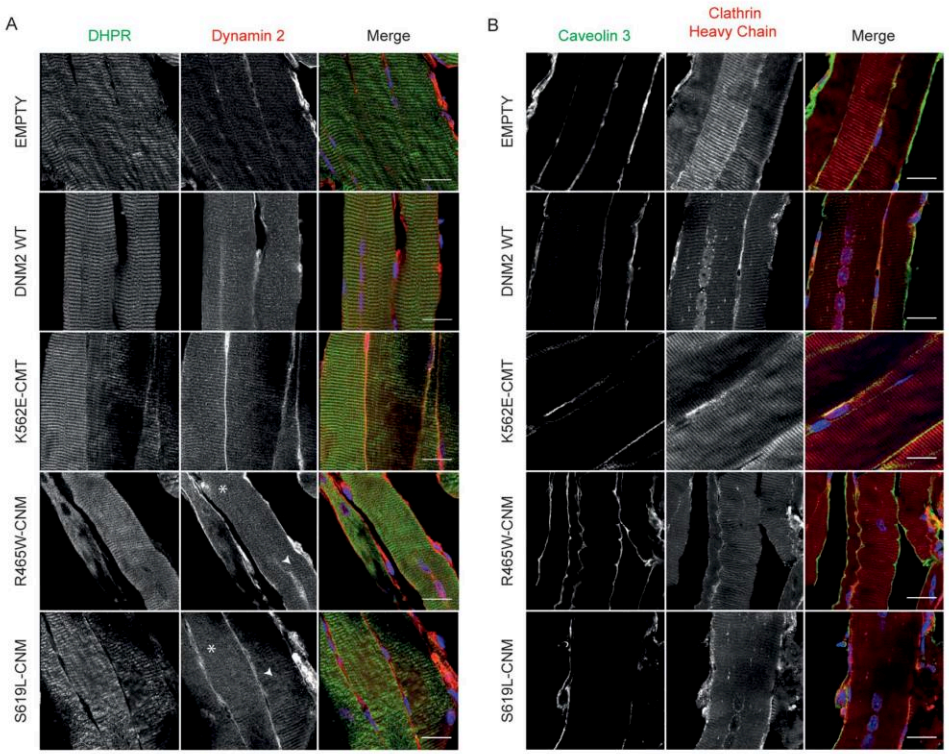

Figure 4. Overexpression of DNM2-WT and DNM2-CNM mutants disrupt muscle organization. (A) Longitudinal 8 µm or TA sections were stained by immunofluorescence using antibodies against DHPR and DNM2. Scale bar = 20 µm. (B) Longitudinal 8 µm TA sections were stained by immunofluorescence using antibodies to detect caveolin-3 and CHC. Images displayed are projections of confocal stacks. Scale bar = 20 µm.

of the PH domain implicated in membrane recognition, and in vitro studies showed CMT mutants exhibit a strong reduction in lipid binding (18). The pathogenesis of CMT and CNM mutations has previously been investigated in cellular systems modeling peripheral nerves. Decreased myelination was observed in cultured motor neurons from dorsal root ganglia explants only upon expression of CMT mutants but not CNM mutants (36). In the same cellular system, DNM2-CMT mutants impaired clathrin-mediated endocytosis in motor neurons and Schwann cells, whereas CNM mutants had no effect. Furthermore, overexpression of CNM but not CMT mutations could rescue endocytosis defects observed in Schwann cells from *Dnm2*-deficient mice (36). In vivo, *Dnm2* deletion in Schwann cells impaired myelination and deletion in adult mice caused demyelination (37), reminiscent of histopathology seen in CMT patients and suggesting that the disease is due to decrease of DNM2 in peripheral nerves. In addition, our finding that AAV1 transduction of the K562E-CMT mutant leads to a significant increase in its RNA expression can be explained if this mutant decreases the overall activity of DNM2, in light of recent data showing that decreasing DNM2 promotes adenovirus replication probably by increasing the release of virus from endosomes (22). Taken together, DNM2-CMT mutants are most probably loss-of-function.

Overall, our in vivo data support that DNM2-CNM mutations are gain-of-function while DNM2-CMT mutants are loss-of-function, suggesting different pathomechanisms are involved in the two diseases.

Different pathomechanisms for DNM2 mutations related to CNM and CMT

The exogenous expression of different DNM2 mutants in muscle revealed marked differences in the structure and organization of the neuromuscular system that may underlay the common decrease in muscle force. In particular, expression of the K562E-CMT mutant is not associated to strong structural defects of the myofibers but correlated with pronounced structural defects of the neuromuscular junctions. For DNM2-CNM mutants, alterations of both NMJ and myofibers potentially cause muscle weakness; obviously, the strong abnormalities in triads, mitochondria and the sarcomere structure should at least partially decrease muscle force. Overall, we propose that muscle weakness in CNM is induced largely from alteration of the myofiber structure while muscle weakness in CMT mainly comes from NMJ defects.

While our AAV serotype 1 injections were intramuscular, we cannot exclude the possibility that AAV1 underwent retrograde transport resulting in expression of DNM2 constructs in motorneurons, as previously found with AAV serotype 2 (38). Primary muscle defects have been shown to induce NMJ defects. For example, muscle-specific deletion of *Dnm2* induced structural defects of myofibers with metabolic alterations, together with irregular NMJs and peripheral nerve damage (39). Also, overexpression of uncoupling protein 1 (UCP1) in skeletal muscle led to defects in mitochondrial function resulting in secondary NMJ

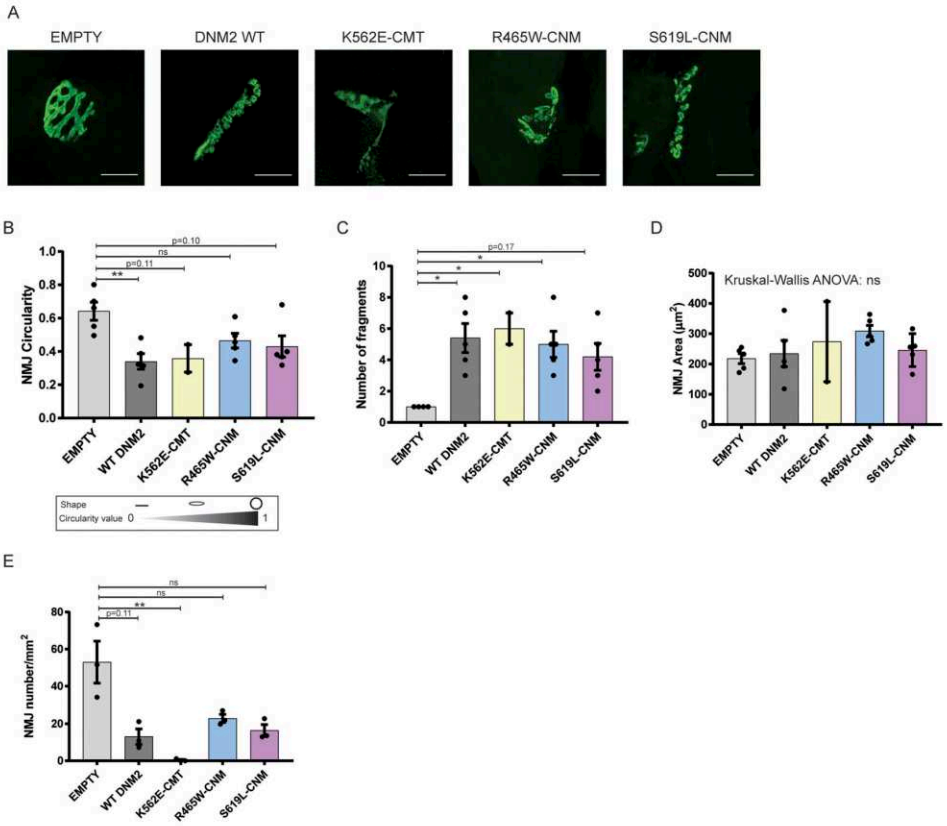

Figure 5. Neuromuscular junction defects due to the overexpression of DNM2-WT, CMT and CNM mutants. (A) Images of representative neuromuscular junctions labeled with using fluorescent alpha-bungarotoxin. Scale bar = 20 µm. (B) NMJ shape; circularity was calculated (value of 1 indicates a perfect circle, as the value approaches 0 it indicates an increasingly elongated shape) ($n = 1$–3 NMJ from 2 mice). (C) Number of fragments per NMJ ($n = 1$–3 NMJ $\times$ 2 mice). (D) NMJ Area ($n = 1$–3 NMJ $\times$ 2 mice). (E) Graph representing the number of NMJs per muscle area calculated using different images of longitudinal 8 µm TA muscle sections. Kruskal–Wallis ANOVA, followed by multiple comparisons test with Dunn's correction; $^{***}P < 0.0001$; $^{*}P < 0.05$; ns not significant. P values > 0.40 are not displayed in the graph.

defects and degeneration of motor neurons (40). Bragato *et al.* overexpressed human DNM2 constructs in zebrafish, harboring different mutations than the one tested here (the R522H CNM mutant and the G537C CMT mutant) and also found that they both impacted on the structure of NMJ (41). Conversely, the CMT mutant also induced a high number of central nuclei in the myofibers. This discrepancy may be due to the different animal models used or the fact that there are two orthologs of DNM2 in zebrafish.

Both CNM mutants tested in this study induced mitochondrial shape defects (Fig. 3A). As mice with muscle-specific deletion of *Dnm2* display abnormal mitochondria as well as increased NMJ area (39), the balance in DNM2 activity is potentially important for mitochondria homeostasis. Contradictory reports were recently published on a direct role of DNM2 in mitochondria fission (42, 43); whether mitochondria structural defects we observed, especially with the S619L-CNM mutant, are caused by a direct role of DNM2 on mitochondria dynamics thus remains unclear. When muscles were injected with K562E-CMT mutant, no obvious disruption in mitochondria was observed, however NMJs were clearly affected (Figs. 3 and 5). DNM2 may affect mitochondria or be directly involved in the maintenance of the NMJ.

The S619L-CNM expression induced a more severe muscle phenotype than R465W-CNM, in alignment with the severity and disease age of onset observed in patients with these mutations. Our in vivo models thus recapitulate faithfully the genotype–phenotype correlation seen in patients, supporting that the increased severity and earlier onset linked to the S619L mutation is not due to genetic modifiers or environmental differences with patients harboring other mutations but is an intrinsic property of the mutated residue.

Conclusions

In this study using AAV1-mediated gene expression, we established *in vivo* models to study DNM2 mutations linked to CNM and CMT in the neuromuscular system. Expression of WT and CNM mutants recreated a CNM-like phenotype, suggesting CNM mutations are gain-of-function. Expression of the CMT mutant in muscle did not lead to severe structural or ultrastructural defects despite similar reduction in muscle force, suggesting that different pathomechanisms are involved in the two diseases.

Materials and Methods

Materials

pAAV plasmids were generated as described before (21) containing full-length human isoform DNM2 cDNA (NCBI Reference Sequence: NM_001005360.2). The different mutations were introduced by primer-directed PCR mutagenesis. All constructs were verified by sequencing.

Primary antibodies used were anti-DNM2 (dilution used 1/100, 2680, described in (21)), anti-DHPR (Santa Cruz Biotechnology; sc-8160; dilution used 1/50), anti-CAV3 (Santa Cruz Biotechnology; sc-5310; dilution used 1/50) and anti-CHC (Abcam; ab21679; dilution used 1/100). Secondary antibodies used were donkey anti-goat Alexa-488, donkey anti-rabbit Alexa-594, goat anti-mouse Alexa-488 and goat anti-rabbit Alexa-594 (Life Technologies). The dilution used for all secondary antibodies was 1/250. To detect neuromuscular junction, we used alpha-Bungarotoxin CF®488A Conjugate (Biotium).

Production and purification of AAV

Recombinant adeno-associated virus serotype 1 were generated by a triple transfection of HEK293T-derived cell line with the expression plasmid pAAV-DNM2 and the auxiliary plasmids pHelper (Agilent) and pXR1 for AAV serotype 1 (UNC Vector Core). DNM2 wild-type and mutated forms were cloned under the control of the CMV promoter in the pAAV-MCS (Agilent). AAV vectors were harvested 48 h after transfection from cell lysate treated with 100 U/ml Benzonase (Merck). AAV1 were purified by iodixanol gradient ultracentrifugation (OptiPrep™, Axis Shield) followed by dialysis and concentration against Dulbecco's PBS containing 0.5 mM $MgCl_2$ using centrifugal filters (Amicon Ultra-15 Centrifugal Filter Device 100 K). Viral titers were determined by Q-PCR using the LightCycler480 SYBR Green I Master (Roche) and primers targeting the CMV enhancer sequence. Viruses were stored at −80°C until use.

Animals

WT 129/SvPAS mice were handled according to the French and European legislation on animal care and experimentation. Protocols were approved by the institutional Ethics Committee. Protocol No. APAFIS #5640-2016061019332648 v4 was granted to perform animal experiments. Mice were kept on a 12 h light/12 h dark cycle in ventilated cages and given free access to food. All mice analyzed in this study were male. Mice were numbered and after AAV1-injection muscles were analyzed blindly.

Intramuscular injection of AAV1

Three-week-old male WT 129/SvPAS were weighed and anesthetized with a solution of ketamine 20 mg/ml and xylazine 0.4% at 5 µl/g of body weight. The solution was administrated by intraperitoneal injection. Both TA muscles were injected with 20 µl of 5×10^{11} vg/ml AAV1 encoding DNM2 (either wild type-DNM2 or including K562E, R465W or S619L mutations), and the same dose of AAV1 containing an empty AAV construct was injected in the contralateral TA as a control.

Muscle contractile properties

Muscle force measurements were evaluated by measuring *in situ* muscle contraction in response to nerve stimulation using the Complete 1300A Mouse Test System (Aurora Scientific) as described previously (44). Animals were anesthetized (intraperitoneal injection of pentobarbital sodium, 50 mg/kg) and maintained under deep anesthesia. The distal tendon of the TA was detached and tied to an isometric transducer. The sciatic nerve was stimulated, and response to stimulation (pulse frequency of 1–125 Hz) was recorded to measure absolute maximal force. To determine specific maximal force, TA muscles were dissected and weighed. Muscles were then stored for further analysis.

Protein extraction and western blot

TA muscle cryosections were lysed in RIPA buffer supplemented with PMSF 1 mM and complete mini EDTA-free protease inhibitor cocktail (Roche Diagnostic). Protein concentrations were determined with the Bio-Rad Protein Assay Kit. Samples were denatured at 95°C for 5 min. Then, 15 µg of protein in 5× Lane Marker Reducing Buffer (Thermo Fisher Scientific) were separated in 10% SDS-PAGE gel and transferred on nitrocellulose membrane for 7 min at 2.5 A using a Trans-Blot Turbo Transfer System (Bio-Rad). Total protein was determined by Ponceau S staining. Membranes were blocked for 1 h in TBS containing 5% non-fat dry milk and 0.1% Tween20 before an incubation overnight with primary rabbit polyclonal antibodies against DNM2 2865 (1:500, described in (21)) diluted in blocking buffer containing 5% milk. The secondary antibody coupled to horseradish peroxidase was goat anti-rabbit (Jackson Immunoresearch) (1:10 000) and was incubated for 2 h. Nitrocellulose membranes were visualized in Amersham Imager 600 (GE Healthcare Life Sciences). Images from full western blot membranes are shown in Supplementary Material, Fig. S1B.

RNA extraction and qRT-PCR

Total RNA was isolated from muscle tissue using with TRI Reagent (Molecular Research Center). To eliminate possible detection of DNA, DNAseI treatment was applied to the samples according to the user guide provided (Thermo Fischer Scientific). cDNA synthesis was performed using Superscript IV Reverse Transcriptase (Thermo Fisher Scientific). Quantitative PCR was done using cDNA amplified with SYBR Green Master Mix I (Roche) together with 0.1 µM forward and reverse interexonic primers. Amplicons were analyzed with a LightCycler® 480 (Roche). Primers used were *DNM2* and *Dnm2*: (F) TGATCCTGCAGTTCATCAGC, (R) ATGACACCGATGGTCCGTAG, *Rpl27* (45) (F) AAGCCGTCATCGTGAAGAACA, (R) CTTGATCTTGGATCGGCTTGGC.

Muscle histology

TA muscles were snap-frozen in liquid nitrogen-cooled isopentane and stored at −80°C for hematoxylin and eosin (H&E), SDH or reduced NADH histology analysis. Transversal cryosections (8 µm) were prepared and stained. Entire muscle sections were imaged with the Hamamatsu 322 NanoZoomer 2HT slide scanner. The percentage of TA muscle fibers with mislocalized (centralized or internalized) nuclei was counted using the cell counter plugin in Fiji image analysis software. The fiber area was measured using the Fiji software. A total of 400–500 fibers from four to six mice were analyzed per group.

Electron microscopy

Transmission electron microscopy (TEM) was carried out on TA muscles fixed in 2.5% paraformaldehyde, 2.5% glutaraldehyde and 50 mM $CaCl_2$ in 0.1 M cacodylate buffer (pH 7.4) as described

previously (28). Briefly, sections of 70 nm were obtained from TA muscles and stained with uranyl acetate and lead citrate. They were observed by TEM (Morgagni 268D, FEI). The ratio of triads to sarcomere was calculated by dividing the number of triads identified by the number of sarcomeres present in the field. A total of 10–15 sarcomeres from two mice were analyzed per group.

Immunostaining of muscle transversal sections

For longitudinal immunostaining, TA muscles were fixed in PFA 4% for 24 h, then transferred to 30% sucrose for 12 h and stored at 4°C, as described previously (28). Isopentane-frozen muscles were used to perform transversal stainings. Transversal or longitudinal (8 µm) cryosections of TA were stained with primary antibodies and secondary antibodies listed in Materials and Methods section. Images were taken in the same Leica SP8-UV confocal microscope (Leica Microsystems).

Statistical analysis

For this study, $n = 4$–5 mice were used. Bar charts show mean ± SEM. All graphs were made with GraphPad Prism software. Normality was tested using the Shapiro–Wilk normality test for each condition to determine if parametric tests were applicable. Differences between groups were analyzed by *t* test or one-way ANOVA followed by post hoc Tukey's or Dunn's multiple-comparison test.

Supplementary Material

Supplementary Material is available at HMG online.

Funding

Institut National de la Santé et de la Recherche Médicale, Centre National de la Recherche Scientifique, Strasbourg University; French State fund managed by the Agence Nationale de la Recherche under the frame program Investissements d'Avenir (ANR-10-IDEX-0002-02, ANR-10-LABX-0030-INRT) and Association Française Contre les Myopathies (AFM 21267-RESCUE). X.M.M. is an Institut de Génétique et de Biologie Moléculaire et Cellulaire International PhD Programme fellow supported by LabEx INRT funds.

Authors' contribution

B.S.C. and J.L. designed and supervised the research; X.M.M. and S.B. performed the research; X.M.M., B.S.C. and J.L. analyzed the data; X.M.M., B.S.C. and J.L. wrote the manuscript.

Acknowledgements

We would like to thank Raquel Gómez Oca and Nadia Messaddeq for excellent technical assistance and Pascal Kessler for building the macro to analyze histological data. We thank the imaging facility (photonic and electron microscopy), animal house and histology platform of the IGBMC for support.

Conflict of interest statement. B.S.C. and J.L. are cofounders of Dynacure. B.S.C. and S.B. are currently employed by Dynacure, and J.L. is a scientific advisor.

References

1. Antonny, B., Burd, C., De Camilli, P., Chen, E., Daumke, O., Faelber, K., Ford, M., Frolov, V.A., Frost, A., Hinshaw, J.E. *et al.* (2016) Membrane fission by dynamin: what we know and what we need to know. *EMBO J*, **35**, 2270–2284.
2. Ferguson, S.M. and De Camilli, P. (2012) Dynamin, a membrane-remodelling GTPase. *Nat. Rev. Mol. Cell. Biol.*, **13**, 75–88.
3. Praefcke, G.J. and McMahon, H.T. (2004) The dynamin superfamily: universal membrane tubulation and fission molecules? *Nat. Rev. Mol. Cell. Biol.*, **5**, 133–147.
4. Faelber, K., Posor, Y., Gao, S., Held, M., Roske, Y., Schulze, D., Haucke, V., Noe, F. and Daumke, O. (2011) Crystal structure of nucleotide-free dynamin. *Nature*, **477**, 556–560.
5. Pisciotta, C. and Shy, M.E. (2018) *Neuropathy. Handb. Clin. Neurol.*, **148**, 653–665.
6. Baets, J., De Jonghe, P. and Timmerman, V. (2014) Recent advances in Charcot-Marie-Tooth disease. *Curr. Opin. Neurol.*, **27**, 532–540.
7. Previtali, S.C., Zhao, E., Lazarevic, D., Pipitone, G.B., Fabrizi, G.M., Manganelli, F., Mazzeo, A., Pareyson, D., Schenone, A., Taroni, F. *et al.* (2019) Expanding the spectrum of genes responsible for hereditary motor neuropathies. *J. Neurol. Neurosurg. Psychiatry*, **90**, 1171–1179.
8. Claeys, K.G., Zuchner, S., Kennerson, M., Berciano, J., Garcia, A., Verhoeven, K., Storey, E., Merory, J.R., Bienfait, H.M., Lammens, M. *et al.* (2009) Phenotypic spectrum of dynamin 2 mutations in Charcot-Marie-Tooth neuropathy. *Brain*, **132**, 1741–1752.
9. Zuchner, S., Noureddine, M., Kennerson, M., Verhoeven, K., Claeys, K., De Jonghe, P., Merory, J., Oliveira, S.A., Speer, M.C., Stenger, J.E. *et al.* (2005) Mutations in the pleckstrin homology domain of dynamin 2 cause dominant intermediate Charcot-Marie-Tooth disease. *Nat. Genet.*, **37**, 289–294.
10. Bitoun, M., Maugenre, S., Jeannet, P.Y., Lacene, E., Ferrer, X., Laforet, P., Martin, J.J., Laporte, J., Lochmuller, H., Beggs, A.H. *et al.* (2005) Mutations in dynamin 2 cause dominant centronuclear myopathy. *Nat Genet*, **37**, 1207–1209.
11. Bohm, J., Biancalana, V., Dechene, E.T., Bitoun, M., Pierson, C.R., Schaefer, E., Karasoy, H., Dempsey, M.A., Klein, F., Dondaine, N. *et al.* (2012) Mutation spectrum in the large GTPase dynamin 2, and genotype-phenotype correlation in autosomal dominant centronuclear myopathy. *Hum. Mutat.*, **33**, 949–959.
12. Fischer, D., Herasse, M., Bitoun, M., Barragan-Campos, H.M., Chiras, J., Laforet, P., Fardeau, M., Eymard, B., Guicheney, P. and Romero, N.B. (2006) Characterization of the muscle involvement in dynamin 2-related centronuclear myopathy. *Brain*, **129**, 1463–1469.
13. Jungbluth, H., Wallgren-Pettersson, C. and Laporte, J. (2008) Centronuclear (myotubular) myopathy. *Orphanet J. Rare Dis.*, **3**, 26.
14. Romero, N.B. and Bitoun, M. (2011) Centronuclear myopathies. *Semin Pediatr Neurol*, **18**, 250–256.
15. Bitoun, M., Bevilacqua, J.A., Prudhon, B., Maugenre, S., Taratuto, A.L., Monges, S., Lubieniecki, F., Cances, C., Uro-Coste, E., Mayer, M. *et al.* (2007) Dynamin 2 mutations cause sporadic centronuclear myopathy with neonatal onset. *Ann. Neurol.*, **62**, 666–670.
16. Susman, R.D., Quijano-Roy, S., Yang, N., Webster, R., Clarke, N.F., Dowling, J., Kennerson, M., Nicholson, G., Biancalana, V., Ilkovski, B. *et al.* (2010) Expanding the clinical, pathological

and MRI phenotype of DNM2-related centronuclear myopathy. *Neuromuscul. Disord.*, **20**, 229–237.
17. Reubold, T.F., Faelber, K., Plattner, N., Posor, Y., Ketel, K., Curth, U., Schlegel, J., Anand, R., Manstein, D.J., Noé, F. *et al.* (2015) Crystal structure of the dynamin tetramer. *Nature*, **525**, 404.
18. Kenniston, J.A. and Lemmon, M.A. (2010) Dynamin GTPase regulation is altered by PH domain mutations found in centronuclear myopathy patients. *Embo J.*, **29**, 3054–3067.
19. Wang, L., Barylko, B., Byers, C., Ross, J.A., Jameson, D.M. and Albanesi, J.P. (2010) Dynamin 2 mutants linked to centronuclear myopathies form abnormally stable polymers. *J. Biol. Chem.*, **285**, 22753–22757.
20. White, R.B., Bierinx, A.S., Gnocchi, V.F. and Zammit, P.S. (2010) Dynamics of muscle fibre growth during postnatal mouse development. *BMC Dev. Biol.*, **10**, 21.
21. Cowling, B.S., Toussaint, A., Amoasii, L., Koebel, P., Ferry, A., Davignon, L., Nishino, I., Mandel, J.L. and Laporte, J. (2011) Increased expression of wild-type or a centronuclear myopathy mutant of dynamin 2 in skeletal muscle of adult mice leads to structural defects and muscle weakness. *Am. J. Pathol.*, **178**, 2224–2235.
22. Lee, J.S., Ismail, A.M., Lee, J.Y., Zhou, X., Materne, E.C., Chodosh, J. and Rajaiya, J. (2019) Impact of dynamin 2 on adenovirus nuclear entry. *Virology*, **529**, 43–56.
23. Bitoun, M., Stojkovic, T., Prudhon, B., Maurage, C.A., Latour, P., Vermersch, P. and Guicheney, P. (2008) A novel mutation in the dynamin 2 gene in a Charcot-Marie-Tooth type 2 patient: clinical and pathological findings. *Neuromuscul. Disord.*, **18**, 334–338.
24. McMahon, H.T. and Boucrot, E. (2011) Molecular mechanism and physiological functions of clathrin-mediated endocytosis. *Nat. Rev. Mol. Cell. Biol.*, **12**, 517–533.
25. Vassilopoulos, S., Gentil, C., Laine, J., Buclez, P.O., Franck, A., Ferry, A., Precigout, G., Roth, R., Heuser, J.E., Brodsky, F.M. *et al.* (2014) Actin scaffolding by clathrin heavy chain is required for skeletal muscle sarcomere organization. *J. Cell. Biol.*, **205**, 377–393.
26. Chen, S., Huang, P., Qiu, Y., Zhou, Q., Li, X., Zhu, M. and Hong, D. (2018) Phenotype variability and histopathological findings in patients with a novel DNM2 mutation. *Neuropathology*, **38**, 34–40.
27. Cowling, B.S., Chevremont, T., Prokic, I., Kretz, C., Ferry, A., Coirault, C., Koutsopoulos, O., Laugel, V., Romero, N.B. and Laporte, J. (2014) Reducing dynamin 2 expression rescues X-linked centronuclear myopathy. *J. Clin. Invest.*, **124**, 1350–1363.
28. Tasfaout, H., Buono, S., Guo, S., Kretz, C., Messaddeq, N., Booten, S., Greenlee, S., Monia, B.P., Cowling, B.S. and Laporte, J. (2017) Antisense oligonucleotide-mediated Dnm2 knockdown prevents and reverts myotubular myopathy in mice. *Nat. Commun.*, **8**, 15661.
29. Tasfaout, H., Lionello, V.M., Kretz, C., Koebel, P., Messaddeq, N., Bitz, D., Laporte, J. and Cowling, B.S. (2018) Single intramuscular injection of AAV-shRNA reduces DNM2 and prevents myotubular myopathy in mice. *Mol. Ther.*, **26**, 1082–1092.
30. Tasfaout, H., Cowling, B.S. and Laporte, J. (2018) Centronuclear myopathies under attack: a plethora of therapeutic targets. *J. Neuromuscul Dis*, **5**, 387–406.
31. Buono, S., Ross, J.A., Tasfaout, H., Levy, Y., Kretz, C., Tayefeh, L., Matson, J., Guo, S., Kessler, P., Monia, B.P. *et al.* (2018) Reducing dynamin 2 (DNM2) rescues DNM2-related dominant centronuclear myopathy. *Proc. Natl. Acad. Sci. U. S. A.*, **115**, 11066–11071.
32. Hohendahl, A., Roux, A. and Galli, V. (2016) Structural insights into the centronuclear myopathy-associated functions of BIN1 and dynamin 2. *J. Struct. Biol.*, **196**, 37–47.
33. Ross, J.A., Digman, M.A., Wang, L., Gratton, E., Albanesi, J.P. and Jameson, D.M. (2011) Oligomerization state of dynamin 2 in cell membranes using TIRF and number and brightness analysis. *Biophys. J.*, **100**, L15–L17.
34. James, N.G., Digman, M.A., Ross, J.A., Barylko, B., Wang, L., Li, J., Chen, Y., Mueller, J.D., Gratton, E., Albanesi, J.P. *et al.* (2014) A mutation associated with centronuclear myopathy enhances the size and stability of dynamin 2 complexes in cells. *Biochim. Biophys. Acta*, **1840**, 315–321.
35. Rabai, A., Reisser, L., Reina-San-Martin, B., Mamchaoui, K., Cowling, B.S., Nicot, A.S. and Laporte, J. (2019) Allele-specific CRISPR/Cas9 correction of a heterozygous DNM2 mutation rescues centronuclear myopathy cell phenotypes. *Mol. Ther. Nucleic Acids*, **16**, 246–256.
36. Sidiropoulos, P.N., Miehe, M., Bock, T., Tinelli, E., Oertli, C.I., Kuner, R., Meijer, D., Wollscheid, B., Niemann, A. and Suter, U. (2012) Dynamin 2 mutations in Charcot-Marie-Tooth neuropathy highlight the importance of clathrin-mediated endocytosis in myelination. *Brain*, **135**, 1395–1411.
37. Gerber, D., Ghidinelli, M., Tinelli, E., Somandin, C., Gerber, J., Pereira, J.A., Ommer, A., Figlia, G., Miehe, M., Nageli, L.G. *et al.* (2019) Schwann cells, but not oligodendrocytes, depend strictly on dynamin 2 function. *Elife*, **8**.
38. Lu, Y.Y., Wang, L.J., Muramatsu, S., Ikeguchi, K., Fujimoto, K., Okada, T., Mizukami, H., Matsushita, T., Hanazono, Y., Kume, A. *et al.* (2003) Intramuscular injection of AAV-GDNF results in sustained expression of transgenic GDNF, and its delivery to spinal motoneurons by retrograde transport. *Neurosci Res*, **45**, 33–40.
39. Tinelli, E., Pereira, J.A. and Suter, U. (2013) Muscle-specific function of the centronuclear myopathy and Charcot-Marie-Tooth neuropathy-associated dynamin 2 is required for proper lipid metabolism, mitochondria, muscle fibers, neuromuscular junctions and peripheral nerves. *Hum. Mol. Genet.*, **22**, 4417–4429.
40. Dupuis, L., Gonzalez de Aguilar, J.L., Echaniz-Laguna, A., Eschbach, J., Rene, F., Oudart, H., Halter, B., Huze, C., Schaeffer, L., Bouillaud, F. *et al.* (2009) Muscle mitochondrial uncoupling dismantles neuromuscular junction and triggers distal degeneration of motor neurons. *PLoS One*, **4**, e5390.
41. Bragato, C., Gaudenzi, G., Blasevich, F., Pavesi, G., Maggi, L., Giunta, M., Cotelli, F. and Mora, M. (2016) Zebrafish as a model to investigate dynamin 2-related diseases. *Sci. Rep.*, **6**, 20466.
42. Kamerkar, S.C., Kraus, F., Sharpe, A.J., Pucadyil, T.J. and Ryan, M.T. (2018) Dynamin-related protein 1 has membrane constricting and severing abilities sufficient for mitochondrial and peroxisomal fission. *Nat. Commun.*, **9**, 5239.
43. Lee, J.E., Westrate, L.M., Wu, H., Page, C. and Voeltz, G.K. (2016) Multiple dynamin family members collaborate to drive mitochondrial division. *Nature*, **540**, 139–143.
44. Cowling, B.S., Prokic, I., Tasfaout, H., Rabai, A., Humbert, F., Rinaldi, B., Nicot, A.S., Kretz, C., Friant, S., Roux, A. *et al.* (2017) Amphiphysin (BIN1) negatively regulates dynamin 2 for normal muscle maturation. *J. Clin. Invest.*, **127**, 4477–4487.
45. Thomas, K.C., Zheng, X.F., Garces Suarez, F., Raftery, J.M., Quinlan, K.G., Yang, N., North, K.N. and Houweling, P.J. (2014) Evidence based selection of commonly used RT-qPCR reference genes for the analysis of mouse skeletal muscle. *PLoS One*, **9**, e88653.

Preliminary data: Rescuing Mtm1-/y by modulating specific DNM2 functions

Introduction

Mtm1$^{-/y}$, a mouse model for XLCNM disease displays high DNM2 protein level. Reduction of DNM2 level by genetic cross improved the CNM phenotype and survival of *Mtm1*$^{-/y}$ animals. This was validated by two other techniques such as ASO and shRNA injections against DNM2 (as discussed in section 4. Therapies in centronuclear myopathies). However, all strategies mentioned aim to reduce the total protein amount of DNM2 without distinguishing which function is responsible for the disease.

Here we created AAV containing DNM2 mutations that were reported to have specific protein functions disrupted in vitro, to evaluate their effect in disease rescue by intramuscular injection in *Mtm1*$^{-/y}$. The effect in WT muscles was also evaluated to elucidate the importance of different DNM2 protein functions in normal muscle physiology.

The following constructs were used:

Mutation	**Domain localization**	**Impacted function**
K44A	GTPase domain	Reduced GTPase activity
K142A	GTPase domain	No conformational change due to GTPase activity
R399A	MIDDLE domain	No high order oligomers
K562E	PH domain	Reduced lipid binding and lipid-stimulated GTPase activity
DeltaPRD	PRD Domain	PRD Domain removed, no interaction with SH3-domain containing proteins
K44A + R465W (KARW)	GTPase + MIDDLE domains	Reduced GTPase activity + Mild CNM mutation
WT-DNM2	WT protein containing exon 13ter (ubiquitous isoform)	

The AAV-injection protocol used as well as all the techniques used in this study are already described in the previous publication (Publication 1: *Different in vivo impacts of Dynamin 2 mutations implicated in Charcot-Marie-Tooth neuropathy or Centronuclear Myopathy*).

NOTE: The number of datapoints in the following experiments does not allow to perform statistical tests. All the data in this section should be considered as preliminary.

Results

WT Animals

AAV-Mediated overexpression of different DNM2 mutants in WT muscle impact on muscle force, fiber size and nuclei position

Expression of human cDNA was achieved by AAV intramuscular injection in 3-week old mice. First, DNM2 overexpression was confirmed by immunoblotting of TA muscle lysates (Figure 1A). DNM2 exogenous expression was confirmed although we observed that some constructs achieve higher levels of protein expression than others even injecting the same amount of viral particles. The same tendency was observed in the previous publication. Expression of all the analyzed constructs seem to have an impact on muscle force (Figure 1B) but no obvious difference is seen at muscle weight level (Figure 1C). Of note, DeltaPRD construct may have an effect reducing muscle weight.

At histological level, there are differences between constructs regarding fiber size and nuclei position (Figure 2A). These differences were confirmed by fiber diameter quantification: while most of the constructs have an impact on fiber size, R399A and K562E seem to follow a similar distribution than empty injected muscles (Figure 2B, C). When analyzing nuclei position, the same two construct seem not to affect nuclei internalization or centralization (Figure 2D).

In summary, we observe differences in the overexpression of different DNM2 mutants that should be confirmed with additional datapoints and further histological and ultrastructural analysis. Interestingly, impacting on DNM2's function of lipid binding or oligomerization is not affecting nuclei position and it seems to have a different effect in skeletal muscle than changing GTPase activity or protein interaction (Figure 2). We also observed that seems that the constructs with abnormal lipid binding or oligomerization are highly expressed than the others even injecting the same amount of viral particles (Figure 1A).

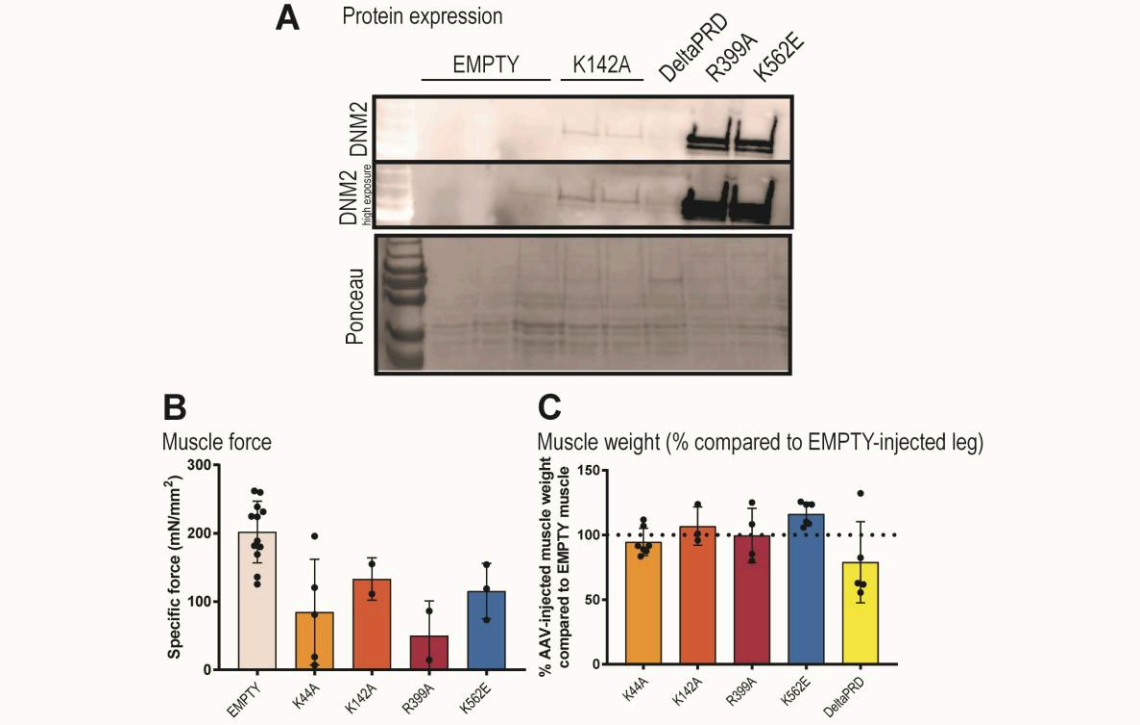

Figure 1. DNM2 overexpression in WT muscles impacts on muscle force but not in muscle weight. (A) Immunoblotting of muscle lysates showing AAV-mediated overexpression of different constructs. (B) In vivo specific muscle force of tibialis anterior muscles expressing different DNM2 mutants. (C) Muscle weight comparing the percentage of weight change versus the EMPTY-injected contralateral muscle.

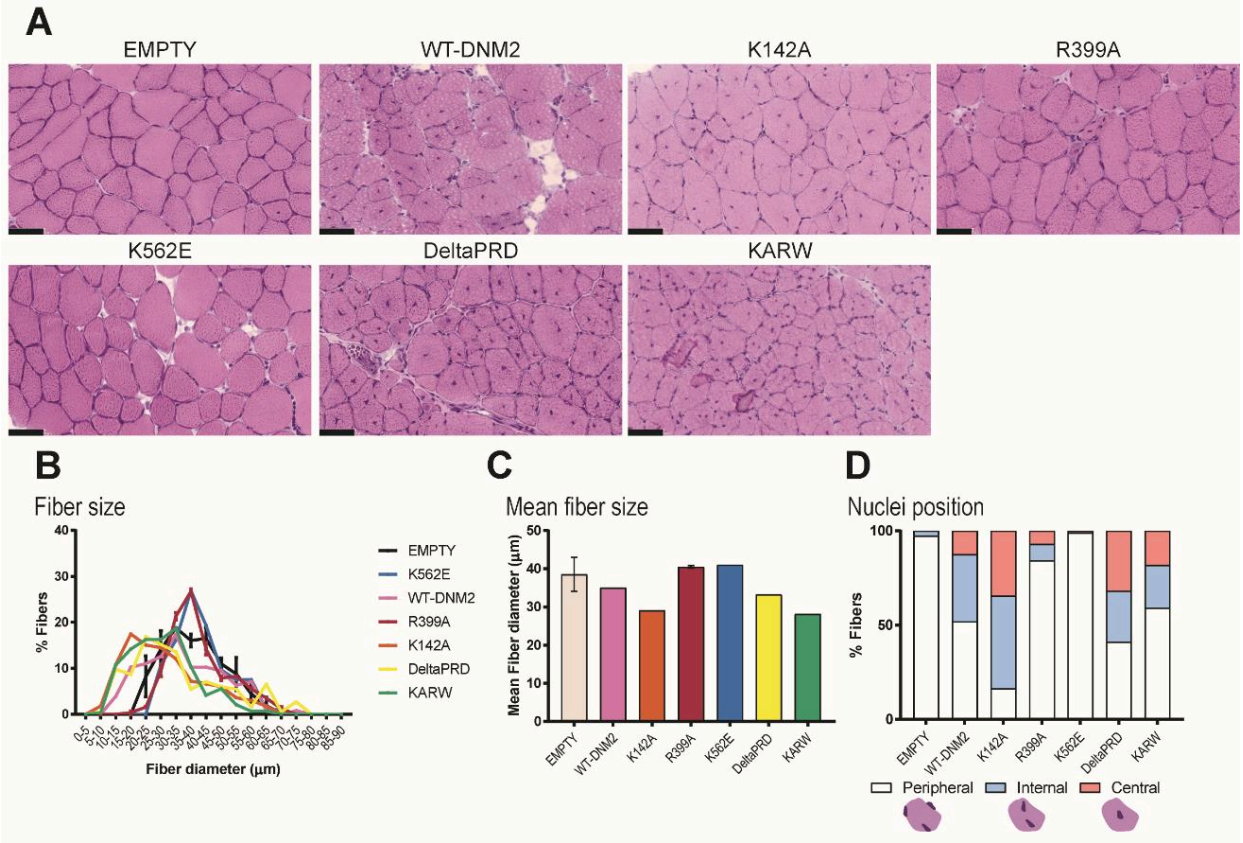

Figure 2. DNM2 overexpression in WT muscle impacts on fiber size and nuclei position. (A) Transverse 8µm TA muscle sections stained with HE (Scalebar=50µm). (B) Fiber diameter distribution and (C) mean fiber diameter. (D) Quantification of percentage of fibers with specific nuclei positions.

Overexpression of DNM2 K562E lipid binding defective mutant seems to improve muscle weight and fiber size of *Mtm1*$^{-/y}$ muscles

We next explored the possibility of improving the CNM phenotype observed in *Mtm1*$^{-/y}$ by modulating different DNM2 functions. DNM2 exogenous expression was confirmed although, as discussed previously, we observed that some constructs achieve higher levels of protein expression than others even injecting the same amount of viral particles (Figure 3A). In vivo muscle force post-injection experiments did not show a clear improvement, although it remains to be confirmed since not all the constructs were tested and some of them present variability (Figure 3A). Surprisingly, injection of K562E mutant seems to increase muscle weight when compared to contralateral empty-injected muscle (Figure 3B). Overexpression of the two mutants impacting GTPase activity seem to decrease the already low muscle force in *Mtm1*$^{-/y}$ animals (Figure 3C). DeltaPRD mutant overexpression needs the confirmation with additional experiments, only one muscle presented a major force increase, making it very difficult to conclude (Figure 3C).

Preliminary histological analysis shows a change in fiber size and nuclei position for the analyzed constructs (Figure 4A). When quantifying fiber size, we observe that WT-DNM2 overexpression aggravates myofiber atrophy whereas K562E increases fiber diameter (Figure 4B, C and Supplementary Figure 1). Surprisingly, nuclei position seems to be improved when overexpressing WT-DNM2 and K562E, although it remains to be confirmed (Figure 4D).

Summarizing, K562E mutant seems to improve muscle weight and fiber size of *Mtm1*-/y muscles (Figure 3B and 4B, C), suggesting lipid binding as a potential DNM2 function that could be used as a therapeutic target. The further study of the remaining constructs should give more information on DNM2 pathomechanism in XLCNM models and the confirmation if other DNM2 functions may be used for this purpose. Unexpectedly, overexpression of WT-DNM2 seems to impact on nuclei position, reducing nuclei internalization (Figure 4D) but still decreasing fiber size (Figure 4B, C), raising the question of how different DNM2 isoforms may impact on XLCNM and their role in skeletal muscle physiology.

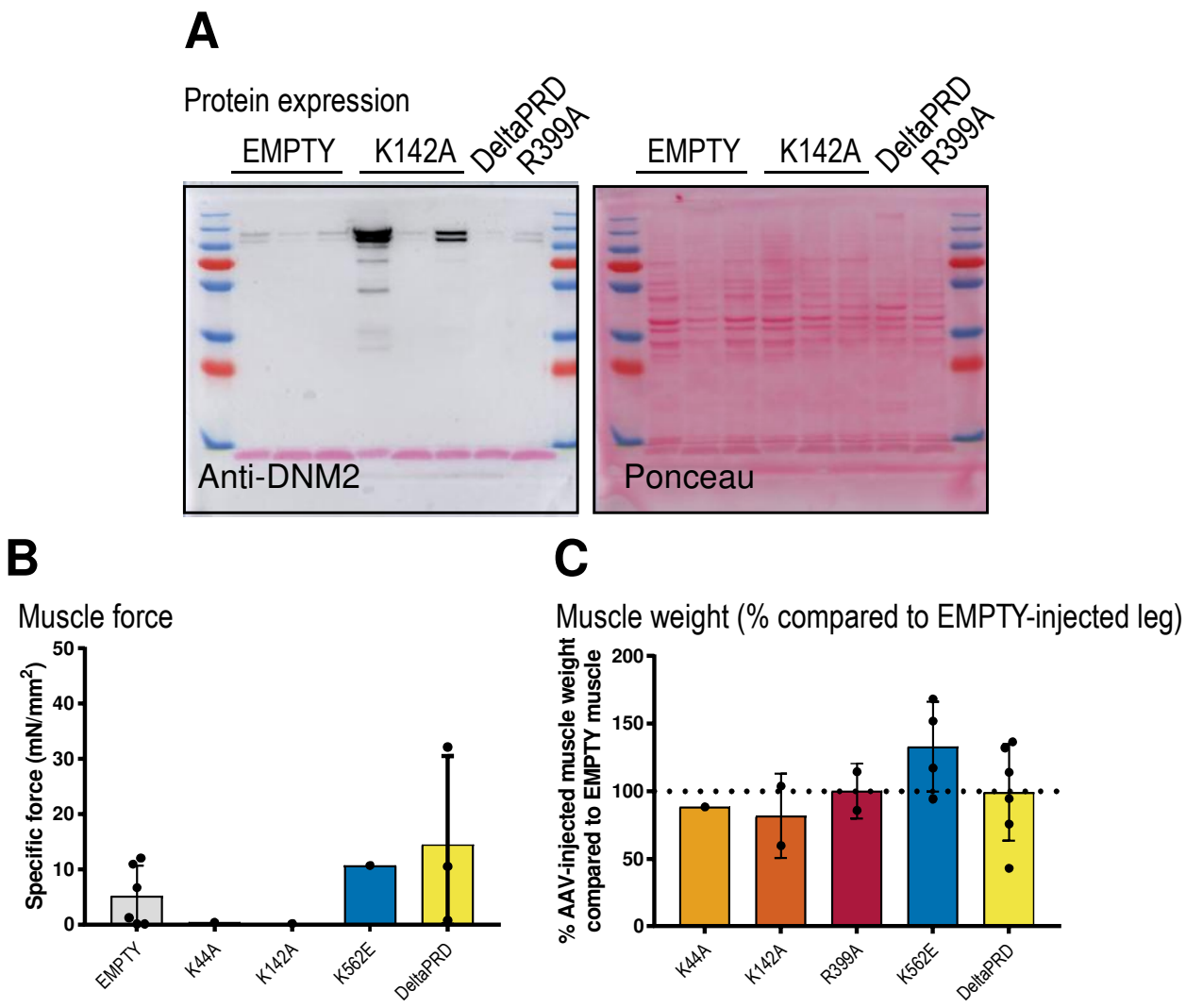

Figure 3. Overexpression of lipid binding defective mutant in *Mtm1*-/y TA seems to have a positive impact on muscle weight. (A) Immunoblotting of muscle lysates showing AAV-mediated overexpression of different constructs in *Mtm1*$^{-/y}$ TA. (B) In vivo specific muscle force in TA from *Mtm1*$^{-/y}$ animals. (C) Percentage of change in muscle weight compared to empty-injected contralateral muscle.

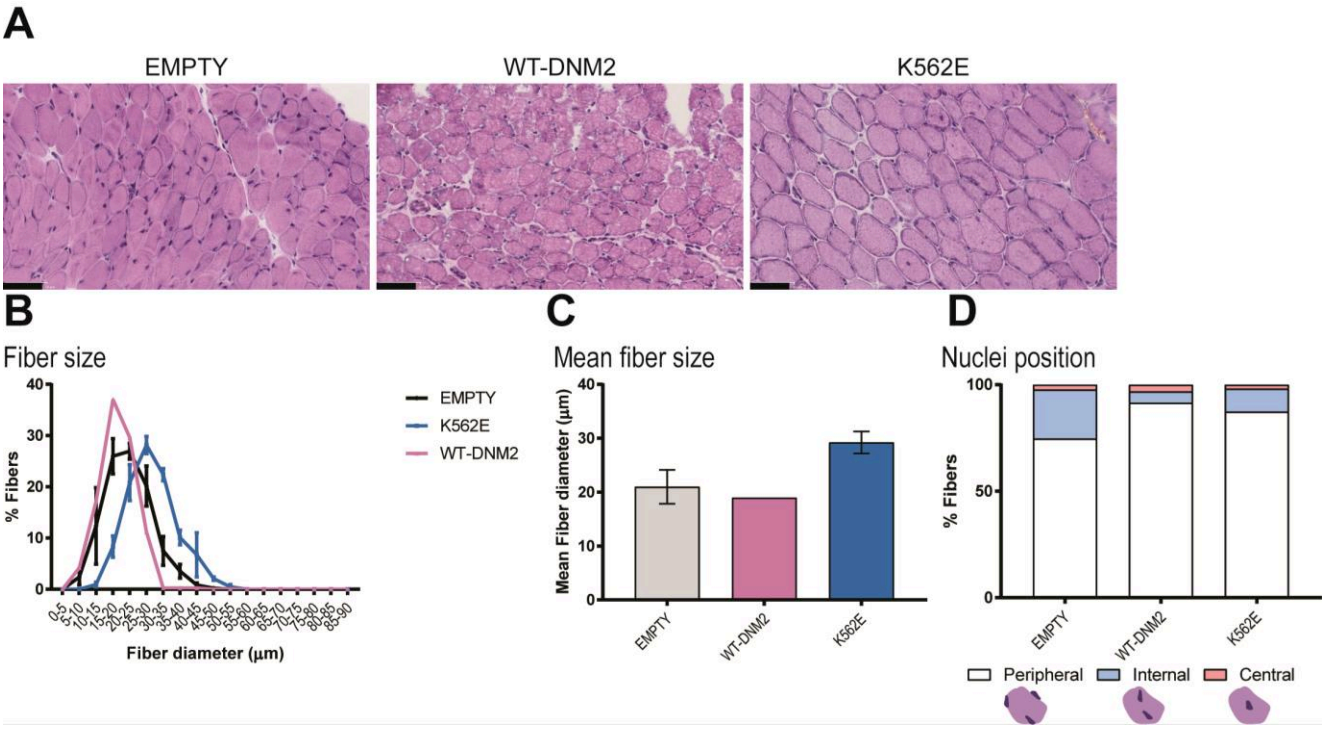

Figure 4. Overexpression of lipid binding defective mutant increases fiber size of *Mtm1*-/y injected TA muscles. (A) 8µm muscle sections stained with HE (Scalebar=50µm). (B) Fiber size distribution and (C) mean fiber size for the different constructs analyzed. (D) Percentage of fibers with specific nuclei position.

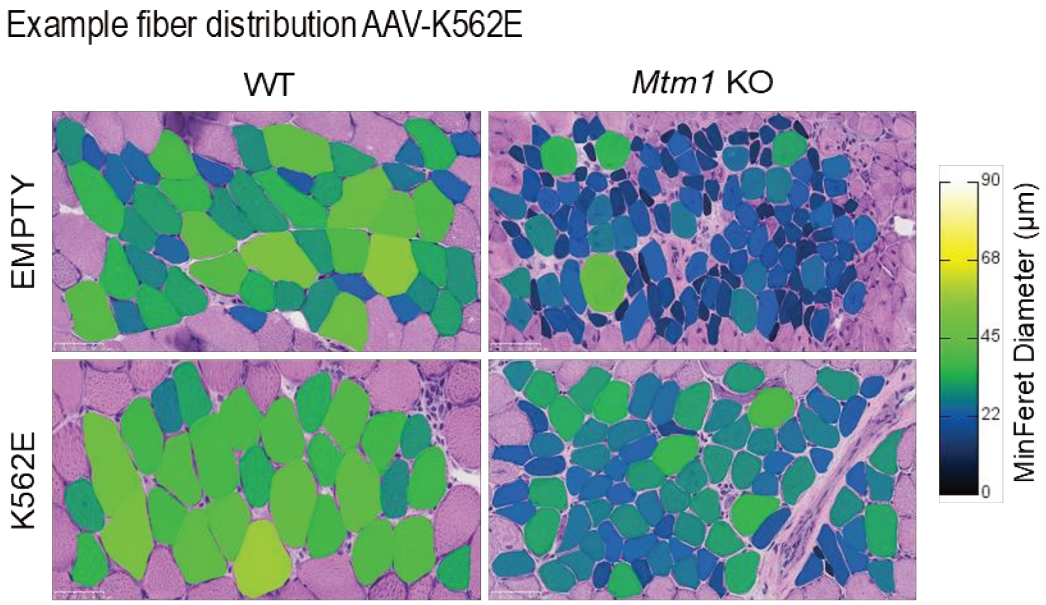

Supplementary Figure 1. Example of fiber size distribution in K562E-expressing muscles.

Conclusion

In conclusion, in WT muscles we observed potential differences with all DNM2 constructs explored although their effect on other DNM2 cellular functions remains to be explored. It seems that K562E and R399A do not impair nuclei position.

Overexpression of lipid defective K562E DNM2 mutant seems to improve some CNM features in *Mtm1*$^{-/y}$. Other constructs should be explored before concluding

Contribution

In this preliminary study I did all AAV injections and muscle analysis.

Suzie Buono cloned and produced all pAAV plasmids.

Pascale Koebel produced the AAV for intramuscular injection.

Roberto Silva-Rojas and Juliana Neves helped in muscle force measurements.

Coralie Borne helped in western blot and fiber size analysis.

Publication 2: Physiological impact and disease reversion for the severe form of centronuclear myopathy linked to Dynamin

Introduction

Mutations in *DNM2* cause CNM or CMT diseases. Between CNM cases, there is an heterogeneity since different mutations can cause severe or mild forms of the disease. The *Dnm2*$^{+/R465W}$ is the only current model for mild-CNM and displays mild signs of myopathy. The lack of a faithful model for severe DNM2-CNM makes it difficult to validate new therapies for this form.

Here we created the novel *Dnm2*$^{+/S619L}$ mouse model carrying a patient mutation that causes neonatal severe form of CNM. This will be a precious tool to study new therapies and understand the pathophysiology of severe forms of CNM.

Graphical abstract

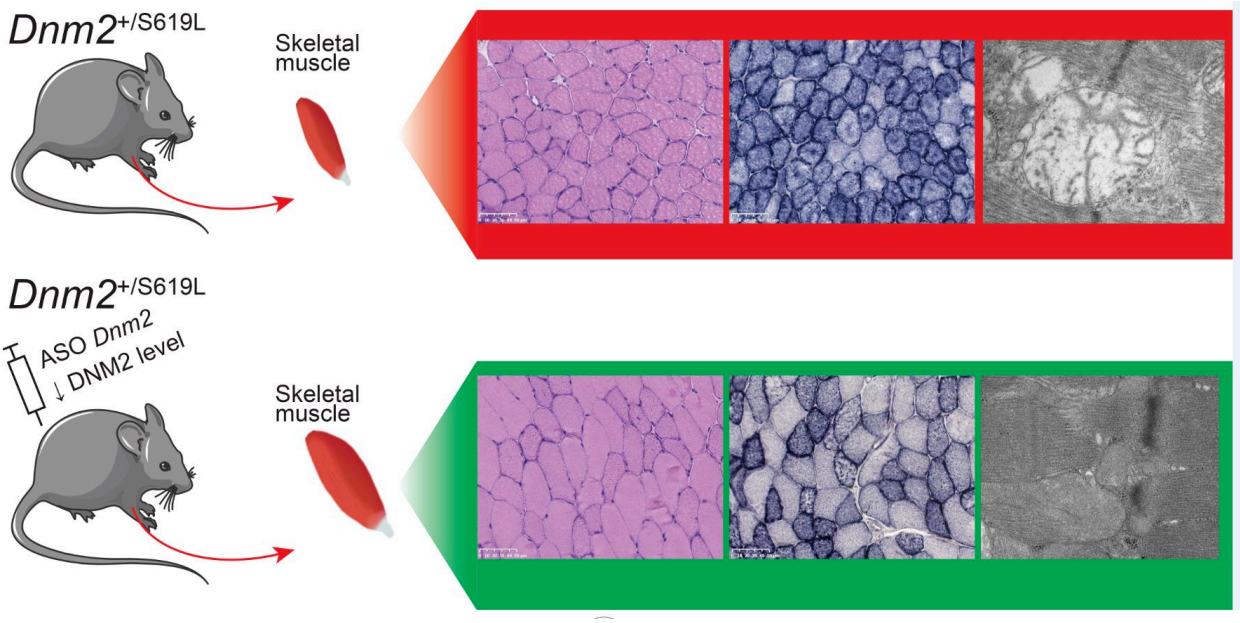

Results

- *Dnm2*$^{+/S619L}$ have early decreased body weight and impaired motor function.
- Muscles from this mice have accumulation of DNM2 protein when evaluated by western blot, this accumulation is not due to an increase in RNA level.
- Homozygous is lethal from E18.5 to P2 and there is a slight mortality of heterozygous animals from P2 to P10.

- At histological level, heterozygous males have smaller fibers and oxidative staining reveals abnormal accumulations in the center of the fiber.
- Electron microscopy analysis revealed a population of swollen and enlarged mitochondria in muscles from heterozygous males.
- Decreasing DNM2 protein level by ASO treatment improved motor function, histological features and mitochondrial defects 3 weeks after treatment.

Conclusion

Here we show the first validation of a mammalian model for the severe form of DNM2-related CNM, associated to S619L mutation. We also found that reducing DNM2 total protein level by ASO treatment improves motor function and muscle histology in *Dnm2*$^{+/S619L}$ animals.

Contribution

In this work I performed mice phenotyping, treatment. I did all histological and ultrastructural analysis, immunofluorescence and molecular biology experiments.

Christine Kretz performed mice phenotyping and animal treatment.

Roberto Silva-Rojas did in vivo muscle force measurements.

Julien Ochala performed all single myofiber experiments.

Alexia Menuet helped in mice phenotyping and animal treatment.

Norma B Romero analysed biopsies from patients at histological, ultrastructural and molecular levels.

This work was supervised by Belinda Cowling and Jocelyn Laporte.

Physiological impact and disease reversion for the severe form of centronuclear myopathy linked to Dynamin

Xènia Massana Muñoz[1,2,3,4], Christine Kretz[1,2,3,4,#], Roberto Silva Rojas[1,2,3,4,#], Julien Ochala[5], Alexia Menuet[1,2,3,4], Norma B Romero[6,7], Belinda S. Cowling[1,2,3,4,8], Jocelyn Laporte[1,2,3,4,*]

[1] Institut de Génétique et de Biologie Moléculaire et Cellulaire, Illkirch, France

[2] Centre National de la Recherche Scientifique, UMR7104, Illkirch, France

[3] Institut National de la Santé et de la Recherche Médicale, U1258, Illkirch, France

[4] Université de Strasbourg, Illkirch, France

[5] Centre of Human and Applied Physiological Sciences, School of Basic and Medical Biosciences, Faculty of Life Sciences and Medicine, King's College London, SE1 1UL London, United Kingdom

[6] Neuromuscular Morphology Unit, Myology Institute, GHU Pitié-Salpêtrière, Paris, France

[7] Sorbonne Université, AP-HP, INSERM, Centre de référence des maladies neuromusculaires Nord/Est/Ile de France, Paris, France

[8] Dynacure, Illkirch, France

[#] equal contributors

* Correspondence and request of materials should be addressed to

Jocelyn Laporte

Mailing address: 1, rue Laurent Fries B.P. 10142 67404 ILLKIRCH (FRANCE)

Phone number: + 33388653412

E-mail address : jocelyn@igbmc.fr

Abstract

Classical dynamins are large GTPases regulating membrane and cytoskeleton dynamics, and are linked to different pathological conditions ranging from neuromuscular diseases to encephalopathy and cancer. Dominant DNM2 (dynamin 2) mutations lead to either mild adult onset or severe neonatal centronuclear myopathy (ADCNM). Our objectives were to better understand the pathomechanism of severe ADCNM and test a potential therapy. Here, we created the *Dnm2*$^{SL/+}$ mouse line harboring the common S619L mutation found in patients with severe ADCNM and impairing the conformational switch regulating dynamin self-assembly and membrane remodeling. The *Dnm2*$^{SL/+}$ mouse faithfully reproduces severe ADCNM hallmarks with early impaired muscle function and force together with myofibers hypotrophy. It revealed swollen mitochondria lacking cristae as the main ultrastructural defect and potential cause of the disease. Patient analysis confirmed this structural hallmark. In addition, DNM2 reduction with antisense oligonucleotides after disease onset efficiently reverted locomotor and force defects after only 3 weeks of treatment. Most histological defects including mitochondria alteration were partially or fully rescued. Overall, this study highlights an efficient approach to revert the severe form of dynamin-related centronuclear myopathy. These data also reveal that the dynamin conformational switch is key for muscle function and should be targeted for future therapeutic developments.

Introduction

Maintenance and remodeling of the intracellular organization is controlled by cytoskeletons and membrane dynamics. Dynamins are mechanochemical GTPases that catalyze membrane remodeling and control actin polymerization (1-3). Within the classical dynamins, dynamin 2 (DNM2) is the only member ubiquitously expressed. Dominant *DNM2* mutations cause different genetic diseases affecting different tissues: centronuclear myopathy (MIM#160150) (4), Charcot-Marie-Tooth peripheral neuropathy (CMT; MIM#606482) (5) and spastic paraplegia (6). A recessive *DNM2* mutation was also reported in a lethal congenital contracture syndrome (MIM#615368) (7).

Autosomal dominant centronuclear myopathy (ADCNM) due to *DNM2* mutations is characterized by progressive muscle weakness, mainly proximal, and facial weakness with ptosis (4, 8). Histological hallmarks are type I fiber predominance and hypotrophy, and a general intracellular disorganization with nuclei centrally located and radial organization of the sarcoplasmic reticulum (9). The age of onset and severity are highly heterogeneous, ranging from the severe neonatal onset form to a mild form with adult onset. The most common mutations in the severe and the adult forms are the S619L and R465W missense mutations, respectively (10). Patients with the S619L mutation have a generalized hypotonia at birth associated with ventilator distress requiring mechanical ventilation, that is not observed for the R465W mutation (11). The pathomechanism is still unclear and the role of DNM2 in muscle is not well understood. Several in cellulo and in vivo models have been created to shed light on DNM2 physiopathological functions, and suggest the disease arises from T-tubule fragmentation and a defect in intracellular organization (12-16). The only genetically stable physiological model is the *Dnm2*$^{RW/+}$ mouse (R465W mutation) that displays a mild phenotype with force reduction from 3 weeks, and muscle atrophy and abnormal oxidative staining from 2 months of age (17). These defects are rather weak and slightly progressive with no impact on lifespan and body weight. To date, no stable animal model for the severe form of ADCNM has been reported. Several *DNM2* ADCNM mutations were exogenously

overexpressed in drosophila, zebrafish and mouse. Drosophila overexpressing S619L DNM2 did not develop to adult stage due to an eclosion defect, and larvae displayed T-tubule disorganization (13). Zebrafish transiently overexpressing S619L DNM2 had decreased movement and structural defects in T-tubules and neuromuscular junctions (12, 15, 18). In mouse, several *DNM2* mutations linked to ADCNM were transiently overexpressed and correlated with CNM-like histological defects (14, 16). A faithful model is thus still needed to study the pathomechanisms and test potential therapies, especially for the severe form.

No therapies are yet available for any ADCNM forms. Palliative treatment with acetylcholine inhibitors showed improvement of motor behavior in zebrafish larvae and muscle strength and fatigability in patients (18, 19). First proof-of-concept with prospective technologies as RNA trans-splicing and RNA inhibition were recently reported. RNA trans-splicing was only tested in WT mice(20), while RNA inhibition with allele-specific shRNA silencing(21) or antisense oligonucleotides targeting the total pool of *Dnm2* both prevented the progression of the phenotypes of the *Dnm2*$^{RW/+}$ mouse (22, 23)

DNM2 mutations in ADCNM are proposed to be gain-of-function. The functions of DNM2 depend on its ability to hydrolyze GTP, oligomerize and bind lipids (24). In vitro, DNM2 ADCNM mutants increased protein oligomerization and its GTPase activity independently of lipid binding (25, 26). Moreover, overexpression of WT DNM2 in mice induced a CNM-like phenotype, milder than overexpressing the R465W mutant (14, 27).

Classical dynamins are composed of a GTPase domain, a middle domain and a GTPase effector domain (GED) which form the stalk and are involved in protein oligomerization, a pleckstrin homology (PH) domain which binds membranes, and a C-terminal proline rich domain (PRD) which binds SH3-containing proteins (Figure 1A) (28, 29). Most ADCNM DNM2 mutations linked to the severe form, including the S619L, are concentrated in the PH-stalk interface, while the mild R465W mutation does not affect this interface. This interface regulates a conformational switch impacting dynamin self-assembly, membrane binding and fission (24, 30). The PH-stalk interface

in the closed conformation is auto-inhibitory, and the release of the PH domain upon membrane binding leads to an open conformation. Several ADCNM mutations weaken this interface, and the severe S619L mutant disrupts this interface which leads to decreased auto-inhibition and aberrant oligomerization in vitro (Figure 1A) (24). However, a modest impact of S619L on endocytosis was noted in culture cells (31) and the physiological impact of this conformational switch has never been investigated.

Here, we aimed to create and validate the first genetically stable mammalian model for the severe ADCNM form to study the disease mechanisms and have the opportunity to test potential therapies in a physiological relevant model. We established the *Dnm2*$^{SL/+}$ mouse harboring the S619L *Dnm2* mutation, and showed that it faithfully reproduces a severe CNM phenotype that was reversed by DNM2 reduction upon antisense oligonucleotide treatment. Importantly, this model allows us to study the physiological impact of the conformational switch regulating the functions of dynamin 2, a protein critical to many cell functions.

Results

Creation and validation of the *Dnm2*$^{SL/+}$ mouse harboring the S619L *Dnm2* mutation

To create a stable mammalian model for the severe ADCNM form, we engineered a transgenic mouse line through homologous recombination in C57BL/6N ES cells (Figure 1, A and B). Both heterozygous male and female *Dnm2*$^{SL/+}$ mice were fertile and were crossed with WT and *Dnm2*$^{SL/+}$ mice to generate the disease model (*Dnm2*$^{SL/+}$ mice) and homozygous *Dnm2*$^{SL/SL}$ mice. Genotypes were confirmed by PCR and DNA sequencing (Figure 1, C and D). At 18.5 days post-coitum (dpc), the expected Mendelian segregation was observed, while no homozygous mice survived to postnatal day 2, and a partial mortality of the heterozygous was noted between 18.5dpc and day 10 (Figure 1E). Homozygous mice which were identified, all died within the first hours of birth. After day 10, all *Dnm2*$^{SL/+}$ mice survived up to at least 18 months (18mo). In the surviving *Dnm2*$^{SL/+}$ mice, DNM2 protein level was increased by around 2 fold in tibialis anterior (TA) muscle compared with WT littermates (Figure 2A). RT-qPCR analysis of the ubiquitous *Dnm2* isoform from TA muscles revealed no significant differences between *Dnm2*$^{SL/+}$ and WT mice (Figure 2B). In addition to the ubiquitous *Dnm2* isoform (Ub-*Dnm2*), we previously reported the presence of a skeletal muscle specific isoform (M-*Dnm2*) containing exon12b encoding for 10 amino acids located between the stalk and PH domains. M-*Dnm2* represents about 71% of all *Dnm2* isoforms in TA muscle and it was slightly decreased in the *Dnm2*$^{SL/+}$ muscle. In a 17 month old patient muscle biopsy that was accessible, DNM2 antibody detected a protein at the expected size and higher molecular weight signals, suggesting possible aggregation or modification specifically of the S619L protein (Figure 2C). In conclusion, the S619L *Dnm2* mutation is incompatible with postnatal life at the homozygous state and affects the survival of heterozygous mice, the latter representing the disease model for ADCNM.

Dnm2$^{SL/+}$ mice develop a severe muscle phenotype resembling centronuclear myopathy

To investigate if the *Dnm2*$^{SL/+}$ mice line represents a faithful model for severe ADCNM, mice were characterized at different timepoints, from 18.5dpc to adulthood, at the clinical and histological levels. At 18.5dpc, while there was no obvious difference in myofiber size and general organization between WT and *Dnm2*$^{SL/+}$ mice by haematoxylin/eosin (HE) of lower limbs muscles, abnormal nuclei shape and central chains of nuclei were seen in the homozygous mice (Figure 3A). Central chains of nuclei are often seen in CNM patient myofibers (9). At day 2, body weight was already significantly decreased in *Dnm2*$^{SL/+}$ mice (Figure 3B). We thus explored feeding ability and identified a decrease in milk intake in the stomach, albeit with unchanged blood glucose levels (Figure 3, C and D). These findings suggest a feeding defect causing decreased body weight. Body weight in males was below WT levels over time up to 8 weeks (8w), when mice were sacrificed for further analyses (Figure 4A). A very strong decrease in hanging ability was noted at all timepoints analyzed in *Dnm2*$^{SL/+}$ mice, reflecting a major impairment in motor function (Figure 4B). ADCNM displays specific histological hallmarks: abnormal oxidative staining, centralized nuclei and fiber size heterogeneity, which are the key for diagnosis (9). HE staining of TA muscles at 8w revealed smaller and rounder muscle fibers in *Dnm2*$^{SL/+}$ mice (Figure 4C-E). There was a slight tendency for increased internal or central nuclei. In addition, succinate dehydrogenase (SDH) and reduced nicotinamide adenine dinucleotide (NADH) staining confirmed fiber hypotrophy and highlighted abnormal accumulation of oxidative activity in the center of fibers (Figure 4, C and F). Overall, the *Dnm2*$^{SL/+}$ mouse displays a severe motor defect and a CNM-like histology, validating this model as faithfully reproducing the severe form of ADCNM.

Pathological mechanisms at the basis of ADCNM

To decipher the defects at the basis of the disease, we first checked the localization of DNM2 in muscle. In WT and *Dnm2*$^{SL/+}$ muscles, DNM2 displayed a striated pattern reminiscent of the sarcomeric organization and fitting with Z-line localization, as previously reported (Figure 5A) (14). The S619L mutation did not obviously affect this localization. Ultrastructural analyses with

transmission electron microscopy showed slight mis-alignment of the Z-line (Figure 5B). The main defect was the presence of vacuole-like structures that were confirmed to be mitochondria on higher magnification. While well-localized between the sarcomeres at the A band, mitochondria were often enlarged and rounded and were devoid of most cristae (Figure 5, C and D; Supplementary Figure 1). Mitochondrial structure was normal in the muscles of the reported *Dnm2*$^{RW/+}$ mouse, supporting that the *Dnm2*$^{SL/+}$ mouse represents a more severe form of myopathy than the *Dnm2*$^{RW/+}$ mouse (17). We did not detect the same type of structural defect in liver and heart tissues, only a decrease in mitochondrial area in liver (Supplementary Figure 2). Based on these findings we analyzed the muscle of an ADCNM patient with the DNM2 S619L mutation by electron microscopy and found similar enlarged mitochondria devoid of most cristae, highlighting an overlooked phenotype in patients (Figure 5E). Other structural alterations found in other congenital myopathies such as cores or rods were absent.

Zebrafish or mice overexpressing the S619L mutant displayed a disrupted distribution and structural fragmentation of the neuromuscular junction (15, 16). However, the transgenic *Dnm2*$^{SL/+}$ mouse has a normal distribution and NMJ area (Supplementary Figure 3), indicating that defects of the neuromuscular junction is not a major hallmark of the disease and is probably due to acute overexpression. As different DNM2 mutations are linked to peripheral CMT neuropathy, peripheral nerves were investigated. No structural defect in the sciatic nerve was detected in the *Dnm2*$^{SL/+}$ mouse (Supplementary Figure 4). Taken together, the most prominent feature was a strong impairment in mitochondria in muscle, which is expected to impact muscle performance.

The defects in muscle force of the *Dnm2*$^{SL/+}$ mouse are reverted upon DNM2 reduction

To further characterize the impact of the S619L mutation and test a potential therapeutic approach, we analyzed an independent cohort of mice with or without injections of antisense oligonucleotides (ASO) targeting the *Dnm2* pre and mature mRNA. Reduction of DNM2 upon injection of ASO-1 antisense oligonucleotide was shown to prevent and revert the phenotypes of

the X-linked CNM model, the *Mtm1*$^{y/-}$ mouse (32). This strategy was also applied to the *Dnm2*$^{RW/+}$ mouse and appeared to ameliorate the mild muscle phenotypes of this model (22). In this last study, ASO injections were done before disease onset, preventing a full reversion study. Here, weekly intraperitoneal (IP) injections of 25mg/kg ASO-1 were performed in *Dnm2*$^{SL/+}$ mice from 3 to 7w and analyzed at 8w. Of note, before 3w, *Dnm2*$^{SL/+}$ mice displayed feeding defects, reduced body and muscle weight and strongly impaired motor performance (Figure 2). Upon treatment, the differences in body and muscle weights compared to treated or untreated WT mice were decreased albeit not fully normalized (Figure 6, A and B). The untreated *Dnm2*$^{SL/+}$ mice displayed a strong decrease in absolute and specific TA muscle force, while the treated animals had a specific force back to WT level after 5w of treatment (Figure 6, C and D). Untreated *Dnm2*$^{SL/+}$ mice had a strongly impaired motor performance at all ages, while it was normalized after 3w of treatment (Figure 6, E and F; Supplementary Movie 1). To assess if the force decrease was due to an intrinsic defect of myofibers, isolated myofibers were analyzed. The absolute force, cross-sectional area and specific force of myofibers from the TA muscle of *Dnm2*$^{SL/+}$ mice were all significantly decreased, while treatment for 5 weeks normalized these parameters (Figure 6G-I). Overall, DNM2 reduction with ASO targeting *Dnm2* efficiently reverted both locomotor and force defects of the *Dnm2*$^{SL/+}$ mouse, supporting the mutation has a gain-of-function activity in vivo.

CNM histological hallmarks of the *Dnm2*$^{SL/+}$ mouse are greatly ameliorated upon DNM2 reduction

We next investigated if the rescue of the muscle force correlated with an improvement of the CNM-like histology by staining TA muscles with HE, SDH and NADH-TR. The decreased fiber size in untreated *Dnm2*$^{SL/+}$ mice was fully normalized upon ASO-1 injections (Figure 7, A and B). Due to the weak defects in nuclei localization, it was difficult to conclude on an improvement (Figure 7C). The oxidative staining was greatly ameliorated in treated *Dnm2*$^{SL/+}$, mice with near

complete loss of the abnormal central accumulation; however, some fibers presented a heterogeneous staining unlike WT (Figure 7, A and D). Western blotting with DNM2 antibody of TA muscles lysates showed that ASO-1 treament efficiently reduced DNM2 protein levels (Figure 7E). While untreated *Dnm2*$^{SL/+}$ mice displayed increased DNM2 levels, the reduction of DNM2 down to the WT level correlated with the phenotypic rescue. We conclude that DNM2 reduction corrected the CNM-like histological abnormalities of the *Dnm2*$^{SL/+}$ mouse.

We uncovered sarcomeres mis-alignment and a strong mitochondrial structural defect in the *Dnm2*$^{SL/+}$ mice (Figure 5). Electron microscopy revealed an improvement of the sarcomere alignment upon treatment, and this was confirmed by immuno-labeling of alpha-actinin and the RYR1 calcium channel, markers of Z-line and sarcoplasmic reticulum respectively (Figure 8, A, C and D). We observed two populations of mitochondria: enlarged mitochondria with highly perturbed cristae structure, as in the untreated, and normal or slightly enlarged mitochondria with normal cristae close to WT conditions (Figure 8B). The second population was not seen in untreated animals, suggesting an improvement in mitochondrial structure upon DNM2 reduction. Overall, ASO treatment had a positive impact on the main structural defects observed on mitochondria and sarcomere correlating with the locomotor and force correction.

Discussion

Here, we created and validated the first mammalian model for the severe form of ADCNM due to DNM2 mutations. In particular, we focused on the S619L missense mutation, affecting a residue strongly implicated in the regulation of the PH domain conformational switch that regulates the self-assembly, membrane binding and fission of dynamin. *Dnm2*$^{SL/+}$ mice display an early and severe motor defect linked to force reduction and mitochondria structural anomalies that faithfully reproduce the phenotype of CNM patients including the histological hallmarks of their muscles. Reduction of DNM2 level with antisense oligonucleotides promoting the degradation of *Dnm2* pre-mRNA after disease onset rescued efficiently the main behavior and histological phenotypes and reverted the early signs of the disease.

A faithful mammalian model for severe centronuclear myopathy linked to DNM2 mutation

The *Dnm2*$^{SL/+}$ mice, like the ADCNM severe form, have muscle weakness from birth (10, 11). Patients were reported to have hypotonia with weak suckling and the *Dnm2*$^{SL/+}$ mice had neonatal feeding defects. *Dnm2*$^{SL/+}$ muscle showed most of the hallmarks of patient histology, including fiber hypotrophy and central accumulation of oxidative staining. However, centralization of nuclei was barely observed in adult mice; the *Dnm2*$^{RW/+}$ mouse did not show any nuclei internalization, suggesting this phenotype in ADCNM is difficult to reproduce in mice (17). Conversely, in the *Dnm2*$^{SL/+}$ mouse at E18.5, central chains of nuclei were often seen as in CNM patient myofibers (9). In addition, we uncovered swollen mitochondria with altered cristae in the *Dnm2*$^{SL/+}$ mouse, leading to a reinvestigation of human muscle in which we confirmed this phenotype. The different phenotypes in the *Dnm2*$^{SL/+}$ mice are much more pronounced and of earlier onset than in the *Dnm2*$^{RW/+}$ mice, confirming the genotype-phenotype correlation observed in patients (10). Moreover, it makes the *Dnm2*$^{SL/+}$ mice a better and more attractive model for testing therapies.

The S619L mutated DNM2 was previously overexpressed in drosophila, zebrafish and mouse. Noteworthy, overexpression of DNM2 by itself could trigger cellular defects, as noted when WT-DNM2 was overexpressed in WT mice (14, 27). In both drosophila and zebrafish, only the larva stage could be explored, as drosophila expressing the S619L mutant could not hatch and only transient overexpression was achieved in zebrafish through RNA injection (12, 13, 18). In mice with exogenous overexpression of the S619L mutant, the development of a CNM disease could not be followed as adult WT mice were injected (16). The *Dnm2*$^{SL/+}$ mouse provides a faithful model to characterize the disease progression and postnatal muscle maturation and function. Neuromuscular junction defects were reported in zebrafish and mice overexpressing S619L mutant while we did not observed obvious defect in the *Dnm2*$^{SL/+}$ adult mouse. This difference could be due to the expression level of the S619L mutant, or to a compensatory mechanism in mice. In accordance to the last hypothesis, some *Dnm2*$^{SL/+}$ mice died by day 10 while all remaining mice survived to at least 18mo. In addition, different DNM2 mutations in the PH domain cause Charcot-Marie-Tooth peripheral neuropathy and it is unclear to date if CNM and CMT phenotypes overlap in the same patient (33, 34). There were no obvious structural defects in the sciatic nerve of the *Dnm2*$^{SL/+}$ mouse, unlike the axonal degeneration and loss of myelinating fibers seen in CMT patients (35), suggesting no overlap.

Physiological impact of dynamin dysregulation

Previous studies in the drosophila and zebrafish overexpressing models reported T-tubule defects that were not evident in the *Dnm2*$^{RW/+}$ mouse and neither in the novel *Dnm2*$^{SL/+}$ mouse (17). In accordance to the mice data, no obvious T-tubule or triad structural defects were reported in patients. However, excitation-contraction coupling was impaired in isolated fibers from the *Dnm2*$^{RW/+}$ mouse, supporting that calcium mis-handling could be an important feature in the pathomechanism (36, 37). Here, we uncover a novel potential cause of the disease as the main ultrastructural defect was enlarged mitochondria lacking cristae. Swollen mitochondria harboring

disorganized cristae were also reported in a skeletal muscle specific knock-out, suggesting the mitochondria defects observed in the *Dnm2*$^{SL/+}$ mouse originates from the muscle (38). DNM2 was recently suggested to fission mitochondria in cooperation with another dynamin DRP1 (39), however, this point is highly controversial (40, 41) and we cannot exclude that the impact of DNM2 alteration on mitochondria in muscle is indirect. The movement of the PH domain was shown to be crucial for regulating self-assembly, membrane binding and fission, and the S619L mutation destabilizes this conformational switch in vitro (24). The physiological relevance of this process was unknown, and preliminary data in cultured cells revealed that the S619L mutation only slightly delayed clathrin mediated endocytosis (31). In DNM2 depleted HeLa cells, DNM2-S619L re-expression has been reported to slightly increase clathrin mediated endocytosis of transferrin (28). Our present data supports that this conformational switch is of main importance specifically for skeletal muscle, despite the ubiquitous expression of DNM2. Of note, skeletal muscles specifically contain the M-DNM2 isoform with exon12b encoding for 10 aa in close proximity to the stalk-PH domains interface (42). We thus hypothesize the M-DNM2 is more sensitive to an alteration in the conformational switch of dynamin, and thus that skeletal muscle is more sensitive to CNM mutations underlying the fact that CNM patients appear specifically affected in skeletal muscle despite the ubiquitous expression of *DNM2*. Taken together, while the main function of classical dynamins described in cultured cells is vesicle fission in clathrin mediated endocytosis, DNM2 role in muscle may primarily involve others mechanisms in addition to endosome fissioning.

Proof-of-concept for phenotypic reversion of the severe ADCNM

As the *Dnm2*$^{SL/+}$ mouse displays a faithful and severe phenotype, it is an attractive model for testing therapies, especially those directed towards the severe CNM form. Here we tested reducing DNM2 through antisense oligonucleotides injection after the onset of phenotypes as a potential therapy for severe ADCNM, as it was reported to be efficient for other CNM forms (32).

We found striking improvement of all clinical, histological and ultrastructural phenotypes upon DNM2 reduction. Strikingly, the disease correction upon DNM2 reduction supports that the phenotypes seen at birth and in early life in affected animals and the structural alterations that may result from a muscle maturation delay or blockade are reversible. Importantly, reversion of the motor and force defects back to normal was achieved after only 3w of treatment (Figure 4F).These data support further pre-clinical developments for future clinical trials in patients with *DNM2* mutations and the severe form of ADCNM. Moreover, as antisense oligonucleotides leading to DNM2 decrease were able to rescue myotubular myopathy (32), our findings support a similar treatment can be apply to several myopathies. In addition, the fact that the rescue was obtained in the *Dnm2*$^{SL/+}$ mouse by decreasing overall DNM2 level suggests that impairment of the conformational switch leads to dominant effects. It remains to determine if specific modulation of this conformational switch will have an impact on the disease.

Methods

Animals

The *Dnm2*$^{SL/+}$ mutant mouse line was created at the Institut Clinique de la Souris (http://www.icsmci.fr/en/). Briefly, C57BL/6N mouse embryonic stem (ES) cells were electroporated with a targeting vector carrying the two transversions T>C and C>T at positions 1855 and 1856, respectively (NM_001039520.2), and a floxed neomycin resistance cassette with an auto-excission transgene. After G148 selection, different clones were analyzed by polymerase chain reaction and southern blot using an internal neomycin probe and an external 5' probe. Before injection into BALB/C blastocysts, the selected clone was karyotyped. The obtained male chimeras were bred with C57BL/6N females. Germline transmission with direct excision of the selection cassette was achieved in the first litter. The following primers were used for genotyping: Ef: CAGAAAGCAGGATCCTCGGTGCC; Er: AGTCCAGCTCTGGCTTTGGATCGC; for sequencing: Mf: CCAGAGCCCATGGTCTTAGTGGCC; Mr: ACCCCAGCGCGCAGGAACAG.

Antisense oligonucleotides treatment

The ASO1 used in this study to target *Dnm2* was produced by IONIS Pharmaceuticals (Carlsbad, California, United States), and validated previously (32). WT and *Dnm2*$^{SL/+}$ mice were treated from 3 to 8 weeks of age with weekly intraperitoneal injections of 25mg/kg of ASO1 diluted in sterile PBS. All WT and *Dnm2*$^{SL/+}$ non treated mice shown in the same graphs with ASO1 treated mice were injected with an equivalent volume of sterile PBS.

Phenotyping

From 3 to 8 weeks mice were phenotyped once per week. Body weight and whole body hanging ability were measured. Hanging test was performed by suspending the mice in a cage lid then turned upside down for up to 60 seconds and the time to fall was recorded. This experiment was repeated three times by each mouse, with a 5 minute interval to allow a recovery period.

Muscle contractile properties

TA muscle contraction properties were evaluated by measuring in situ muscle contraction after sciatic nerve stimulation using the Complete1300A mouse Test System (Aurora scientific, Aurora, Canada) as described previously (43). Mice were anesthetized by sequential intraperitoneal injections of domitor/fentanyl mix (2/0.28 mg/Kg), diazepam (8 mg/Kg) and fentanyl (0.28 mg/Kg). After, TA distal tendon was detached and tied to an isometric transducer. The sciatic nerve was then stimulated by pulses of 1-125Hz and the absolute maximal force was determined. The specific maximal force was obtained by dividing the absolute muscle force by the TA muscle weight.

Single myofiber force production

On the day of experiment, single myofibers were dissected from TA bundles in a relaxing solution. They were then individually attached between connectors leading to a force transducer and a lever arm system (model 1400A; Aurora Scientific). Sarcomere length was set to ≈2.50 µm and the temperature to 15°C. Fiber cross-sectional area (CSA) was estimated from the width and depth, assuming an elliptical circumference. The absolute maximal isometric force generation was calculated as the difference between the total tension in the activating solution (pCa 4.50) and the resting tension measured in the same myofiber while in the relaxing solution (pCa 9.0). Specific force was defined as absolute force divided by CSA. Relaxing and activating solutions contained 4 mM Mg-ATP, 1 mM free Mg^{2+}, 20 mM imidazole, 7 mM EGTA, 14.5 mM creatine phosphate, and KCl to adjust the ionic strength to 180 mM and pH to 7.0. The concentrations of free Ca^{2+} were $10^{-9.0}$ M (relaxing solution) and $10^{-4.5}$ M (activating solution).

Muscle histology

TA muscles were dissected and weighted. Muscles were then frozen in liquid nitrogen-cooled isopentane and stored at -80°C for HE, SDH and NADH histology analysis. 8 µm transversal

cryosections were prepared and stained. They were observed using the Hamamatsu 322 NanoZoomer 2HT slide-scanner (Hamamatsu, Japan).

Protein extraction and western blot

TA muscles were lysed in RIPA buffer supplemented with PMSF 1mM and complete mini-EDTA free protease inhibitor cocktail (Roche Diagnostic) using a Precellys 24 tissue homogenizer (Bertin Technologies, France). Protein concentrations were calculated using the BIO-RAD Protein Assay Kit. 20μg of protein in 5x Lane Marker Reducing Buffer (ThermoFisher Scientific) were separated in 10% SDS-PAGE gel. The gel was transferred on nitrocellulose membrane using Transblot® TurboTM RTA transfer kit (BioRad) for 7 minutes at 2.5A. Protein loading was determined by Ponceau S staining. Membranes were blocked for 1h in TBS containing 5% non-fat dry milk and 0.1% Tween20 before a 2h room-temperature or overnight 4°C incubation with DNM2 primary antibody (2865, 1/700 described in (14)). Subsequently, membranes were incubated with secondary antibody coupled to horseradish peroxidase. Nitrocellulose membranes were visualized in Amersham Imager 600 (GE Healthcare Life Sciences).

RNA extraction and qRT-PCR

RNA was isolated from TA muscle using TRI Reagent (Molecular Research Center, Cincinnati, USA). cDNA synthesis was achieved using SuperScriptIV Reverse Transcriptase (Thermo Fisher Scientific). Quantitative PCR was done with cDNA amplified and SYBER Green Master Mix I (Roche) together with 0.1 μM of forward and reverse interexonic primers. Amplicons were analyzed using a Lightcycler® 480 (Roche). The following primers were used Ub_*Dnm2*_F: ACCTACATCAGGGAGCGAGA; Ub_*Dnm2*_R: GCTCCTCTGCTGGGCATT; pan_*Dnm2*_F: ACCCCACACTTGCAGAAAAC; pan_*Dnm2*_R: CGCTTCTCAAAGTCCACTCC; 12b_*Dnm2*_F: ACCTACATCAGGGAGCGAGA; 12b_*Dnm2*_R: TGTGACCAGCTCCTCAGTATAGA; *Rpl27*_F:

AAGCCGTCATCGTGAAGAACA; *Rpl27*_R: CTTGATCTTGGATCGCTTGGC (*Rpl27* primers were described in (44)).

Electron Microscopy

Transmission electron microscopy was performed on TA muscles fixed in 2.5% paraformaldehyde (PFA), 2.5% glutaraldehyde and 50 mM CaCl2 in cacodylate buffer (0.1M, pH=7.4). Muscles were then postfixed in 1% osmium tetroxide in 0.1 M cacodylate buffer for 1 h at 4°C and incubated with 5% uranyl acetate for 2 h at 4°C. The samples were embedded in Epon 812. Ultrathin sections were cut at 70 nm and contrasted with uranyl acetate and lead citrate, they were finally observed with a Philips CM12 electron microscope equipped with a Gatan OneView Camera (Gatan, USA).

Immunostaining of muscle longitudinal sections

For longitudinal immunostaining, TA muscles were fixed as described before (32). After PFA 4% and sucrose 30% incubation, fiber bundles were manually isolated and mounted in SuperFrost Plus™ adhesion microscopy slides (Thermo Fisher Scientific). Subsequent immunostaining was performed using the following primary antibodies: anti-DNM2 (dilution used 1/100, 2680, described in (14)), anti-RYR1 (dilution used 1/100, R129, Sigma-Aldrich) and anti-Alpha-actinin (dilution used 1/100, A7811, Sigma-Aldrich). The secondary antibody used was donkey anti-rabbit Alexa-594 or goat anti-mouse Alexa-647 (Life Technologies), the dilution used was 1/250. To detect neuromuscular junction we used alpha-Bungarotoxin CF®488A Conjugate (Biotium), the dilution used was 1/1000.

Statistical analysis

All data was verified for normal distribution using Shapiro-Wilk test and for homoscedascity with the Brown-Forsythe test. Normal and homoscedastic data was analyzed using T-test, in case of two-group comparison, or One-way ANOVA followed by post hoc Tukey's test in case of multiple

group analysis. For non-normally distributed or heteroscedastic data, T test with Welch's correction or non-parametric one-way ANOVA (Kruskal Wallis) with posthoc Dunn's test were done respectively. All statistical tests used were two-sided. Multiple timepoints were analyzed separately. Charts show individual points with additional lines indicating mean ± SEM. Curves and graphs were made using GraphPad Prism software.

Study approval

Animal care and experimentation was in accordance with French and European legislation and approved by the institutional ethics committee (project numbers 01594.02, 2016052510176016 and 2016031110589922). Mice were kept on 12h day light and 12h dark cycle with free access to standard food and water. Lifespan and body weight were followed during this study.

Authors contribution

JL conceived the project. XMM, RSR, JO, NBR, BSC, JL designed the experiments and analyzed the data. XMM, CK, RSR, JO, AM performed experiments. XMM and JL wrote the manuscript.

Acknowledgements

We would like to thank Raquel Gómez Oca, Charlotte Gineste, David Reiss, William Magnant, Nadia Messaddeq Jean-Luc Weickert, Guy Brochier and Clémence Labasse for help and excellent technical assistance, Shuling Guo and Brett Monia for providing the ASO1 oligonucleotide, ICS and IGBMC animal houses. We thank Ayesha Eduljee for constructive criticism of the manuscript. The creation of the *Dnm2*$^{SL/+}$ mouse was done with Phenomin-ICS, Illkirch, France. This study was supported by INSERM, CNRS, Strasbourg University, ANR Dynather (ANR-18-CE17-0006-02), and ANR-10-LABX-0030-INRT, a French State fund managed by the Agence Nationale de la Recherche under the frame program Investissements d'Avenir ANR-10-IDEX-0002-02. Xènia Massana Muñoz is an IGBMC International PhD Programme fellow supported by LabEx INRT funds. Roberto Silva-Rojas is funded by Fondation Recherche Médicale fellowship (PLP20170939073).

Conflict of interest statement

B.S.C. and J.L. are cofounders of Dynacure. B.S.C. is currently employed by Dynacure.

References

1. Antonny B, Burd C, De Camilli P, Chen E, Daumke O, Faelber K, Ford M, Frolov VA, Frost A, Hinshaw JE, et al. Membrane fission by dynamin: what we know and what we need to know. *EMBO J.* 2016;35(21):2270-84.
2. Ferguson SM, and De Camilli P. Dynamin, a membrane-remodelling GTPase. *Nat Rev Mol Cell Biol.* 2012;13(2):75-88.
3. Schmid SL, and Frolov VA. Dynamin: functional design of a membrane fission catalyst. *Annu Rev Cell Dev Biol.* 2011;27(79-105.
4. Bitoun M, Maugenre S, Jeannet PY, Lacene E, Ferrer X, Laforet P, Martin JJ, Laporte J, Lochmuller H, Beggs AH, et al. Mutations in dynamin 2 cause dominant centronuclear myopathy. *Nat Genet.* 2005;37(11):1207-9.
5. Zuchner S, Mersiyanova IV, Muglia M, Bissar-Tadmouri N, Rochelle J, Dadali EL, Zappia M, Nelis E, Patitucci A, Senderek J, et al. Mutations in the mitochondrial GTPase mitofusin 2 cause Charcot-Marie-Tooth neuropathy type 2A. *Nat Genet.* 2004;36(5):449-51.
6. Sambuughin N, Goldfarb LG, Sivtseva TM, Davydova TK, Vladimirtsev VA, Osakovskiy VL, Danilova AP, Nikitina RS, Ylakhova AN, Diachkovskaya MP, et al. Adult-onset autosomal dominant spastic paraplegia linked to a GTPase-effector domain mutation of dynamin 2. *BMC Neurol.* 2015;15(223.
7. Koutsopoulos OS, Kretz C, Weller CM, Roux A, Mojzisova H, Bohm J, Koch C, Toussaint A, Heckel E, Stemkens D, et al. Dynamin 2 homozygous mutation in humans with a lethal congenital syndrome. *Eur J Hum Genet.* 2013;21(6):637-42.
8. Wallgren-Pettersson C, Clarke A, Samson F, Fardeau M, Dubowitz V, Moser H, Grimm T, Barohn RJ, and Barth PG. The myotubular myopathies: differential diagnosis of the X linked recessive, autosomal dominant, and autosomal recessive forms and present state of DNA studies. *JMedGenet.* 1995;32(673-9.

9. Romero NB. Centronuclear myopathies: a widening concept. *Neuromuscul Disord.* 2010;20(4):223-8.

10. Bohm J, Biancalana V, Dechene ET, Bitoun M, Pierson CR, Schaefer E, Karasoy H, Dempsey MA, Klein F, Dondaine N, et al. Mutation spectrum in the large GTPase dynamin 2, and genotype-phenotype correlation in autosomal dominant centronuclear myopathy. *Hum Mutat.* 2012;33(6):949-59.

11. Bitoun M, Bevilacqua JA, Prudhon B, Maugenre S, Taratuto AL, Monges S, Lubieniecki F, Cances C, Uro-Coste E, Mayer M, et al. Dynamin 2 mutations cause sporadic centronuclear myopathy with neonatal onset. *Ann Neurol.* 2007;62(6):666-70.

12. Gibbs EM, Davidson AE, Telfer WR, Feldman EL, and Dowling JJ. The myopathy-causing mutation DNM2-S619L leads to defective tubulation in vitro and in developing zebrafish. *Dis Model Mech.* 2014;7(1):157-61.

13. Chin YH, Lee A, Kan HW, Laiman J, Chuang MC, Hsieh ST, and Liu YW. Dynamin-2 mutations associated with centronuclear myopathy are hypermorphic and lead to T-tubule fragmentation. *Hum Mol Genet.* 2015;24(19):5542-54.

14. Cowling BS, Toussaint A, Amoasii L, Koebel P, Ferry A, Davignon L, Nishino I, Mandel JL, and Laporte J. Increased expression of wild-type or a centronuclear myopathy mutant of dynamin 2 in skeletal muscle of adult mice leads to structural defects and muscle weakness. *Am J Pathol.* 2011;178(5):2224-35.

15. Bragato C, Gaudenzi G, Blasevich F, Pavesi G, Maggi L, Giunta M, Cotelli F, and Mora M. Zebrafish as a Model to Investigate Dynamin 2-Related Diseases. *Sci Rep.* 2016;6(20466.

16. Massana Muñoz X, Buono S, Koebel P, Laporte J, and Cowling BS. Different in vivo impacts of dynamin 2 mutations implicated in Charcot–Marie–Tooth neuropathy or centronuclear myopathy. *Human Molecular Genetics.* 2019.

17. Durieux AC, Vignaud A, Prudhon B, Viou MT, Beuvin M, Vassilopoulos S, Fraysse B, Ferry A, Laine J, Romero NB, et al. A centronuclear myopathy-dynamin 2 mutation impairs skeletal muscle structure and function in mice. *Hum Mol Genet.* 2010;19(24):4820-36.

18. Gibbs EM, Clarke NF, Rose K, Oates EC, Webster R, Feldman EL, and Dowling JJ. Neuromuscular junction abnormalities in DNM2-related centronuclear myopathy. *J Mol Med (Berl).* 2013;91(6):727-37.

19. Robb SA, Sewry CA, Dowling JJ, Feng L, Cullup T, Lillis S, Abbs S, Lees MM, Laporte J, Manzur AY, et al. Impaired neuromuscular transmission and response to acetylcholinesterase inhibitors in centronuclear myopathies. *Neuromuscul Disord.* 2011;21(6):379-86.

20. Trochet D, Prudhon B, Jollet A, Lorain S, and Bitoun M. Reprogramming the Dynamin 2 mRNA by Spliceosome-mediated RNA Trans-splicing. *Mol Ther Nucleic Acids.* 2016;5(9):e362.

21. Tasfaout H, Lionello VM, Kretz C, Koebel P, Messaddeq N, Bitz D, Laporte J, and Cowling BS. Single Intramuscular Injection of AAV-shRNA Reduces DNM2 and Prevents Myotubular Myopathy in Mice. *Mol Ther.* 2018;26(4):1082-92.

22. Buono S, Ross JA, Tasfaout H, Levy Y, Kretz C, Tayefeh L, Matson J, Guo S, Kessler P, Monia BP, et al. Reducing dynamin 2 (DNM2) rescues DNM2-related dominant centronuclear myopathy. *Proc Natl Acad Sci U S A.* 2018;115(43):11066-71.

23. Trochet D, Prudhon B, Beuvin M, Peccate C, Lorain S, Julien L, Benkhelifa-Ziyyat S, Rabai A, Mamchaoui K, Ferry A, et al. Allele-specific silencing therapy for Dynamin 2-related dominant centronuclear myopathy. *EMBO Mol Med.* 2018;10(2):239-53.

24. Srinivasan S, Dharmarajan V, Reed DK, Griffin PR, and Schmid SL. Identification and function of conformational dynamics in the multidomain GTPase dynamin. *EMBO J.* 2016;35(4):443-57.

25. Kenniston JA, and Lemmon MA. Dynamin GTPase regulation is altered by PH domain mutations found in centronuclear myopathy patients. *Embo J.* 2010;29(18):3054-67.

26. Wang L, Barylko B, Byers C, Ross JA, Jameson DM, and Albanesi JP. Dynamin 2 mutants linked to centronuclear myopathies form abnormally stable polymers. *J Biol Chem.* 2010;285(30):22753-7.

27. Liu N, Bezprozvannaya S, Shelton JM, Frisard MI, Hulver MW, McMillan RP, Wu Y, Voelker KA, Grange RW, Richardson JA, et al. Mice lacking microRNA 133a develop dynamin 2-dependent centronuclear myopathy. *J Clin Invest.* 2011;121(8):3258-68.

28. Faelber K, Posor Y, Gao S, Held M, Roske Y, Schulze D, Haucke V, Noe F, and Daumke O. Crystal structure of nucleotide-free dynamin. *Nature.* 2011;477(7366):556-60.

29. Jimah JR, and Hinshaw JE. Structural Insights into the Mechanism of Dynamin Superfamily Proteins. *Trends Cell Biol.* 2019;29(3):257-73.

30. Mattila JP, Shnyrova AV, Sundborger AC, Hortelano ER, Fuhrmans M, Neumann S, Muller M, Hinshaw JE, Schmid SL, and Frolov VA. A hemi-fission intermediate links two mechanistically distinct stages of membrane fission. *Nature.* 2015;524(7563):109-13.

31. Koutsopoulos OS, Koch C, Tosch V, Bohm J, North KN, and Laporte J. Mild functional differences of dynamin 2 mutations associated to centronuclear myopathy and charcot-marie-tooth peripheral neuropathy. *PLoS One.* 2011;6(11):e27498.

32. Tasfaout H, Buono S, Guo S, Kretz C, Messaddeq N, Booten S, Greenlee S, Monia BP, Cowling BS, and Laporte J. Antisense oligonucleotide-mediated Dnm2 knockdown prevents and reverts myotubular myopathy in mice. *Nat Commun.* 2017;8(15661.

33. Bitoun M, Stojkovic T, Prudhon B, Maurage CA, Latour P, Vermersch P, and Guicheney P. A novel mutation in the dynamin 2 gene in a Charcot-Marie-Tooth type 2 patient: clinical and pathological findings. *Neuromuscul Disord.* 2008;18(4):334-8.

34. Chen S, Huang P, Qiu Y, Zhou Q, Li X, Zhu M, and Hong D. Phenotype variability and histopathological findings in patients with a novel DNM2 mutation. *Neuropathology : official journal of the Japanese Society of Neuropathology.* 2018;38(1):34-40.

35. Claeys KG, Zuchner S, Kennerson M, Berciano J, Garcia A, Verhoeven K, Storey E, Merory JR, Bienfait HM, Lammens M, et al. Phenotypic spectrum of dynamin 2 mutations in Charcot-Marie-Tooth neuropathy. *Brain.* 2009;132(Pt 7):1741-52.

36. Fraysse B, Guicheney P, and Bitoun M. Calcium homeostasis alterations in a mouse model of the Dynamin 2-related centronuclear myopathy. *Biology Open.* 2016;5(1691-6.

37. Kutchukian C, Szentesi P, Allard B, Trochet D, Beuvin M, Berthier C, Tourneur Y, Guicheney P, Csernoch L, Bitoun M, et al. Impaired excitation-contraction coupling in muscle fibres from the dynamin2(R465W) mouse model of centronuclear myopathy. *J Physiol.* 2017;595(24):7369-82.

38. Tinelli E, Pereira JA, and Suter U. Muscle-specific function of the centronuclear myopathy and Charcot-Marie-Tooth neuropathy-associated dynamin 2 is required for proper lipid metabolism, mitochondria, muscle fibers, neuromuscular junctions and peripheral nerves. *Hum Mol Genet.* 2013;22(21):4417-29.

39. Lee JE, Westrate LM, Wu H, Page C, and Voeltz GK. Multiple dynamin family members collaborate to drive mitochondrial division. *Nature.* 2016;540(7631):139-43.

40. Fonseca TB, Sanchez-Guerrero A, Milosevic I, and Raimundo N. Mitochondrial fission requires DRP1 but not dynamins. *Nature.* 2019;570(7761):E34-E42.

41. Kamerkar SC, Kraus F, Sharpe AJ, Pucadyil TJ, and Ryan MT. Dynamin-related protein 1 has membrane constricting and severing abilities sufficient for mitochondrial and peroxisomal fission. *Nat Commun.* 2018;9(1):5239.

42. Cowling BS, Prokic I, Tasfaout H, Rabai A, Humbert F, Rinaldi B, Nicot AS, Kretz C, Friant S, Roux A, et al. Amphiphysin (BIN1) negatively regulates dynamin 2 for normal muscle maturation. *J Clin Invest.* 2017;127(12):4477-87.

43. Silva-Rojas R, Treves S, Jacobs H, Kessler P, Messaddeq N, Laporte J, and Bohm J. STIM1 over-activation generates a multi-systemic phenotype affecting the skeletal muscle, spleen, eye, skin, bones and immune system in mice. *Hum Mol Genet.* 2019;28(10):1579-93.

44. de Jonge HJ, Fehrmann RS, de Bont ES, Hofstra RM, Gerbens F, Kamps WA, de Vries EG, van der Zee AG, te Meerman GJ, and ter Elst A. Evidence based selection of housekeeping genes. *PLoS One.* 2007;2(9):e898.

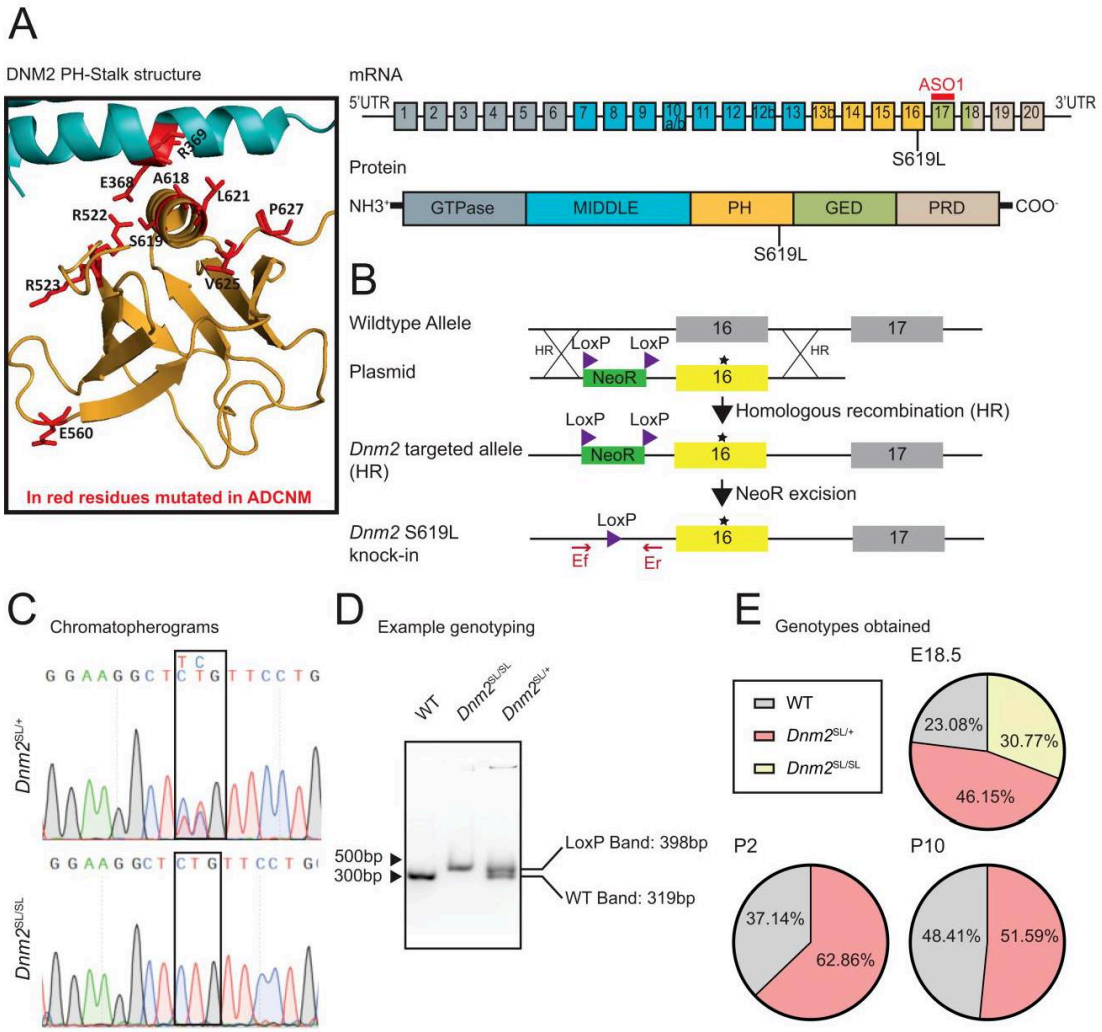

Figure 1. Creation and validation of the *Dnm2*$^{SL/+}$ mouse with the S619L *Dnm2* mutation. (A) Left: Structure of the PH-stalk interface in a closed conformation modelled from the structure of dynamin 3 tetramer (PDB ID:5A3F). Residues mutated in ADCNM are in red. The S619 residue is located on the PH domain at the PH-stalk interface. Right: Exonic and protein domain structure of DNM2. ASO1 is an antisense oligonucleotide targeting murine *Dnm2*. Exons 10a, 10b, 12b, 13b are alternatively spliced exons. PH: Pleckstrin Homology; GED: GTPase Effector Domain; PRD: Proline Rich Domain; the middle and GED domains form the stalk. (B) Genomic region, plasmid and strategy for homologous recombination. (C) Chromatopherograms of the *Dnm2* mutation identified in heterozygous and homozygous mice. (D) Example of DNA genotyping. (E) Proportion of genotypes obtained at 18.5 days post-coitum (dpc) (n=15), postnatal day 2 (n=35) and day 10 (n=130).

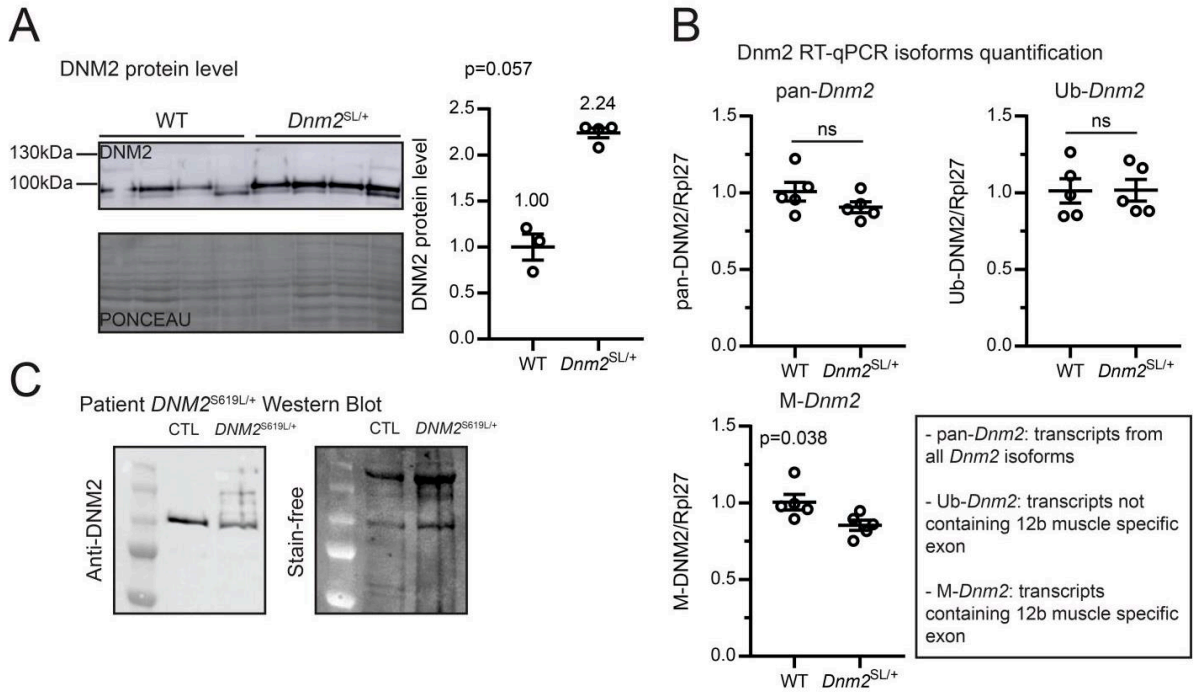

Figure 2. *Dnm2*$^{SL/+}$ animals display an increased DNM2 level. (A) DNM2 protein level in TA muscles of 8w old WT and *Dnm2*$^{SL/+}$ ($3 \leq n \leq 5$; Mann-Whitney Test). (B) *Dnm2* isoforms quantification. Pan-*Dnm2* corresponds to all isoforms, Ub-*Dnm2* to ubiquitous isoforms not including the muscle-specific exon 12b, M-*Dnm2* to isoforms including the muscle-specific exon 12b (n=5; Unpaired t Test). (C) Western blot of DNM2 in muscle from a patient with the *DNM2* S619L mutation compared to control. ns not significant comparing WT vs *Dnm2*$^{SL/+}$. Charts show individual points with additional lines indicating mean ± SEM.

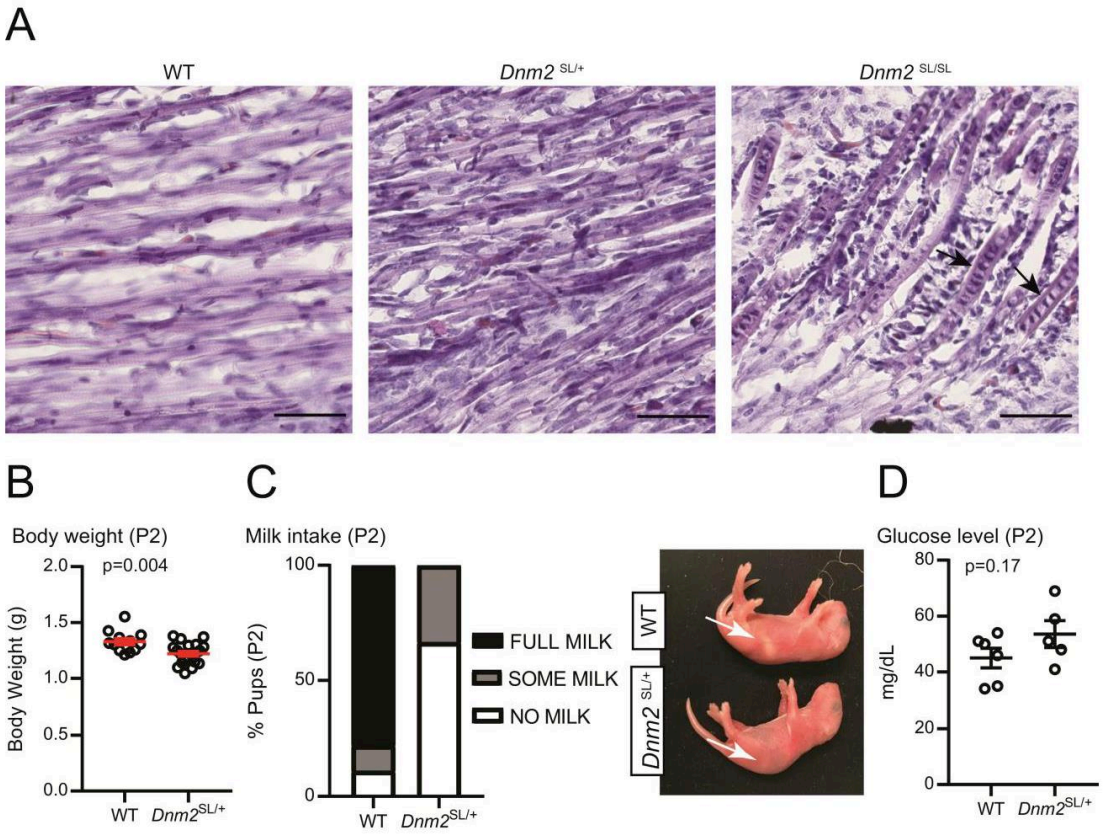

Figure 3. *Dnm2*$^{SL/+}$ pups display reduced body weight and delayed muscle maturation. (A) Haematoxylin-eosin (HE) staining of lower limb muscles from E18.5 WT, *Dnm2*$^{SL/+}$ and *Dnm2*$^{SL/SL}$ embryos. Arrows point to myonuclei chains. Scale bar=50μm. (B-D) Body weight ($12 \leq n \leq 20$; Unpaired t Test) (B), milk intake (graph shows average for each group and genotype, $12 \leq n \leq 20$) (C), and glucose level in blood ($5 \leq n \leq 6$; Unpaired t Test) (D) in P2 WT and *Dnm2*$^{SL/+}$ pups. Charts show individual points with additional lines indicating mean ± SEM.

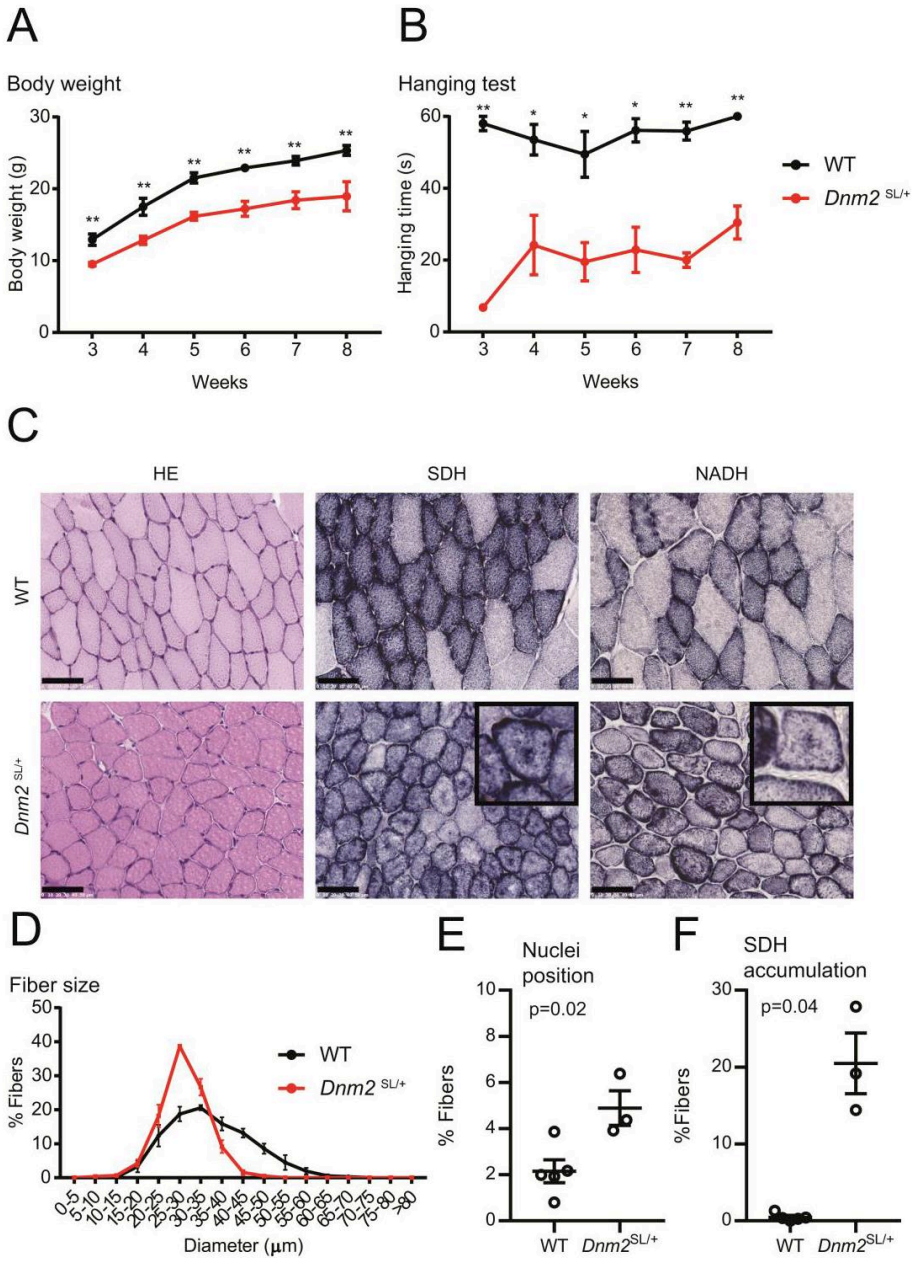

Figure 4. *Dnm2*$^{SL/+}$ develop a severe muscle phenotype resembling centronuclear myopathy (A) Body weight (n=5; Unpaired T test for each individual timepoint) (B) and hanging test performance (n=5; Unpaired t Test for each individual timepoint) between 3 and 8 weeks in WT and *Dnm2*$^{SL/+}$ mice. Maximum hanging time is 60 s. Both graphs show average value for each timepoint and genotype with additional lines indicating SEM. (C) HE, Succinate dehydrogenase (SDH) and reduced nicotinamide adenine dinucleotide (NADH) staining of TA muscle sections from WT and *Dnm2*$^{SL/+}$ mice at 8w (n=5 per staining and group). Note the central accumulation of SDH stain specifically in the *Dnm2*$^{SL/+}$ muscle. Scale bar=50µm. (D-F) Quantifications of fiber size ($3 \le n \le 5$, graph shows average value ± SEM for each diameter and genotype) (D), nuclei internalization and centralization ($3 \le n \le 5$; Unpaired t Test) (E), and percentage of fibers with central accumulation of SDH stain ($3 \le n \le 5$; Welch's t Test) (F). **p<0.01; *p < 0.05 comparing WT vs *Dnm2*$^{SL/+}$. Charts show individual points with additional lines indicating mean ± SEM unless differently stated.

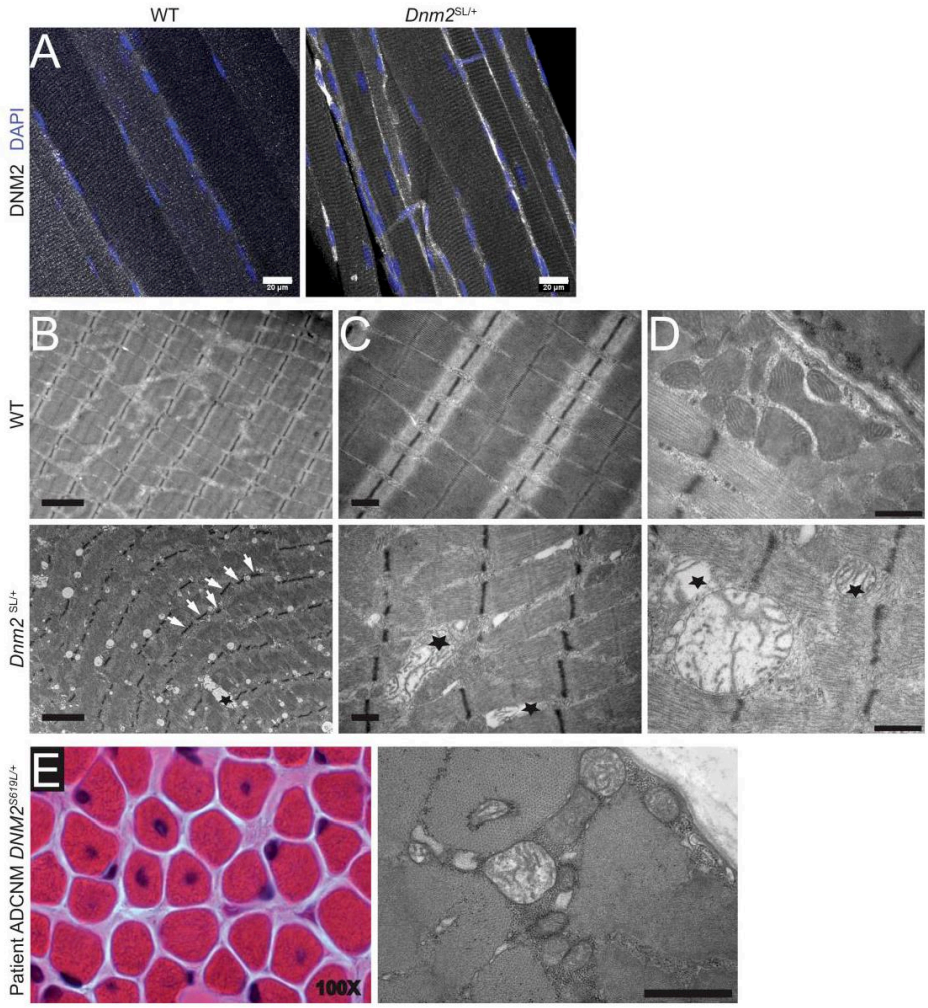

Figure 5. Abnormal mitochondria structure in the *Dnm2*$^{SL/+}$ mice. (A) Subcellular localization of DNM2 by immunofluorescence in longitudinal sections from TA muscles at 8w. Scale bar=20µm. (B) Ultrastructural analysis by electron microscopy in WT and *Dnm2*$^{SL/+}$ TA muscles at 8w (n=2 replicates per group). Arrows point to Z-line mis-alignment and stars indicate swollen mitochondria. Scale bar=2µm. (C-D) Higher magnification showing swollen mitochondria with disrupted cristae in the *Dnm2*$^{SL/+}$ muscle only. (C) Scale bar=0.5µm (D) Scale bar=500nm. (E) Electron microscopy (scale bar = 2µm) and HE (100x magnification) representative images from a muscle from a patient carrying the S619L mutation.

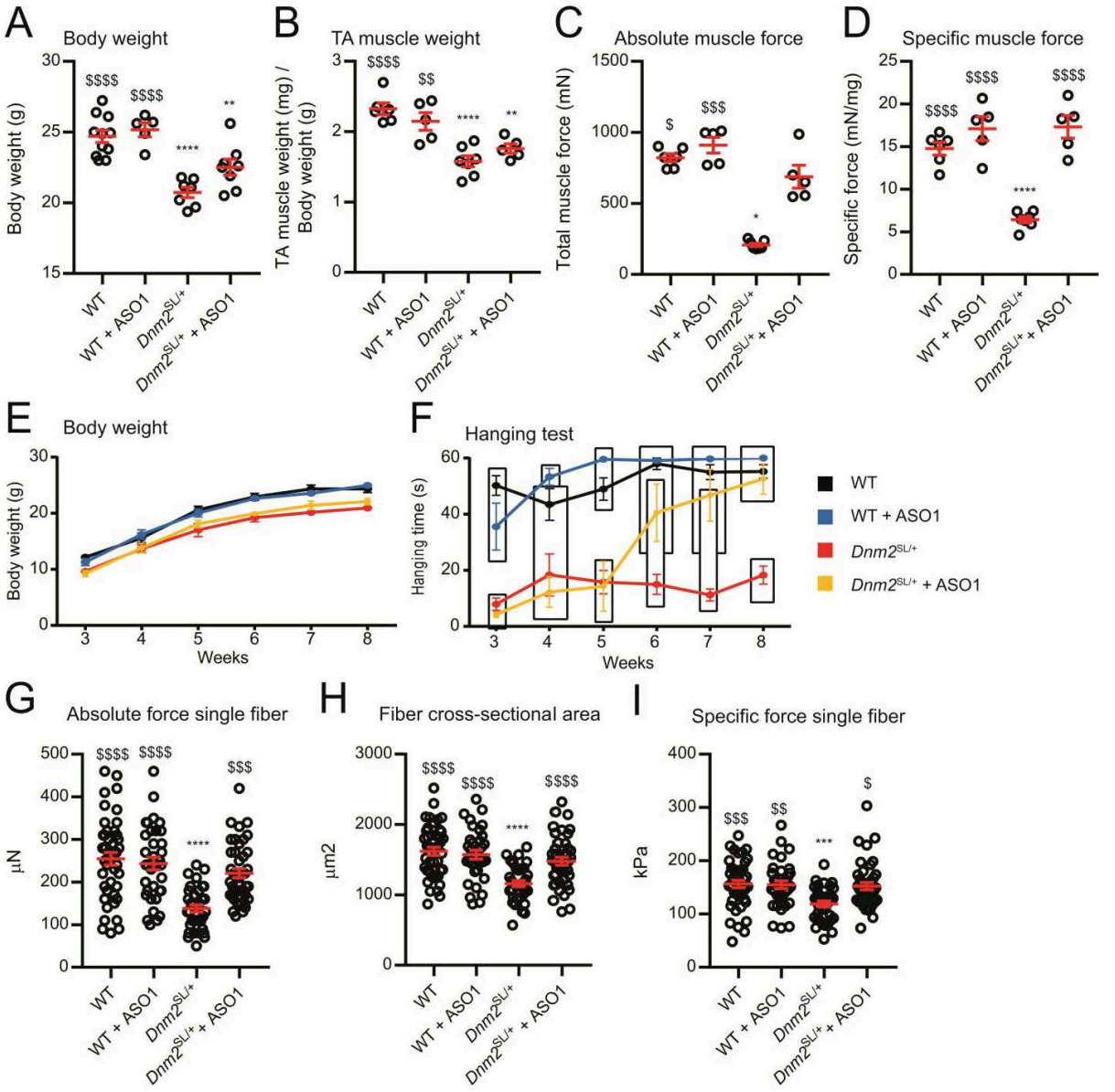

Figure 6. DNM2 reduction reverts the motor defects of the *Dnm2*$^{SL/+}$ mice. (A-D) Body weight (5 ≤ n ≤ 11; One-way ANOVA with Tukey's post hoc test) (A), TA muscle weight (5 ≤ n ≤ 7; One-way ANOVA with Tukey's post hoc test) (B), absolute muscle force (5 ≤ n ≤ 7; Kruskal-Wallis Test with Dunn's post hoc test) (C) and specific muscle force (5 ≤ n ≤ 7; One-way ANOVA with Tukey's post hoc test) (D) measured at 8w in WT and *Dnm2*$^{SL/+}$ mice treated or not with ASO1 antisense oligonucleotide targeting *Dnm2*. (E-F) Body weight and hanging performance of WT and *Dnm2*$^{SL/+}$ mice treated or not with ASO1 between 3 and 8 weeks (6 ≤ n ≤ 7). Blocks show groups with non-significant difference in hanging test performance (One-way ANOVA with Tukey's posthoc test for each individual timepoint). Note the hanging performance of the treated *Dnm2*$^{SL/+}$ mice reaches non statistical significance with WT at week 6. Both curves show average values ± SEM for each timepoint and genotype. (G-I) Absolute muscle force (Kruskal-Wallis test with Dunn's post hoc test) (G), fiber cross-sectional area (One-way ANOVA with Tukey's post hoc test) (H) and specific muscle force (Kruskal-Wallis test with Dunn's post hoc test) (I) measured in single myofibers from 8w old WT and Dnm2SL/+ mice treated or not with ASO1 antisense oligonucleotide targeting Dnm2 (35 ≤ n ≤ 43). ****p<0.0001; ***p < 0.001; **p<0.01; *p < 0.05 comparing vs WT. $$$$p<0.0001; $$$p < 0.001; $$p<0.01; $p < 0.05 vs *Dnm2*$^{SL/+}$. Charts show individual points with additional lines indicating mean ± SEM unless differently stated.

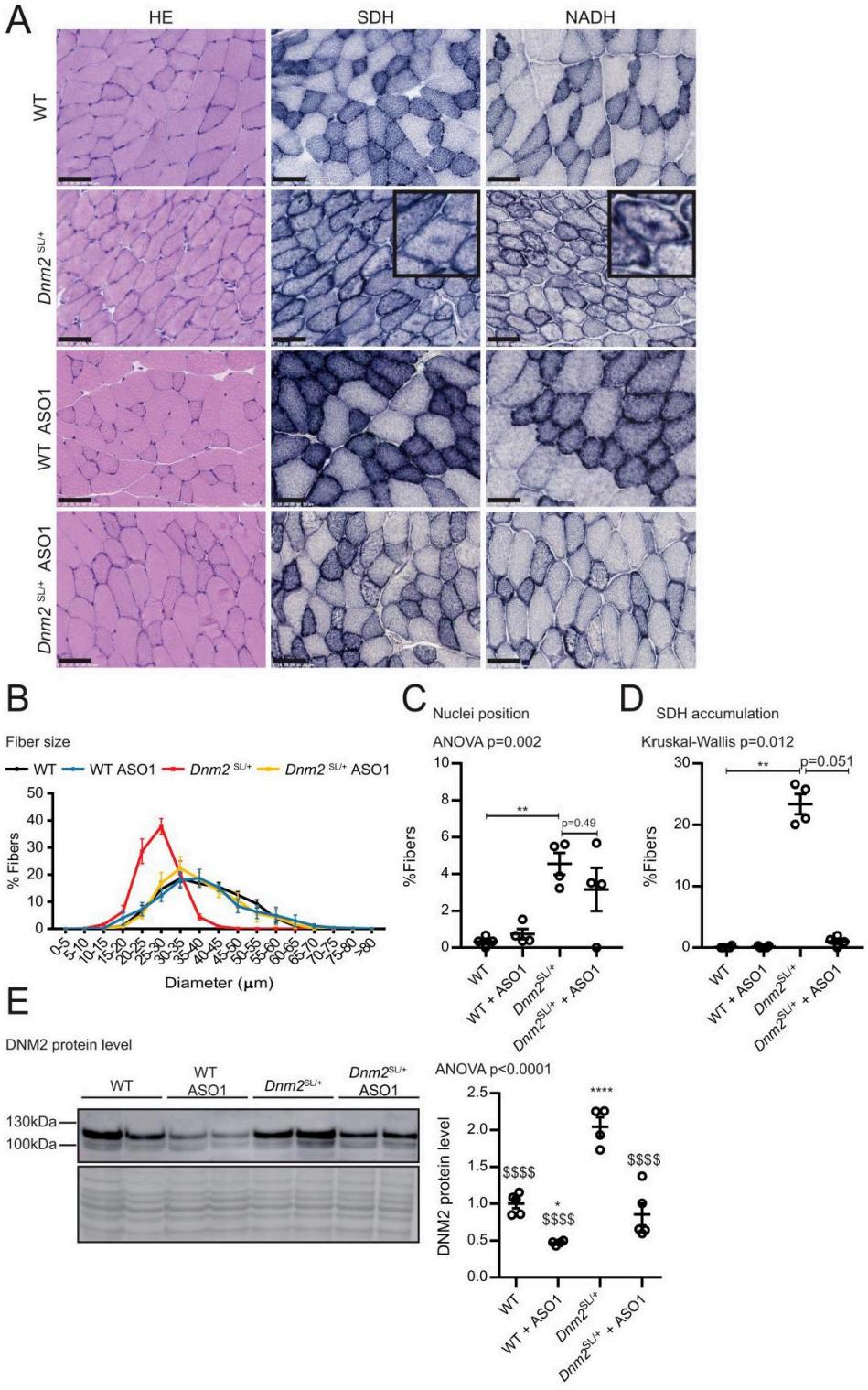

Figure 7. CNM histological hallmarks of *Dnm2*$^{SL/+}$ mice are ameliorated upon DNM2 reduction. (A) HE, SDH and NADH stainings of TA muscle sections from 8w old WT and *Dnm2*$^{SL/+}$ mice treated or not with ASO1. Scale bar=50µm (n=5 per group and staining). (B-D) Quantification of fiber size (n=4, graph shows average value ± SEM for each diameter and genotype) (B), nuclei internalization and centralization (n=4) (C), and percentage of fibers with central accumulation of SDH stain (n=4) (D). (E) DNM2 protein level in TA muscles of 8w old WT and *Dnm2*$^{SL/+}$ mice treated or not with ASO1

(4 ≤ n ≤ 5; One way ANOVA with Tukey's post hoc test). ****p<0.0001; ***p < 0.001; **p<0.01; *p < 0.05 comparing vs WT. $$$$p<0.0001; $$$p < 0.001; $$p<0.01; $p < 0.05 vs *Dnm2*$^{SL/+}$. Charts show individual points with additional lines indicating mean ± SEM unless differently stated.

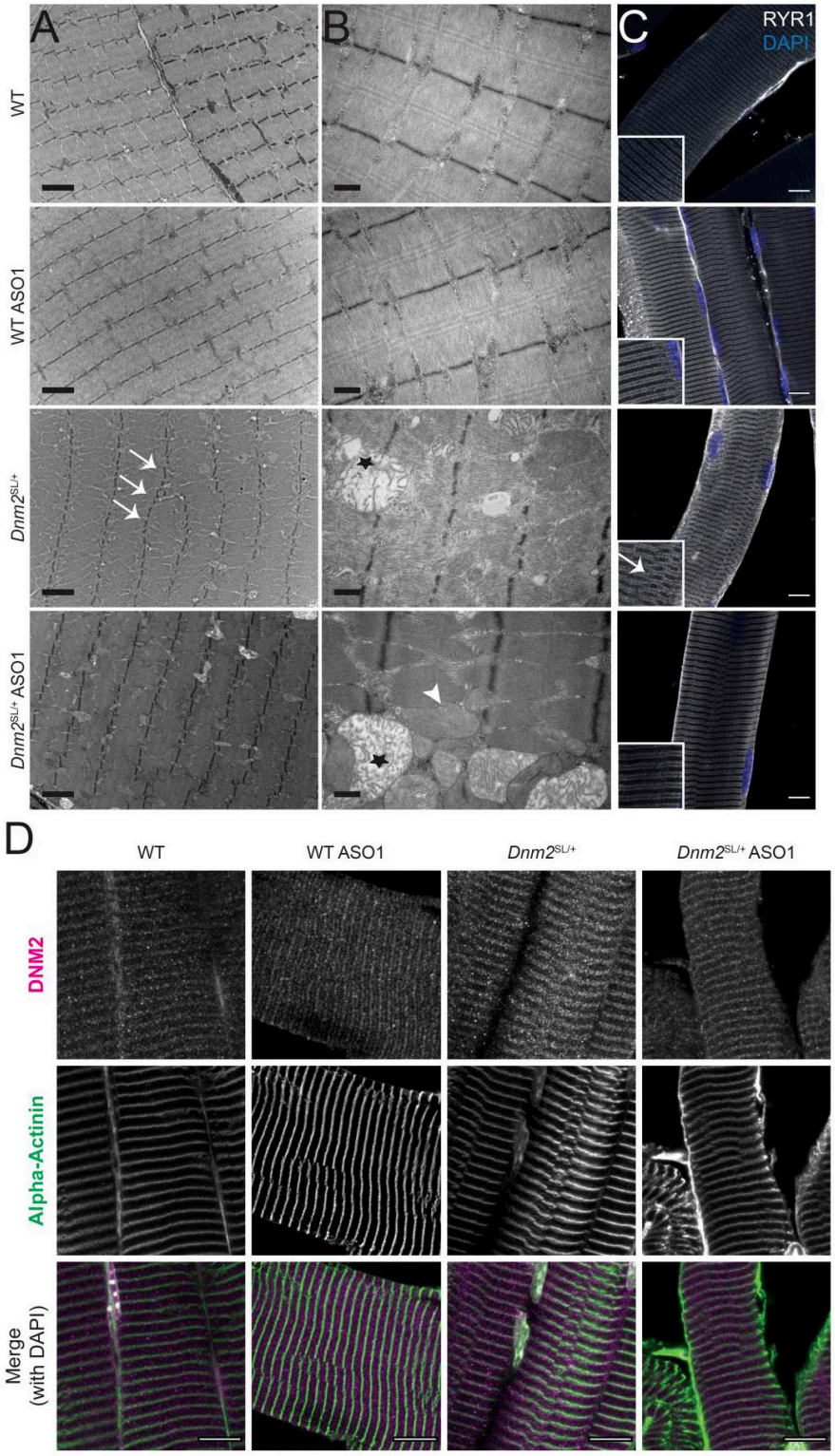

Figure 8. Ultrastructural analysis of *Dnm2*$^{SL/+}$ muscles upon DNM2 reduction (A) Ultrastructural view by electron microscopy in TA muscles from 8w old WT and *Dnm2*$^{SL/+}$ treated or not with ASO1 antisense oligonucleotide targeting *Dnm2* (n=2). Arrows point to Z-line mis-alignment and stars indicate swollen mitochondria. Scale bar=2μm. (B) Higher

magnification on mitochondria showing two populations in the ASO1 treated *Dnm2*$^{SL/+}$ mice: swollen mitochondria with disrupted cristae (indicated by a star) and normal mitochondria (indicated by arrowhead). Scale bar=0.5μm. (C-D) Immunofluorescence in TA muscles from 8w old mice (n=2) of RYR1 (ryanodine receptor, a marker of sarcoplasmic reticulum at the triad) and DAPI for nuclei. Arrow point to mis-alignment (C) and of DNM2 together with Alpha-actinin (a marker of Z-line) and DAPI for nuclei. Scale bar = 10μm.

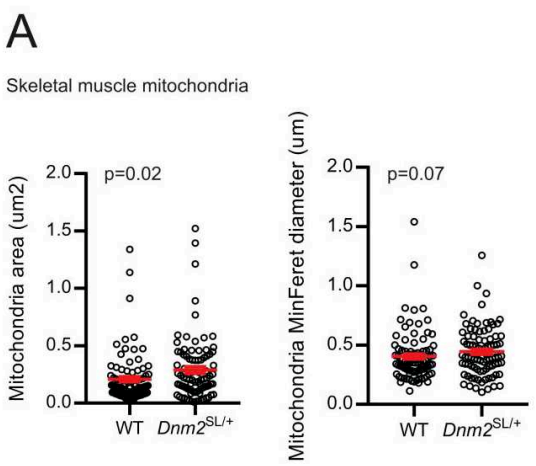

Supplementary Figure 1. Increased area of *Dnm2*$^{SL/+}$ tibialis anterior mitochondria.

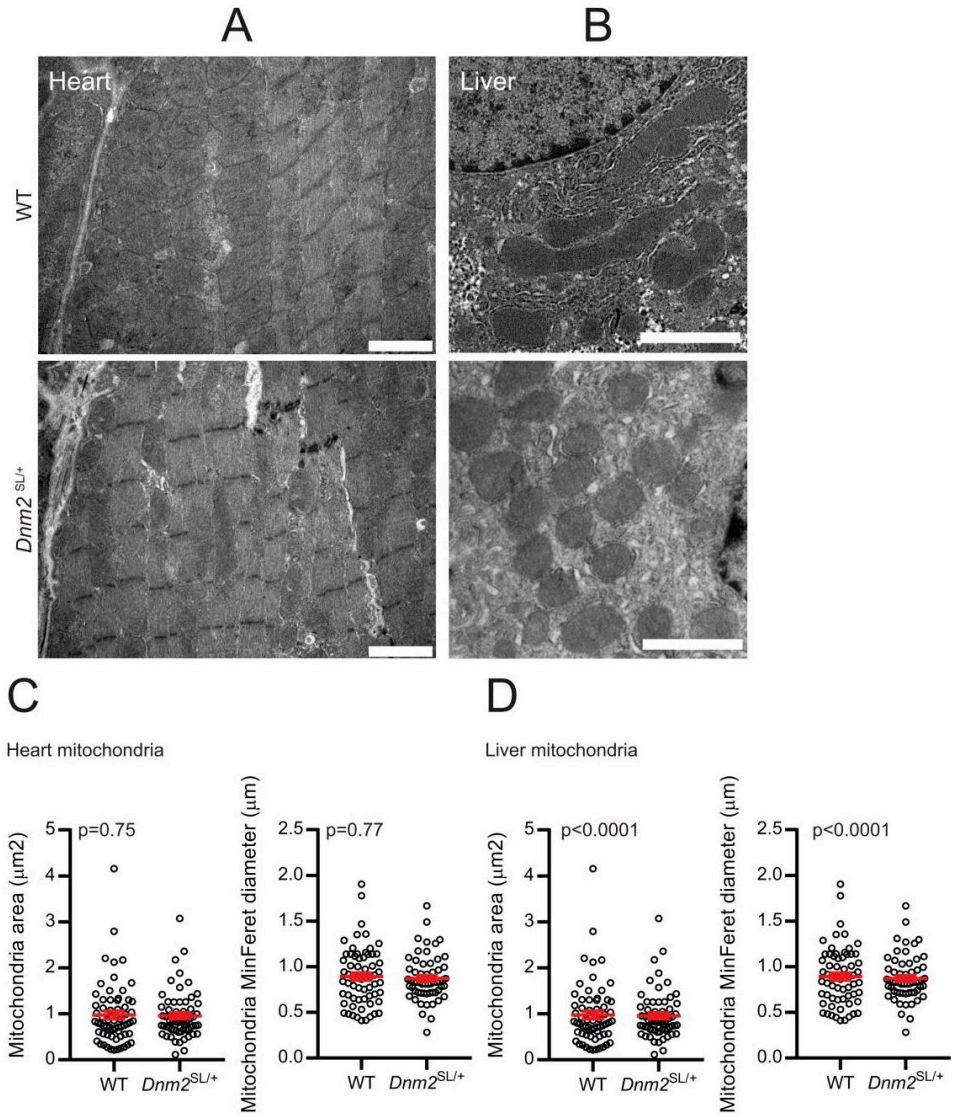

Supplementary Figure 2. Analysis of heart and liver mitochondria. (A-B) Representative images from heart (A) and liver (B) mitochondria (Scalebar = 2µm). (C-D) Quantification of area and Minimum Feret diameter in heart (C) and liver (D) reporting differences in liver mitochondrial size. (In both cases 60≤n≤88 mitochondria (2 animals, 3 different regions of interest), Mann Whitney test).

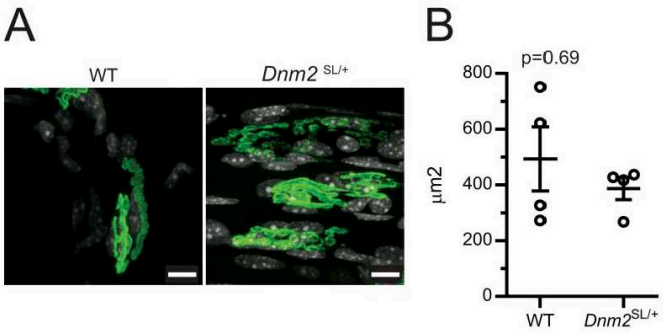

Supplementary Figure 3. Neuromuscular junction staining. (A) Representative images of α-bungarotoxin staining (in green) and DAPI (in gray) in fibers from 8w old WT and *Dnm2*$^{SL/+}$ mice. Scale bar=10µm. (B) Quantification of neuromuscular junction area (n=4).

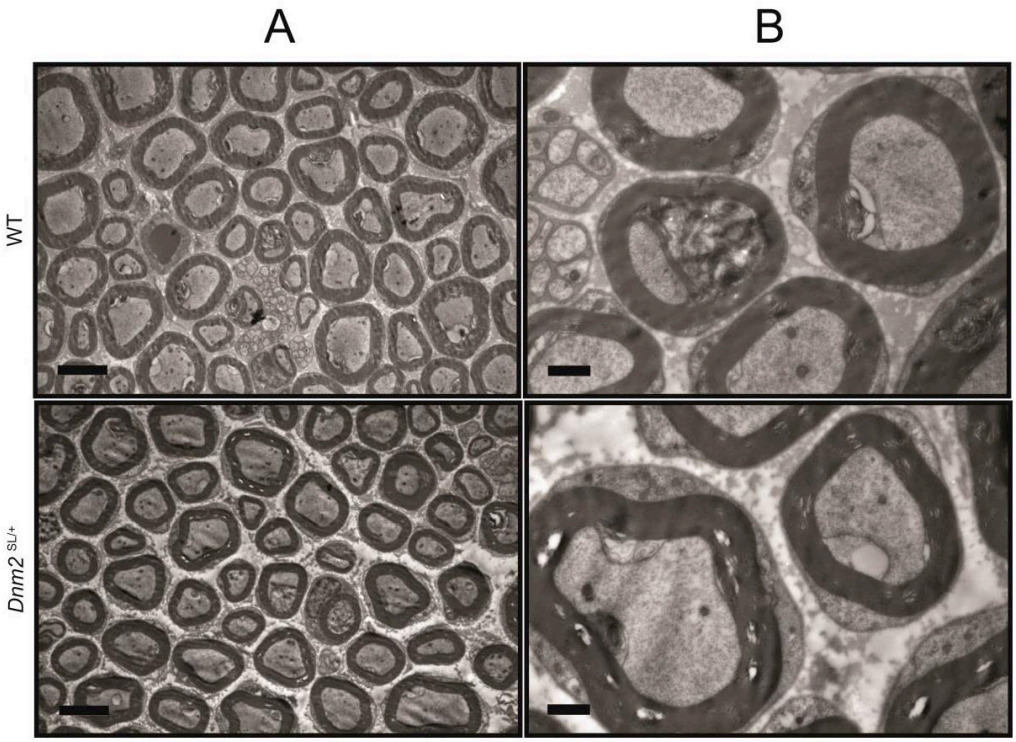

Supplementary Figure 4. Transmission electron microscopy images from sciatic nerve. (A) Transversal sections of sciatic nerve from 8w old WT and *Dnm2*$^{SL/+}$ mice. Scale bar=5μm. (B) Higher magnification of the same sciatic nerves from 8w old WT and *Dnm2*$^{SL/+}$ mice. Scale bar=1μm.

Figure 1F

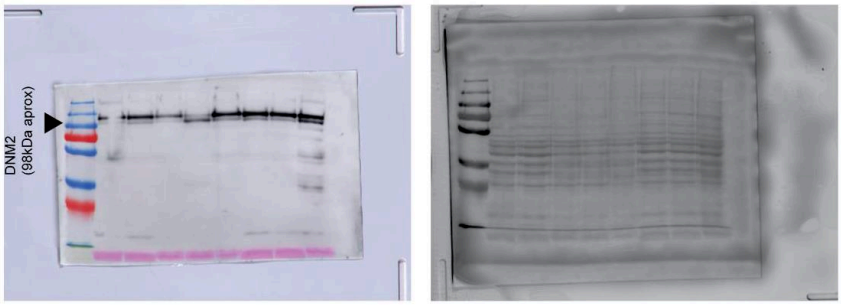

Figure 5H

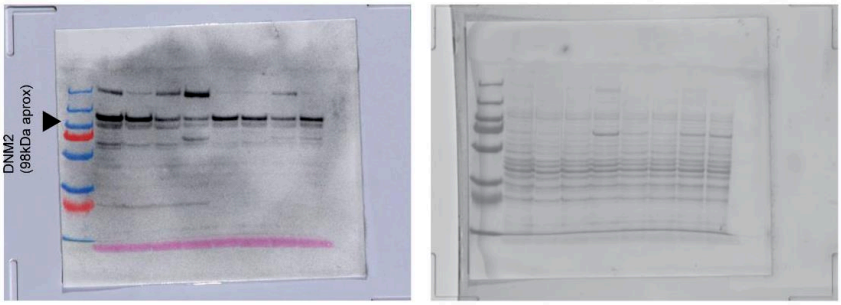

Supplementary figure 5. Uncropped full-length Western blot images.

Supplementary movie 1. Hanging test performance of *Dnm2*$^{SL/+}$ treated with ASO. Video showing two 8 weeks old *Dnm2*$^{SL/+}$ mice untreated and treated with ASO performing hanging test.

Publication 3: Tamoxifen prolongs survival and alleviates symptoms in mice with fatal X-linked myotubular myopathy

Introduction

XLCNM is a severe congenital muscle disease caused by mutations in the *MTM1* gene. Patients display generalized muscle weakness and hypotonia usually leading to early death in the first years of life. Nowadays, no specific treatment exists.

Tamoxifen is a drug commonly used in breast cancer treatment. Tamoxifen treatment of mouse models of Duchenne muscle disease counteracted the symptoms, showing this drug as a potential candidate to improve symptoms of skeletal muscle diseases.

In this study the effect of Tamoxifen treatment in *Mtm1*$^{-/y}$ mouse model was evaluated.

Results

- Tamoxifen treatment increases *Mtm1*$^{-/y}$ lifespan in a dose-dependent manner.
- *Mtm1*$^{-/y}$ treated animals display better performance in motor function tests such as hanging test (named grid test in the paper).
- In vivo force measurements of *Mtm1*$^{-/y}$ treated animals showed that tamoxifen promotes an increase in muscle force.
- At histological level, there is a reduction in the percentage of fibers with internalized nuclei but there is no change in myofiber size in treated animals.
- At ultrastructural level, there is an improvement of sarcomeric structure and increase in the number of identifiable triads per sarcomere in treated *Mtm1*$^{-/y}$ animals.

Conclusion

This study demonstrates that tamoxifen, a drug that has been approved and used for long time, has the ability to improve the CNM phenotype and survival of *Mtm1*$^{-/y}$ mice, appearing as a promising candidate for repurposing to treat XLCNM.

Contribution

In this work I participated doing all the histological (fiber size, nuclei position) and ultrastructural analysis (triad count, T tubule circularity) from all the cohorts.

I was supervised by Belinda Cowling and Jocelyn Laporte. The work was done in a collaboration with Olivier Dorchies' team.

nature COMMUNICATIONS

ARTICLE

DOI: 10.1038/s41467-018-07058-4 OPEN

Tamoxifen prolongs survival and alleviates symptoms in mice with fatal X-linked myotubular myopathy

Elinam Gayi[1], Laurence A. Neff[1], Xènia Massana Muñoz[2,3,4,5], Hesham M. Ismail[1], Marta Sierra[1], Thomas Mercier[6], Laurent A. Décosterd[6], Jocelyn Laporte[2,3,4,5], Belinda S. Cowling[2,3,4,5], Olivier M. Dorchies[1] & Leonardo Scapozza[1]

X-linked myotubular myopathy (XLMTM, also known as XLCNM) is a severe congenital muscular disorder due to mutations in the myotubularin gene, *MTM1*. It is characterized by generalized hypotonia, leading to neonatal death of most patients. No specific treatment exists. Here, we show that tamoxifen, a well-known drug used against breast cancer, rescues the phenotype of *Mtm1*-deficient mice. Tamoxifen increases lifespan several-fold while improving overall motor function and preventing disease progression including lower limb paralysis. Tamoxifen corrects functional, histological and molecular hallmarks of XLMTM, with improved force output, myonuclei positioning, myofibrillar structure, triad number, and excitation-contraction coupling. Tamoxifen normalizes the expression level of the XLMTM disease modifiers DNM2 and PI3KC2B, likely contributing to the phenotypic rescue. Our findings demonstrate that tamoxifen is a promising candidate for clinical evaluation in XLMTM patients.

[1] Pharmaceutical Biochemistry Group, School of Pharmaceutical Sciences, University of Lausanne, University of Geneva, CMU 5-6, Rue Michel-Servet 1, Geneva 1211, Switzerland. [2] Department of Translational Medicine and Neurogenetics, Institut de Génétique et de Biologie Moléculaire et Cellulaire (IGBMC), Illkirch 67404, France. [3] Centre National de la Recherche Scientifique (CNRS), UMR7104, Illkirch 67404, France. [4] Institut National de la Santé et de la Recherche Médicale (INSERM), U1258, Illkirch 67404, France. [5] Université de Strasbourg, Illkirch 67404, France. [6] Division and Laboratory of Clinical Pharmacology, Service of Biomedicine, Department of Laboratories, Lausanne University Hospital, Lausanne 1011, Switzerland. These authors contributed equally: Laurence A. Neff, Xènia Massana Muñoz, Hesham M. Ismail. Correspondence and requests for materials should be addressed to O.M.D. (email: olivier.dorchies@unige.ch) or to L.S. (email: leonardo.scapozza@unige.ch)

X-linked centronuclear myopathy (XLCNM; OMIM #310400), the most severe form of centronuclear myopathy (CNM), affects ~1 in 50,000 males[1]. XLCNM is commonly known as X-linked myotubular myopathy (XLMTM) as characteristic histological features include small-caliber myofibers and centrally located nuclei resembling myotubes[2,3]. XLMTM patients present with profound and generalized muscle weakness from birth. Most XLMTM male patients die in the first 2 years of life; some develop a milder form and may survive into adulthood while female carriers display a more heterogeneous disease[1,4–6]. XLMTM is due to the lack of myotubularin (MTM1), a lipid phosphatase that dephosphorylates phosphatidylinositol 3-phosphate (PtdIns(3)P) and PtdIns(3,5)P_2 into PtdIns and PtdIns(5)P[7–9]. Imbalance in these lipids impairs membrane trafficking, nuclei positioning, and t-tubule organization[10].

No specific treatment exists for XLMTM. AAV-mediated *MTM1* replacement therapy showed great promise in murine and canine models and has reached clinical stage (ClinicalTrials.gov Identifier: NCT03199469)[11–14]. Down-regulating dynamin-2 (DNM2), a protein mutated in autosomal forms of CNM, is another promising approach to rescue several CNM forms[15–17]. The development of these innovative therapies, however, may be hampered by technical and safety issues and be further complicated by cost issues in case of clinical efficacy. By contrast, repurposing well-known drugs might offer time- and cost-effective therapeutic options[18].

Tamoxifen has been used for almost 40 years to treat estrogen receptor-positive breast cancers in both women and men[19–21] and has been tried in a variety of other disorders[22–27]. Importantly, tamoxifen proved safe in pediatric patients[28–35]. Our earlier published[36,37] and unpublished findings that tamoxifen potently counteracted the symptoms in a mouse model of Duchenne muscular dystrophy (DMD) have been translated into compassionate use and a phase 3 clinical trial in underway on DMD boys (ClinicalTrials.gov Identifiers NCT02835079 and NCT03354039, respectively).

We thus thought to evaluate tamoxifen in *Mtm1*$^{-/y}$ mice, a validated model of XLMTM[15,38–40]. In the present work, we demonstrate that oral tamoxifen given to pups from weaning onwards significantly corrects functional, histological, and molecular hallmarks of the disease, resulting in a remarkable enhancement in survival. Tamoxifen is the first EMA- and FDA-approved drug to show such a promising therapeutic potential for patients with XLMTM.

Results

Effects of oral tamoxifen treatments on food and drug intake. *Mtm1*$^{-/y}$ mice and wild type (WT) littermates were weaned on post-natal day 23 ± 1, slightly after disease onset, at which time they were given a control diet or pellets supplemented with tamoxifen citrate (equivalent to 30, 10, and 3 mg tamoxifen free base per kg of diet). Food intake was similar on control and high-tamoxifen diets throughout the study time for *Mtm1*$^{-/y}$ and wild type mice (Supplementary Figure 1). On the highest dose (30 mg kg^{-1} of diet), tamoxifen intake was approximately 6, 5, and 4 mg kg^{-1} d^{-1} in treated mice aged 42, 84, and 200 days, respectively. The levels of tamoxifen and major metabolites in plasma and leg muscle tissue were consistent with levels found previously in treated dystrophic mice[36] (Supplementary Table 1).

Tamoxifen improves life span and slows disease progression. Untreated *Mtm1*$^{-/y}$ mice showed early hind limb paralysis with rapid progression of muscle weakness to the trunk and forelimbs, resulting in marked kyphosis, frailty (Fig. 1a) and premature death at a median age of 45 days (Fig. 1b). By contrast, all doses of tamoxifen extended the life span of *Mtm1*$^{-/y}$ mice, which on the highest dose, reached a median age of 290 days. Shortly before dying, all untreated *Mtm1*$^{-/y}$ mice showed paralyzed hindlimbs and dragging feet. By contrast, adult-treated mice remained mobile and retained ability to rear and to climb onto objects using both forelimbs and hindlimbs (Supplementary Movies 1–4). Remarkably, one *Mtm1*$^{-/y}$ mouse on high tamoxifen reached 464 days of age. Consistent with tamoxifen-mediated enhanced survival, disease progression was significantly delayed in treated *Mtm1*$^{-/y}$ mice (Fig. 1c), which performed almost as well as WT mice in an anti-gravity assay assessing whole-body force (Fig. 1d). Old *Mtm1*$^{-/y}$ mice on high tamoxifen diet presented less clinical features of disease and relatively spared upper body (Fig. 1a), suggesting slower retrograde disease progression. This was illustrated by the ability of the treated mice to climb onto objects using their forelimbs, preserved neck and head control, and relatively large thoracic cage suggestive of spared trunk muscles (Supplementary Movies 3, 4; Fig. 1a). In spite of overwhelming protection from the disease, tamoxifen-treated *Mtm1*$^{-/y}$ mice remained small (Fig. 1e). Similarly, tamoxifen-treated WT mice were smaller than their untreated counterparts, partly due to smaller muscles (Supplementary Tables 2, 3), and presumably also because of reduced amount of white adipose tissue, which was evident upon dissection and similar to our observation in dystrophic mice reported earlier[36].

In order to examine the impact of tamoxifen on muscle mechanical properties, muscle structure and molecular adaptation underpinning tamoxifen-mediated protection, we next treated mice for various periods with optimal tamoxifen dosing (30 mg kg^{-1} of diet).

Tamoxifen improves the size of leg muscles and diaphragm. Compared with WT mice, most locomotor muscles examined in *Mtm1*$^{-/y}$ mice showed severe atrophy at D42 (Supplementary Table 2, 3). That atrophy was partly prevented by tamoxifen even after normalization for improved body weight (from +10% in the quadriceps to +18% in the gastrocnemius). Overall, the effect of tamoxifen at increasing muscle size of *Mtm1*$^{-/y}$ mice persisted until D210. The diaphragm of *Mtm1*$^{-/y}$ mice showed a distinct response to tamoxifen: although the diaphragm was atrophic at D42 and D84, its absolute size doubled between D84 and D210. As a consequence of changes in body weight, the relative size of the diaphragm was gradually bigger over time (from 67 to 198% of wild-type counterparts at D42 and D210, respectively).

Tamoxifen improves the strength and features of leg muscles. Muscle weakness is a key pathological feature of XLMTM patients that is also prominent in the *Mtm1*$^{-/y}$ murine model. We investigated if and to what extent tamoxifen ameliorated the force generated by the triceps surae (hereafter referred to as triceps), a large muscle group of the lower leg that makes up most of the calf volume and contains gastrocnemius, plantaris, and soleus muscles.

We first analyzed phasic (also known as twitch) force at D42, at which time a substantial proportion of untreated *Mtm1*$^{-/y}$ mice survived. The absolute phasic force of untreated *Mtm1*$^{-/y}$ mice was highly compromised, representing only 17.3% of that of untreated wild-type mice. Tamoxifen significantly enhanced the absolute force of *Mtm1*$^{-/y}$ mice almost threefold (Fig. 2a). The absolute phasic traces were normalized to the triceps cross-sectional area in order to express the specific phasic tension, i.e., the force generated per unit of muscle cross-section (Fig. 2b). This revealed that tamoxifen markedly augmented the specific phasic force of *Mtm1*$^{-/y}$ mice (+155%), reaching 61% of the force developed by WT mice. We then compared the specific phasic force at D42, D84, and D210 (Fig. 2c). Tamoxifen

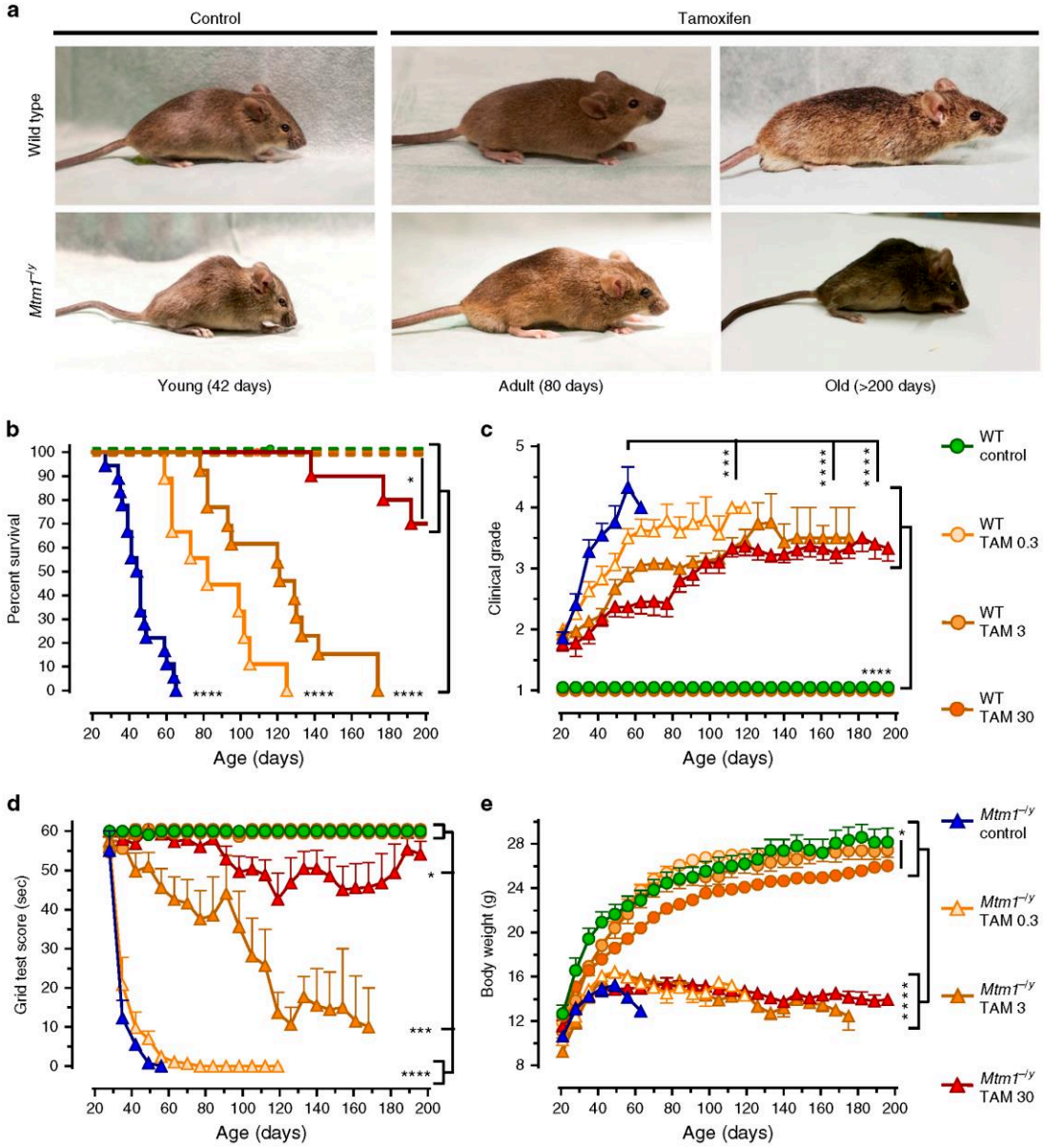

Fig. 1 Tamoxifen rescues the phenotype of XLMTM mice. Life-long oral tamoxifen delays disease progression in XLMTM mice. Wild type (WT) and *Mtm1*$^{-/y}$ mice were fed control or tamoxifen (TAM)-supplemented diets from weaning onward. **a** Photographs of WT and *Mtm1*$^{-/y}$ mice, illustrating disease severity in young untreated mice and protection conferred by tamoxifen in adult and old mice. **b** Kaplan–Meier curves showing the effects of treatments on mouse survival. Early death of untreated *Mtm1*$^{-/y}$ mice contrasts with prolongation of life span in tamoxifen-treated littermates. Data are from 8 to 18 mice per group. $^{*}P \leq 0.05$; $^{****}P \leq 0.0001$. Log-rank (Mantel–Cox) test. **c** Disease progression was assessed three times per week using a 5-grades clinical scale: muscle function was scored as 1 (normal function of hind limbs), 2 (difficulty in spreading toes), 3 (evident weakness in legs), 4 (paralysis of one hind limb), or 5 (complete paralysis of both legs). WT mice had a clinical score of 1 (normal) throughout the study. Untreated *Mtm1*$^{-/y}$ mice quickly reached a high clinical grade, whereas disease progressed much slower in tamoxifen-treated littermates. **d** Mouse motor function was assessed weekly via a horizontal grid-hanging test. The score of untreated *Mtm1*$^{-/y}$ mice declined quickly. Tamoxifen preserved motor function of *Mtm1*$^{-/y}$ mice close to WT values. **e** Mouse body weight was recorded 3 times per week. Tamoxifen affected the growth of WT but not of *Mtm1*$^{-/y}$ mice. *Mtm1*$^{-/y}$ mice remained smaller than WT mice throughout. **b**–**e** Symbols and TAM doses (0.3, 3, and 30 mg kg^{-1} of diet) are shown on the right-hand side. **c**, **d**, **e** Data represent the mean ± s.e.m. of 8 to 18 mice as defined in **a**. $^{*}P \leq 0.05$; $^{**}P \leq 0.01$; $^{****}P \leq 0.0001$; ns non-significant. One-way ANOVA with Fisher's least significance difference (LSD) post-test

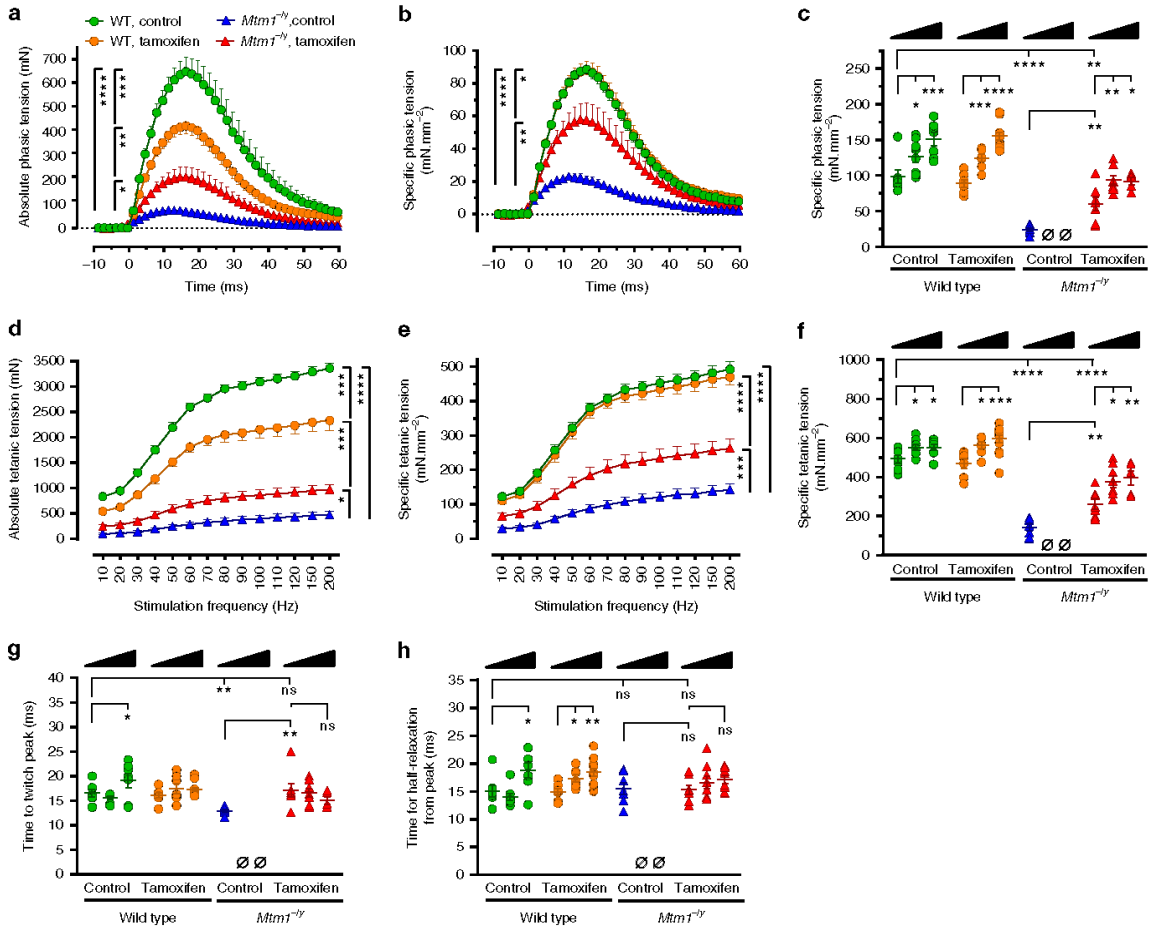

Fig. 2 Tamoxifen augments the strength of leg muscles of XLMTM mice. Electrically evoked triceps contractions were recorded under isometric conditions and contractile features analyzed in 42, 84, and 210-day-old mice fed placebo or tamoxifen-supplemented (30 mg kg^{-1}) diets. **a** Average traces showing absolute phasic (twitch) contraction of the triceps at 42 days (D42). Tamoxifen significantly enhanced the force (tension) in *Mtm1*$^{-/y}$ mice. **b** Specific phasic force (see Online Methods for details) of D42 *Mtm1*$^{-/y}$ mice augmented with tamoxifen. **c** Specific phasic force of *Mtm1*$^{-/y}$ mice increased with tamoxifen at all examined ages. **d** Average traces showing triceps absolute force-frequency curves at D42. Tamoxifen more than doubled the tetanic force of *Mtm1*$^{-/y}$ mice. **e** Specific force of *Mtm1*$^{-/y}$ mice markedly augmented with tamoxifen at all stimulation frequencies. **f** Specific tetanic force of *Mtm1*$^{-/y}$ mice was considerably improved at all studied ages. In triceps examined after various treatment durations, tamoxifen rescued the impaired time to twitch peak of *Mtm1*$^{-/y}$ mice (**g**) but had no impact on the time required for half-relaxation from peak (**h**). D42 panels: WT wild type; legend in **a** stands for **a**, **b**, **d**, **e**; data represent the mean ± s.e.m. of $n = 7$ triceps per group. **c**, **f**, **g**, **h**: black triangles illustrate increasing age (42–84 and 210 days) within each treatment group; columns from left to right: data represent the mean ± s.e.m. of 7; 8; 7; 7; 7; 13; 7; 0; 0; 7; 8; 6 triceps, respectively. $^{*}P \leq 0.05$; $^{**}P \leq 0.01$; $^{***}P \leq 0.001$; $^{****}P \leq 0.0001$; ns non-significant, Ø no surviving mice. One-way ANOVA followed by Fisher's LSD post-test

considerably increased this parameter in *Mtm1*$^{-/y}$ mice at all ages studied compared to untreated *Mtm1*$^{-/y}$ mice at D42 (Fig. 2c). Functional benefits culminated to 74.1% of WT values at D84 and showed only marginal decrease at D210.

Then, the tetanic forces were determined from force–frequency curves. Tamoxifen more than doubled (2.1-fold increase) the absolute tetanic force of *Mtm1*$^{-/y}$ mice at D42, which, after correction for muscle size, reached 53.2% of WT values (Fig. 2d, e). Similar to phasic force, tamoxifen remarkably increased the specific tetanic force of *Mtm1*$^{-/y}$ mice at all ages studied (Fig. 2f). Maximum benefits were found at D210, when tetanic force reached 71.7% of age-matched wild type values (68.2% at D84).

Further analysis of the phasic traces revealed a significant reduction in the time required by the triceps of untreated *Mtm1*$^{-/y}$ mice for reaching twitch peak force, indicative of impaired excitation–contraction coupling (Fig. 2g). Tamoxifen fully restored the time to twitch peak to normal values at all ages. Tamoxifen did not significantly alter the time for half-relaxation from twitch peak at D42 (indicative of SERCA activity and kinetics of inactivation of actin–myosin cross-bridges) (Fig. 2h). Nevertheless, this feature tended to increase with age in both WT and *Mtm1*$^{-/y}$ mice treated with tamoxifen.

In striking contrast with its beneficial actions in *Mtm1*$^{-/y}$ mice, tamoxifen caused generalized muscle hypotrophy in WT mice, which was only partly explained by decreased body weight (Supplementary Table 2, 3). In WT triceps at D42, this translated into decreased absolute force output (Fig. 2a, d), which correlated with decreased muscle mass (Fig. 2b, e). However, specific force

was not altered suggesting that intrinsic mechanical properties of WT myofibers were globally preserved. The specific phasic and tetanic tensions of WT mice augmented with age independently of tamoxifen (Fig. 2c, f).

Tamoxifen improves leg muscle structure and ultrastructure. Histological analyses showed that the tibialis anterior (TA) muscle of *Mtm1*$^{-/y}$ mice contained many fibers in which organelles, including nuclei and mitochondria, were abnormally distributed, forming necklace patterns of oxidative staining essentially in large-caliber fibers[41]. Tamoxifen did not correct these specific features and had a minor impact on fiber type composition (Fig. 3a, b; Supplementary Figure 2). However, tamoxifen reduced by ~50% the number of myofibers displaying nuclei in abnormal position, a prominent histological feature of XLMTM (Fig. 3c). Tamoxifen also induced overall improvement of the myofibrillar structure, including improved organization of the Z-lines, highly ordered protein complexes that keep the sarcomeres in register, and better defined M-line, A-band, and I-band (Fig. 3d; Supplementary Figure 3).

Tamoxifen reduces disease modifiers and alters ER levels. We examined the consequence of tamoxifen treatment on muscular transcript and protein levels of targets selected for their known contribution to CNM pathogenesis, for modulating *Mtm1*$^{-/y}$ mouse phenotype, or mediating tamoxifen actions (Fig. 4; Supplementary Tables 4, 5). In the *Mtm1*$^{-/y}$ mouse, as well in CNM patients, both BIN1 and DNM2 are overexpressed. Here we report that BIN1 mRNA is also more abundant in *Mtm1*$^{-/y}$ mouse muscle. Overall, in both WT and *Mtm1*$^{-/y}$ gastrocnemius muscles, tamoxifen tended to down-regulate BIN1 and DNM2 (Fig. 4a–c), both postulated to act downstream of myotubularin[42]. Of note, the ability of tamoxifen to reduce DNM2 levels was reproduced, at least partly, in a human muscle cell line established from an XLMTM individual[43,44] (Supplementary Figure 4; see Supplementary Tables 6, 7 for details on the human muscle cell lines and the primers used for RT-PCR). In mice, tamoxifen also significantly corrected the elevated levels of desmin (a muscle-specific intermediate filament that controls nuclei positioning via binding myotubularin[45]), of PI3KC2B (an enzyme whose genetic muscle-specific ablation rescues the disease[40]) and of dysferlin (involved in membrane repair and t-tubule biogenesis[46,47]) (Fig. 4a, b, d). Muscle extracts from untreated *Mtm1*$^{-/y}$ mice massively accumulated a putative dysferlin degradation product (~160 kDa) whose proportion was reduced to near-normal levels with tamoxifen (Supplementary Figure 5). Tamoxifen decreased ERα but not ERβ protein levels, presumably via post-transcriptional mechanisms since these effects were not mirrored by mRNA expression (Fig. 4a, b, e). Tamoxifen also partly restored sarcomeric myosin content, which was significantly reduced in *Mtm1*$^{-/y}$ muscle (Fig. 4b, f).

Tamoxifen increases triad density and restores EC coupling. Well-formed triads are required for efficient calcium release from intracellular stores and subsequent muscle contraction in response to nerve stimulation. Tamoxifen restored triad quantity and improved their morphology (Fig. 5a, b). Consistent with these findings, tamoxifen normalized the amplitude of calcium fluxes elicited by depolarization in myofibers from *Mtm1*$^{-/y}$ mice (Fig. 5c–e). Moreover, tamoxifen almost corrected the levels of DHPR, a voltage-sensitive calcium channel that tightly regulates excitation–contraction (EC) coupling. The DHPR effector, RyR1, was found at normal levels in all groups (Fig. 5f–g).

Long-term tamoxifen mitigates myopathic feature progression. TA muscles of *Mtm1*$^{-/y}$ mice treated until D84 and D210 still contained small caliber myofibers with abnormally distributed organelles (Fig. 6a, b). The diameter of TA myofiber significantly increased with age in WT mice while it remained virtually stable over time in tamoxifen-treated *Mtm1*$^{-/y}$ mice (Fig. 6c). At D42, tamoxifen more than halved myofibres with nuclei in abnormal position in *Mtm1*$^{-/y}$ mice. Then, these pathological myofibres gradually accumulated as treated *Mtm1*$^{-/y}$ mice became older (Fig. 6d). At D42, tamoxifen reduced by 42%, the deficit in triad number of *Mtm1*$^{-/y}$ mice. Between D42 and D210, triad number declined similarly in both WT and *Mtm1*$^{-/y}$-treated mice (Fig. 6e).

Discussion

XLMTM is a rare myopathy due to the lack of the lipid phosphatase myotubularin (MTM1)[1,48]. Most affected boys die during early infancy[6]. Despite extremely high unmet medical need, very few pharmacological options have been explored so far in animal models[49,50] or in CNM patients[51].To date, no approved pharmacological treatment has been shown to alleviate the symptoms and increase the life expectancy of the patients.

The rationale for repurposing tamoxifen for XLMTM was based on previous success of our group with the drug in several murine models of debilitating muscular diseases, including *mdx*^{5Cv} mice, a model of DMD[36]. We reasoned that the many protective actions exerted by tamoxifen on diverse muscular conditions might provide a therapeutic avenue for XLMTM. Our findings largely support this view.

In brief, oral tamoxifen, administered from shortly after weaning (i.e., after *Mtm1*$^{-/y}$ mice started to develop overt muscular symptoms), improved overall body strength, increased force generation in leg muscles, slowed disease progression through clinical stages, and importantly, prolonged the lifespan several-fold. These functional improvements correlated with reduced number of centrally located myonuclei, better excitation–contraction coupling, and normalization of molecular markers of the disease, all of which likely contribute to tamoxifen-mediated protection.

Efficient transduction of the muscular action potential into release of Ca^{2+} from sarcoplasmic reticulum stores is a critical step in excitation–contraction coupling (ECC) and a major determinant of force generation. Triads are key structures in this process. Triad disorganization and impaired ECC have a major role in the profound muscle weakness displayed by *Mtm1*$^{-/y}$ mice and is associated with a decreased level of DHPR[52–55]. Tamoxifen not only restored about 42% of triad number deficit in the TA, but also almost fully normalized DHPR expression and dramatically enhanced Ca^{2+} release in isolated *flexor digitorum brevis* (FDB) fibers exposed to a physiological stimulus that triggers DHPR-mediated RyR activation. Altogether, beneficial actions of tamoxifen on triad count, structural components, and function very likely explain the much improved muscle function of *Mtm1*$^{-/y}$ mice. The augmented muscle function was measured not only locally in the triceps, but also at the whole body level with the grid hanging test, suggesting that tamoxifen-mediated enhancement of ECC took place in the whole musculature. Moreover, *Mtm1*$^{-/y}$ diaphragm weight was gradually increased over time.

Noteworthy, although body weight deficit was not corrected and improved muscle structure and muscle force did not reach WT level, the lifespan of tamoxifen-treated *Mtm1*$^{-/y}$ mice was extended by 6.4-fold (45 days median survival of untreated KO vs 290 days) on high dose tamoxifen. Overall, it suggests that the beneficial effects of tamoxifen on life-sustaining physiological

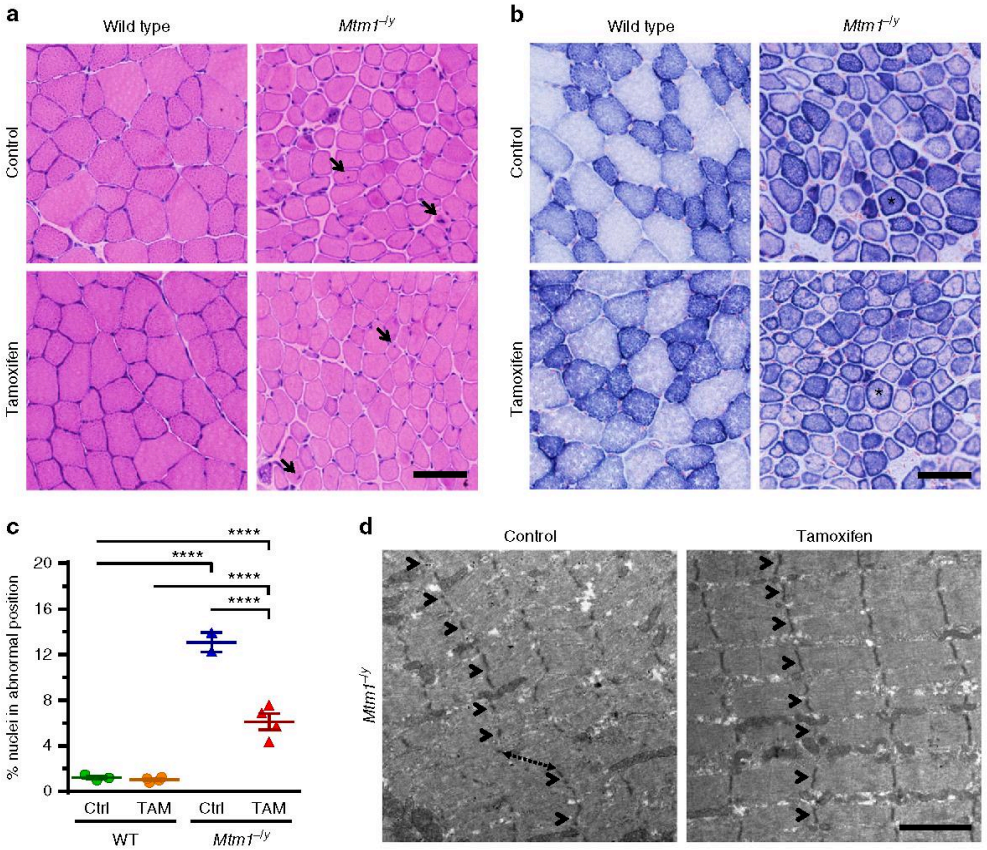

Fig. 3 Tamoxifen mitigates muscle structure and improves sarcomeric organization in XLMTM mice. Muscle structure and sarcomere ultrastructure were examined by histology and transmission electron microscopy, respectively, in 42-day-old (D42) mice either untreated (control; Ctrl) or treated with tamoxifen (TAM; 30 mg kg^{-1} of diet). **a** Representative pictures of hematoxylin–eosin stained sections from the tibialis anterior (TA) of D42 mice. Note the small size of the $Mtm1^{-/y}$ myofibres and the presence of mislocalized nuclei, a hallmark of $Mtm1^{-/y}$ mice and XLMTM patients (arrows). **b** Representative pictures of succinate dehydrogenase (SDH) activity in TA sections of D42 mice, demonstrating abnormal distribution of oxidative staining. The intense staining forming a ring at the periphery of many $Mtm1^{-/y}$ myofibres (examples shown by asterisks) is due to accumulated mitochondria and other organelles and is a hallmark of the pathology. **c** The percentage of nuclei abnormally positioned (either internally or centrally located) in TA myofibres of D42 mice were counted from hematoxylin–eosin-stained sections. That feature was reduced by 53.3% with TAM. Data represent the mean ± s.e.m. of $n = 2$–4 TA per group. $^{****}P \leq 0.0001$. One-way ANOVA followed by Fisher's LSD post-test. **d** Sarcomere ultrastructure revealed by transmission electron microscopy in the TA from untreated (control) and tamoxifen-treated $Mtm1^{-/y}$ mice at D42. Note overall disorganization of the sarcomeres in untreated TA with disruption of the Z-lines (structures running perpendicular to the sarcomeres and holding myofibrils together; arrowheads) and shifted sarcomeres (dashed arrow). Tamoxifen ameliorated the organization of the sarcomeres as demonstrated by in-register Z-lines in adjacent myofibrils (arrowheads). The bar represents 50 µm in **a** and **b**, and 2 µm in **d**

functions are sufficient to greatly extend the lifespan of the animals. Most morphological, functional, and histological outcomes were stable until around 210 days of age. Preliminary observation of long-term $Mtm1^{-/y}$ mouse survivors (4 mice; average 369 days; range 271–464 days; i.e., up to 10-fold the median survival of untreated mice) suggested that the beneficial effects of tamoxifen persisted on extended periods of time.

Here we also investigated potential molecular mechanisms of the rescue. Our earlier work with tamoxifen in mdx^{5Cv} mice[36] provided evidence that tamoxifen (i) is pro-estrogenic on striated muscles (as on bone and uterus[56]), a view supported by a recent meta-analysis in treated women[57], and (ii) exerts beneficial actions through high affinity estrogen receptors. Typical of hormone-dependent receptor degradation, binding of tamoxifen (or its active metabolites) to ERα likely explains the lower levels of that receptor in muscles of treated $Mtm1^{-/y}$ mice mice[58–60].

Myotubularin is intricately linked to BIN1 and DNM2, which collectively control membrane dynamics from production of phosphoinositides to membrane curvature and vesicle fission[42]. Noteworthy, mutations in BIN1 and DNM2 cause autosomal forms of CNM[42]. MTM1 and BIN1 were proposed to act as negative regulators of DNM2 in muscle. Accordingly, diminishing DNM2 rescues the phenotype of $Mtm1^{-/y}$ and $Bin1^{-/-}$ mice[15–17]. We found that tamoxifen almost normalized BIN1 and DNM2. On their own, these molecular actions taking place just downstream of MTM1 might explain most tamoxifen-driven benefits. Furthermore, we showed that tamoxifen also reduced DNM2 levels in a human muscle cell line established from an XLMTM individual[43,44]. This further demonstrates the value of the $Mtm1^{-/y}$ mouse as a model for XLMTM[15,38–40] and supports future translation of tamoxifen efficacy findings from $Mtm1^{-/y}$ mice to XLMTM patients.

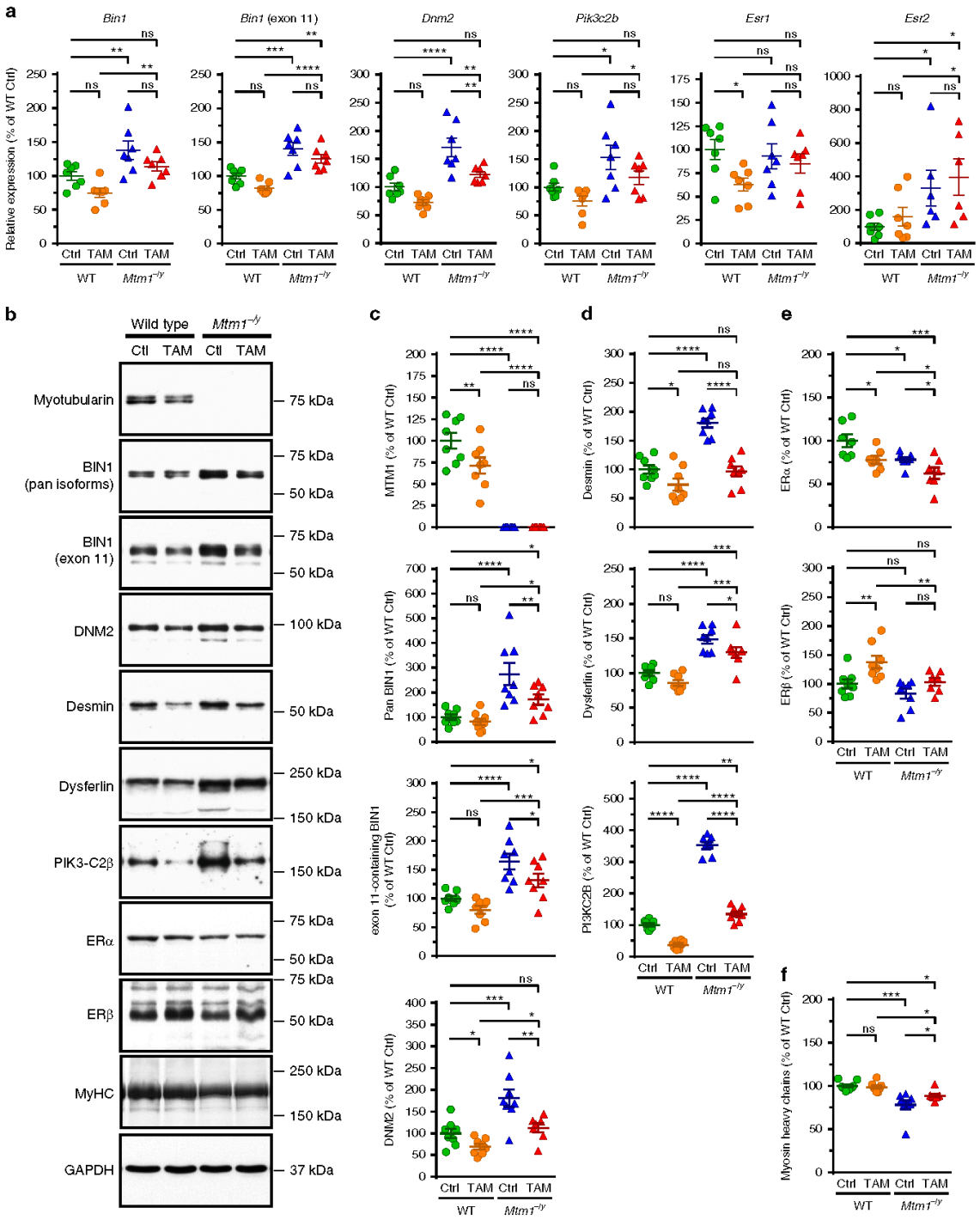

Interestingly, a recent study in MCF7 cells linked DNM2 reduction to impaired autophagy—a prominent feature in *Mtm1*$^{-/y}$ mice[39,61]—and to ERα accumulation in response to estradiol[62]. Although impaired autophagy have been reported in *Mtm1*$^{-/y}$ mice, DNM2 levels are usually increased (and not reduced) in XLMTM and relevant model organisms. In line with these reports, our observations suggest that other mechanisms prevail in *Mtm1*$^{-/y}$ muscle since tamoxifen (i) decreased not only DNM2 but also ERα levels, and (ii) improved overall muscle architecture and nuclei positioning, hardly consistent with further

Fig. 4 Tamoxifen reduces the expression of XLMTM disease modifiers and alters the expression of estrogen receptors. The mRNA and protein levels of known XLMTM disease modifiers and of estrogen receptors, which mediate most tamoxifen actions, were determined in gastrocnemius muscle of 42-days old (D42) wild type (WT) and *Mtm1*$^{-/y}$ mice, either untreated (control; Ctrl) or tamoxifen (TAM)-treated (30 mg kg^{-1} of diet). **a** mRNA levels normalized to glyceraldehyde-3-phosphate dehydrogenase (*Gapdh*). From left to right, relative expression (as percentage of WT Ctrl) of mRNA encoding amphiphysin 2/BIN1 (*Bin1*; all transcripts), muscle-specific BIN1 (*Bin1*; exon 11-containing transcript), dynamin-2 (*Dnm2*), PI3KC2B (*Pik3c2b*), estrogen receptor (ER) α (*Esr1*), and ERβ (*Esr2*). **b** Representative immunoblots of proteins of interest, as indicated. DNM2: dynamin 2; MyHC: myosin heavy chains; GAPDH: glyceraldehyde-3-phosphate dehydrogenase. Position of molecular weight markers (kDa) is shown. **c**–**f** Levels (normalized to GAPDH and expressed as percentage of WT Ctrl) of proteins selected for their role in XLMTM and tamoxifen signaling. **c** Proteins involved in the "MAD"-pathway. From top to bottom: myotubularin (MTM1), amphiphysin 2/BIN1 (pan-isoforms), amphiphysin 2/BIN1 (muscle-specific isoform), dynamin-2 (DNM2). **d** Other disease modifiers and protein deregulated in absence of MTM1. From top to bottom: desmin, dysferlin, PI3KC2B. **e** Estrogen receptors. Top: ERα; bottom: ERβ. **f** Myosin heavy chains, a major constituent of sarcomeres. Data represent the mean ± s.e.m. of $n = 6$–8 muscles per group. $^{*}P \le 0.05$; $^{**}P \le 0.01$; $^{***}P \le 0.001$; $^{****}P \le 0.0001$; ns non-significant. One-way ANOVA followed by Fisher's LSD post-test

worsening of autophagic flux subsequent to DNM2 down-regulation.

Phosphatidylinositol 3-phosphate (PtdIns3*P*) is a main substrate of myotubularin and is produced by PI3-kinases including class II PI3KC2B. Consistent with the hypothesis that altered PtdIns3*P* level account for myotubular myopathy, recent studies showed that inhibiting or down-regulating PI3KC2B rescued the phenotype of *Mtm1*$^{-/y}$ mice, likely via improvement of ECC[40,55]. The PI3KC2B kinase was over-expressed several-fold in *Mtm1*$^{-/y}$ gastrocnemius muscle. Remarkably, we found that tamoxifen almost normalized PI3KC2B expression, thereby very likely contributing to the overall protection exerted by tamoxifen. It is not established, however, if the reduced levels of PI3KC2B is a direct effect of tamoxifen or if it is a secondary consequence of an overall improvement of muscle structure and function. Of note, our findings on PI3KC2B levels diverge from those by Dr. James Dowling and colleagues (see ref. [63]), suggesting they might be dependent on the mouse genetic background and/or disease severity.

Desmin is a muscle-specific intermediate filament that shows discrete sarcomeric expression. It helps maintaining the myofibrils in-register and ensuring mechanical integrity of the myofibers during contraction. In *Mtm1*$^{-/y}$ muscle and in XLMTM patients, desmin level is increased[45,64] and its distribution resembles that in immature myotubes[44,64]. Desmin also controls nuclei and mitochondria positioning, a function that is altered by mutations in *MTM1*[45]. We showed here that tamoxifen normalized the elevated levels of desmin in *Mtm1*$^{-/y}$ mice and this correlated with improved nuclei position and better sarcomeric structure, along with partial correction of myosin heavy chain levels, the major component of myofibrils.

Although tamoxifen significantly reduced DNM2, PI3KC2B and desmin in muscle of both WT and *Mtm1*$^{-/y}$ mice, these molecular changes led to dramatically different consequences. In *Mtm1*$^{-/y}$ mice, normalization of elevated levels of these proteins likely improved the phenotype. By contrast, muscle growth and function in normal mice was impaired with tamoxifen. We speculate that this is a consequence of the reduction of these proteins and of MTM1 to sub-optimal levels. Considering the roles of the MTM1–BIN1–DNM2 pathway in t-tubule biogenesis and in excitation-contraction coupling[17,52,53,65], it is possible that muscle cramps experienced by breast cancer patients[66–68] result from tamoxifen-induced changes in the levels of these proteins. By contrast, we believe that tamoxifen-induced muscle atrophy observed in WT mice is likely species-specific as, to our knowledge, alteration of muscle volume has not been reported in human, not even in breast cancer patients having been on tamoxifen for several years.

In this study, we show that tamoxifen, given orally to a mouse model of XLMTM, considerably ameliorated muscle function and prolonged survival. As reported earlier in a murine model of DMD[36], tamoxifen also caused relative hypertrophy of the diaphragm of aged *Mtm1*$^{-/y}$ mice, which warrants further investigation for assessing the potential benefit on respiratory function. The most efficacious dose tested (30 mg of tamoxifen per kg of diet, yielding 4–6 mg of tamoxifen per kg of body weight per day) was similar to that producing optimal disease prevention in a mouse model of DMD[36]. Considering differences in drug exposure between species, this dose is clinically relevant as it matches that used for breast cancer therapy, compassionate use for DMD boys and TAMDMD, the phase 3 clinical trial (respectively ClinicalTrials.gov identifiers NCT02835079 and NCT03354039). Growth pattern in tamoxifen-treated mice was not restored to normal, which should be distinguished from a potential toxicity of tamoxifen on growth. As tamoxifen modulates molecular events downstream of myotubularin, not all pathogenic features were corrected to normal values as would be expected with gene-restoration therapies[13]. Interestingly, tamoxifen has been used as an alternative to growth hormone in short boys[31] and improved predicted adult height in girls with McCune–Albright syndrome[35]. Thus, side effects related to sub-optimal growth of XMLTM patients in future tamoxifen trials are extremely unlikely.

Interestingly, during the course of our study, Professor James Dowling and collaborators (Sick Kids Hospital, Toronto, Canada) made observations similar to ours with tamoxifen in *Mtm1*$^{-/y}$ mice, confirming the clinically relevant findings that we present here.

Importantly, tamoxifen is a readily available EMA- and FDA-approved drug used for several decades for treating breast cancer[19–21]. It is also efficacious in other hormone-related disorders[22–27]and is safe in diverse male pediatric conditions[28–35]. We believe that the Orphan Drug Designation recently granted by the EMA for tamoxifen use in DMD[36,37], the launching of the TAMDMD trial, and simultaneous report of the therapeutic potential of tamoxifen in *Mtm1*$^{-/y}$ mice by two independent groups should encourage priority consideration for clinical evaluation for XLMTM. Tamoxifen fulfils all criteria[18] for timely repurposing as a symptomatic treatment for XLMTM, either as a monotherapy or combined with AAV-*MTM1* restoration or DNM2 downregulation approaches that will hopefully prove efficacious in clinical trials. Tamoxifen might also prove useful in other myopathies where t-tubule defects secondary to increased DNM2 levels contribute to the pathogenesis, such as BIN1-related CNM and caveolin-3 and dysferlin-related myopathies[15,17,65,69].

Methods

Animals and housing conditions. All procedures involving mice complied with the Swiss Federal Law on Animal Welfare. Procedures were reviewed by the veterinary office of Geneva and authorized under the license numbers GE/61/16 and GE/13/17.

Mtm1-deficient mice in the 129Pas genetic background were obtained from Dr. J. Laporte (IGBMC, Illkirch, France). A colony was established and maintained at the animal facility of the Geneva-Lausanne School of Pharmaceutical Sciences by

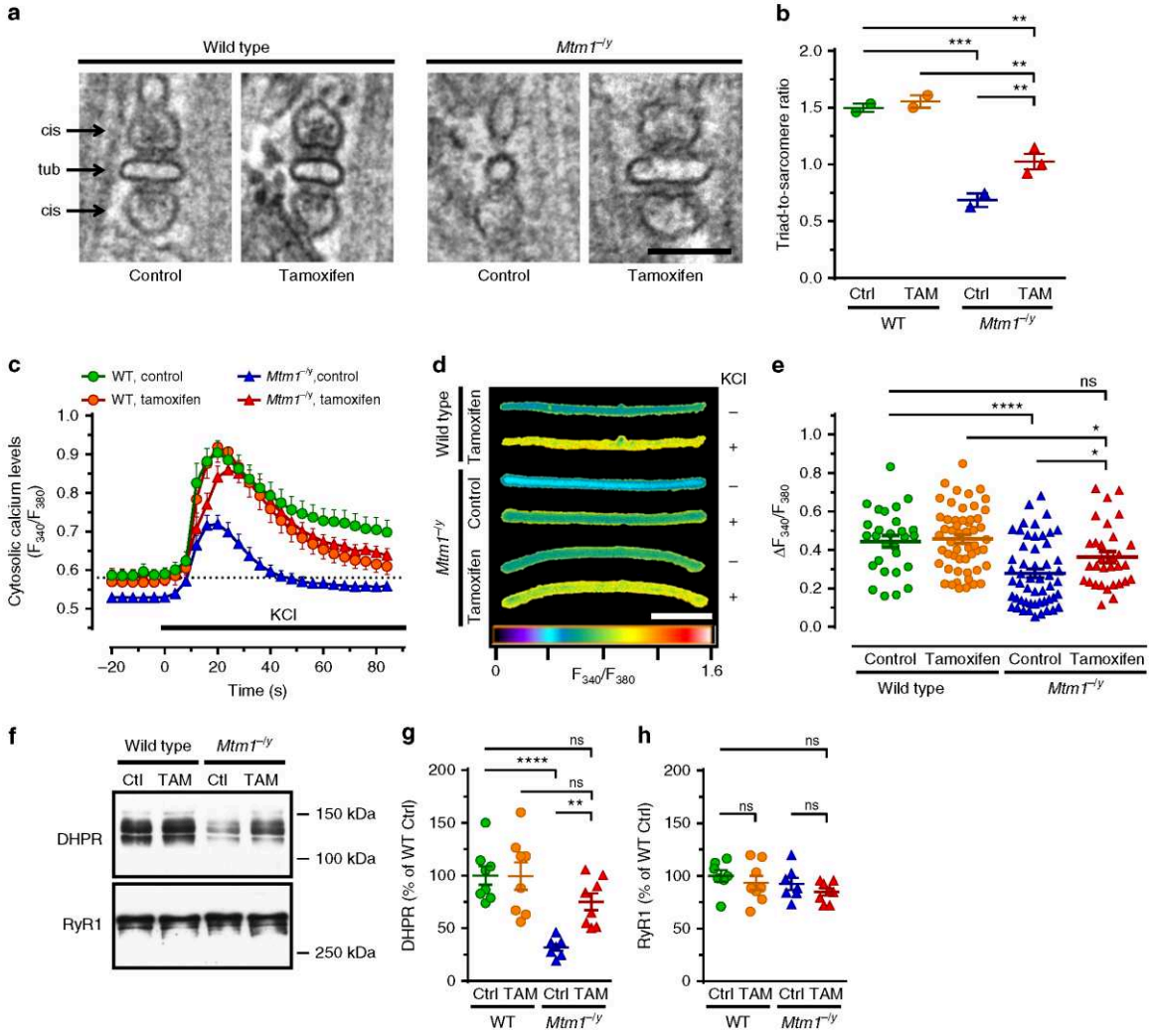

Fig. 5 Tamoxifen improves triad density and excitation-contraction coupling, Triads and excitation-contraction coupling were examined in 42 days old (D42) mice either untreated (control; Ctrl) or treated with tamoxifen (TAM; 30 mg kg^{-1} in diet). **a** Triads—specialized membrane structures made of a t-tubule (tub) flanked by terminal cisternae (*cis*) arising from the sarcoplasmic reticulum and controlling Ca^{2+} release—were visualized by transmission electron microscopy (TEM) in the tibialis anterior (TA) of mice at D42. Note the abnormal shape of the remaining triads in the *Mtm1*$^{-/y}$ mouse and recovery with tamoxifen treatment. The bar represents 100 nm. **b** The number of well-positioned triads per sarcomere unit was determined from TEM pictures in TA from wild type (WT) and Mtm1$^{-/y}$ mice at D42. TAM partly rescued the much decreased triad density in *Mtm1*$^{-/y}$ mice. Mean ± s.e.m. of $n = 2$–3 mice. **c**–**e** Excitation-contraction coupling assessed via live imaging of Ca^{2+} fluxes induced by KCl depolarization in single FDB myofibers (see Online Methods for details). **c** Average traces of the responses of FDB fibers to KCl, an experimental setting that mimics muscle depolarization ($n = 17$–29 fibers). **d** Representative images (pseudo-colored) illustrating cytosolic Ca^{2+} levels in FDB fibers at baseline (−; before KCl pulse) and at the peak of KCl-induced response (+). The bar represents 100 µm. **e** Quantification of cytosolic Ca^{2+} at the peak response. TAM enhanced *Mtm1*$^{-/y}$ cytosolic Ca^{2+} to levels found in WT. Data shown in e represent, from left to right, the mean ± s.e.m. of $n = 29$, 53, 53, and 31 fibers. **f** Representative western blots of DHPR and RyR1. **g**, **h** Quantification of DHPR and RyR1, respectively. Mean ± s.e.m. of $n = 7$ muscles. $^{*}P \le 0.05$; $^{**}P \le 0.01$; $^{***}P \le 0.001$; $^{****}P \le 0.0001$; ns non-significant. One-way ANOVA followed by Fisher's LSD post-test

breeding wild type males with *Mtm1*$^{+/-}$ heterozygous females. The *Mtm1*$^{+/y}$ (wild type) and *Mtm1*$^{-/y}$ (mutant) males in the progeny were used in experiments. Mice were housed on wood granule bedding in either Eurostandard type II or type III polycarbonate cages equipped with filter tops (Indulab AG, Gams, Switzerland). They were kept on a 12-h dark/12-h light cycle, under constant temperature (22 ± 1 °C) and humidity (50–60%). Mice were allowed unlimited access to food and water throughout the study. Environment enrichment consisted in a Mouse House (Indulab AG), shredded paper, and cylinders of pure cellulose (Cocoon, Datesand, Manchester, UK).

Genotyping. Toe biopsies were taken at 7–10 days post-natal for combined genotyping and permanent marking of individuals. DNA was prepared using DirectPCR Lysis Reagent/Mouse Tail (AxonLab AG, Le Mont-sur-Lausanne, Switzerland) according to the manufacturer's instructions. The final lysate was diluted fivefold in molecular biology grade water. One µL of DNA was used for PCR amplification using ready to load 2x GoTaq® Master Mix (Promega, Dübendorf, Switzerland). The following primers (Microsynth AG, Balgach, Switzerland) were added: MTM1 Forward 1 (5′-AGACAGTGATGCAC AGAGAGGAG-3′), binding upstream of exon 4 (used at 0.25 µM); MTM1

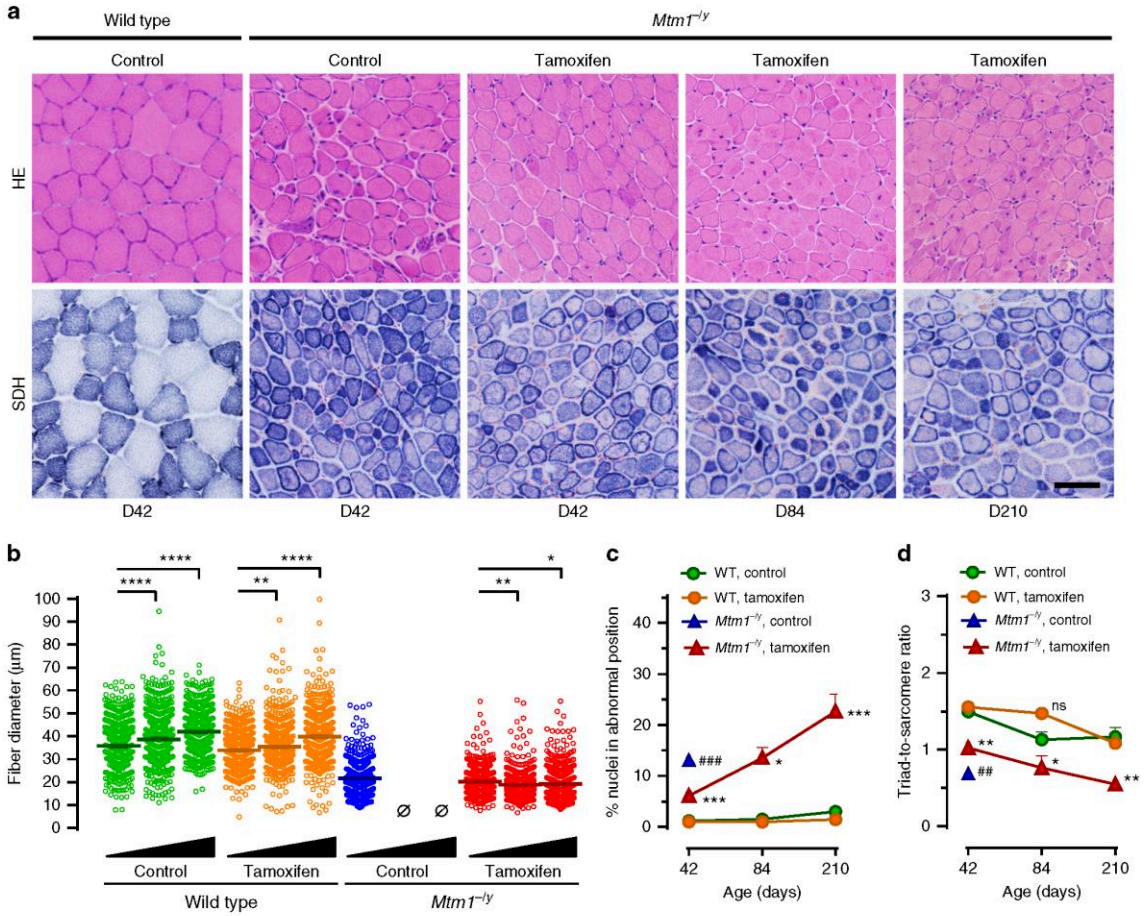

Fig. 6 Myopathic features after long-term tamoxifen treatment, Muscle structure and triads were examined by histology and transmission electron microscopy, respectively, in wild type (WT) and $Mtm1^{-/y}$ mice during long-term treatment with tamoxifen (30 mg kg^{-1} in diet). **a** Representative pictures of tibialis anterior (TA) sections from untreated WT and $Mtm1^{-/y}$ mice at D42, and tamoxifen-treated $Mtm1^{-/y}$ mice at D42, D84, and D210 stained with hematoxylin–eosin (HE) or for succinate dehydrogenase (SDH) activity. Muscle structure of $Mtm1^{-/y}$ mice was stable over the duration of tamoxifen treatment. The bar represents 50 µm. **b** Scatter plots showing the distribution of TA myofiber diameter in mice at D42, D84, and D210 (black triangles illustrate increasing age). Fiber size remained almost constant from D42 to D210. $N = 600$ myofibers per group. **c** The percentage of abnormally positioned nuclei (either internally or centrally located) in TA myofibres of mice at D42, D84, and D210 were counted from hematoxylin–eosin-stained sections. The density of abnormally positioned nuclei increased significantly with ageing. Mean ± s.e.m. of $n = 2$–5 TA per group. **d** The number of well-positioned triads relative to sarcomere number, determined from TEM pictures in TA from wild type and $Mtm1^{-/y}$ mice, showed no significant change from D42 to D84. Black triangles illustrate increasing age (42–84 and 210 days). Mean ± s.e.m. of $n = 2$–3 TA per group. $^{*}P \leq 0.05$; $^{**}P \leq 0.01$; $^{***}P \leq 0.001$; $^{****}P \leq 0.0001$. $^{\#\#}P \leq 0.01$; $Mtm1^{-/y}$ control vs tamoxifen at D42. ns non-significant; Ø no surviving mice. One-way ANOVA followed by Fisher's LSD post-test

Forward 2 (5′-AATGGCCCCATTAAGGGAAG-3′), binding within exon 4 (used at 0.50 µM); MTM1 Reverse (5′-GTGTGCATGTTTGGACCATGG-3′), binding downstream of exon 4 (used at 0.50 µM). The PCR reaction (10 µL final volume) was run on a Biometra Tpersonal thermocycler (AxonLab) as follows: initial denaturation at 95 °C for 5 min; amplification: denaturation at 95 °C for 20 s, annealing at 55 °C for 30 s, elongation at 72 °C for 60 s, 35 cycles; final elongation at 72 °C for 5 min; holding temperature, 10 °C. PCR products were analyzed on 1% agarose gels containing SYBR Safe DNA Gel Stain (Thermo Fisher Scientific AG, Reinach, Switzerland), at a 1:20,000 dilution. The mutant allele was identified as a band of 165 bp and the wild type one as a band of 437 bp (a band of 920 bp arising from the primers binding outside exon 4 was expected but not efficiently amplified).

Groups and treatments. $Mtm1^{+/-}$ carrier females are clinically healthy. Only male mice were used in experiments. Male pups were weaned on post-natal day 23 ± 1, at which time treatments were initiated. Randomization was not feasible because small cohorts were generally produced and each group had to comprise enough wild type mice to foster the mutants. Sub-groups of mice, usually made of 2–4 wild type and 1–4 $Mtm1^{-/y}$ mice, were given pellets of diet supplemented with different amounts of tamoxifen citrate (Haohua Industry Co., Jinan City, China) to achieve to 3, 10, and 30 mg of tamoxifen free base per kg of chow. The modified chow was prepared by Cargill, Provimi-Kliba AG (Kaiseraugst, Switzerland).

Specific care was systematically implemented in order to restrict suffering of the fragile $Mtm1^{-/y}$ mice. This included food pellets placed inside the cages, bottles equipped with long nozzles, bedding granules to raise the ground and facilitate access to drinking water, nestling and enrichment materials, and non-experimental chaperone mice in case not enough wild type littermates were generated along with the $Mtm1^{-/y}$ mice.

For survival analyses, mice were followed up to 200–210 days of age. For the other experiments, treatments were maintained until post-natal day 42 (±1) days (D42, young mice), at which time around 60% of the untreated $Mtm1^{-/y}$ mice were still alive; 84 (±2) days (D84, adult mice), at which time none of the untreated $Mtm1^{-/y}$ mice survived; and 210 (±3) days (D210, old mice).

Longitudinal monitoring of disease progression. Body weight, food consumption, and clinical score were recorded three times per week on each sub-group of mice. Food consumption (in g diet per g body weight per day) was calculated from the amount of diet (in g) consumed by each cage (average total body weight in g) during periods of 2–3 consecutive days. Disease progression was assessed three times per week using a clinical grade scale adapted from that described earlier[38]. In brief, the mice were given a score of 1 (normal function of hind limbs), 2 (difficulty in spreading toes), 3 (evident weakness in legs), 4 (paralysis of one hind limb), or 5 (both hind limbs are paralyzed). Moribund mice were killed, usually soon after reaching stage 5.

Mice were subjected once a week to a horizontal grid-hanging test that measured their ability to sustain their own body weight against gravity. In brief, a mouse was placed on the center of a wire grid (dimension 35 × 50 cm, made of 1 mm-diameter metal wire and forming a 1.26 cm square mesh). The grid was gently inverted upside-down and maintained approximately 50 cm above a thick layer of soft bedding material to avoid causing damage to the animals in case of fall. The time until which the mouse fell from the grid was recorded. In the event of a fall, the timer was stopped, the grid put back to its original position, the mouse promptly returned to the grid and the test was continued. The test was ended when the final time score (set at 60 s) was reached or when the mouse was not able to hold the grid for more than 10 s between consecutive falls.

Electrically evoked contractions of the triceps surae. Muscle mechanical properties of the triceps surae (hereafter referred to as "triceps") were recorded in situ in deeply sedated, freely breathing mice without disturbing triceps innervation and blood supply. The triceps is a large muscle group that makes up most of the calf volume and comprises the gastrocnemius, the plantaris and the soleus muscles. Its balanced composition of slow- and fast-contracting fibers makes it similar to most human leg muscles, hence its value for physiology, experimental pharmacology and evaluating therapeutics. In an isometric setting such as the one we used, the muscle is set to a fixed length. Electrical stimulation causes attempts of the muscle to contract; the mechanical tension ("force") exerted on its extremities is measured via a force transducer. Meaningful parameters are determined from two extreme mechanical responses that are phasic and tetanic contractions. A phasic (also known as twitch) contraction consists in an elementary muscle contraction, comprising a rising phase followed by full muscle relaxation (return to baseline), from which kinetics of contraction and relaxation can be calculated. The phasic force is measured as the amplitude of the response (see Fig. 2a, b in the main text). On the other end of the spectrum, stimulating the muscle at high frequency generates a tetanic contraction, which is the maximum force that the muscle can produce (Fig. 2d, e).

At the end of the treatment period, mice were briefly sedated by inhalation of isoflurane before i.p. injection of a mixture of urethane–diazepam–buprenorphine (1.5 g kg $^{-1}$, 5 mg kg $^{-1}$, and 100 µg kg $^{-1}$, respectively), ensuring deep anesthesia and adequate analgesia for over 2 h. Mechanical responses of the right triceps to electrical stimulations were recorded isometrically using a custom-made device as previously described[36,70–74]. In brief, the knee joint was firmly immobilized, and the Achilles tendon was linked to a force transducer coupled to a LabView interface (National Instruments, Austin, TX). Two thin steel electrodes were inserted into the triceps for delivering 0.5-ms pulses of controlled intensity and frequency. After manual settings of optimal muscle length and optimal current intensity, 5–6 phasic responses to single stimuli were recorded at a sampling rate of 3 kHz to determine absolute peak twitch tension, time to peak twitch tension and time for half relaxation from peak twitch tension. Then, force–frequency curves were constructed at a sampling rate of 1 kHz: the triceps was subjected to 200-ms trains of stimuli at increasing frequencies (10 to 120 Hz by increments of 10 Hz, then 150 and 200 Hz) delivered at 30-s intervals. The maximum response was taken as the absolute tetanic tension. Absolute phasic and absolute tetanic tensions were converted into specific tensions (in mN mm $^{-2}$ of muscle section) after normalization for the muscle cross-sectional area. The cross-sectional area (in mm^2) was determined by dividing the triceps mass (in mg) by the product of the optimal muscle length (in mm) and the density of mammalian skeletal muscle (1.06 mg mm $^{-3}$).

Blood and tissue sampling. Immediately after isometric force recordings, mice were thoracotomized, heparin (LKT labs, Enzo Life Sciences, Lausen, Switzerland) (MW 4–6 kDa; 30 µL; 30 U mL $^{-1}$) was injected into the heart, and the descending aorta was cut. Total blood was collected in a 1.5-mL microcentrifuge tube, and centrifuged (10 min, 4 °C, 10,000×*g*). Plasma was snap-frozen in liquid nitrogen before being stored at −80 °C. Volumes of total blood and plasma were recorded. Selected muscles were quickly dissected and weighed (Supplementary Table 2 and 3). Tibialis anterior (TA) were processed for histology and transmission electron microscopy. The gastrocnemius were saved for RT-PCR and western-blot analyses. The remaining leg muscles were collected and pooled. That muscle bulk was saved for determining levels of tamoxifen and its metabolites. In some instances, flexor digitorum brevis (FDB) muscles were used for live imaging of calcium fluxes in single intact fibers.

Histological analysis of skeletal muscle. TA muscles were embedded in tragacanth gum (Sigma-Aldrich) (5% w/v in water), frozen in liquid nitrogen-cooled isopentane and stored at −80 °C until further processing. Air-dried 10 µm-thick transverse sections were fixed with 4% PFA and stained with hematoxylin and eosin (HE) or for succinate dehydrogenase (SDH) activity using conventional procedures[16,17]. Image acquisition was performed with a NanoZoomer 2.0-HT slide scanner equipped with the fluorescence module L11600–21 (Hamamatsu Photonics). Myofiber cross-sectional area (CSA) was analyzed using FIJI image analysis software (ImageJ 1.51s version, available at http://imagej.net/) from fluorescence pictures taken from HE-stained TA sections. CSA (µm^2) was determined from at least 300 fibers per muscle. The percentage of myofibers with abnormally positioned nuclei (either centralized or internalized) was calculated from at least 300 fibers per TA using the cell counter plugin in FIJI analysis software. The total number of myofibers in each TA was also counted using FIJI.

Transmission electron microscopy. The proximal half of TA muscles was cut into small pieces that were fixed with 2.5% glutaraldehyde, 2.5% paraformaldehyde and 50 mM $CaCl_2$ in 0.1 M cacodylate buffer (pH 7.2). Samples were post-fixed with 2% OsO_4, 0.8% $K_3Fe(CN)_6$ in 0.1 M cacodylate buffer (pH7.4) for 2 h a t 4 °C and incubated with 5% uranyl acetate for 2 h at 4 °C. Muscles were dehydrated in a graded series of ethanol and embedded in epon resin. Thin (70-nm) sections were stained with uranyl acetate and lead citrate and examined by transmission electron microscope. The number of triads per sarcomere (around 40 per mouse) was quantified from electron micrographs using the Metamorph 3 software[15,75]. The ratio of triads/sarcomere was calculated by dividing number of triads clearly identified and correctly localized by the total number of sarcomeres present in the image[15,76].

Analysis of mRNA expression by quantitative RT-PCR. The left gastrocnemius muscle (non-exposed to the isometric contraction protocol) was snap-frozen in liquid nitrogen and stored at −80 °C until processed for quantitative PCR (qPCR) essentially as described[36]. The muscles were ground to a fine powder in mortars cooled in liquid nitrogen. RNA were extracted from approximately 10 mg of muscle powder using RNeasy Fibrous Tissue mini kit (Qiagen, Hombrechtikon, Switzerland). Tissue disruption was enhanced by sonicating three times for 3 s on ice. Then 100 ng of total RNA were reverse-transcribed with Super-Script II Reverse Transcriptase (Invitrogen). The resulting cDNA was subjected to quantitative PCR (qPCR) amplification using PowerUp SYBR^{TM} Green Master mix (Applied Biosystems, Thermo Fisher Scientific) according to the manufacturer's instructions. Briefly, 10 µL reaction mixtures were prepared containing 1 µL of cDNA (equivalent to 2.5 ng of initial RNA), forward and reverse primers (500 nM each) for *Bin1* (pan isoforms), *Bin1* (isoform 8), *Dnm2*, *Esr1*, *Esr2*, *Pik3c2b* or *Gapdh* (used as the housekeeping gene) (Supplementary Table 4), the kit Master mix and RNAse-free water. They were subjected to PCR amplification using a StepOnePlus Real-Time PCR System thermocycler (Thermo Fisher Scientific) under the following conditions: initial denaturation at 95 °C for 60 s; amplification: denaturation at 95 °C for 20 s, annealing at 55 °C for 30 s, elongation at 72 °C for 60 s, 40 cycles; final elongation at 72 °C for 5 min. The expression level of each transcript was expressed relative to that of *Gapdh* using the $2^{-\Delta\Delta Ct}$ method[36].

Semi-quantitative western-blots. Gastrocnemius muscles were pulverized on liquid nitrogen and extracts were prepared as previously described[36,73,74]. The final protein concentration was adjusted to 3 mg mL $^{-1}$ with reducing Laemmli buffer. Muscle extracts (30 to 60 µg per lane) were resolved by SDS-PAGE, and proteins were transferred onto nitrocellulose membranes using standard procedures. Equal loading and transfer efficiency were verified with Ponceau Red staining. Membranes were blocked for 1 h in TBST (20 mM Tris-base, 150 mM NaCl, 0.05% Tween-20, pH 7.5) containing 5% non-fat dry milk and incubated overnight at 4 °C with one of the primary antibodies listed in Supplementary Table 5.

After extensive wash in TBST, the membranes were incubated with a HRP-conjugated secondary reagent (Donkey anti-Rabbit (Amersham, GE Healthcare Life Sciences, Thermo Fisher Scientific), Goat anti-mouse (Bio-Rad), or kappa light chain binding protein (Santa Cruz Biotechnologies)) as required before signal detection on X-ray Fuji films (Thermo Fisher Scientific) using an enhanced chemiluminescence kit (ECL Prime Western Blotting Detection Reagent) (Amersham). The X-ray films were scanned at high resolution (720 dpi) on an Epson Perfection V750 PRO scanner using settings for transparent documents in order to avoid signal saturation and augment the linear range of the signals. Bands were quantified using ImageJ (version 1.48; freely available at http://imagej.nih.gov/ij). Specific care allowing semi-quantitative analysis has been described in details elsewhere[36,74]. Briefly, in order to allow intra-gel and inter-gel comparison and semi-quantitative analysis of the signals, the following procedure was applied: (i) for each muscle protein to be quantified, 4 gels were run simultaneously (PerfectBlue™ Dual Gel System Twin ExW S, Peqlab) and processed in parallel, (ii) the samples (6–8 muscles per group) were loaded as quadruplets, each consisting of extracts from non-treated and TAM-treated WT and non-treated and TAM-treated *Mtm1*-null mice (iii) each quadruplet was flanked by a standard extract (Std), consisting of a mixture of all muscle extracts, (iv) the portions of the gels that contained the protein of interest were transferred onto a single nitrocellulose membrane, ensuring that all samples and flanking standard extracts were

simultaneously exposed to the blocking solution, primary antibodies, secondary HRP-conjugated secondary antibody, ECL reagent, and X-ray film. Signals were normalized to GAPDH and the resulting values were normalized to that of the flanking standard samples. The standard sample being a mixture of all samples to be compared the ones with the others, this ensured that its signal has an average, non-saturating, intensity. Finally, the values were expressed as the percentage of the WT control group.

Larger views of the blots for which portions are shown in Figs. 4 and 5 are presented in Supplementary Figure 6.

Culture of isolated flexor digitorum brevis (FDB) fibers. Hind feet were dissected and immersed in transfer buffer (Hank's buffered salt solution supplemented with 10 mM HEPES, pH 7.4). FDB muscles were dissected under a binocular microscope, transferred to warmed (37 °C) maintenance medium (Dulbecco's Modified Eagle's Medium (DMEM) containing 10% fetal bovine serum and 10 μg mL^{-1} ciprofloxacin (Sigma)), and 1 mg mL^{-1} collagenase type IA (Sigma) was finally added[77]. The full process took no more than 1 h. The mixture was maintained for 60 min at 37 °C with frequent shaking in a humidified incubator gassed with air containing 5% CO_2. Then, muscles were carefully rinsed twice in warmed maintenance medium to remove enzyme excess and individual fibers were released by triturating gently with fire-polished Pasteur pipettes of decreasing opening widths. Throughout that process, aliquots of maintenance medium containing single fibers were transferred onto clean 18 mm-diameter glass coverslips coated with 15 μg cm^{-2} Matrigel (BD biosciences) in 12-well tissue culture plates. Ca^{2+} measurement was performed the next day.

Live imaging of cytosolic calcium in FDB fibers. Ca^{2+} levels in the cytosol of FDB fibers was monitored via fluorescence microscopy using the calcium-sensitive probe Fura-2 essentially as described previously[77]. Fura-2-AM (Molecular Probes, Invitrogen, Thermo Fisher Scientific), the acetoxymethyl ester of Fura-2, was used to facilitate loading into fibers and the subsequent de-esterification and intracellular trapping. The Fura-2-AM stock solution was prepared extemporaneously by mixing Fura-2-AM (5 mM) with an equal volume of Pluronic acid F-127 (20% w/v solution, Molecular probes). Fibers were washed twice with physiological salt solution containing Ca^{2+} (PSS^{+}; composition in mM: HEPES 5, KCl 5, $MgCl_2{\cdot}6H_2O$ 1, NaCl 145, $CaCl_2{\cdot}2H_2O$ 1.7, glucose 10) before incubation in the loading solution (PSS^{+} containing 2 μL mL^{-1} of the Fura-2-AM/Pluronic acid working solution; final Fura-2 concentration 5 μM). Loading was done at 37 °C for 45 min after which the cells were washed twice with PSS^{+} and Fura-2-AM allowed to de-esterify at room temperature for another 20 min. Loading and de-esterification buffers were supplemented with 100 μM *N*-benzyl-*p*-toluenesulfonamide (BTS) (Medchem Express, Lucerna-Chem, Luzern, Switzerland) to prevent fiber contraction and detachment. All loading steps were done in the dark. Coverslips holding fibers were placed in a perfusion chamber that was continuously perfused at 1.5 mL min^{-1} using a peristaltic pump. The imaging setup consisted of a high speed monochromator (Visitron Systems, Puchheim, Germany) allowing selection of alternating excitation wavelengths and an ORCA-Flash4.0LT Digital sCMOS camera mounted on an Axiovert 200 microscope (Carl Zeiss AG, Feldbach, Switzerland) equipped with objectives for high resolution fluorescence imaging. The experiments were done ratiometrically with alternating excitation wavelengths of 340 and 380 nm and emission at wavelengths above 510 nm using a long pass filter. Images were acquired every 2 s. After recording baseline calcium, fibers were perfused with a modified PSS^{+} containing high concentration of KCl (125 mM) and reduced concentration of NaCl (10 mM). Ca^{2+} increment during depolarization was calculated as the difference between resting Ca^{2+} levels and the maximum levels of Ca^{2+} reached during depolarization. Data acquisition and analysis was performed using VisiView software version 3.3.0.3 (Visitron Systems).

Data analysis and statistics. Survival curves were analyzed using the Log-rank (Mantel–Cox) test. All other comparisons were assessed by ANOVA followed by Fisher's least significance difference (LSD) test. The overall changes in body weights, grid test scores and clinical grades over time were assessed from the areas under the curves calculated from every mouse.

Data availability

The authors declare that all data supporting the findings of this study are available within the paper and its supplementary information files. A reporting summary for this Article is available as a Supplementary Information file.

Received: 10 September 2018 Accepted: 12 October 2018
Published online: 19 November 2018

References

1. Jungbluth, H. & Gautel, M. Pathogenic mechanisms in centronuclear myopathies. *Front. Aging Neurosci.* **6**, 339 (2014).
2. Lawlor, M. W. et al. Skeletal muscle pathology in X-Linked myotubular myopathy: review with cross-species comparisons. *J. Neuropathol. Exp. Neurol.* **75**, 102–110 (2016).
3. Romero, N. B. Centronuclear myopathies: a widening concept. *Neuromuscul. Disord.* **20**, 223–228 (2010).
4. Barth, P. G. & Dubowitz, V. X-linked myotubular myopathy--a long-term follow-up study. *Eur. J. Paediatr. Neurol.* **2**, 49–56 (1998).
5. Buj-Bello, A., Biancalana, V., Moutou, C., Laporte, J. & Mandel, J.-L. Identification of novel mutations in the MTM1 gene causing severe and mild forms of X-linked myotubular myopathy. *Hum. Mut.* **14**, 320–325 (1999).
6. Biancalana, V. et al. Affected female carriers of MTM1 mutations display a wide spectrum of clinical and pathological involvement: delineating diagnostic clues. *Acta Neuropathol.* **134**, 889–904 (2017).
7. Blondeau, F. et al. Myotubularin, a phosphatase deficient in myotubular myopathy, acts on phosphatidylinositol 3-kinase and phosphatidylinositol 3-phosphate pathway. *Hum. Mol. Genet.* **9**, 2223–2229 (2000).
8. Tronchère, H. et al. Production of phosphatidylinositol 5-phosphate by the phosphoinositide 3-phosphatase myotubularin in mammalian cells. *J. Biol. Chem.* **279**, 7304–7312 (2004).
9. Taylor, G. S., Maehama, T. & Dixon, J. E. Myotubularin, a protein tyrosine phosphatase mutated in myotubular myopathy, dephosphorylates the lipid second messenger, phosphatidylinositol 3-phosphate. *Proc. Natl Acad. Sci. USA* **97**, 8910–8915 (2000).
10. Bachmann, C. et al. Cellular, biochemical and molecular changes in muscles from patients with X-linked myotubular myopathy due to MTM1 mutations. *Hum. Mol. Genet.* **26**, 320–332 (2017).
11. Elverman, M. et al. Long-term effects of systemic gene therapy in a canine model of myotubular myopathy. *Muscle Nerve* **56**, 943–953 (2017).
12. Mack, D. L. et al. Systemic AAV8-mediated gene therapy drives whole-body correction of myotubular myopathy in dogs. *Mol. Ther.* **25**, 839–854 (2017).
13. Childers, M. K. et al. Gene therapy prolongs survival and restores function in murine and canine models of myotubular myopathy. *Sci. Transl. Med.* **6**, 220ra210 (2014).
14. Buj-Bello, A. et al. AAV-mediated intramuscular delivery of myotubularin corrects the myotubular myopathy phenotype in targeted murine muscle and suggests a function in plasma membrane homeostasis. *Hum. Mol. Genet.* **17**, 2132–2143 (2008).
15. Cowling, B. S. et al. Reducing dynamin 2 expression rescues X-linked centronuclear myopathy. *J. Clin. Invest.* **124**, 1350–1363 (2014).
16. Tasfaout, H. et al. Antisense oligonucleotide-mediated Dnm2 knockdown prevents and reverts myotubular myopathy in mice. *Nat. Commun.* **8**, 15661 (2017).
17. Cowling, B. S. et al. Amphiphysin (BIN1) negatively regulates dynamin 2 for normal muscle maturation. *J. Clin. Invest.* **127**, 4477–4487 (2017).
18. Ismail, H. M., Dorchies, O. M. & Scapozza, L. The potential and benefits of repurposing existing drugs to treat rare muscular dystrophies. *Exp. Opin. Orphan Drugs* **6**, 259–271 (2018).
19. Hayes, T. G. Pharmacologic treatment of male breast cancer. *Expert. Opin. Pharmacother.* **10**, 2499–2510 (2009).
20. Shagufta, Ahmadl. Tamoxifen a pioneering drug: an update on the therapeutic potential of tamoxifen derivatives. *Eur. J. Med. Chem.* **143**, 515–531 (2018).
21. Peddi, P. F. Hormone receptor positive breast cancer: state of the art. *Curr. Opin. Obstet. Gynecol.* **30**, 51–54 (2018).
22. Moein, M. R., Tabibnejad, N. & Ghasemzadeh, J. Beneficial effect of tamoxifen on sperm recovery in infertile men with nonobstructive azoospermia. *Andrologia* **44**, 194–198 (2012).
23. Chua, M. E. et al. Revisiting oestrogen antagonists (clomiphene or tamoxifen) as medical empiric therapy for idiopathic male infertility: a meta-analysis. *Andrology* **1**, 749–757 (2013).
24. Patel, D. P., Chandrapal, J. C. & Hotaling, J. M. Hormone-based treatments in subfertile males. *Curr. Urol. Rep.* **17**, 56 (2016).
25. Kunath, F., Keck, B., Antes, G., Wullich, B. & Meerpohl, J. Tamoxifen for the management of breast events induced by non-steroidal antiandrogens in patients with prostate cancer: a systematic review. *BMC Med.* **10**, 96 (2012).
26. Payne, W. G. et al. Down-regulating causes of fibrosis with tamoxifen: a possible cellular/molecular approach to treat rhinophyma. *Ann. Plast. Surg.* **56**, 301–305 (2006).
27. van Bommel, E. F., Hendriksz, T. R., Huiskes, A. W. & Zeegers, A. G. Brief communication: tamoxifen therapy for nonmalignant retroperitoneal fibrosis. *Ann. Intern. Med.* **144**, 101–106 (2006).
28. Walter, A. W. et al. Tamoxifen and carboplatin for children with low-grade gliomas: a pilot study at St. Jude Children's Research Hospital. *J. Pediatr. Hematol. Oncol.* **22**, 247–251 (2000).
29. Lawrence, S. E., Arnold Faught, K., Vethamuthu, J. & Lawson, M. L. Beneficial effects of raloxifene and tamoxifen in the treatment of pubertal gynecomastia. *J. Pediatr.* **145**, 71–76 (2004).

30. Skapek, S. X. et al. Safety and efficacy of high-dose tamoxifen and sulindac for desmoid tumor in children: results of a Children's Oncology Group (COG) Phase II Study. *Pediatr. Blood. Cancer* **60**, 1108–1112 (2013).
31. Kreher, N. C., Eugster, E. A. & Shankar, R. R. The use of tamoxifen to improve height potential in short pubertal boys. *Pediatrics* **116**, 1513–1515 (2005).
32. Lapid O., van Wingerden J. J., & Perlemuter L. Tamoxifen therapy for the management of pubertal gynecomastia: a systematic review. *J. Pediatr. Endocrinol. Metab.* **26**, 803–807 (2013).
33. Derman, O., Kanbur, N., Kilic, I. & Kutluk, T. Long-term follow-up of tamoxifen treatment in adolescents with gynecomastia. *J. Pediatr. Endocrinol. Metab.* **21**, 449–454 (2008).
34. Eugster, E. A. et al. Tamoxifen treatment for precocious puberty in McCune-Albright syndrome: a multicenter trial. *J. Pediatr.* **143**, 60–66 (2003).
35. de, G. et al. Tamoxifen improves final height prediction in girls with McCune-Albright syndrome: a long follow-up. *Horm. Res. Paediatr.* **84**, 184–189 (2015).
36. Dorchies, O. M. et al. The anticancer drug tamoxifen counteracts the pathology in a mouse model of duchenne muscular dystrophy. *Am. J. Pathol.* **182**, 485–504 (2013).
37. Gayi, E. et al. Repurposing the selective oestrogen receptor modulator tamoxifen for the treatment of Duchenne muscular dystrophy. *Chimia* **72**, 238–240 (2018).
38. Buj-Bello, A. et al. The lipid phosphatase myotubularin is essential for skeletal muscle maintenance but not for myogenesis in mice. *Proc. Natl Acad. Sci. USA* **99**, 15060–15065 (2002).
39. Al-Qusairi, L. et al. Lack of myotubularin (MTM1) leads to muscle hypotrophy through unbalanced regulation of the autophagy and ubiquitin-proteasome pathways. *Faseb J.* **27**, 3384–3394 (2013).
40. Sabha, N. et al. PIK3C2B inhibition improves function and prolongs survival in myotubular myopathy animal models. *J. Clin. Invest.* **126**, 3613–3625 (2016).
41. Bevilacqua, J. A. et al. "Necklace" fibers, a new histological marker of late-onset MTM1-related centronuclear myopathy. *Acta Neuropathol.* **117**, 283 (2008).
42. Cowling, B. S., Toussaint, A., Muller, J. & Laporte, J. Defective membrane remodeling in neuromuscular diseases: Insights from animal models. *PLoS Genet.* **8**, e1002595 (2012).
43. Laporte, J., Kress, W. & Mandel, J. L. Diagnosis of X-linked myotubular myopathy by detection of myotubularin. *Ann. Neurol.* **50**, 42–46 (2001).
44. Dorchies, O. M. et al. Normal innervation and differentiation of X-linked myotubular myopathy muscle cells in a nerve-muscle coculture system. *Neuromuscul. Disord.* **11**, 736–746 (2001).
45. Hnia, K. et al. Myotubularin controls desmin intermediate filament architecture and mitochondrial dynamics in human and mouse skeletal muscle. *J. Clin. Invest.* **121**, 70–85 (2011).
46. Kerr, J. P., Ward, C. W. & Bloch, R. J. Dysferlin at transverse tubules regulates Ca(2+) homeostasis in skeletal muscle. *Front. Physiol.* **5**, 89 (2014).
47. Hofhuis, J. et al. Dysferlin mediates membrane tubulation and links T-tubule biogenesis to muscular dystrophy. *J. Cell. Sci.* **130**, 841 (2017).
48. Hnia, K., Vaccari, I., Bolino, A. & Laporte, J. Myotubularin phosphoinositide phosphatases: cellular functions and disease pathophysiology. *Trends Mol. Med.* **18**, 317–327 (2012).
49. Lawlor, M. W. et al. Inhibition of activin receptor type IIB increases strength and lifespan in myotubularin-deficient mice. *Am. J. Pathol.* **178**, 784–793 (2011).
50. Dowling, J. J. et al. Myotubular myopathy and the neuromuscular junction: a novel therapeutic approach from mouse models. *Dis. Model Mech.* **5**, 852–859 (2012).
51. Robb, S. A. et al. Impaired neuromuscular transmission and response to acetylcholinesterase inhibitors in centronuclear myopathies. *Neuromuscul. Disord.* **21**, 379–386 (2011).
52. Al-Qusairi, L. et al. T-tubule disorganization and defective excitation-contraction coupling in muscle fibers lacking myotubularin lipid phosphatase. *Proc. Natl Acad. Sci. USA* **106**, 18763–18768 (2009).
53. Al-Qusairi, L. & Laporte, J. T-tubule biogenesis and triad formation in skeletal muscle and implication in human diseases. *Skelet. Muscle* **1**, 26–26 (2011).
54. Royer, B. et al. The myotubularin–amphiphysin 2 complex in membrane tubulation and centronuclear myopathies. *EMBO Rep.* **14**, 907–915 (2013).
55. Kutchukian, C. et al. Phosphatidylinositol 3-kinase inhibition restores Ca^{2+} release defects and prolongs survival in myotubularin-deficient mice. *Proc. Natl. Acad. Sci. USA* **113**, 14432–14437 (2016).
56. Vogel, V. G. et al. Effects of tamoxifen vs raloxifene on the risk of developing invasive breast cancer and other disease outcomes. *JAMA* **295**, 2727–2741 (2006).
57. Van der Weijden-Van Doornik, E. M., Slot, D. E., Burtin, C. & van der Weijden, G. A. Grip strength in women being treated for breast cancer and receiving adjuvant endocrine therapy: systematic review. *Phys. Ther.* **97**, 904–914 (2017).
58. Baltgalvis, K. A., Greising, S. M., Warren, G. L. & Lowe, D. A. Estrogen regulates estrogen receptors and antioxidant gene expression in mouse skeletal muscle. *PLoS ONE* **5**, e10164 (2010).
59. Saceda, M. et al. Regulation of the estrogen receptor in MCF-7 cells by estradiol. *Mol. Endocrinol.* **2**, 1157–1162 (1988).
60. Lonard, D. M., Nawaz, Z., Smith, C. L. & O'Malley, B. W. The 26S proteasome is required for estrogen receptor-a and coactivator turnover and for efficient estrogen receptor-a transactivation. *Mol. Cell* **5**, 939–948 (2000).
61. Fetalvero, K. M. et al. Defective autophagy and mTORC1 signaling in myotubularin null mice. *Mol. Cell. Biol.* **33**, 98–110 (2013).
62. Totta, P., Busonero, C., Leone, S., Marino, M. & Acconcia, F. Dynamin II is required for 17β-estradiol signaling and autophagy-based ERα degradation. *Sci. Rep.* **6**, 23727 (2016).
63. Maani, N. et al. Tamoxifen therapy in a murine model of myotubular myopathy. *Nat Commun.* https://doi.org/41467-018-07057-5 (2018).
64. Sarnat, H. B. Myotubular myopathy: arrest of morphogenesis of myofibres associated with persistence of fetal vimentin and desmin. Four cases compared with fetal and neonatal muscle. *Can. J. Neurol. Sci.* **17**, 109–123 (1990).
65. Demonbreun, A. R. & McNally, E. M. Dynamin 2 the rescue for centronuclear myopathy. *J. Clin. Invest.* **124**, 976–978 (2014).
66. Pemmaraju, N., Munsell, M. F., Hortobagyi, G. N. & Giordano, S. H. Retrospective review of male breast cancer patients: analysis of tamoxifen-related side-effects. *Ann. Oncol.* **23**, 1471–1474 (2011).
67. Karatas, F. et al. Leg cramps associated with tamoxifen use—possible mechanism and treatment recommendations. *J. Buon.* **21**, 520 (2016).
68. Lintermans, A. et al. A prospective assessment of musculoskeletal toxicity and loss of grip strength in breast cancer patients receiving adjuvant aromatase inhibitors and tamoxifen, and relation with BMI. *Breast Cancer Res. Treat.* **146**, 109–116 (2014).
69. Bohm, J. et al. Altered splicing of the BIN1 muscle-specific exon in humans and dogs with highly progressive centronuclear myopathy. *PLoS Genet.* **9**, e1003430 (2013).
70. Dorchies, O. M. et al. Green tea extract and its major polyphenol (−)-epigallocatechin gallate improve muscle function in a mouse model for Duchenne muscular dystrophy. *Am. J. Physiol. Cell. Physiol.* **290**, C616–C625 (2006).
71. Hibaoui, Y., Reutenauer-Patte, J., Patthey-Vuadens, O., Ruegg, U. T. & Dorchies, O. M. Melatonin improves muscle function of the dystrophic mdx^{5Cv} mouse, a model for Duchenne muscular dystrophy. *J. Pineal Res.* **51**, 163–171 (2011).
72. Reutenauer, J., Dorchies, O. M., Patthey-Vuadens, O., Vuagniaux, G. & Ruegg, U. T. Investigation of Debio 025, a cyclophilin inhibitor, in the dystrophic mdx mouse, a model for Duchenne muscular dystrophy. *Br. J. Pharmacol.* **155**, 574–584 (2008).
73. Reutenauer-Patte, J., Boittin, F.-X., Patthey-Vuadens, O., Ruegg, U. T. & Dorchies, O. M. Urocortins improve dystrophic skeletal muscle structure and function through both PKA- and Epac-dependent pathways. *Am. J. Pathol.* **180**, 749–762 (2012).
74. De Andrade, P. B. M. et al. Caloric restriction induces energy-sparing alterations in skeletal muscle contraction, fiber composition and local thyroid hormone metabolism that persist during catch-up fat upon refeeding. *Front. Physiol.* **6**, 254 (2015).
75. Cowling, B. S. et al. Increased expression of wild-type or a centronuclear myopathy mutant of dynamin 2 in skeletal muscle of adult mice leads to structural defects and muscle weakness. *Am. J. Pathol.* **178**, 2224–2235 (2011).
76. Amoasii, L. et al. Phosphatase-dead myotubularin ameliorates X-linked centronuclear myopathy phenotypes in mice. *PLoS Genet.* **8**, e1002965 (2012).
77. Boittin, F.-X. et al. Ca^{2+}-independent phospholipase A_2 enhances store-operated Ca^{2+} entry in dystrophic skeletal muscle fibers. *J. Cell. Sci.* **119**, 3733–3742 (2006).

Acknowledgements

This work was supported by intramural research support from the University of Geneva, University of Lausanne and University of Strasbourg, as well as by grants to O.M.D. and L.S. from the Swiss Foundation for Research on Muscle Diseases (SFRMD/FSRMM/SSEM), the French Muscular Dystrophy Association (AFM-Telethon; Grants #17821, #20959), and the Dutch Duchenne Parent Project (DPP-NL) and grants to B.S.C. and J.L. from INSERM, CNRS, Agence Nationale de la Recherche (ANR-14-CE12–0009, -10-LABX-0030-INRT and -10-IDEX-0002–02). M.S. is supported by the European Union's Horizon 2020 research and innovation programme under the Marie Sklodowska-Curie grant agreement No 800198. X.M.M. is an IGBMC International PhD Programme fellow supported by LabEx INRT funds. We are grateful to Colette Sauty for excellent assistance with animal care, Barbara Pinheiro-Tonneau and Stefane Melancia for help with histological analyses, Pascal Kessler for help with image quantification and Nadia Messaddeq for help with electron microscopy.

Author contributions

E.G., L.A.N., X.M.M., H.M.I., M.S., T.M., B.S.C., and O.M.D. designed and performed the experiments, E.G., L.A.N., X.M.M., H.M.I., M.S., T.M., B.S.C., and O.M.D. analyzed the data; E.G., L.A.N., H.M.I., and O.M.D. wrote the manuscript; X.M.M., M.S., T.M., L.A.D.,

J.L., B.S.C., and L.S. edited the manuscript; L.A.D., J.L., B.S.C., L.S., and O.M.D. provided support and supervised the work.

Additional information

Supplementary Information accompanies this paper at https://doi.org/10.1038/s41467-018-07058-4.

Competing interests: J.L. and B.S.C. are scientific advisors for Dynacure. The remaining authors declare no competing interests.

Reprints and permission information is available online at http://npg.nature.com/reprintsandpermissions/

Publisher's note: Springer Nature remains neutral with regard to jurisdictional claims in published maps and institutional affiliations.

Part 3
Discussion and perspectives

Discussion

During my PhD I investigated the role of DNM2 in different forms of CNM using two different systems: AAV-mediated overexpression and a genetically modified mouse model carrying a *Dnm2* mutation.

I compared the effect of overexpressing different DNM2 mutations in WT skeletal muscle, pointing at different mechanisms that could be implicated in the pathogenic effect of those mutations. I also tried to disrupt different DNM2 protein functions to find the main activities related to its pathogenicity in *Mtm1*-/y animal model.

I validated a novel mouse model carrying the S619L mutation in the *Dnm2* gene. This mutation in human causes a neonatal severe form of DNM2-related CNM. This mouse faithfully reproduces many features also present in patients. I found that this model had an increase in DNM2 protein level and treatment with ASO to reduce it had a significant therapeutic effect after 3 weeks of weekly injections.

Lastly, I participated in a project to study the effect of tamoxifen treatment in *Mtm1*$^{-/y}$ mouse model. With this study we showed that tamoxifen improves survival and some CNM phenotypes. Since tamoxifen is an FDA approved drug currently used in clinic for other indications, this therapeutic effect in XLCNM mouse model opens the possibility of repurposing this drug for XLCNM patients.

DNM2: a mechanoenzyme with signaling abilities

After several years of research, our vision of how DNM2 functions has progressed. Initially, its role was mainly related to membrane fission in endocytosis, but nowadays we know that DNM2 plays a role in many different cellular aspects from cellular adhesion to cytoskeleton remodeling. Currently we have a model that can explain membrane fission activity, as explained previously (Introduction, 2.2. Dynamin protein).

In summary below are the key steps for DNM2-related membrane fission:

1) Protein switch to open conformation
2) Potential interaction with additional partners that would facilitate membrane binding
3) Dynamic membrane binding
4) Change in GDP/GTP load
5) High order oligomerization stabilizing membrane binding
6) GTP hydrolysis and powerstroke

7) Membrane fission and release

Similarly to the way it tubulates membranes, DNM2 can bundle actin filaments and microtubules by direct binding (Gu et al., 2010; Hamao, Morita, & Hosoya, 2009) affecting its organization. It can also participate in actin remodeling by interacting with other proteins like for example NWASP (Franck et al., 2019).

In these two processes it seems the mechanism of action as a mechanoenzyme is very similar.

However, there are other cellular processes where DNM2 plays a role and it is not clear how is working. For example, it was mentioned before that DNM2 can play a role in apoptosis but the mechanism of action it remains unknown (Fish et al., 2000).

Overall, considering all the activities where DNM2 is implicated in the cell, this may suggest the mechanism of action may not be the same in all cell types. In conclusion, DNM2 should be considered as a mechanoenzyme with additional cell signaling abilities.

Several CNM models have increased DNM2 protein level

In this thesis I presented two studies where I overexpressed human WT or mutated DNM2 in mouse skeletal muscle (Publication 1 and preliminary data). Interestingly, overexpression of WT-DNM2 caused a CNM-like phenotype, as shown previously (Cowling et al., 2011). This is in accordance with the CNM phenotype observed in XLCNM mouse model, where DNM2 is increased (Cowling et al., 2014). At that time, only one DNM2 mouse model was available, with the mutation R465W, causing mild CNM. The DNM2 protein level in these animals is equivalent to WT (Durieux, Vignaud, et al., 2010). Here I presented the creation of a novel model for severe DNM2-related CNM in which we detected an approximate 2 protein fold-increase compared to WT (Publication 2). In both CNM-DNM2 models it has been shown that reducing DNM2 level improves their phenotype ((Buono et al., 2018), Publication 2).

It remains to be confirmed if the increase in DNM2 protein is also seen in patients carrying the same mutations. In Publication 2 an immunoblot for a S619L patient shows no obvious protein increase but an abnormal protein band pattern that may indicate an increased protein oligomerization or oligomer stability. All this raises the question if DNM2 pathogenic mutations for CNM and CMT play also a role in protein stability.

All these results point to DNM2 protein increase as a pathogenic mechanism in CNM disease.

Hypothetical mechanisms leading to DNM2 protein increase

It is still not well understood how DNM2 protein increase can be responsible for CNM pathogenicity.

Taking the example of the *Mtm1*$^{-/y}$ mouse model, different strategies have been shown to improve its phenotype:

- Gene replacement, in which the gene was provided by an AAV vector (Buj-Bello et al., 2008)
- Enzyme replacement, in which MTM1 was fused to a mice antibody and injected in *Mtm1*$^{-/y}$ improving the clinical phenotype (Lawlor et al., 2013)
- BIN1 overexpression, which is a protein involved in CNM and directly binding MTM1 (Lionello et al., 2019)
- MTMR2 expression, which is a protein from the same family than MTM1 (Raess, Cowling, et al., 2017)
- Tamoxifen treatment, which normalized DNM2 level in treated animals (Publication 3 and (Maani et al., 2018).
- Genetic ablation of PI3KC2B, which is the kinase acting in the reverse direction to the phosphoinositide phosphatase MTM1 (Sabha et al., 2016)
- DNM2 reduction by genetic cross, shRNA-AAV or ASO treatment (Cowling et al., 2014; Tasfaout et al., 2017; Tasfaout et al., 2018)

Whether the latter three therapeutic approaches may relate to each other by playing on DNM2 expression it is not clear. Only tamoxifen treatment showed a normalization of DNM2 protein level similar to what is achieved by ASO treatment or genetic cross (Publication 3).

Recently, an additional pathomechanism involving DNM2 regulation was proposed for *Mtm1*-/y mouse model. Chen et al. pointed to miR199A1, a DNM2 intragenic microRNA, as a key player responsible for XLCNM disease in this mouse (X. Chen et al., 2020). They proposed that, similarly to DNM2 upregulation in this mouse, there is an upregulation of miR199A1 and pointed to STAT3 as the key transcriptional factor involved in this mechanism. A genetic cross between *Mtm1*$^{-/y}$ and miR199A1$^{-/-}$ animals showed that double KO animals have improved lifespan and muscle function (X. Chen et al., 2020). Further studies are required to understand if the same mechanism may be responsible for the increased DNM2 protein level detected in other CNM animal models. However, considering that miR199a1 is located at the intronic part of DNM2 (Aranda et al., 2015), and as

shown in Publication 1, WT-DNM2 overexpression induces a CNM-like phenotype, suggesting DNM2 cDNA expression has a pathogenic effect in CNM.

miR133a is a microRNA involved in cardiac and skeletal muscle development. Its role is mainly related to heart development and function and myoblast proliferation and differentiation (J. F. Chen et al., 2006; Liu et al., 2008). One of the targets from miR133a is DNM2 (Horak, Novak, & Bienertova-Vasku, 2016). Liu et al. showed that miR133a KO mice develop a DNM2-related CNM (Liu et al., 2011). Those animals displayed a 2-fold increase in *Dnm2* RNA together with a 7-fold increased protein level. miR133a KO animals had abnormal mitochondria localization and shape, together with a strong increase in the proportion of fibers with internalized nuclei. Myofiber size was also shown to be heterogeneous (Liu et al., 2011). The target site of miR133a in DNM2 is located at the 3'UTR region. It seems unlikely that a mutation in the coding region of the gene can have an effect on miR133a binding. Also, only protein was found to be increased with a normal RNA level in our novel *Dnm2*$^{+/S619L}$ mouse model (Publication 2). However, we cannot conclude if there is a possible dysregulation of miR133a level in the different animal models with an increased DNM2 level that may contribute to the pathology. Nevertheless, similarly to what I mentioned before, the expression of DNM2 cDNA is already causing a CNM-like phenotype, meaning not only miR133a dysregulation can play a role in the disease.

Artificial mutations and DNM2 role in nuclei position

In previous sections, I presented AAV-mediated expression of different DNM2 artificial or pathogenic mutations (Publication 1 and preliminary data). In both cases, one of the aims was to evaluate how different mutations impact skeletal muscle physiology. Surprisingly, we found differences for each artificial mutation studied. In summary:

Mutation	**Main defect(s) observed**
K44A	Reduction in force *No histology data is available at the moment*
K142A	Reduction in force Nuclei mislocalization
R399A	Reduction in force Mild improvement of muscle weight
ΔPRD	Nuclei mislocalization

	Mild improvement of muscle weight

As discussed previously, DNM2 overexpression, of WT or some artificial mutants, caused myonuclei mislocalization. One of the possible explanations of this is the potential effect caused by overexpressing DNM2 itself since WT-DNM2 overexpression strongly affects nuclei position. Interestingly, not all the mutants studied here have the ability to induce nuclei mislocalization when overexpressed in muscle. More precisely, R399A and K562E-CMT do not have a strong impact on myonuclei position unlike the other mutants explored (Publication 1 and preliminary data). These two mutants have in common a defect in lipid binding: R399A has 50% less affinity to bind lipids than WT-DNM2 and K562E-CMT is not able to bind them at all (Kenniston & Lemmon, 2010; Ramachandran et al., 2007). Furthermore both mutants have reduced GTPase activity. Additionally, R399A has a strong defect in forming high order oligomers (Ramachandran et al., 2007). Taking together these points and the fact that we did not observe the same effect in GTPase-defective mutants (Preliminary data), it seems that lipid binding is one of the most important functions involved in nuclei position.

Playing on DNM2 activity in XLCNM mouse model: DNM2 lipid binding as a potential therapeutic target

It has been shown that reducing DNM2 protein level has a therapeutic effect in several CNM mouse models. Here we wanted to explore how targeting specific DNM2 protein functions could impact on improving CNM-related phenotypes.

With the preliminary data included in this thesis (Preliminary data), it seems K562E expression causes an improvement in muscle phenotypes analyzed. We observed an improvement in the histology and ultrastructure of the skeletal muscle of *Mtm1*$^{-/y}$ animals expressing K562E. However, further analysis is needed of the other mutants injected. Interestingly, ΔPRD and R399A may have a milder positive effect when expressed in *Mtm1*$^{-/y}$ mice since we observe an increase of muscle weight although to a lesser extent than in the case of expressing DNM2-K562E mutant. In accordance with the discussion above, it looks like lipid binding may be one of the most pathogenic functions of DNM2 that should be targeted to improve CNM disease. However, we cannot exclude that due to the lack of lipid binding the real reason of this improvement is that DNM2 is not able to form high order oligomers, which may have a strong impact in membrane remodeling and fission.

We also observed a mild improvement in muscle weight expressing ΔPRD, a mutant that prevents the interaction with SH3 domain containing proteins. There are several SH3-domain containing proteins involved in the first-stages of endocytosis that interact with DNM2 (Sundborger & Hinshaw, 2014). This interaction may be an alternative way for DNM2 to be recruited to the membrane, so inhibiting this interaction may have a mild positive effect.

A further analysis of muscles injected with these mutants is needed to better understand the effect of inhibiting specific DNM2 functions in an XLCNM mouse model.

What we can learn from DNM2 animal models: similarities and differences

Since DNM2 was related to CNM and CMT diseases, several animal models have been generated to further understand their pathomechanism, from zebrafish to mouse models. Here I presented the creation of a novel mouse model that faithfully reproduces some CNM features. Nowadays, there are 4 DNM2 mouse models available: 3 of them carrying pathogenic mutations and 1 KO. The different features are listed in the following table.

Comparison of available mouse models

	Dnm2 **muscle-specific KO**	***Dnm2*** **R465W (Adolescent/adult onset CNM)**	***Dnm2*** **K562E (CMT)**	***Dnm2*** **S619L (Neonatal onset severe CNM)**
Mouse generation	Floxed exon 2	Mutation inserted by homologous recombination.	Mutation inserted by homologous recombination.	Mutation inserted by homologous recombination.
Reference	(Tinelli, Pereira, & Suter, 2013)	(Durieux, Vignaud, et al., 2010)	(Pereira et al., 2020)	Publication 2
Main genotype analyzed	Homozygous for muscle-specific KO of *Dnm2*	Heterozygous	Heterozygous	Heterozygous
GENERAL CLINICAL PHENOTYPING				
Survival	Complete KO is lethal.	Equivalent to WT. (Maximum age analyzed: 1.5 years of age)	Equivalent to WT (Maximum age analyzed: 1 year of age)	From P2 to P10 some pups are dying. After P10 survival is

	***Dnm2* muscle-specific KO**	***Dnm2* R465W (Adolescent/adult onset CNM)**	***Dnm2* K562E (CMT)**	***Dnm2* S619L (Neonatal onset severe CNM)**
	Muscle specific KO animals live until 10 days of age.	Few homozygous mice survived until weaning		equivalent to WT. (Maximum age analyzed: 2 years of age) Only one homozygous found born but dead, most of homozygous not found from E18.5 onwards.
Body weight	Decreased at P2 and P10.	Equivalent to WT	Decreased at 8 weeks	Decreased at P2 and from 3 weeks of age
Tibialis anterior muscle weight	Not analyzed but gastrocnemius muscle weight was decreased at P2 and P10.	Decreased at 8 and 32 weeks of age	Decreased at 8 weeks	Decreased at 8 weeks
Motor function	Not analyzed.	Decreased TA muscle force at 3, 8 and 32 weeks of age.	Less distance travelled in open-field	Impaired hanging test and in vivo force measurements.
Nerve physiology	Axonal degeneration.	Not analyzed	Muscle response to motor axon stimulation is reduced (compound	Not analyzed

	***Dnm2* muscle-specific KO**	***Dnm2* R465W (Adolescent/adult onset CNM)**	***Dnm2* K562E (CMT)**	***Dnm2* S619L (Neonatal onset severe CNM)**
			muscle action potential amplitude). Very mild changes in g-ratio.	
MOLECULAR BIOLOGY ANALYSIS				
DNM2 protein level	Low protein expression at P5, almost no protein at P10.	Equivalent to WT	Not analyzed	Increased
***Dnm2* RNA level**	Not analyzed	Equivalent to WT. Homozygous animals had a small decrease.	Not analyzed	Same than WT, small decrease in skeletal muscle isoform
DNM2 protein localization in muscle	Not analyzed	Equivalent to WT, striated and perinuclear. Some fibers have internal accumulation that collocalizes with dysferlin.	Not analyzed	Equivalent to WT
NEUROMUSCULAR PHENOTYPING				
Skeletal muscle histology	Muscles from P5 and P10 displayed less number of fibers. At P5 increase of large caliber fibers whereas at P10	Mild reduction in fiber size.	Reduced fiber size	Smaller fibers and abnormal oxidative staining

	***Dnm2* muscle-specific KO**	***Dnm2* R465W (Adolescent/adult onset CNM)**	***Dnm2* K562E (CMT)**	***Dnm2* S619L (Neonatal onset severe CNM)**
	increase of small caliber fibers.			
Oxidative staining	Not analyzed	Accumulation of oxidative staining in the center of myofibers	Not analyzed	Accumulation of oxidative staining in the center of myofibers
Nuclei position in skeletal muscle	Not analyzed	Equivalent to WT. In old mice defects in the number of nuclei per fiber, suggesting defects in myocyte fusion.	Not analyzed, but no obvious defect observed in histological images.	Equivalent to WT.
Skeletal muscle ultrastructure	Reduction in mitochondrial density.	Equivalent to WT with a slight increase in mitochondrial density and reduced myofibril size.	Not analyzed	Alteration in mitochondrial density and sarcomere organization
T tubules	Not analyzed	Equivalent to WT	Not analyzed	Not analyzed
Mitochondria	Swollen and disrupted cristae system appearing at P10. No mitochondria alterations observed at P5.	Increased mitochondrial content in transversal ultrastructural images	Not analyzed	Swollen and disrupted cristae system

	***Dnm2* muscle-specific KO**	***Dnm2* R465W (Adolescent/adult onset CNM)**	***Dnm2* K562E (CMT)**	***Dnm2* S619L (Neonatal onset severe CNM)**
Neuromuscular junction	Enlarged NMJ area	Not analyzed	Only checked by electrostimulation analysis and no major defect observed.	Equivalent to WT
ADDITIONAL PHENOTYPES				
Immune system	Not analyzed	Not analyzed	Increase in number of macrophages populating skeletal muscle. There is not neutropenia as in some K562E patients.	Not analyzed
Lipid droplet	Dysregulation of lipid droplets in skeletal muscle from KO animals at P5 and P10.	Defect in autophagosome maturation that may impact in lipid droplet degradation, but no obvious defect observed by ultrastructural analysis.	No obvious defects observed.	No obvious defects observed.
Phenotype relative to AAV-mediated expression (Publication 1)		Force reduction. Nuclei internalization Myofiber size reduction. Abnormal mitochondria size and location.	Force reduction. No nuclei mislocalization. No change in fiber size.	Force reduction. Strong nuclei mislocalization. Reduction in myofiber size.

	***Dnm2* muscle-specific KO**	***Dnm2* R465W (Adolescent/adult onset CNM)**	***Dnm2* K562E (CMT)**	***Dnm2* S619L (Neonatal onset severe CNM)**
	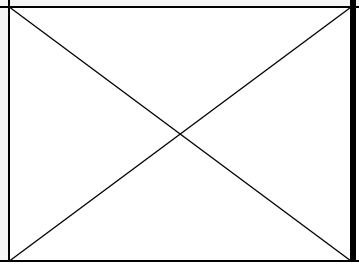	Increased T tubule circularity NMJ fragmentation	Strong defect in NMJ with decreased number and area.	Abnormally enlarged mitochondria with strongly disrupted cristae system. NMJ fragmentation.

Investigation of the *Dnm2*-KO animal model provided a better understanding of which neuromuscular functions DNM2 may be involved in. A strong defect in axons and neuromuscular junction was described, along with reduced muscle weight and the number of mitochondria was reduced with abnormal shape (Tinelli et al., 2013). Recently, several studies confirmed a possible involvement of DNM2 in neuromuscular junction and mitochondria fission. DNM2 seems to play a role in neuromuscular junction maturation by its actin bundling ability (Lin et al., 2020). It may be also involved in mitochondrial fission by partnering with DRP1, although different reports found contrary results on this topic (Kamerkar, Kraus, Sharpe, Pucadyil, & Ryan, 2018; Lee et al., 2016). Taking together these studies, we decided to investigate these features in the new mouse model carrying the S619L mutation and found a defect in muscle and body weights together with a strong defect in mitochondria. No defect was observed at neuromuscular junction or sciatic nerve. One of the most interesting points is that the abnormal mitochondria observed in S619L has the same shape than the one present in *Dnm2*-KO. However it remains unclear how introducing a mutation that has been shown to increase protein activity in vitro may cause a similar effect than removing the protein in mitochondrial wellness.

Nuclei centralization is not a common feature in DNM2-CNM mouse models and a comparable percentage of fibers with internalized nuclei was only achieved in mice by exogenous overexpression of human DNM2 (Publication 2). In XLCNM patients, the percentage of fibers with internalized nuclei is very heterogeneous among patients, with a range from 2% to 60% (Pierson, Tomczak, Agrawal, Moghadaszadeh, & Beggs, 2005), which is similar to what is observed in *Mtm1*$^{-/y}$ mouse model (Buj-Bello et al., 2002) (and also Preliminary data, EMPTY injected *Mtm1*$^{-/y}$ muscles). In ADCNM patients a range of 20% to 40% of fibers with internalized nuclei was observed (Jeannet et al., 2004). Two different hypothesis may explain why this phenotype is not easily reproduced in DNM2 mouse models: (i) that human and mouse DNM2 may not have equivalent functions or (ii) that the level of overexpression achieved by AAV injection is too high and pushes the system to an abnormal situation.

Similarly to patients, R465W mouse model shows a milder phenotype than S619L, since no obvious differences were observed in body weight and motor function is less impaired than in S619L. Interestingly, not the same defects are observed in both animals. For example, DNM2 localization is not affected in the *Dnm2*$^{+/S619L}$ and it was reported to be altered in the *Dnm2*$^{+/R465W}$. Myofibers of *Dnm2*$^{+/R465W}$ mice had an abnormal DNM2 accumulation in the center of the fiber that was colocalizing with dysferlin, a protein involved in muscle contraction (Durieux, Vignaud, et al., 2010). Muscle ultrastructural analysis of *Dnm2*$^{+/R465W}$ animals was similar to WT littermates,

only a slight increase in mitochondrial density and reduced myofibril size was reported (Durieux, Vignaud, et al., 2010). In Publication 1, by AAV-mediated expression we were able to recreate some of these phenotypes in WT skeletal muscle. Overexpressing R465W lead to an increase of mitochondrial density and size. Whereas S619L overexpression caused a strong disruption of mitochondria cristae system. Considering the combined results, it seems that a different pathomechanism may be linked to each mutation, which may also explain the difference of severity.

In Publication 2 we also presented a biopsy from a patient with an S619L mutation and found that mitochondria was similarly affected. In other CNM models, mitochondria was found mislocalized, in most cases collapsing in the perinuclear area (Buj-Bello et al., 2002), but no such alterations (i.e. swollen mitochondria with strongly disrupted cristae system) were reported before. Here we showed that ultrastructural analysis from the *Dnm2*$^{+/S619L}$ mice was very similar to what was observed in a S619L affected patient, making this animal an attractive model to study *DNM2*-related severe CNM pathomechanisms and therapies.

Very recently, the creation of a novel mouse model carrying the K562E mutation, linked to CMT disease, was reported (Pereira et al., 2020). Unexpectedly, this animal has no obvious signs of a peripheral neuropathy but shows signs of a mild myopathy. Only a mild defect was detected at muscle response to motor axon stimulation. However, body weight and muscle weight were reduced and there was a reduction of myofiber size. No ultrastructural data is available for this animal (Pereira et al., 2020). In Publication 1, we also overexpressed K562E in WT skeletal muscle. We observed no obvious change in muscle ultrastructure or histology, but detected a strong decrease of neuromuscular junction number and area. A patient carrying another DNM2-related CMT mutation was biopsied and no strong defect was observed at skeletal muscle level (Bitoun et al., 2008). It is difficult to conclude how K562E may affect muscle physiology, here we reported a strong alteration of neuromuscular junction that did not correlate with what was observed in the *Dnm2*$^{+/K562E}$ animal model. However, the analysis of this animal raised the question again if K562E patients may have an overlooked defect in skeletal muscle that should be further analyzed.

Lastly, a similar study to Publication 1 was published at the same time and reported no strong defects at the neuromuscular junction or skeletal muscle level when expressing another CMT mutation (G537C) in zebrafish (Zhao, Smith, Volpatti, Fabian, & Dowling, 2019).

DNM2 mutations in CMT have been typically categorized as loss of function, since they display lower GTPase activity and lipid binding in vitro. On the other hand, as mentioned in the introduction (2.6. Insights into DNM2 pathogenic mutations), CNM mutants have higher GTPase activity that is not regulated by lipid binding (Kenniston & Lemmon, 2010). For this reason, it has been typically said that CNM-DNM2 mutations lead to a gain of function whereas DNM2-CMT mutations cause a loss of function of the protein. However, here I presented a defect in NMJ due to DNM2-CMT expression in skeletal muscle (Publication 1), and Pereira et al. reported that *Dnm2*$^{+/K562E}$ animals display signs of a myopathy, indicating that we cannot exclude that CMT mutations cause additional muscle defects. However, the defect at NMJ level was not reproduced in zebrafish or in a mouse model with the same mutation. For this reason, further studies are needed to determine if DNM2-CMT mutations affect not only peripheral nerves but also muscle physiology. Additionally, the results from the different studies (AAV-mediated human DNM2 expression in mouse skeletal muscle, mouse model generation with *Dnm2* mutation and zebrafish stable transgenic expressing human DNM2) suggest that the conservation of DNM2 function may be different through species (Publication 1 and (Pereira et al., 2020; Zhao et al., 2019).

Conclusion and perspectives

During my thesis project, I used two different approaches to study DNM2 pathophysiology linked to different mutations: AAV-mediated expression and a genetically modified mouse model. On one hand I focused in pathogenic mutations to better understand which is the mechanism that leads to CNM and CMT diseases. On the other hand, I used different artificial DNM2 mutations already described to affect specific DNM2 functions with two different aims: to understand how they would affect WT skeletal muscle physiology and to determine which function of DNM2 should be inhibited to rescue a XLCNM mouse model.

Regarding CNM mutations, I presented the creation of a novel mouse model that mimics some of the phenotypes observed in a patient carrying the same mutation. I also showed that reducing DNM2 in this mouse has a positive effect in motor function together with an improvement in mitochondrial wellness and muscle ultrastructure. However, considering the controversy with DNM2's role in mitochondrial fission, it remains to be clarified how reducing DNM2 may have such an effect in this mouse model.

AAV-mediated expression of DNM2 mutants linked to CNM or CMT diseases in WT skeletal muscle lead to different defects. Overexpression of CNM mutants altered muscle ultrastructure with a strong effect on mitochondria, whereas overexpression of K562E-CMT mutant affected NMJ, causing a decrease of NMJ number and area. In this thesis I showed that, although CMT is a peripheral neuropathy, some defects may appear in skeletal muscle. Interestingly, expression of CNM mutants caused NMJ fragmentation. These results suggest that an overlap may exist between CNM and CMT diseases.

I also showed preliminary data of AAV-mediated expression of different DNM2 artificial mutants. In an *Mtm1*$^{-/y}$ mouse model I obtained promising results overexpressing K562E mutation, linked to CMT disease and that impairs lipid binding. Further analysis are needed to confirm this improvement and several question will need to be answered. For example, it will be needed to assess the preferential location for each DNM2 mutant and confirm to which cellular structures is preferentially located. Since they are DNM2 mutants, their overexpression may have additional pathogenic phenotypes. Before establishing which function of DNM2 should be targeted possible on-target effects should be analyzed across tissues and for cellular functions. This of special importance for K562E, a mutant that in patients causes a peripheral neuropathy, making it necessary to evaluate how neuromuscular junctions and nerves respond to its expression as a therapy in CNM.

In line with this point, I found that mutants impairing lipid binding do not cause nuclei centralization. This raises the question to understand how DNM2 lipid binding may be responsible for nuclei centralization. Further studies will be needed to conclude if lipid binding or the consequent high order oligomerization are responsible for this abnormal feature, which is a hallmark of CNM disease.

In conclusion, in this thesis I obtained new data that will help to better understand DNM2 pathophysiology in CNM and CMT diseases as well as its normal function in skeletal muscle.

Bibliography

Aghbolaghi, A. G., & Lechpammer, M. (2017). A rare case of centronuclear myopathy with DNM2 mutation: genotype-phenotype correlation. *Autops Case Rep, 7*(2), 43-48. doi:10.4322/acr.2017.020

Al-Qusairi, L., & Laporte, J. (2011). T-tubule biogenesis and triad formation in skeletal muscle and implication in human diseases. *Skelet Muscle, 1*(1), 26. doi:2044-5040-1-26 [pii]

10.1186/2044-5040-1-26

Al-Qusairi, L., Prokic, I., Amoasii, L., Kretz, C., Messaddeq, N., Mandel, J. L., & Laporte, J. (2013). Lack of myotubularin (MTM1) leads to muscle hypotrophy through unbalanced regulation of the autophagy and ubiquitin-proteasome pathways. *FASEB J, 27*(8), 3384-3394. doi:10.1096/fj.12-220947

fj.12-220947 [pii]

Amoasii, L., Hnia, K., Chicanne, G., Brech, A., Cowling, B. S., Muller, M. M., . . . Laporte, J. (2013). Myotubularin and PtdIns3P remodel the sarcoplasmic reticulum in muscle in vivo. *J Cell Sci, 126*(Pt 8), 1806-1819. doi:10.1242/jcs.118505

jcs.118505 [pii]

Antonny, B., Burd, C., De Camilli, P., Chen, E., Daumke, O., Faelber, K., . . . Schmid, S. (2016). Membrane fission by dynamin: what we know and what we need to know. *EMBO J, 35*(21), 2270-2284. doi:10.15252/embj.201694613

Aranda, J. F., Canfran-Duque, A., Goedeke, L., Suarez, Y., & Fernandez-Hernando, C. (2015). The miR-199-dynamin regulatory axis controls receptor-mediated endocytosis. *J Cell Sci, 128*(17), 3197-3209. doi:10.1242/jcs.165233

Bashkirov, P. V., Akimov, S. A., Evseev, A. I., Schmid, S. L., Zimmerberg, J., & Frolov, V. A. (2008). GTPase cycle of dynamin is coupled to membrane squeeze and release, leading to spontaneous fission. *Cell, 135*(7), 1276-1286. doi:10.1016/j.cell.2008.11.028

Beggs, A. H., Bohm, J., Snead, E., Kozlowski, M., Maurer, M., Minor, K., . . . Shelton, G. D. (2010). MTM1 mutation associated with X-linked myotubular myopathy in Labrador Retrievers. *Proc Natl Acad Sci U S A, 107*(33), 14697-14702. doi:1003677107 [pii]

10.1073/pnas.1003677107

Berciano, J. (2011). Peripheral neuropathies: Molecular diagnosis of Charcot-Marie-Tooth disease. *Nat Rev Neurol, 7*(6), 305-306. doi:10.1038/nrneurol.2011.72

Bethoney, K. A., King, M. C., Hinshaw, J. E., Ostap, E. M., & Lemmon, M. A. (2009). A possible effector role for the pleckstrin homology (PH) domain of dynamin. *Proc Natl Acad Sci U S A, 106*(32), 13359-13364. doi:10.1073/pnas.0906945106

Bitoun, M., Bevilacqua, J. A., Prudhon, B., Maugenre, S., Taratuto, A. L., Monges, S., . . . Guicheney, P. (2007). Dynamin 2 mutations cause sporadic centronuclear myopathy with neonatal onset. *Ann Neurol, 62*(6), 666-670.

Bitoun, M., Durieux, A. C., Prudhon, B., Bevilacqua, J. A., Herledan, A., Sakanyan, V., . . . Guicheney, P. (2009). Dynamin 2 mutations associated with human diseases impair clathrin-mediated receptor endocytosis. *Hum Mutat, 30*(10), 1419-1427. doi:10.1002/humu.21086

Bitoun, M., Maugenre, S., Jeannet, P. Y., Lacene, E., Ferrer, X., Laforet, P., . . . Guicheney, P. (2005). Mutations in dynamin 2 cause dominant centronuclear myopathy. *Nat Genet, 37*(11), 1207-1209. doi:10.1038/ng1657

Bitoun, M., Stojkovic, T., Prudhon, B., Maurage, C. A., Latour, P., Vermersch, P., & Guicheney, P. (2008). A novel mutation in the dynamin 2 gene in a Charcot-Marie-Tooth type 2 patient: clinical and pathological findings. *Neuromuscul Disord, 18*(4), 334-338.

Bohm, J., Biancalana, V., Dechene, E. T., Bitoun, M., Pierson, C. R., Schaefer, E., . . . Laporte, J. (2012). Mutation spectrum in the large GTPase dynamin 2, and genotype-phenotype correlation in autosomal dominant centronuclear myopathy. *Hum Mutat, 33*(6), 949-959. doi:10.1002/humu.22067

Bohm, J., Biancalana, V., Malfatti, E., Dondaine, N., Koch, C., Vasli, N., . . . Laporte, J. (2014). Adult-onset autosomal dominant centronuclear myopathy due to BIN1 mutations. *Brain, 137*(Pt 12), 3160-3170. doi:10.1093/brain/awu272

awu272 [pii]

Brinas, L., Vassilopoulos, S., Bonne, G., Guicheney, P., & Bitoun, M. (2013). Role of dynamin 2 in the disassembly of focal adhesions. *J Mol Med (Berl), 91*(7), 803-809. doi:10.1007/s00109-013-1040-2

Buj-Bello, A., Biancalana, V., Moutou, C., Laporte, J., & Mandel, J. L. (1999). Identification of novel mutations in the MTM1 gene causing severe and mild forms of X-linked myotubular myopathy. *Hum Mutat, 14*(4), 320-325.

Buj-Bello, A., Fougerousse, F., Schwab, Y., Messaddeq, N., Spehner, D., Pierson, C. R., . . . Mandel, J. L. (2008). AAV-mediated intramuscular delivery of myotubularin corrects the myotubular myopathy phenotype in targeted murine muscle and suggests a function in plasma membrane homeostasis. *Hum Mol Genet, 17*(14), 2132-2143. doi:ddn112 [pii]

10.1093/hmg/ddn112

Buj-Bello, A., Laugel, V., Messaddeq, N., Zahreddine, H., Laporte, J., Pellissier, J. F., & Mandel, J. L. (2002). The lipid phosphatase myotubularin is essential for skeletal muscle maintenance but not for myogenesis in mice. *Proc Natl Acad Sci U S A, 99*(23), 15060-15065.

Buono, S., Ross, J. A., Tasfaout, H., Levy, Y., Kretz, C., Tayefeh, L., . . . Cowling, B. S. (2018). Reducing dynamin 2 (DNM2) rescues DNM2-related dominant centronuclear myopathy. *Proc Natl Acad Sci U S A*. doi:10.1073/pnas.1808170115

Cadot, B., Gache, V., & Gomes, E. R. (2015). Moving and positioning the nucleus in skeletal muscle - one step at a time. *Nucleus, 6*(5), 373-381. doi:10.1080/19491034.2015.1090073

Cao, H., Garcia, F., & McNiven, M. A. (1998). Differential distribution of dynamin isoforms in mammalian cells. *Mol Biol Cell, 9*(9), 2595-2609.

Chal, J., & Pourquie, O. (2017). Making muscle: skeletal myogenesis in vivo and in vitro. *Development, 144*(12), 2104-2122. doi:10.1242/dev.151035

Chappie, J. S., Acharya, S., Leonard, M., Schmid, S. L., & Dyda, F. (2010). G domain dimerization controls dynamin's assembly-stimulated GTPase activity. *Nature, 465*(7297), 435-440.

Chen, J. F., Mandel, E. M., Thomson, J. M., Wu, Q., Callis, T. E., Hammond, S. M., . . . Wang, D. Z. (2006). The role of microRNA-1 and microRNA-133 in skeletal muscle proliferation and differentiation. *Nat Genet, 38*(2), 228-233. doi:10.1038/ng1725

Chen, X., Gao, Y. Q., Zheng, Y. Y., Wang, W., Wang, P., Liang, J., . . . Zhu, M. S. (2020). The intragenic microRNA miR199A1 in the dynamin 2 gene contributes to the pathology of X-linked centronuclear myopathy. *J Biol Chem*. doi:10.1074/jbc.RA119.010839

Chen, Y., & Yu, L. (2017). Recent progress in autophagic lysosome reformation. *Traffic, 18*(6), 358-361. doi:10.1111/tra.12484

Chin, Y. H., Lee, A., Kan, H. W., Laiman, J., Chuang, M. C., Hsieh, S. T., & Liu, Y. W. (2015). Dynamin-2 mutations associated with centronuclear myopathy are hypermorphic and lead to T-tubule fragmentation. *Hum Mol Genet, 24*(19), 5542-5554. doi:10.1093/hmg/ddv285

Claeys, K. G., Zuchner, S., Kennerson, M., Berciano, J., Garcia, A., Verhoeven, K., . . . De Jonghe, P. (2009). Phenotypic spectrum of dynamin 2 mutations in Charcot-Marie-Tooth neuropathy. *Brain, 132*(Pt 7), 1741-1752.

Cocanougher, B. T., Flynn, L., Yun, P., Jain, M., Waite, M., Vasavada, R., . . . Foley, A. R. (2019). Adult MTM1-related myopathy carriers: Classification based on deep phenotyping. *Neurology, 93*(16), e1535-e1542. doi:10.1212/WNL.0000000000008316

Cowling, B. S., Chevremont, T., Prokic, I., Kretz, C., Ferry, A., Coirault, C., . . . Laporte, J. (2014). Reducing dynamin 2 expression rescues X-linked centronuclear myopathy. *J Clin Invest, 124*(3), 1350-1363. doi:10.1172/JCI71206

Cowling, B. S., Prokic, I., Tasfaout, H., Rabai, A., Humbert, F., Rinaldi, B., . . . Laporte, J. (2017). Amphiphysin (BIN1) negatively regulates dynamin 2 for normal muscle maturation. *J Clin Invest, 127*(12), 4477-4487. doi:10.1172/JCI90542

Cowling, B. S., Toussaint, A., Amoasii, L., Koebel, P., Ferry, A., Davignon, L., . . . Laporte, J. (2011). Increased expression of wild-type or a centronuclear myopathy mutant of dynamin 2 in skeletal muscle of adult mice leads to structural defects and muscle weakness. *Am J Pathol, 178*(5), 2224-2235. doi:10.1016/j.ajpath.2011.01.054

Cowling, B. S., Toussaint, A., Muller, J., & Laporte, J. (2012). Defective membrane remodeling in neuromuscular diseases: insights from animal models. *PLoS Genet, 8*(4), e1002595. doi:10.1371/journal.pgen.1002595

PGENETICS-D-11-02246 [pii]

Damke, H., Baba, T., Warnock, D. E., & Schmid, S. L. (1994). Induction of mutant dynamin specifically blocks endocytic coated vesicle formation. *J Cell Biol, 127*(4), 915-934.

Damke, H., Binns, D. D., Ueda, H., Schmid, S. L., & Baba, T. (2001). Dynamin GTPase domain mutants block endocytic vesicle formation at morphologically distinct stages. *Mol Biol Cell, 12*(9), 2578-2589. doi:10.1091/mbc.12.9.2578

Danino, D., Moon, K. H., & Hinshaw, J. E. (2004). Rapid constriction of lipid bilayers by the mechanochemical enzyme dynamin. *J Struct Biol, 147*(3), 259-267. doi:10.1016/j.jsb.2004.04.005

De Craene, J. O., Bertazzi, D. L., Bar, S., & Friant, S. (2017). Phosphoinositides, Major Actors in Membrane Trafficking and Lipid Signaling Pathways. *Int J Mol Sci, 18*(3). doi:10.3390/ijms18030634

Dong, J., Misselwitz, R., Welfle, H., & Westermann, P. (2000). Expression and purification of dynamin II domains and initial studies on structure and function. *Protein Expr Purif, 20*(2), 314-323. doi:10.1006/prep.2000.1305

Dowling, J. J., Vreede, A. P., Low, S. E., Gibbs, E. M., Kuwada, J. Y., Bonnemann, C. G., & Feldman, E. L. (2009). Loss of myotubularin function results in T-tubule disorganization in zebrafish and human myotubular myopathy. *PLoS Genet, 5*(2), e1000372.

Durieux, A. C., Prudhon, B., Guicheney, P., & Bitoun, M. (2010). Dynamin 2 and human diseases. *J Mol Med, 88*(4), 339-350. doi:10.1007/s00109-009-0587-4

Durieux, A. C., Vassilopoulos, S., Laine, J., Fraysse, B., Brinas, L., Prudhon, B., . . . Bitoun, M. (2012). A centronuclear myopathy--dynamin 2 mutation impairs autophagy in mice. *Traffic, 13*(6), 869-879. doi:10.1111/j.1600-0854.2012.01348.x

Durieux, A. C., Vignaud, A., Prudhon, B., Viou, M. T., Beuvin, M., Vassilopoulos, S., . . . Bitoun, M. (2010). A centronuclear myopathy-dynamin 2 mutation impairs skeletal muscle structure and function in mice. *Hum Mol Genet, 19*(24), 4820-4836. doi:10.1093/hmg/ddq413

ddq413 [pii]

Fabrizi, G. M., Ferrarini, M., Cavallaro, T., Cabrini, I., Cerini, R., Bertolasi, L., & Rizzuto, N. (2007). Two novel mutations in dynamin-2 cause axonal Charcot-Marie-Tooth disease. *Neurology, 69*(3), 291-295. doi:10.1212/01.wnl.0000265820.51075.61

Faelber, K., Posor, Y., Gao, S., Held, M., Roske, Y., Schulze, D., . . . Daumke, O. (2011). Crystal structure of nucleotide-free dynamin. *Nature, 477*(7366), 556-560. doi:10.1038/nature10369

nature10369 [pii]

Ferguson, S. M., & De Camilli, P. (2012). Dynamin, a membrane-remodelling GTPase. *Nat Rev Mol Cell Biol, 13*(2), 75-88. doi:10.1038/nrm3266

Fetalvero, K. M., Yu, Y., Goetschkes, M., Liang, G., Valdez, R. A., Gould, T., . . . Murphy, L. O. (2013). Defective autophagy and mTORC1 signaling in myotubularin null mice. *Mol Cell Biol, 33*(1), 98-110. doi:10.1128/MCB.01075-12

MCB.01075-12 [pii]

Fish, K. N., Schmid, S. L., & Damke, H. (2000). Evidence that dynamin-2 functions as a signal-transducing GTPase. *J Cell Biol, 150*(1), 145-154. doi:10.1083/jcb.150.1.145

Fongy, A., Falcone, S., Laine, J., Prudhon, B., Martins-Bach, A., & Bitoun, M. (2019). Nuclear defects in skeletal muscle from a Dynamin 2-linked centronuclear myopathy mouse model. *Sci Rep, 9*(1), 1580. doi:10.1038/s41598-018-38184-0

Fonseca, T. B., Sanchez-Guerrero, A., Milosevic, I., & Raimundo, N. (2019). Mitochondrial fission requires DRP1 but not dynamins. *Nature, 570*(7761), E34-E42. doi:10.1038/s41586-019-1296-y

Franck, A., Laine, J., Moulay, G., Lemerle, E., Trichet, M., Gentil, C., . . . Vassilopoulos, S. (2019). Clathrin plaques and associated actin anchor intermediate filaments in skeletal muscle. *Mol Biol Cell, 30*(5), 579-590. doi:10.1091/mbc.E18-11-0718

Frontera, W. R., & Ochala, J. (2015). Skeletal muscle: a brief review of structure and function. *Calcif Tissue Int, 96*(3), 183-195. doi:10.1007/s00223-014-9915-y

Gavriilidis, C., Laredj, L., Solinhac, R., Messaddeq, N., Viaud, J., Laporte, J., . . . Hnia, K. (2018). The MTM1-UBQLN2-HSP complex mediates degradation of misfolded intermediate filaments in skeletal muscle. *Nat Cell Biol, 20*(2), 198-210. doi:10.1038/s41556-017-0024-9

Gerber, D., Ghidinelli, M., Tinelli, E., Somandin, C., Gerber, J., Pereira, J. A., . . . Suter, U. (2019). Schwann cells, but not Oligodendrocytes, Depend Strictly on Dynamin 2 Function. *Elife, 8*. doi:10.7554/eLife.42404

Gibbs, E. M., Clarke, N. F., Rose, K., Oates, E. C., Webster, R., Feldman, E. L., & Dowling, J. J. (2013). Neuromuscular junction abnormalities in DNM2-related centronuclear myopathy. *J Mol Med (Berl), 91*(6), 727-737. doi:10.1007/s00109-013-0994-4

Gibbs, E. M., Davidson, A. E., Telfer, W. R., Feldman, E. L., & Dowling, J. J. (2014). The myopathy-causing mutation DNM2-S619L leads to defective tubulation in vitro and in developing zebrafish. *Dis Model Mech, 7*(1), 157-161. doi:10.1242/dmm.012286

dmm.012286 [pii]

Gonzalez-Jamett, A. M., Baez-Matus, X., Olivares, M. J., Hinostroza, F., Guerra-Fernandez, M. J., Vasquez-Navarrete, J., . . . Cardenas, A. M. (2017). Dynamin-2 mutations linked to Centronuclear Myopathy impair actin-dependent trafficking in muscle cells. *Sci Rep, 7*(1), 4580. doi:10.1038/s41598-017-04418-w

Gonzalez-Jamett, A. M., Haro-Acuna, V., Momboisse, F., Caviedes, P., Bevilacqua, J. A., & Cardenas, A. M. (2014). Dynamin-2 in nervous system disorders. *J Neurochem, 128*(2), 210-223. doi:10.1111/jnc.12455

Gonzalez-Jamett, A. M., Momboisse, F., Haro-Acuna, V., Bevilacqua, J. A., Caviedes, P., & Cardenas, A. M. (2013). Dynamin-2 Function and Dysfunction Along the Secretory Pathway. *Front Endocrinol (Lausanne), 4*, 126. doi:10.3389/fendo.2013.00126

Grabs, D., Slepnev, V. I., Songyang, Z., David, C., Lynch, M., Cantley, L. C., & De Camilli, P. (1997). The SH3 domain of amphiphysin binds the proline-rich domain of dynamin at a single site that defines a new SH3 binding consensus sequence. *J Biol Chem, 272*(20), 13419-13425.

Gu, C., Yaddanapudi, S., Weins, A., Osborn, T., Reiser, J., Pollak, M., . . . Sever, S. (2010). Direct dynamin-actin interactions regulate the actin cytoskeleton. *EMBO J, 29*(21), 3593-3606. doi:emboj2010249 [pii]

10.1038/emboj.2010.249

Hamao, K., Morita, M., & Hosoya, H. (2009). New function of the proline rich domain in dynamin-2 to negatively regulate its interaction with microtubules in mammalian cells. *Exp Cell Res, 315*(7), 1336-1345.

Henley, J. R., Krueger, E. W., Oswald, B. J., & McNiven, M. A. (1998). Dynamin-mediated internalization of caveolae. *J Cell Biol, 141*(1), 85-99. doi:10.1083/jcb.141.1.85

Herskovits, J. S., Shpetner, H. S., Burgess, C. C., & Vallee, R. B. (1993). Microtubules and Src homology 3 domains stimulate the dynamin GTPase via its C-terminal domain. *Proc Natl Acad Sci U S A, 90*(24), 11468-11472.

Hinshaw, J. E., & Schmid, S. L. (1995). Dynamin self-assembles into rings suggesting a mechanism for coated vesicle budding. *Nature Cell Biol., 374*, 190-192.

Horak, M., Novak, J., & Bienertova-Vasku, J. (2016). Muscle-specific microRNAs in skeletal muscle development. *Dev Biol, 410*(1), 1-13. doi:10.1016/j.ydbio.2015.12.013

Jeannet, P. Y., Bassez, G., Eymard, B., Laforet, P., Urtizberea, J. A., Rouche, A., . . . Romero, N. B. (2004). Clinical and histologic findings in autosomal centronuclear myopathy. *Neurology, 62*(9), 1484-1490.

Jones, D. M., Alvarez, L. A., Nolan, R., Ferriz, M., Sainz Urruela, R., Massana-Munoz, X., . . . Padilla-Parra, S. (2017). Dynamin-2 Stabilizes the HIV-1 Fusion Pore with a Low Oligomeric State. *Cell Rep, 18*(2), 443-453. doi:10.1016/j.celrep.2016.12.032

Jones, S. M., Howell, K. E., Henley, J. R., Cao, H., & McNiven, M. A. (1998). Role of dynamin in the formation of transport vesicles from the trans-Golgi network. *Science, 279*, 573-577.

Jungbluth, H., Wallgren-Pettersson, C., & Laporte, J. (2008). Centronuclear (myotubular) myopathy. *Orphanet J Rare Dis, 3*, 26.

Kamerkar, S. C., Kraus, F., Sharpe, A. J., Pucadyil, T. J., & Ryan, M. T. (2018). Dynamin-related protein 1 has membrane constricting and severing abilities sufficient for mitochondrial and peroxisomal fission. *Nat Commun, 9*(1), 5239. doi:10.1038/s41467-018-07543-w

Kasai, K., Shin, H. W., Shinotsuka, C., Murakami, K., & Nakayama, K. (1999). Dynamin II is involved in endocytosis but not in the formation of transport vesicles from the trans-Golgi network. *J Biochem, 125*(4), 780-789. doi:10.1093/oxfordjournals.jbchem.a022349

Kenniston, J. A., & Lemmon, M. A. (2010). Dynamin GTPase regulation is altered by PH domain mutations found in centronuclear myopathy patients. *EMBO J, 29*(18), 3054-3067. doi:10.1038/emboj.2010.187

Kessels, M. M., Engqvist-Goldstein, A. E., Drubin, D. G., & Qualmann, B. (2001). Mammalian Abp1, a signal-responsive F-actin-binding protein, links the actin cytoskeleton to endocytosis via the GTPase dynamin. *J Cell Biol, 153*(2), 351-366. doi:10.1083/jcb.153.2.351

Kierdaszuk, B., Berdynski, M., Karolczak, J., Redowicz, M. J., Zekanowski, C., & Kaminska, A. M. (2013). A novel mutation in the DNM2 gene impairs dynamin 2 localization in skeletal muscle of a patient with late onset centronuclear myopathy. *Neuromuscul Disord, 23*(3), 219-228. doi:10.1016/j.nmd.2012.12.007

S0960-8966(12)00721-3 [pii]

Klein, D. E., Lee, A., Frank, D. W., Marks, M. S., & Lemmon, M. A. (1998). The pleckstrin homology domains of dynamin isoforms require oligomerization for high affinity phosphoinositide binding. *J Biol Chem, 273*(42), 27725-27733. doi:10.1074/jbc.273.42.27725

Koch, C., Buono, S., Menuet, A., Robe, A., Djeddi, S., Kretz, C., . . . Cowling, B. S. (2020). Myostatin: a Circulating Biomarker Correlating with Disease in Myotubular Myopathy Mice and Patients. *Mol Ther Methods Clin Dev, 17*, 1178-1189. doi:10.1016/j.omtm.2020.04.022

Koenig, J. H., & Ikeda, K. (1989). Disappearance and reformation of synaptic vesicle membrane upon transmitter release observed under reversible blockage of membrane retrieval. *J Neurosci, 9*(11), 3844-3860.

Kosaka, T., & Ikeda, K. (1983). Possible temperature-dependent blockage of synaptic vesicle recycling induced by a single gene mutation in Drosophila. *J Neurobiol, 14*(3), 207-225. doi:10.1002/neu.480140305

Koutsopoulos, O. S., Koch, C., Tosch, V., Bohm, J., North, K. N., & Laporte, J. (2011). Mild functional differences of dynamin 2 mutations associated to centronuclear myopathy and charcot-marie-tooth peripheral neuropathy. *PLoS One, 6*(11), e27498. doi:10.1371/journal.pone.0027498

PONE-D-11-11319 [pii]

Koutsopoulos, O. S., Kretz, C., Weller, C. M., Roux, A., Mojzisova, H., Bohm, J., . . . Laporte, J. (2013). Dynamin 2 homozygous mutation in humans with a lethal congenital syndrome. *Eur J Hum Genet, 21*(6), 637-642. doi:10.1038/ejhg.2012.226

ejhg2012226 [pii]

Krueger, E. W., Orth, J. D., Cao, H., & McNiven, M. A. (2003). A dynamin-cortactin-Arp2/3 complex mediates actin reorganization in growth factor-stimulated cells. *Mol Biol Cell, 14*(3), 1085-1096.

Kuo, I. Y., & Ehrlich, B. E. (2015). Signaling in muscle contraction. *Cold Spring Harb Perspect Biol, 7*(2), a006023. doi:10.1101/cshperspect.a006023

Laporte, J., Biancalana, V., Tanner, S. M., Kress, W., Schneider, V., Wallgren-Pettersson, C., . . . Mandel, J. L. (2000). MTM1 mutations in X-linked myotubular myopathy. *Hum Mutat, 15*(5), 393-409.

Laporte, J., Hu, L. J., Kretz, C., Mandel, J. L., Kioschis, P., Coy, J. F., . . . Dahl, N. (1996). A gene mutated in X-linked myotubular myopathy defines a new putative tyrosine phosphatase family conserved in yeast. *Nat Genet, 13*(2), 175-182. doi:10.1038/ng0696-175

Laporte, J., Kioschis, P., Hu, L. J., Kretz, C., Carlsson, B., Poustka, A., . . . Dahl, N. (1997). Cloning and characterization of an alternatively spliced gene in proximal Xq28 deleted in two patients with intersexual genitalia and myotubular myopathy. *Genomics, 41*(3), 458-462.

Lawlor, M. W., Armstrong, D., Viola, M. G., Widrick, J. J., Meng, H., Grange, R. W., . . . Beggs, A. H. (2013). Enzyme replacement therapy rescues weakness and improves muscle pathology in mice with X-linked myotubular myopathy. *Hum Mol Genet, 22*(8), 1525-1538. doi:10.1093/hmg/ddt003

ddt003 [pii]

Lee, J. E., Westrate, L. M., Wu, H., Page, C., & Voeltz, G. K. (2016). Multiple dynamin family members collaborate to drive mitochondrial division. *Nature, 540*(7631), 139-143. doi:10.1038/nature20555

Lin, S.-S., Hsieh, T.-L., Liou, G.-G., Li, T.-N., Lin, H.-C., Chang, C.-W., . . . Liu, Y.-W. (2020). Dynamin-2 regulates synaptic podosome maturation to facilitate neuromuscular junction development. *BioRxiv*, 2020.2005.2030.125062. doi:10.1101/2020.05.30.125062

Lionello, V. M., Nicot, A. S., Sartori, M., Kretz, C., Kessler, P., Buono, S., . . . Cowling, B. S. (2019). Amphiphysin 2 modulation rescues myotubular myopathy and prevents focal adhesion defects in mice. *Sci Transl Med, 11*(484). doi:10.1126/scitranslmed.aav1866

Liu, N., Bezprozvannaya, S., Shelton, J. M., Frisard, M. I., Hulver, M. W., McMillan, R. P., . . . Olson, E. N. (2011). Mice lacking microRNA 133a develop dynamin 2-dependent centronuclear myopathy. *J Clin Invest, 121*(8), 3258-3268. doi:46267 [pii]

10.1172/JCI46267

Liu, N., Bezprozvannaya, S., Williams, A. H., Qi, X., Richardson, J. A., Bassel-Duby, R., & Olson, E. N. (2008). microRNA-133a regulates cardiomyocyte proliferation and suppresses smooth muscle gene expression in the heart. *Genes Dev, 22*(23), 3242-3254. doi:10.1101/gad.1738708

Lorenzo, O., Urbe, S., & Clague, M. J. (2006). Systematic analysis of myotubularins: heteromeric interactions, subcellular localisation and endosome related functions. *J Cell Sci, 119*(Pt 14), 2953-2959.

Lundmark, R., & Carlsson, S. R. (2004). Regulated membrane recruitment of dynamin-2 mediated by sorting nexin 9. *J Biol Chem, 279*(41), 42694-42702. doi:10.1074/jbc.M407430200

Maani, N., Sabha, N., Rezai, K., Ramani, A., Groom, L., Eltayeb, N., . . . Dowling, J. J. (2018). Tamoxifen therapy in a murine model of myotubular myopathy. *Nat Commun, 9*(1), 4849. doi:10.1038/s41467-018-07057-5

Marks, B., Stowell, M. H., Vallis, Y., Mills, I. G., Gibson, A., Hopkins, C. R., & McMahon, H. T. (2001). GTPase activity of dynamin and resulting conformation change are essential for endocytosis. *Nature, 410*(6825), 231-235.

McNiven, M. A., Kim, L., Krueger, E. W., Orth, J. D., Cao, H., & Wong, T. W. (2000). Regulated interactions between dynamin and the actin-binding protein cortactin modulate cell shape. *J Cell Biol, 151*(1), 187-198.

Mercier, L., Bohm, J., Fekonja, N., Allio, G., Lutz, Y., Koch, M., . . . Laporte, J. (2016). In vivo imaging of skeletal muscle in mice highlights muscle defects in a model of myotubular myopathy. *Intravital, 5*(1), e1168553. doi:10.1080/21659087.2016.1168553

Mettlen, M., Pucadyil, T., Ramachandran, R., & Schmid, S. L. (2009). Dissecting dynamin's role in clathrin-mediated endocytosis. *Biochem Soc Trans, 37*(Pt 5), 1022-1026. doi:10.1042/BST0371022

Mooren, O. L., Kotova, T. I., Moore, A. J., & Schafer, D. A. (2009). Dynamin2 GTPase and cortactin remodel actin filaments. *J Biol Chem, 284*(36), 23995-24005.

Mukund, K., & Subramaniam, S. (2020). Skeletal muscle: A review of molecular structure and function, in health and disease. *Wiley Interdiscip Rev Syst Biol Med, 12*(1), e1462. doi:10.1002/wsbm.1462

Nave, K. A., & Werner, H. B. (2014). Myelination of the nervous system: mechanisms and functions. *Annu Rev Cell Dev Biol, 30*, 503-533. doi:10.1146/annurev-cellbio-100913-013101

Nicot, A. S., Toussaint, A., Tosch, V., Kretz, C., Wallgren-Pettersson, C., Iwarsson, E., . . . Laporte, J. (2007). Mutations in amphiphysin 2 (BIN1) disrupt interaction with dynamin 2 and cause autosomal recessive centronuclear myopathy. *Nat Genet, 39*(9), 1134-1139.

Nishimune, H., & Shigemoto, K. (2018). Practical Anatomy of the Neuromuscular Junction in Health and Disease. *Neurol Clin, 36*(2), 231-240. doi:10.1016/j.ncl.2018.01.009

Oh, P., McIntosh, D. P., & Schnitzer, J. E. (1998). Dynamin at the neck of caveolae mediates their budding to form transport vesicles by GTP-driven fission from the plasma membrane of endothelium. *J Cell Biol, 141*(1), 101-114. doi:10.1083/jcb.141.1.101

Pereira, J. A., Gerber, J., Ghidinelli, M., Gerber, D., Tortola, L., Ommer, A., . . . Suter, U. (2020). Mice carrying an analogous heterozygous Dynamin 2 K562E mutation that causes neuropathy in humans develop predominant characteristics of a primary myopathy. *Hum Mol Genet*. doi:10.1093/hmg/ddaa034

Peterson, C. M., Johannsen, D. L., & Ravussin, E. (2012). Skeletal muscle mitochondria and aging: a review. *J Aging Res, 2012*, 194821. doi:10.1155/2012/194821

Pierson, C. R., Dulin-Smith, A. N., Durban, A. N., Marshall, M. L., Marshall, J. T., Snyder, A. D., . . . Beggs, A. H. (2012). Modeling the human MTM1 p.R69C mutation in murine Mtm1 results in exon 4 skipping and a less severe myotubular myopathy phenotype. *Hum Mol Genet, 21*(4), 811-825. doi:ddr512 [pii]

10.1093/hmg/ddr512

Pierson, C. R., Tomczak, K., Agrawal, P., Moghadaszadeh, B., & Beggs, A. H. (2005). X-linked myotubular and centronuclear myopathies. *J Neuropathol Exp Neurol, 64*(7), 555-564.

Praefcke, G. J., & McMahon, H. T. (2004). The dynamin superfamily: universal membrane tubulation and fission molecules? *Nat Rev Mol Cell Biol, 5*(2), 133-147.

Rabai, A., Reisser, L., Reina-San-Martin, B., Mamdchoui, K., Cowling, B., Nicot, A. S., & Laporte, J. (2019). Allele-specific CRISPR-Cas9-mediated inactivation or correction of a heterozygous dynamin 2 mutation rescues centronuclear myopathy cellular phenotypes. *Mol. ther. Nucleic Acids, in press*.

Raess, M. A., Cowling, B. S., Bertazzi, D. L., Kretz, C., Rinaldi, B., Xuereb, J. M., . . . Laporte, J. (2017). Expression of the neuropathy-associated MTMR2 gene rescues MTM1-associated myopathy. *Hum Mol Genet, 26*(19), 3736-3748. doi:10.1093/hmg/ddx258

Raess, M. A., Friant, S., Cowling, B. S., & Laporte, J. (2017). WANTED - Dead or alive: Myotubularins, a large disease-associated protein family. *Adv Biol Regul, 63*, 49-58. doi:10.1016/j.jbior.2016.09.001

Ramachandran, R., Pucadyil, T. J., Liu, Y. W., Acharya, S., Leonard, M., Lukiyanchuk, V., & Schmid, S. L. (2009). Membrane insertion of the pleckstrin homology domain variable loop 1 is critical for dynamin-catalyzed vesicle scission. *Mol Biol Cell, 20*(22), 4630-4639. doi:10.1091/mbc.E09-08-0683

Ramachandran, R., & Schmid, S. L. (2018). The dynamin superfamily. *Curr Biol, 28*(8), R411-R416. doi:10.1016/j.cub.2017.12.013

Ramachandran, R., Surka, M., Chappie, J. S., Fowler, D. M., Foss, T. R., Song, B. D., & Schmid, S. L. (2007). The dynamin middle domain is critical for tetramerization and higher-order self-assembly. *EMBO J, 26*(2), 559-566.

Reid, A. T., Lord, T., Stanger, S. J., Roman, S. D., McCluskey, A., Robinson, P. J., . . . Nixon, B. (2012). Dynamin regulates specific membrane fusion events necessary for acrosomal exocytosis in mouse spermatozoa. *J Biol Chem, 287*(45), 37659-37672. doi:10.1074/jbc.M112.392803

Relaix, F. (2006). Skeletal muscle progenitor cells: from embryo to adult. *Cell Mol Life Sci, 63*(11), 1221-1225. doi:10.1007/s00018-006-6015-9

Reubold, T. F., Faelber, K., Plattner, N., Posor, Y., Ketel, K., Curth, U., . . . Eschenburg, S. (2015). Crystal structure of the dynamin tetramer. *Nature, 525*, 404. doi:10.1038/nature14880

https://www.nature.com/articles/nature14880#supplementary-information

Robb, S. A., Sewry, C. A., Dowling, J. J., Feng, L., Cullup, T., Lillis, S., . . . Muntoni, F. (2011). Impaired neuromuscular transmission and response to acetylcholinesterase inhibitors in centronuclear myopathies. *Neuromuscul Disord, 21*(6), 379-386. doi:S0960-8966(11)00037-X [pii]

10.1016/j.nmd.2011.02.012

Romero, N. B. (2010). Centronuclear myopathies: a widening concept. *Neuromuscul Disord, 20*(4), 223-228. doi:S0960-8966(10)00053-2 [pii]

10.1016/j.nmd.2010.01.014

Romero, N. B., & Bitoun, M. (2011). Centronuclear myopathies. *Semin Pediatr Neurol, 18*(4), 250-256. doi:10.1016/j.spen.2011.10.006

Rosendale, M., Van, T. N. N., Grillo-Bosch, D., Sposini, S., Claverie, L., Gauthereau, I., . . . Perrais, D. (2019). Functional recruitment of dynamin requires multimeric interactions for efficient endocytosis. *Nat Commun, 10*(1), 4462. doi:10.1038/s41467-019-12434-9

Sabha, N., Volpatti, J. R., Gonorazky, H., Reifler, A., Davidson, A. E., Li, X., . . . Dowling, J. J. (2016). PIK3C2B inhibition improves function and prolongs survival in myotubular myopathy animal models. *J Clin Invest, 126*(9), 3613-3625. doi:10.1172/JCI86841

Schlunck, G., Damke, H., Kiosses, W. B., Rusk, N., Symons, M. H., Waterman-Storer, C. M., . . . Schwartz, M. A. (2004). Modulation of Rac localization and function by dynamin. *Mol Biol Cell, 15*(1), 256-267.

Schulze, R. J., Weller, S. G., Schroeder, B., Krueger, E. W., Chi, S., Casey, C. A., & McNiven, M. A. (2013). Lipid droplet breakdown requires dynamin 2 for vesiculation of autolysosomal tubules in hepatocytes. *J Cell Biol, 203*(2), 315-326. doi:10.1083/jcb.201306140

Seth, P. P., Siwkowski, A., Allerson, C. R., Vasquez, G., Lee, S., Prakash, T. P., . . . Swayze, E. E. (2008). Design, synthesis and evaluation of constrained methoxyethyl (cMOE) and constrained ethyl (cEt) nucleoside analogs. *Nucleic Acids Symp Ser (Oxf)*(52), 553-554. doi:10.1093/nass/nrn280

Shpetner, H. S., & Vallee, R. B. (1989). Identification of dynamin, a novel mechanochemical enzyme that mediates interactions between microtubules. *Cell, 59*(3), 421-432.

Sidiropoulos, P. N., Miehe, M., Bock, T., Tinelli, E., Oertli, C. I., Kuner, R., . . . Suter, U. (2012). Dynamin 2 mutations in Charcot-Marie-Tooth neuropathy highlight the importance of

clathrin-mediated endocytosis in myelination. *Brain, 135*(Pt 5), 1395-1411. doi:10.1093/brain/aws061

Sun, Y., & Tien, P. (2013). From endocytosis to membrane fusion: emerging roles of dynamin in virus entry. *Crit Rev Microbiol, 39*(2), 166-179. doi:10.3109/1040841X.2012.694412

Sundborger, A. C., Fang, S., Heymann, J. A., Ray, P., Chappie, J. S., & Hinshaw, J. E. (2014). A dynamin mutant defines a superconstricted prefission state. *Cell Rep, 8*(3), 734-742. doi:10.1016/j.celrep.2014.06.054

S2211-1247(14)00556-7 [pii]

Sundborger, A. C., & Hinshaw, J. E. (2014). Regulating dynamin dynamics during endocytosis. *F1000Prime Rep, 6*, 85. doi:10.12703/P6-85

Sweeney, H. L., & Hammers, D. W. (2018). Muscle Contraction. *Cold Spring Harb Perspect Biol, 10*(2). doi:10.1101/cshperspect.a023200

Tanabe, K., & Takei, K. (2009). Dynamic instability of microtubules requires dynamin 2 and is impaired in a Charcot-Marie-Tooth mutant. *J Cell Biol, 185*(6), 939-948.

Tanabe, K., & Takei, K. (2012). Dynamin 2 in Charcot-Marie-Tooth disease. *Acta Med Okayama, 66*(3), 183-190. doi:10.18926/AMO/48557

Tasfaout, H., Buono, S., Guo, S., Kretz, C., Messaddeq, N., Booten, S., . . . Laporte, J. (2017). Antisense oligonucleotide-mediated Dnm2 knockdown prevents and reverts myotubular myopathy in mice. *Nat Commun, 8*, 15661. doi:10.1038/ncomms15661

Tasfaout, H., Lionello, V. M., Kretz, C., Koebel, P., Messaddeq, N., Bitz, D., . . . Cowling, B. S. (2018). Single Intramuscular Injection of AAV-shRNA Reduces DNM2 and Prevents Myotubular Myopathy in Mice. *Mol Ther, 26*(4), 1082-1092. doi:10.1016/j.ymthe.2018.02.008

Thomas, N. S., Williams, H., Cole, G., Roberts, K., Clarke, A., Liechti-Gallati, S., . . . et al. (1990). X linked neonatal centronuclear/myotubular myopathy: evidence for linkage to Xq28 DNA marker loci. *J.Med.Genet., 27*, 284-287.

Thompson, H. M., Cao, H., Chen, J., Euteneuer, U., & McNiven, M. A. (2004). Dynamin 2 binds gamma-tubulin and participates in centrosome cohesion. *Nat Cell Biol, 6*(4), 335-342.

Thompson, H. M., Skop, A. R., Euteneuer, U., Meyer, B. J., & McNiven, M. A. (2002). The large GTPase dynamin associates with the spindle midzone and is required for cytokinesis. *Curr Biol, 12*(24), 2111-2117.

Tinelli, E., Pereira, J. A., & Suter, U. (2013). Muscle-specific function of the centronuclear myopathy and Charcot-Marie-Tooth neuropathy-associated dynamin 2 is required for proper lipid metabolism, mitochondria, muscle fibers, neuromuscular junctions and peripheral nerves. *Hum Mol Genet, 22*(21), 4417-4429. doi:10.1093/hmg/ddt292

Toussaint, A., Cowling, B. S., Hnia, K., Mohr, M., Oldfors, A., Schwab, Y., . . . Laporte, J. (2011). Defects in amphiphysin 2 (BIN1) and triads in several forms of centronuclear myopathies. *Acta Neuropathol, 121*(2), 253-266. doi:10.1007/s00401-010-0754-2

Trochet, D., Prudhon, B., Beuvin, M., Peccate, C., Lorain, S., Julien, L., . . . Bitoun, M. (2018). Allele-specific silencing therapy for Dynamin 2-related dominant centronuclear myopathy. *EMBO Mol Med, 10*(2), 239-253. doi:10.15252/emmm.201707988

Trochet, D., Prudhon, B., Jollet, A., Lorain, S., & Bitoun, M. (2016). Reprogramming the Dynamin 2 mRNA by Spliceosome-mediated RNA Trans-splicing. *Mol Ther Nucleic Acids, 5*(9), e362. doi:10.1038/mtna.2016.67

Tronchere, H., Laporte, J., Pendaries, C., Chaussade, C., Liaubet, L., Pirola, L., . . . Payrastre, B. (2004). Production of phosphatidylinositol 5-phosphate by the phosphoinositide 3-phosphatase myotubularin in mammalian cells. *J Biol Chem, 279*(8), 7304-7312. doi:10.1074/jbc.M311071200

M311071200 [pii]

Trouillon, R., & Ewing, A. G. (2013). Amperometric measurements at cells support a role for dynamin in the dilation of the fusion pore during exocytosis. *Chemphyschem, 14*(10), 2295-2301. doi:10.1002/cphc.201300319

van der Bliek, A. M., & Meyerowitz, E. M. (1991). Dynamin-like protein encoded by the Drosophila shibire gene associated with vesicular traffic. *Nature, 351*(6325), 411-414.

van der Bliek, A. M., Redelmeier, T. E., Damke, H., Tisdale, E. J., Meyerowitz, E. M., & Schmid, S. L. (1993). Mutations in human dynamin block an intermediate stage in coated vesicle formation. *J Cell Biol, 122*(3), 553-563. doi:10.1083/jcb.122.3.553

Vandersmissen, I., Biancalana, V., Servais, L., Dowling, J. J., Vander Stichele, G., Van Rooijen, S., & Thielemans, L. (2018). An integrated modelling methodology for estimating the prevalence of centronuclear myopathy. *Neuromuscul Disord, 28*(9), 766-777. doi:10.1016/j.nmd.2018.06.012

Vassilopoulos, S., Gentil, C., Laine, J., Buclez, P. O., Franck, A., Ferry, A., . . . Bitoun, M. (2014). Actin scaffolding by clathrin heavy chain is required for skeletal muscle sarcomere organization. *J Cell Biol, 205*(3), 377-393. doi:10.1083/jcb.201309096

Velichkova, M., Juan, J., Kadandale, P., Jean, S., Ribeiro, I., Raman, V., . . . Kiger, A. A. (2010). Drosophila Mtm and class II PI3K coregulate a PI(3)P pool with cortical and endolysosomal functions. *J Cell Biol, 190*(3), 407-425. doi:jcb.200911020 [pii]

10.1083/jcb.200911020

Wang, J., Fan, Y., Sanger, J. M., & Sanger, J. W. (2018). Nonmuscle myosin II in cardiac and skeletal muscle cells. *Cytoskeleton (Hoboken), 75*(8), 339-351. doi:10.1002/cm.21454

Warnock, D. E., Baba, T., & Schmid, S. L. (1997). Ubiquitously expressed dynamin-II has a higher intrinsic GTPase activity and a greater propensity for self-assembly than neuronal dynamin-I. *Mol Biol Cell, 8*(12), 2553-2562.

Yamada, H., Kobayashi, K., Zhang, Y., Takeda, T., & Takei, K. (2016). Expression of a dynamin 2 mutant associated with Charcot-Marie-Tooth disease leads to aberrant actin dynamics and lamellipodia formation. *Neurosci Lett, 628*, 179-185. doi:10.1016/j.neulet.2016.06.030

Yu, R., Lendahl, U., Nister, M., & Zhao, J. (2020). Regulation of Mammalian Mitochondrial Dynamics: Opportunities and Challenges. *Front Endocrinol (Lausanne), 11*, 374. doi:10.3389/fendo.2020.00374

Zhang, P., & Hinshaw, J. E. (2001). Three-dimensional reconstruction of dynamin in the constricted state. *Nat Cell Biol, 3*(10), 922-926. doi:10.1038/ncb1001-922

Zhao, M., Maani, N., & Dowling, J. J. (2018). Dynamin 2 (DNM2) as Cause of, and Modifier for, Human Neuromuscular Disease. *Neurotherapeutics, 15*(4), 966-975. doi:10.1007/s13311-018-00686-0

Zhao, M., Smith, L., Volpatti, J., Fabian, L., & Dowling, J. J. (2019). Insights into wild type dynamin 2 and the consequences of DNM2 mutations from transgenic zebrafish. *Hum Mol Genet*. doi:10.1093/hmg/ddz260

Zheng, J., Cahill, S. M., Lemmon, M. A., Fushman, D., Schlessinger, J., & Cowburn, D. (1996). Identification of the binding site for acidic phospholipids on the pH domain of dynamin: implications for stimulation of GTPase activity. *J Mol Biol, 255*(1), 14-21. doi:10.1006/jmbi.1996.0002

Zoncu, R., Perera, R. M., Sebastian, R., Nakatsu, F., Chen, H., Balla, T., . . . De Camilli, P. V. (2007). Loss of endocytic clathrin-coated pits upon acute depletion of phosphatidylinositol 4,5-bisphosphate. *Proc Natl Acad Sci U S A, 104*(10), 3793-3798. doi:0611733104 [pii]

10.1073/pnas.0611733104

Zuchner, S., Noureddine, M., Kennerson, M., Verhoeven, K., Claeys, K., De Jonghe, P., . . . Vance, J. M. (2005). Mutations in the pleckstrin homology domain of dynamin 2 cause dominant intermediate Charcot-Marie-Tooth disease. *Nat Genet, 37*(3), 289-294.

Résumé scientifique 'Physiopathologie et thérapies dans les myopathies liées à la mecanoenzyme dynamine'

1) Introduction

La dynamine 2 (DNM2) est une GTPase exprimée ubiquitairement et impliquée dans plusieurs processus allant de la régulation du cytosquelette au remodelage de la membrane et de l'endocytose. Des mutations dominantes de DNM2 ont été associées à deux maladies : la myopathie centronucléaire (CNM) et la neuropathie de Charcot-Marie-Tooth (CMT). Le rôle de la DNM2 est peu connu, c'est pourquoi dans cette thèse on cherche à :

- Comprendre les effets de différentes mutations en lien avec CNM et CMT dans le muscle squelettique qui pourront aider à comprendre la physiopathologie des deux maladies.
- Établir un modèle de la forme sévère de CNM due à DNM2 et valider une approche thérapeutique.
- Identifier les fonctions importantes de la DNM2 dans le muscle et impactées dans les CNM. Ce travail de thèse permettra de mieux comprendre le rôle physiologique de DNM2 et son rôle dans la maladie. Cela permettra également d'avoir un outil précieux pour étudier de potentielles thérapies pour la CNM due à des mutations de la DNM2.

2) Méthodologie

Ce travail de thèse étudie les phénotypes associés à la surexpression du transgène humain DNM2 dans un modèle de souris en utilisant des AAV (virus adéno-associé - AAV) qui ont été injectés dans le muscle de souris sauvages. Pour comprendre les fonctions de la DNM2 impliquées dans les CNMs, un modèle de souris de la forme sévère liée au chromosome X (XLCNM) a été utilisé, dans lequel des injections d'AAV intramusculaire ont été faites. Enfin, un nouveau modèle de souris portant la mutation DNM2 S619L liée à la CNM et une approche thérapeutique par thérapie antisens (Antisens oligonucléotide ASO) contre DNM2 ont été validés.

3) Résultats essentiels

Étude du mécanisme physiopathologique des mutations de DNM2 liées aux CNM dans le muscle squelettique comparé aux mutations de DNM2 impliquées dans les CMT pour mieux comprendre

pourquoi certaines mutations de la DNM2 mènent à une maladie affectant davantage le muscle et d'autres à une maladie neurologique, différentes mutations ont été introduites grâce à des AAV. Dans des modèles de souris sauvages, différentes mutations ont été introduites par voie intramusculaire:

- La DNM2 sauvage a été introduite
- Deux mutations causant soit une forme néonatale ou une forme adulte de CNM ont été introduites, respectivement la mutation DNM2 S619L ou la mutation R465W
- La mutation K562E causant la CMT a été introduite

L'expression de la DNM2 sauvage et des mutants CNM recréent un phénotype de myopathie centronucléaire, ce qui suggère que les mutations CNM sont de type gain de fonction. Les souris qui ont été injectées avec de différentes mutations de la DNM2 CNM ou CMT présentent une localisation anormale de la DNM2 autour du noyau et de la membrane plasmique. Étonnamment, la surexpression de la DNM2 sauvage et des mutants CNM chez une souris WT altèrent la position du noyau dans beaucoup de fibres alors que ce n'est pas le cas pour la mutation retrouvée dans la CMT. Toutes ces mutations ont résulté en une distribution anormale des tailles des fibres. De plus, des défauts histologiques ont été observés par la coloration SDH (activité oxidative mitochondriale) dans les muscles injectés par la DNM2 sauvage et dans les muscles où les mutations CNM ont été ajoutées. De même, des défauts histologiques ont été observés par la coloration NADH (activité oxidative générale) dans les muscles injectés par la DNM2 sauvage, les DNM2-CNM et la DNM2-CMT, ce qui suggère des défauts dans l'organisation du réticulum sarcoplasmique et/ou de la fonction mitochondriale. Enfin, des défauts de localisation de protéines connues pour être importantes dans la fonction musculaire ont été observés, comme la desmine, la dysferline et la bêta-intégrine. En résumé, l'expression de DNM2 sauvage ou CNM induit un phénotype CNM alors que l'expression de DNM2 CMT induit des défauts neuromusculaires différents.

Comprendre la physiopathologie de la forme néonatale autosomale dominante de la myopathie centronucléaire et validation d'un traitement

Un précédent modèle murin avec une forme modérée de la CNM-DNM2 portant la mutation R465W (forme adulte modérée) présente un phénotype progressif très faible du muscle, excluant une analyse détaillée du mécanisme pathologique et la validation de l'effet de potentielles thérapies. Pour ce faire, le modèle de souris Dnm2S619L a été généré, reproduisant la mutation

hétérozygote la plus commune associée à la forme sévère néonatale. Les patients porteurs de cette mutation ont des symptômes associés au CNM comme une faiblesse musculaire, notamment dans les membres inférieurs et des muscles faciaux, une ophtalmoparésie et une prédominance des fibres de type I. J'ai montré que les souris Dnm2S619L/+ ont une forte faiblesse musculaire précoce avec un fort impact sur l'homéostasie mitochondriale. Par stimulation du nerf sciatique, des défauts de contraction musculaire ont pu être observés. Une augmentation du niveau protéique de DNM2 a été observée dans ce modèle, c'est pourquoi une thérapie antisens a été initiée afin de normaliser le niveau total de DNM2.

Cette augmentation du niveau protéique de DNM2 a été reportée dans d'autres modèles de CNM, comme dans le modèle Mtm1y/- (XLCNM), et la réduction du niveau protéique par thérapie antisens a permis d'améliorer le phénotype de la maladie (Tasfaout et al. 2017). La thérapie antisens a également été testée dans le modèle Dnm2S619L, ce qui a permis une amélioration très substantielle de la force musculaire ainsi qu'un rétablissement partiel de la mitochondrie et des tailles des fibres.

Identification des fonctions importantes de la DNM2 pour le muscle et qui sont impliqués dans les CNM

Pour comprendre quelles sont les fonctions essentielles à la DNM2 dans le muscle, les domaines responsables de l'activité GTPase, de l'oligomérisation, de la liaison des protéines et des lipides, ont été mutés artificiellement. Par l'usage d'AAV, la DNM2 sauvage et les mutations perte/gain de fonction ont été insérées dans le muscle squelettique de souris sauvage et chez des souris *Mtm1*$^{-/y}$. Les muscles ont été analysés au niveau de leur fonction et de leur masse, ainsi qu'au niveau histopathologique et moléculaire.

Mutation AAV-DNM2 perte de fonction : notre équipe a récemment montré que la réduction génétique de la DNM2 dans un modèle de souris *Mtm1*$^{-/y}$ permet de rallonger l'espérance de vie des souris, de prévenir le phénotype myopathique et d'améliorer le poids des souris. Dans cette thèse, l'évaluation de différents AAVs, exprimant soit la GTPase inactive de DNM2, soit une la DNM2 ne liant plus ces partenaires protéiques ou lipidiques dans le modèle de souris *Mtm1*$^{-/y}$ a été étudiée ; le but étant de tester quelle activité de DNM2 il faut réduire pour rétablir le phénotype. La mutation DNM2-K44A induit l'impossibilité de liaison au GTP.

La mutation DNM2-K124A permet l'hydrolyse du GTP en GDP, mais ne subit pas de changement de conformation en raison de ce processus. Une construction portant la mutation DNM2-K562E (mutation CMT) ne permet pas la liaison aux lipides. Enfin, la construction DNM2-ΔPRD a été réalisée, où le domaine PRD de la DNM2, responsable de l'interaction avec des protéines régulatrices contenant le domaine SH3, a été retiré. Toutes ces constructions ont été clonées, et les AAV ont été préparés et injectés intra-musculairement chez les souris. Les résultats préliminaires ont montré que les muscles de souris issus du phénotype *Mtm1*$^{-/y}$ ne présentent pas d'amélioration après la surexpression de la DNM2-K142A ou DNM2- ΔPRD. Mais l'injection de l'AAV-DNM2 K562E a un effet positif sur les souris de phénotype *Mtm1*$^{-/y}$, ce qui suggère que la liaison aux lipides de DNM2 est une des potentielles cibles thérapeutiques pour traiter les souris MTM1-CNM et potentiellement les patients XLCNM.

4) Conclusion

Dans cette thèse, diverses mutations de DNM2 liées aux maladies CNM et CMT ont été étudiées. L'expression de la DNM2-sauvage ou de DNM2-CNM recrée le phénotype CNM, ce qui suggère que ces mutations sont de type gain de fonction, alors que l'expression du mutant DNM2-CMT n'entraine pas une internalisation des noyaux, qui est une caractéristique des CNMs, ce qui laisse penser que les mutations causant des CMT altèrent différentes fonctions de la DNM2 ou ont un impact différent (perte de fonction au lieu de gain de fonction). Par la même approche, différentes fonctions de DNM2 ont été étudiées et j'ai montré que la liaison de DNM2 aux lipides est une des potentielles cibles thérapeutiques pour traiter les myopathies centronucléaires liées au chromosome X. Cette thèse fournit également la validation d'une nouvelle lignée de souris DNM2KI-S619L comme un modèle fiable pour les mutations DNM2 affectant les enfants. Nous avons également montré que la diminution du niveau de DNM2 par des injections d'antisens permet d'améliorer le phénotype de myopathie. Enfin, cette étude a permis l'identification de potentiels pathomécanismes lié à la DNM2 dans les CNM et CMT.

Xènia MASSANA MUÑOZ

Physiopathology and therapies in myopathies linked to the mechanoenzyme dynamin

Résumé

La dynamine 2 (DNM2) est une GTPase exprimée ubiquitairement et impliquée dans plusieurs processus allant de la régulation du cytosquelette au remodelage des membranes et le contrôle de l'endocytose. Des mutations dominantes de DNM2 ont été associées à deux maladies : la myopathie centronucléaire (CNM) et la neuropathie de Charcot-Marie-Tooth (CMT). De plus le rôle de la DNM2 dans les tissus impliqués est peu connu. Dans cette thèse, diverses mutations de DNM2 liées aux maladies CNM et CMT ont été étudiées. L'expression de la DNM2-sauvage ou de DNM2-CNM recrée le phénotype CNM, ce qui suggère que ces mutations CNM sont de type gain de fonction, alors que l'expression du mutant DNM2-CMT n'entraine pas une internalisation des noyaux, qui est une caractéristique des CNMs, laissant penser que les mutations causant des CMT altèrent différentes fonctions de la DNM2 ou ont un impact différent (perte de fonction).
Par la même approche, différentes fonctions de DNM2 ont été étudiées et j'ai montré que la liaison de DNM2 aux lipides est une des cibles thérapeutiques potentielles pour traiter les myopathies centronucléaires liées au chromosome X.
Cette thèse fournit également la validation d'une nouvelle lignée de souris DNM2KI-S619L comme modèle reproduisant fiablement les phénotypes des enfants avec mutations DNM2. Nous avons également montré que la diminution du niveau de DNM2 par des injections d'antisens permet d'améliorer le phénotype musculaire de ce modèle.
Enfin, cette étude a permis l'identification de pathomécanismes liés à la DNM2 dans les CNM et CMT.

Résumé en anglais

Dynamin 2 (DNM2) is an ubiquitously expressed GTPase involved in many cellular functions from cytoskeleton regulation to membrane remodeling and endocytosis. DNM2 dominant mutations have been associated to two different diseases: Centronuclear Myopathy (CNM) and Charcot-Marie-Tooth peripheral neuropathy (CMT). In this thesis, different DNM2 mutations linked to CNM and CMT have been studied. The expression of WT-DNM2 or CNM-DNM2 recreates a CNM phenotype, suggesting CNM mutations are gain of function. On the other hand, CMT-DNM2 expression did not cause nuclei internalization, which is the typical phenotype observed in CNM disease, suggesting CMT mutations affect different DNM2 functions or lead to a loss of function of the protein. Using the same approach, different DNM2 protein functions have been studied, showing that DNM2 lipid binding is one of the potential therapeutic targets that could be used to treat X-linked CNM.
This thesis also provides a validation of a novel mouse line, the DNM2KI-S619L, as a model that faithfully reproduces the phenotypes observed in children affected with the S619L mutation. We also showed that reducing DNM2 using antisense oligonucleotide injections improves the muscle phenotype of this mouse.
In conclusion, this study allowed to identify pathomechanisms linked to DNM2 in CNM and CMT diseases.